Development of Novel Polymer Monoliths for Fast Ion Chromatography

by

David Schaller

A thesis submitted in fulfilment of the requirements for the degree

of

Doctor of Philosophy

UNIVERSITY OF TASMANIA

Submitted November 2012

Acknowledgements

Firstly, I'd like to thank my supervisors, Professors Emily F. Hilder and Paul Haddad, without whom this work would have not been possible. You have supported me through all stages of my candidature, so thank you both for your supervision and encouragement. Emily in particular for supporting me in situations that were somewhat delicate at times (details shall not be mentioned here-in, but no hard feelings Bob) sobering yet humorous on reflection. Your knowledge of the field, writing and presentation skills, layout and holistic view of this work have helped make it what it is today. Likewise I'm very grateful of your experienced input and scrutiny Paul, for taking me on-board in the first place and not holding back on painful yet healthy criticism, which sufficiently challenged me to ensure the quality of the work was accepted into the realm of PhD publications, approved and supported by my examiners Prof Sebastian Eeltink and with some discussion (8 pages of tabled correction suggestions) by Dr Damien Conolly.

I also wish to thank Dr Chris Evenhuis, who contributed to several aspects of this research and provided me with supervision over a period of my candidature. I would like to thank my colleagues at ACROSS and the school of Chemistry at UTAS. Dr Joseph Hutchinson for the monolith development groundwork in the lead-up to this project and always offering friendly and helpful advice when needed. Milko Novic gets a mention for great hospitality and good advice and showing me around Slovenia!

I'd like to thank Dr Tom (Artachez) Kazarian, Dr Oscar Potter, Ryan Nay, Dr Tim Causon, Will Percey and of course Madam Esme Candish for company, support, friendship and entertainment within the research group.
My gratitude extends to all other members of the ACROSS team, including Dr Anna Nordborg and Dr Lea Mauko, Mark Guijt and Prof Pavel Nesterenko and the former AST, now Endocrinologist and soon to be Dr - Laura Parsley. Furthermore I'd like to extend my gratitude to A. Prof Jason Smith, A. Prof Michael Breadmore, Dr Wolfgang Buchberger and A. Prof Rob 'Bone Rollin' Shellie. Mirek Macka will also get a mention for cultural diversity.

And to round up the Chemistry crew I couldn't go without saying thanks to the larger than life secretary in action Kerry-Anne Berger!

Following my naturalisation 'into' the remote island down-under called Tasmania, I have found great mates and partners in crime on and off campus, primarily over the alley within the Engineering faculty. Thanks to you guys I had one of the best times in my life in this place, memories that will be with us for the rest of our lives (may it be long enough to remember). Thank you Dr Sushilo, Dr Stecker, Dr MJ Lim (the first of the bunch to depart with floppy hat), Dr Lavroff, Master Aman, Master Vien, Master Chanchai, soon to be Dr Ahsan Latheef and though he might not deserve it I shall acknowledge my gratefulness to the larger than life Master Obi (Steffen)! A love - hate relationship that surprisingly can be fostered…

To all my off-campus buddies, Rob K, Duncan Wilks, Jared Ratray, Jeremy Price, Robin Cooper, Andrew Glidden, Chris Townend and Rose Grayson from the Valley of Lower Longley, and of course Martin Kaelbe the adopted Schaller family member and my Honey GL Ronny Vogel for Tassie TLC and his family Tina Winter and Bela Wintervogel! Also a special thank-you to Heidi Laugesen for positive support and friendship over these years.

I want to extend my special thanks and appreciation to James Fox, contributing significantly to the practical and theoretical understanding and modelling of the C4D chapter. As my adopted Tassie family, Flora and James provided mental and physical support together with their extended family helping out when I needed it. I'd also like to acknowledge my former host-parents, David and Jenny Boyer who invited me into their house 15 years ago and little did they know I was going to stay on the island ever since! So this achievement is also in your honour. I will also recall the encouragement from my Maths Stage 3 teacher Chris Boyles back then at Friend's School, it all adds up.

I'd also like to acknowledge my team at EM&C. Thank you Rhonda and Simon Chislett for giving me a job, putting up with my seemingly chaotic way of approaching projects and your patience and assistance in that matter. And of course for the regular finances that proped up the bank account. Thank you also Nathan Jensen and Malin Flukes for good mateship in the office and field.

Since they are a big bunch and tight unit, I will address the Prichard and Giudici clan as a whole. Thank you all for your support and accepting me in your family circle without much fuss, can't quite say the first German to break the Italian ranks since the two sisters were there before me and some german blood exists from the Hundt family three or so Generations back, also from Stuttgart! Thank you Michael, Karen, Oscar and Oliver Giudici, my inlaws!

Of course my own family will get a mention, thanks guys for sticking (up) it to (for) me… We work in our own way and make each other proud. My bro Felix for winning the Querdenker award at the same time as I officially get this work approved and my little 'big' bro Stephan for following in my footsteps. At least I left you a long enough window to improve on… I'd like to thank my Sis Manuela and BiL Matt Simmo, thank you both for looking after me and for all your support. And that little cheeky offspring of yours, Leah, oh what a joy!

Last but definitely not least! My wonderful wife, love of my life and mother of our children to be, thank you Rosie Schaller (still a Giudici deep down) for all you have done for me and will do, standing by me with encouragement and TLC, starting with our early morning rendezvous at York Store, sweet lunchtime catch-ups in the tearoom, accompanying me to Germany for 4 months while I formulated Chapter 4, your continuing support back here, letting me crash at Nelson (thanks Vanessa and Eleanor) and of course saying yes and marrying me on the 7th of the 7th this year!

I look forward to our continued path together with all the challenges we will face and conquer. I have a feeling parenthood will be the biggest yet!

So in good Aussie fashion I say: ON YAS ALL and if you must do a PhD then be ready to embrace many frustrating moments; you will however be adequately rewarded with joy, accomplishment and the feeling of taking on (a fraction) of the world!

"If you write 3 sentences a day you will complete your thesis in 3 years" Dieter Schaller, sometime in 2011.

Declaration

To the best of my knowledge, this thesis contains no copy or paraphrase of material previously published or written by another person, except where due reference is made in the text of the thesis.

David Schaller

7th November 2012

David Schaller

7th November 2012

Abstract

This thesis focuses on the development of latex agglomerated ion-exchange materials for applications in capillary ion chromatography (IC). The continuous rod, monolithic polymer columns were predominantly synthesised *in-situ* in micro-format – within capillaries of 1 mm internal diameter and below - useable in traditional as well as current high-end capillary IC instruments. Recent developments in monolithic stationary phases for the fast analysis of inorganic ions and other small molecules in IC and capillary electrochromatography (CEC) concentrate in particular on the properties of organic (polymer) monolithic materials and inorganic (silica-based) monoliths and specific applications.

The project path has encompassed fabrication, characterisation and chromatographic investigation of monolayer AS18 latex-coated, sulfonated poly(chloromethylstyrene-*co*-divinylbenzene) (poly(CMS-*co*-DVB)) monoliths and their commercial counterpart – the Dionex Ionswift^{TM} Max Series. Subsequent to the synthesis work, the non-destructive morphology and capacity assessment by capacitively-coupled contactless conductivity detection (C^4D) and the comprehensive study of this technique in relation to methacrylate based, strong anion-exchanger (SAX) polymer monoliths in capillary format revealed the potential and shortfalls of the detection technique to predict monolithic column performance. Monolayer latex-coated, functionalised poly(CMS-*co*-DVB) monolithic porous polymer scaffolds were measured with capacities of 34 μequiv/g and plate heights of 26,000 plates/m. The direct surface functionalised (non-coated) SAX version exhibited values in both capacity and plate number more than double in

magnitude, which is ascribed to the actual surface and pore morphology of the polymer materials with different levels of hydrophobicity.

C^4D was used to non-invasively evaluate the internal make-up of the capillary columns, consisting of a combination of morphology and surface chemistry. Measurements were made by scanning the conductance of the mobile phase filling the pores of the substrate, with and without the surface functional conductivity of the scaffold, over the length of the capillary section using an automated, motorized stage. The findings were well matched with scanning electron microscopy (SEM) images of the capillary cross-sections at discrete locations and further confirmed with chromatographic testing, such that higher conducting, smooth profile yielding columns were predictably exhibiting better separation performance over versions that yielded more irregular conductivity profiles.

The extension of this work on latex-coated, functionalised poly(CMS-*co*-DVB) monoliths in capillary format to coatings with differently sized AS11 latex particles showed that the extent and type of coating are of lower influence on the chromatographic performance in comparison to well defined, uniformly porous morphology of the polymer substrate. Other material surface effects, such as gel porosity and the level of hydrophobicity in relation to the eluents and solvents used, appear to have significant effects on both the synthesis process and the final column chromatographic performance.

Glossary of Terms

Symbol	Quantity	Unit
i.d.	Internal diameter of capillary	*µ*m
o.d.	Outer diameter of capillary	*µ*m
G	Conductance	S
I	Electric current	A
V	Applied voltage	V
Z	Impedance	

Abbreviation

ACN	Acetonitrile
AIBN	2,2'-azobisisobutyronitrile
AMPS	2-acrylamido-2-methyl-1-propane-sulphonic acid
BET	Brunauer-Emmet-Teller model (surface area by N_2 Adsorption)
BJH	Barret-Joyner-Halenda model (surface area by N_2 Adsorption)
BuMA	Butyl methacrylate
C^4D	Capacitively Coupled, Contactless Conductivity Detection
CEC	Capillary Electrochromatography
CLD	Chord Length Distribution
CLSM	Confocal Laser Scanning Microscopy
CMS	Chloromethylstyrene
CTAB	Cetyltrimethylammonium bromide
DDAB	Didodecyldimethylammonium bromide

DDMAU	*N*-dodecyl-*N,N*-(dimethylammonio)undecanoate
DCM	Dichloromethane
DCE	1,2-dichloroethane
DMA	Dimethylamine
DMPAP	2,2-dimethoxy-2-phenylacetophenone
DOSS	Dioctylsulfosuccinnate
DVB	Divinylbenzene
EPMA	Electron Probe Micro-Analysis
EDAX	Energy Dispersive X-ray spectroscopy (Elemental Analysis)
EDMA	Ethyl dimethacrylate
EOF	Electro Osmotic Flow
GMA	Glycidal methacrylate
GNP	Gold Nanoparticle
$HAuCl_4$	Chloroauric acid
IC	Ion Chromatography
ICP	Inductively Coupled Plasma
IDA	Iminodiacetic acid
META	2(methacryloyloxl)ethyl trimethylammonium chloride
MIP	Mercury Intrusion Porosimetry
MIR	Mid-Infrared Spectroscopy
MOAC	Metal Oxide Affinity Chromatography
MVA	Multivariate Data Analysis
MWNT	Multi Walled (Carbon) Nanotubes
NIR	Near-Infrared Spectroscopy
NMR	Nuclear Magnetic Resonance

ODS	Octadecylsilyl
PAHs	Polycyclic Aromatic Hydrocarbons
PDDAC	Poly(diallyldimethylammonium chloride)
PEI	Polyethyleneimine
PEM	Polyelectrolyte Multilayers
RD-MRI	Remotely Detected Magnetic Resonance Imaging
RP	Reversed Phase
RSD	Relative Standard Deviation
SAX	Strong Anion Exchanger
SDS	Sodium dodecylsulfate
SEM	Scanning Electron Microscopy
SPM	3-sulfopropylmethacrylate
sC^4D	Scanning C^4D
SWNT	Single Walled (Carbon) Nanotubes
TEM	Transmission Electron Microscopy
THF	Tetrahydrofuran

Publications

Review: *Monolithic stationary phases for fast ion chromatography and capillary electrochromatography of inorganic ions*
David Schaller, Emily F. Hilder and Paul R. Haddad
J. Sep. Sci. **2006,** *29*, 1705 - 1719.

Monoliths for fast Ion Chromatography

Mr David Schaller, Dr Emily F. Hilder and Prof. Paul R. Haddad
GIT Laboratory Journal **2006***, 6,* 2 - 3.

Development of novel polymer monoliths for fast ion chromatography (IC) **–**

David Schaller, Joseph P. Hutchinson, Emily F. Hilder and Paul R. Haddad - ***HPLC 2006****, San Francisco, US* – *(*Poster).

Development of novel polymer monoliths for fast ion chromatography (IC) **-**

David Schaller, Joseph P. Hutchinson, Emily F. Hilder and Paul R. Haddad - *29th Australasian Polymer Symposium February 2007*

Hobart, Tasmania – *(*Poster).

Development of novel polymer monoliths for fast ion chromatography (IC) **-**

David Schaller, Joseph P. Hutchinson, Chris Evenhuis, Emily F. Hilder and Paul R. Haddad – *RACI R&D Topics Adelaide 2007- Oral (3rd Prize).*

Table of Contents

1. Introduction and Literature Review

The term "Ion Chromatography" was first introduced by the Dionex Corporation upon licensing of the technology based on the principles of ion-exchange chromatography, which was originally established by Baumann *et al.* in 1975 [1]. Today, the separation methods encompassed under the banner of IC include ion-exchange chromatography, ion-interaction (or ion-pair) chromatography, ion-exclusion chromatography and miscellaneous ionic analyte and stationary phase interactions, such as reversed-phase or chelating ion chromatography [2]. Inorganic ion analysis is predominantly carried out by ion-exchange chromatography, nonetheless for simplicity reasons this review includes all relevant techniques under the general term of ion chromatography (IC).

The popularity of IC has to a large extent been generated by the success of the technique in both inorganic and biological ion analysis and has ensured its status as one of the key analytical techniques over the last two decades [2]. Related aspects of ion analysis by liquid chromatography have been covered thoroughly by previous reviews, ranging from historical developments [3-4], principles, application and progress in capillary IC [5] and CEC [6] and microfluidic systems [7] to current column technologies in commercial instrumentation for the analysis of complex sample matrices [8], as well as some degree of future outlook for monolithic stationary phases [9].

Comprehensive reviews on the properties of polymer monoliths as continuous porous polymer rods and their precursors in liquid capillary chromatography have been published by Svec [10-12], providing a good overview and description of the applications and possibilities of these new

generation stationary phases. Other excellent reviews on the use of monolithic columns in CEC [13-15], including comprehensive documentation of the different synthetic processes for sol-gel, acrylate-, polystyrene- and polyacrylamide-based porous monolith media with numerous applications [16], provide further insight into the progress of these materials in chromatographic analysis. Surfactant and latex-coated monoliths have since been reviewed by Chambers *et al.* [17]. The use of ion-exchange monoliths for the separation of proteins and polynucleotides has also been reviewed elsewhere [18-19].

The latest developments of tailored functional polymer monoliths to improve the efficient separation of small molecules in HPLC have recently been reviewed by Svec [20], highlighting the potential of these modifications already trialled as well as those yet to be tested. Similarly, the various advantages and limitations of monoliths used for separations of small molecules in HPLC (and to some extent in CEC) have been recently reviewed by Nischang *et al.* [21], drawing attention to the scaffold chemistry as the main focus requiring improvement.

More specifically in the field of IC, a recent comprehensive review by Nordborg *et al.* [22] outlines material benefits and drawbacks of both polymer and silica monolith scaffolds and their modification as well as alternative monolithic materials. Various characterisation techniques for evaluating the column morphology and modification are also included in this review, with application-specific matching of suitable monolithic columns and commercial analogues also included.

The review presented here [23] considers two different classes of monolithic stationary phases, namely organic polymer-based and silica-based monolithic separation media for application in IC. Since initial research efforts into continuous separation media began in the early 1970s, much progress has been made, particularly after the introduction of a new class of rigid macroporous polymer monoliths by Svec and Fréchet [24] in the early 1990s. The first application of methacrylate monoliths as stationary phases in IC was published in 1995 [25]. This was followed closely by the reproducible synthesis of uniform monolithic silica media, using a hydrolysis-based sol-gel process, by Tanaka and co-workers [26] and followed by surface modification reaction with alkylsilane to create reversed-phase continuous separation media.

Monolithic silica columns are now well established as commercially available HPLC columns. Examples such as the Chromolith RP-18 range (Merck) and the Onyx Monolithic C_{18} range (Phenomenex) are becoming more popular for inorganic and biological analysis due to their advantages over packed particle columns [9]. For analytes such as small organic molecules (MW<500) and ions, the reversed-phase C_{18} silica structures have been coated with ionic surfactants to create anionic [27], cationic [28-30] or zwitterionic [31-32] stationary phases suitable for fast IC. The ProSwift monolithic ion-exchange columns by Dionex (Inc.) are some of the columns of choice for fast protein separations, offering high resolution for separation and purification.

Terms such as fast and ultra-fast separations have become more common in recent literature with the availability of commercial IC columns

(*i.e.* Speed ROD) allowing sub-minute separations of 10 or more ionic analytes.

For the purpose of this study, fast IC separations are conducted in less than 5 minutes.

At present, the robust and reproducible analysis of small ions is successfully performed on commercial IC columns packed with surface-functionalised polymer beads. When considering analysis of small inorganic ions on standard IC instrumentation, the currently available IC columns showing best performance are those using latex-coated or grafted polymer particles manufactured by the Dionex Corporation. Nevertheless, particle-packed columns have significant disadvantages at higher flow-rates, predominantly evident in the loss of separation efficiency and also the rapid build-up of backpressure, which can damage both instrumentation and columns. Packed particle columns are thus not the best option for fast IC analysis on conventional IC equipment [33].

Over the last decade research efforts on monolithic media for IC have focused on high throughput and efficient separation of proteins and large organic molecules (MW>500), where the speed of analysis is a key factor for analysing large numbers of biological samples, while maintaining or even increasing separation efficiency [25]. The rapid mass transfer characteristics of these analytes on monolithic media can be attributed predominantly to convective rather than diffusive mass transfer. This occurs because the eluent is forced to flow through the pores of the monolithic media, in contrast to polymer beads, where the majority of the flow is directed around the particles and separation relies on the diffusive mass transfer of analytes into

the pores of the particles, which is very slow and unfavourable for large, high molecular weight molecules [34].

The permeability and open pore structure of the flow-through channels ensures dynamic interaction between mobile phase and functional groups on the stationary phase surface, which provides increased mass transfer at high flow-rates by minimising the presence of stagnant mass transfer zones reliant on diffusive mechanisms. This relationship is illustrated in Van Deemter plots of monolithic stationary phases. A recent characterisation of silica monoliths [35] calculated the permeability for packed columns to be equivalent to the monolithic format for particles with a diameter of 15 μm and the diffusion-limited mass transfer equivalent for particles of 3 μm diameter. However, one of the main drawbacks of current monolithic formats for fast IC of small ions is the apparent lack of ion-exchange capacity. While this tends to be less of an issue for the separation of large organic molecules such as proteins, it considerably affects the separation efficiency and sensitivity of inorganic ions, as these are reliant on individual functionalities present on the stationary phase surface rather than spanning over an extended range of interaction sites [36].

Besides the advantage of high flow at lower backpressure, both polymer and silica based monolithic stationary phases can readily be modified to suit a variety of applications. Given the single phase polymerisation mixture in monolith synthesis, the choice of possible porogens, functional monomers and reaction conditions is far greater than in suspension polymerisation of macroporous beads [33].

The fabrication method used to create monolithic polymer and silica stationary phases can be performed *in-situ*, directly inside a variety of columns or moulds. Furthermore, the monolithic media can simultaneously be attached to the pre-treated column walls during synthesis, through formation of covalent bonds. This is particularly advantageous for fabrication in microchips and microcolumns, where packing with particles poses difficulties and usually requires the use of retaining frits. Regardless of the type of column, the rigidity of the porous network allows these materials to be used in combination with conventional IC systems, withstanding backpressures up to 20 MPa without deformation of the internal porous structure [33].

Monolithic materials are now well established for the analysis of biomolecules with several commercial products already available [33]. However, the field of fast anion chromatography has only recently included the use of monolithic stationary phases and judging by the current limitations is still very much in the development stage. This review therefore aims to provide an insight into the principles and potential uses of polymer- and silica-based monolithic materials for fast IC of inorganic and small organic ions and further to comment on likely future developments in this field.

1.1 Monolithic silica stationary phases

Silica monoliths prepared by the polymerisation of sol-gel precursors [26] or immobilisation of silica particles [37] yield highly uniform monolithic skeletons. The methods of fabrication, characterisation and various

applications of monolithic silica materials have been the subject of several comprehensive reviews [38-40].

The original sol-gel process employed by Nakanishi and Soga [41] was later adapted [26] to create silica monoliths of reversed-phase nature by derivatisation with alkyl-silanes for applications in CEC and IC. Silica monoliths prepared in this way offer a very uniform morphology, consisting of an array of well-ordered, equally sized, interlinked skeleton branches of 1-2 μm in diameter, separated by continuous flow-through pores. The synthesis of silica monoliths using the sol-gel method is predominantly carried out in capillary columns and micro channels, where covalent attachment of the monolithic skeleton to the column or channel wall prevents shrinking of the silica during preparation, which would otherwise create physical gaps between column wall and the porous material [42]. Synthesis of monolithic silica columns in the larger scale HPLC format, for columns with internal diameters in the mm range, is more difficult and involves a shaving and cladding step of the shrunken silica rod released from the mould. For fabrication in capillaries or microchip channels, anchoring of the material by covalent attachment is essential to prevent flushing the porous network from the channel. As the covalent attachment during the phase transition reaction prevents the shrinkage away from the capillary or channel wall, the morphology of micro-channel silica monoliths is similar to their polymer analogues, consisting of aggregated silica globules rather than the smooth cylindrical structures found in HPLC-scale formats [33].

Synthesis occurs in three stages and involves gelation, ageing and drying. After phase separation has occurred in the gelation step, the curing

agents are removed by washing with water. The aging process involves curing of the formed silica skeleton with ammonium hydroxide solution in order to develop the mesopore structure [15]. Although the tailoring of flow properties is governed by the control in macroporous structure, it is the independent control of mesopore formation that occurs during the aging process which is ultimately responsible for the unique chromatographic performance [33].

Columns prepared by this method are now available commercially for use with conventional IC instrumentation and have been post-modified in various approaches to create functional monolithic silica ion-exchange stationary phases. Studies using unmodified commercial silica monolith columns have already reported considerable improvement in selectivity, efficiency and limit of detection over conventional columns simply by allowing higher sample throughput while maintaining the favourable mass transfer characteristics, which is not possible with conventional packed particle columns [43]. Several examples of post-modification have been reported, including surfactant-coated reversed-phase silica monoliths for ion-exchange [28-29], covalent attachment of substrates containing functional groups [44-46], as well as silica monoliths fabricated in a capillary and coated with latex nanoparticles via electrostatic interaction [47].

1.1.1 IC on modified commercial columns

Adapted from an ion-interaction method previously employed by Connolly and Paull [48-49] for fast IC in packed octadecylsilyl (ODS) particle columns, Hatsis and Lucy [50] used a reversed-phase monolithic silica column (Merck

Chromolith SpeedROD RP-18, 50 x 4.6 mm) to demonstrate the potential of real-time monitoring of chemical processes. Eight anions were separated in only 15 s at flow-rates as high as 16 mL/min, using reversed-phase ion-interaction chromatography with direct conductivity detection and reported detection limits in the low ppm range.

A surfactant coating procedure employed by Connolly and Paull in packed ODS particle columns [51] was also adapted by Hatsis and Lucy to perform a high speed ion-exchange separation on a surfactant coated, reversed-phase monolithic silica column [28]. Seven anions were separated with baseline resolution in 30 s, using suppressed conductivity detection at pH 7.0, with a maximum flow-rate of 10 mL/min, affording detection limits in the low ppb range. As efficiency was not significantly affected by the flow-rate, it was indicated that faster flow-rates would yield even shorter separation times. The limited stability of the surfactant coating was found to cause a reduction in column performance after 3000 - 4000 column volumes, giving an increase in backpressure by up to 25%. Stripping with acetonitrile and recoating of the monolith regenerated the performance and original backpressure. The authors suggested the use of a surfactant-coated guard column as a preventative step for column coating degradation, based on findings by Cassidy *et al.* [52].

Similar sub-minute separations on surfactant-coated monolithic silica columns have also been demonstrated by Connolly *et al.* [29], who developed a combined anion- and cation exchange column by coating the silica substrate with a solution containing both the cationic surfactant didodecyldimethylammonium bromide (DDAB) and the anionic surfactant

dioctylsulfosuccinnate (DOSS). At flow-rates between 4.0 and 8.0 mL/min, up to 8 anions and 5 cations were separated in under 100 s using indirect conductivity detection with analyte concentrations of 10 - 100 mg/L. The potential for simultaneous detection of anions and cations in water samples was demonstrated by connecting both columns in parallel. Injection of analytes was performed prior to flow-splitting for separate eluent delivery.

Unique anion selectivity was reported by O'Riordain *et al.* [31] for a zwitterionic surfactant-coated C_{18} silica monolith (Merck Chromolith Performance C_{18}). Stability of the dynamically coated carboxybetaine layer was maintained by using eluents containing 0.2 m*M* of the surfactant. A day-to-day reproducibility of less than 5% RSD could thus be achieved. Elevated flow-rates resulted in considerably lower separation times than for the particle-packed equivalent. The authors found that the presence of surfactant in the eluent significantly affected the relationship between eluent pH, peak efficiency and the retention time of the analytes. Further investigations were deemed necessary to fully understand the nature of this relationship, which may quite possibly be connected to ion-interaction effects between the eluent surfactant and analytes.

A further study was conducted by this same group [32] using short Chromolith C_{18} columns coated with a long chained carboxybetaine surfactant. The unique structure of the *N*-dodecyl-*N,N*-(dimethylammonio) undecanoate (DDMAU) surfactant was predicted to create a double layer assembly on the monolith surface, consisting of a strong anionic internal layer and a weak cationic outer layer. Due to the higher coating stability of this surfactant, the system had the advantage of not requiring the presence

of surfactant in the eluent for layer stability, which was confirmed with several hundred subsequent runs producing near identical chromatograms. Investigation of surfactant retention on different reversed-phase silica materials was also described, confirming the high affinity of DDMAU for the hydrophobic C_{18} modified silica materials. The predicted nature of the double layer was supported by the observed relationship between eluent pH and analyte retention, which confirmed the presence of a weak shielding layer, in which the repulsion of analyte anions was related to the dissociation of the terminal carboxyl groups. The average efficiency was reported at 29,000 plates/m, with detection limits the range of 40-830 ppb.

Victory *et al.* [53] demonstrated the possibility of a compact micro-IC with suppressed conductivity detection, using an ultra-short (1.0 x 0.4 cm) monolithic silica column coated with DDAB for the analysis of common anions. The practicality of this approach was limited due to system constraints; nevertheless, the work demonstrated the potential of performing compact micro-IC on currently available columns, using a combination of micropumps, microinjector, packed-bed suppressor cartridge and a conductivity cell. Further system evaluation was deemed necessary, in particular for robustness and reproducibility.

Xu *et al.* [27, 54] modified a coating procedure previously used in silica particle-packed columns to determine H^+ concentrations in the *μM* range. Following this principle, a reversed-phase monolithic silica column (Merck Chromolith SpeedROD, 5.0 x 0.46 cm) was coated with the surfactant dodecylsulfate to create a sulfonated cation-exchange stationary phase. By choosing the right eluent conditions, the authors showed the quantification of

H^+ in rainwater with detection limits as low as 1 *μM* using conductiometric detection. They further found good stability of the column coating over 2 months, affording constant efficiency and peak retention. This method is a significant improvement over previously reported IC methods, in that it offers high speed analysis with lower detection limits over a wider linear range.

In a continuation of this work the authors employed a double-layer approach [30] to coat a reversed-phase silica monolith (Merck Chromolith Performance RP-18, 10 x 0.46 cm), based on encouraging results reported earlier by Fritz *et al.* [55]. First, the column was coated with the non-ionic surfactant poly(oxyethylene) (POE), followed by a layer of the cationic surfactant cetyltrimethylammonium bromide (CTAB), which produced a stable anion-exchange stationary phase. The aim of the double-coating procedure was to reduce the influence of the hydrophobic monolith backbone and to stabilise the second layer of cationic surfactant. The improvement in efficiency and coating stability was confirmed by comparison to an equivalent, single coated cation-exchange column using Van Deemter plots and separations of equivalent sample compositions. Detection of hydroxide concentrations in the low *μM* range using conductiometric detection showed good correlation with conventional potentiometric pH measurements. These findings demonstrate an interesting principle for column modification, particularly for reducing unfavourable hydrophobic interactions between some analytes and the stationary phase backbone [55].

Sugrue [56] demonstrated the separation of divalent metal ions on a bare porous silica monolith column (Merck Chromolith Si) using a predominantly organic mobile phase composition at a reported efficiency of

25,000 plates/m. The authors referred to this as “solvent enhanced ion chromatography” due to the fact that the organic nature of the mobile phase enhanced the ion-interaction of the metal analytes with the dissociated silanol groups through reduced hydration effects of the aqueous constituent. The extent of hydration was found to be strongly dependent on the nature of the solvent, which was further verified by variations in buffer pH and concentration. Detection was conducted after post-column reaction of the analytes with resorcinol, using UV absorbance at 510 nm.

In a previous study [44], the same column (Merck Chromolith Si) was used for the covalent attachment of lysine. The resultant novel zwitterionic type stationary phase was used to separate inorganic anions and transition metal cations. The authors reported selective complexation between the transition metal ions and the lysine group using variations in eluent pH, in particular for Zn(II) and Pb(II), in line with previously published data on lysine-metal complexes. Given the variation in ionic nature of the zwitterionic functionality with respect to the eluent pH, the effect of eluent pH, concentration and flow-rate on the separation efficiency of common anions was examined. The anion-exchange capacity of the column was found to vary with pH levels, with measured values of 4 *μM* and 12 *μM* at pH 6 and 3 respectively, so a variable capacity anion exchanger could be produced using eluent pH gradients. The optimised separation of 6 anions was conducted in around 100 s, with peak efficiencies of 50,000 plates/m. Variations in retention time were reported to be below 0.4% RSD, indicating excellent reproducibility.

By immobilising metal chelating functionalities Sugrue *et al.* [45] demonstrated the separation of 10 mg/L Mg(II) and Ca(II) in a 2 *M* KCl solution in 40 s using a high-performance monolithic silica chelating ion-exchange column. Modification of the silica monolith was achieved by covalent attachment of iminodiacetic acid (IDA) to the silica skeleton of a Merck Performance Si column. In a continuation of this study, the same technique was used to generate different selectivity towards alkali, alkaline earth and selected transition metal ions [46]. With further improvement, this technique could become a powerful tool for real time analysis of specific metals in complex sample matrices, such as mining run-off and industrial wastewaters.

1.1.2 CEC using surface modified sol-gel silica monoliths

Synthesis of monolithic silica structures with various pore sizes was carried out by Breadmore *et al.* [57] in fused silica capillaries. The monoliths were modified by dynamic coating with poly(diallyldimethylammonium chloride) (PDDAC) and evaluated by ion-exchange capillary electrochromatography (CEC). The morphology of the silica monolith was varied using polyethylene oxide (of different molecular weights) as the water-soluble polymer in the sol-gel mixture used to control the onset of phase separation. Slight changes in polymer concentration were reported to significantly affect the size of the macropores. The authors reported surface and pore size measurements only prior to coating with PDDAC and showed that identical surface areas could be obtained for monolithic structures of very different morphology. When these materials were used as ion-exchange stationary phases, the presence

of PDDAC in the mobile phase was required to maintain an otherwise unstable absorbed coating. The separations of four common anions on the coated silica monoliths of different morphology resulted in different retention times despite measuring identical surface areas. This was attributed to the difference in open pore structure, governing the distribution of the flow.

In a continuation of this study, Breadmore and co-workers [58] employed polyelectrolyte multilayers (PEM) consisting of PDDAC and dextran sulfate for use as ion-exchange stationary phases in CEC. The successive coating of an *in-situ* synthesised silica monolith with multiple ionic polymers significantly enhanced the coating stability compared to single-layer coatings, providing highly reproducible EOF, even for columns prepared from different sol-gel batches. Individual layer thickness was accurately controlled by the composition of the ionic polymer solution, whereas overall coating thickness was governed by the number of coating layers. Furthermore, the surface properties were modified to suit the required chromatographic interaction by changing the nature of the exposed polyelectrolyte. As small ions could freely penetrate the PEM layers, the ion-exchange capacity could be tuned by controlling the thickness of the layers, as demonstrated by the increase in retention of inorganic anions with the increase in the number of adsorbed layers. This illustrated the potential use of PEM's to provide readily adjustable modifications of chromatographic supports for CEC, which should be invaluable for separations performed in microchip devices. A review on PEM coatings in CEC separations has been published by Kamande *et al.* [59] and provides a good overview of the topic.

A different coating approach has been published by Hutchinson *et al*. [60], where capillary-immobilised silica monoliths were coated with functional latex nanoparticles, creating anion-exchange columns for CEC. Despite good retention of latex particles in the coating phase, the increase in surface area after coating with latex particles was comparatively small and capacity measurements suggested that only a partial coverage of latex particles had been achieved. Nevertheless, the separation of 5 weakly retained anions could be performed with considerable efficiency of 80,000 plates per 25 cm column. The disadvantage of this system was the requirement of high ionic strength eluents in order to suppress the extent of the ion-exchange interactions between analytes and the latex functionalities.

When considered in comparison to open-tubular latex-coated columns [61], the magnitude of analyte retention was comparable to particle-packed columns, yet did not display the backpressure limitations. However, due to the applied electric field in electrophoretic analysis, considerable Joule heating was observed and the system was not suitable for the analysis of more strongly retained analytes. Furthermore, the authors recognised some difficulties in creating monolithic stationary phases of equivalent chromatographic performance.

1.1.3 Summary and discussion

The research publications considered above predominantly illustrate the effective transfer of modification methods previously demonstrated for particle packed columns onto a monolithic silica format. The highly uniform structure of silica monoliths results in superior flow properties compared to

most other continuous materials, providing a very promising permeability to surface area ratio.

The variety of modifications discussed here provides a relatively restricted overview of the potential surface alterations that can be performed on these materials. Most of the studies described here make use of commercially available silica columns for subsequent post-modification. No further morphology characterisation was conducted to examine the degree of coating in general and within the mesopores of the silica skeleton. Surface area measurements of coated silica monoliths have only been reported for dry, latex-coated monoliths. As the drying process most likely affects the integrity of the surfactant or polyelectrolyte layers, the understanding of morphology changes imposed by the coating procedure is to some extent still limited and warrants further investigation in the future.

Monolithic silica columns have so far provided very promising results in achieving fast IC separations. Post-modification of current commercial columns have been used as a logical first step in achieving this goal on current IC instrumentation. The success of monolithic stationary phases used with generic IC instruments will be essential in generating an increase in demand for these materials and to provide a stepping stone for the development of better, miniaturised columns and instrumentation.

However, most of the work described here utilizes a variety of different pump, eluent generation and detection modules which are matched to suit the system requirements. Current commercial IC instrumentation equipped for anion analysis is purchased as a complete unit that predominantly employs alkaline hydroxide or carbonate eluent generation followed by eluent

suppressed conductivity detection. Further developments in monolithic IC columns for high speed analysis on existing instrumentation thus has to take account of the pH restriction imposed by the typical hydroxide eluents used. The rapid degradation of silica-based stationary phases at alkaline pH implies that these materials have limited suitability for hydroxide eluent suppressed conductivity detection.

Some of the work described above [28] has utilised suppressed conductivity detection using *o*-cyanophenol titrated to pH 7.0 with sodium hydroxide and this approach has provided the lowest detection limit in the above examples. As electrostatic shielding of hydroxide by equivalent charged surfactant layers affords some degree of protection, a variation of this method may become a viable option for mild hydroxide shielding of silica monoliths using a suitable array of charged surface coatings. It may be sufficient to use slightly alkaline eluents in order to achieve similar detection limits to current packed polymer particle IC columns. Conversely, low pH eluents are applicable to silica stationary phases and these have been used for cation analysis on complete IC systems where a suppressible acid such as methanesulfonic acid is used in the eluent, followed by suppressed conductivity detection.

Applications of silica monolithic stationary phases for ion separations in CEC face some major challenges. First, CEC instruments are most commonly equipped only with UV detection and thus suffer from higher detection limits, unless some form of sample preconcentration or stacking is used [60]. Second, the fragility of the silica skeleton requires good immobilisation in the capillary column and shrinking of the monolithic

structure during synthesis can result in void spaces generated between the silica material and column walls if insufficient covalent bonding between the silica skeleton and the capillary wall is present. This can lead to detachment of the silica rod and subsequent removal from the column with applied pressure. Furthermore, for improved batch-to-batch reproducibility, meticulous attention to experimental detail is necessary to reproducibly control the onset of phase separation.

Alkyl silanes are easily oxidised and should thus be stored under an inert atmosphere if required for prolonged use. Although silica monoliths have been successfully fabricated in fused- silica capillaries, the ends of a monolith contained in a capillary have to be trimmed off as large voids in both ends form during the synthesis procedure [42]. Thus, the fabrication procedure developed by Tanaka and co-workers [26] is not easily amenable for microchip channels, where the end parts cannot be simply trimmed off. CEC applications using monolithic silica stationary phases suffer from an additional factor which leads to reduced detection limits. Since the monolithic material is present throughout the entire capillary, including the detection window, optical detection is impaired unless a detection capillary is joined to the separation capillary [61]. However, the *in-situ* synthesis of reversed-phase sol-gel monoliths in silica capillaries demonstrated by Zare and co-workers [62] using photopolymerised sol-gel (PSG) offers an interesting alternative. The nature of the photoinitiated polymerisation allowed the confinement of the monolith in the irradiated part of the capillary column and furthermore has been demonstrated in the successful preparation within microchip channels [63].

Derivatisation of the reversed-phase sol-gel monoliths was demonstrated for the analysis of peptides [64] and proteins [65], thus validating the viability of these sol-gel monoliths as IC stationary phases. However, besides SEM images of the micro-globular structure, the authors did not conduct any morphology studies for these sol-gel polymerised monoliths. The electron-micrograph indicates similar morphological properties of the silica based monolith to the polymer analogues, with an array of microglobular clusters separated by through-pores. Further assessment of the porous structure is required however in order to draw a more comprehensive morphological comparisons with the conventional sol-gel silica monoliths.

1.2 Monolithic polymer stationary phases

Although polymer based chromatographic supports may not seem to offer any clear advantage over silica monoliths with regard to separation efficiency, their ease of *in-situ* preparation in a range of formats is currently unmatched. Furthermore, these porous polymer monoliths are ideal for preparation in microfluidic channels and can be confined to specific locations in the channel or a capillary by using UV-initiated polymerisation with a suitable photomask [66]. A further significant advantage of polymer monoliths is their resistance to high pH and temperature [33], so that they are more readily applicable for use as IC columns used in commercial IC instrumentation employing continuously generated hydroxide eluents. The development of monolithic polymer supports by Svec and Fréchet [24] has

since found application in HPLC, CEC and most other related analytical techniques, especially for fast and efficient protein separations.

The advantage of *in-situ* fabrication lies in the individual tailoring of each column during synthesis. Physical properties are extremely flexible and can be varied by simply changing the composition of the polymerisation mixture, allowing a high level of control over pore size and distribution, surface area and functionalities, density and degree of rigidity and swelling [33, 67-69]. The typical polymerisation mixture consists of 20-40% monomers and 80-60% porogens, plus a small amount of thermal or photo-initiator. The types of porogens as well as monomers govern the solubility of the forming polymer globules, governing the onset of the phase separation, which in turn affects the pore size. The relative distribution of globules within the polymer network depends on reaction parameters such as concentration, reaction temperature and time.

The *in-situ* fabrication proceeds as follows. The deoxygenated polymerisation mixture containing the required ratios of monomers and porogens is introduced into a mould (such as a silica capillary or a polymeric HPLC column body) and exposed either to heat [70], UV light [66] or γ-radiation [71] to initiate and maintain the radical polymerisation process over a certain period of time. After the polymerisation is complete (10-20 min for UV initiation depending on UV intensity and usually between 18-24 h for thermal initiation depending on temperature) the porogens are removed by washing with methanol or another porogen soluble solvent, leaving behind the continuous pores that present around 50-70% of the average cross-sectional volume (depending on the amount of monomer in the initial mixture)

in the column [24]. The resulting morphology normally reflects the choice in reaction conditions, and reproducible fabrication can be accomplished.

High permeability is generally achieved with flow-through pores in the range of 1-10 μm. The influence of monomer composition on the monolith morphology is based on the different solubilities of the mixture constituents. In the initial stages of polymerisation, the unreacted monomers generally exhibit better solvent properties for the forming polymer globules as opposed to the porogens and are thus more concentrated in the swollen polymer nuclei. As the reaction proceeds, the incorporation of solvated monomers within the forming polymer globule are kinetically more favoured, governing the extent of globule formation with less cross-linked chains more dominant in the outer globule layers. Thus the morphology of the formed polymer monoliths is further governed by the respective solubilities of monovinyl and divinyl (cross-linking) monomers, such that cross-linking is more favoured at the early stages of polymerisation and chain propagation in the later stages. As most of the knowledge on porous control in monolithic polymerisation has been derived from published data relating to macroporous beads, the application of the same principles in monolithic synthesis remains questionable, as the use of identical polymerisation mixtures for bead and monolith synthesis yields very different porous morphologies.

Svec *et al.* [33] attribute this to the gravitational effect on forming polymer nuclei, a predominant force governing the coalescence of globules in the lower end of the mould during the unstirred synthesis of monolithic polymers. The different system dynamics in suspension polymerisation of macroporous beads, where constant stirring induces rotational motion in the

organic phase droplets, negates this gravitational effect, such that the forming nuclei move randomly as result of the stirring and centrifugal force. The nuclei are therefore able to keep their individuality longer, grow separately and “pack” better. As a result, the voids between the globules that constitute a single bead are smaller [33].

Furthermore, the interfacial tension between the organic droplets and the aqueous phase in suspension polymerisation governs the distribution of the solvents in the droplet, such that constituents containing polar groups are predominantly present at the droplet interface to reduce the surface tension. Thus, the forming polymer nuclei are better solvated and do not coalesce, which means that monomer concentration is more evenly distributed rather than swelling the forming nuclei. By contrast, the unstirred synthesis procedure of monolith fabrication makes use of a single phase polymerisation mixture. Weak interfacial tensions, if any, may occur only towards the column wall, however estimating the extent of this effect requires preparation and characterisation of monolithic porous polymers in different moulds using identical polymerisation mixtures. In the absence of stirring, the phase transition of forming nuclei occurs earlier on, resulting in larger micro-globules and increased pore size. In addition, the material morphology is further controlled by the rate of radical polymerisation, either by varying the temperature of thermally initiated mixtures or the intensity of radiation for mixtures containing UV initiators. Higher temperatures or radiation intensities reduce the half-life of the initiators, generating more radicals at any time of the reaction. Thus more and therefore smaller globules are produced,

yielding a smaller pore size distribution, due to reduced swelling of the nuclei with monomers.

Surface functionalities are introduced to the monolith surface either by including specific functional monomers in the polymerisation mixture or by post-modification of the porous template. Reactive modification of epoxide groups are generally carried out, based on the original publication by Svec and Fréchet [24]. However, grafting of functional monomers [72] and semi-permanent coating procedures [9] are emerging as popular alternatives with increasing promise.

1.2.1 Micro-IC

Hilder *et al.* [73] reported the use of sulfonic acid functionalised butyl methacrylate-*co*-ethylene-dimethacrylate-*co*-2-acrylamido-2-methyl-propane-sulfonic acid (BuMA-*co*-EDMA-*co*-AMPS) monoliths prepared in 250 *µ*m *i.d.* fused silica capillaries and then coated with quaternary amine functionalised latex nanoparticles for the anion exchange separation of 7 saccharides in less than 10 min. The porogen composition was optimised to allow sufficient flow-rate, while maintaining separation efficiency by adequate surface area coverage with the functionalised latex nanoparticles.

The positively charged latex particles were retained on the negatively charged sulfonic acid functionalities by electrostatic interaction. A polymerisation mixture consisting of BuMA (22%), EDMA (16%), AMPS (2%) in 1,4-butandiol (13%), 1-propanol (37%) and water (10%) was used to produce a monolithic stationary phase with an average pore size of 0.97 *µ*m and a corresponding dry surface area of 35 m^2/g. Coating with the

functionalised latex particles increased this value to 47 m^2/g. The effect of surface coverage was visualised by SEM. As only a small proportion of sulfonic acid functionalities from the incorporated AMPS monomer are present on the monolith surface, the degree of latex coating was confined to individual particles rather than being present as a continuous surface layer. The ratio of AMPS in the polymerisation mixture was limited to 5% of the total monomers, as higher ratios induced swelling of the hydrophilic polymer chains, which in turn decreased the pore size to the extent of complete blockage. This work also presents changes to the median pore diameter resulting in significant changes in the separation resolution.

A glycidyl methacrylate-*co*-ethylene dimethacrylate (GMA-*co*-EDMA) monolithic polymer synthesised in a 250 *μ*m *i.d.* capillary was sulfonated by Ueki *et al.* [74], using a 1 M aqueous Na_2SO_3 solution at pH 11. Under optimised conditions, the authors achieved a maximum reported epoxide group conversion of 13% (300 *μ*equiv/mL), which was attributed to the fraction of incorporated glycidyl methacrylate monomers within the polymer structure rather than on the monolith surface. Furthermore, hydrolysis of available epoxide groups into stable diols was considered as the main competing reaction. Unfortunately the authors did not provide any detail on how the ion-exchange capacity measurements were performed. A combination of a micro-pump, injector and on-capillary UV detector was used for the ion-exchange separations of common cations on the lower capacity (6.5%) sulfonated GMA-*co*-EDMA monolith, affording around 20,000 plates/m. Reproducibility over several days was shown to be very good, as no significant changes in selectivity or resolution were reported. The authors

further prepared and coated a Develosil OD-5 silica particle packed 250 *μ*m-*i.d.* capillary column with the anionic surfactant sodium dodecylsulfate (SDS).

Under identical separation conditions, a packed silica column achieved twice the efficiency of the monolithic material, but suffered from a seven fold increase in backpressure at the same flow-rate. The authors also demonstrated the potential inertness of the sulfonated methacrylate monolith to protein fouling by direct injection of aqueous protein samples, including saliva. Values of 13 to 20 m*M* of Na^+, 17 to 43 m*M* for K^+, 0.10 to 0.55 m*M* for Mg^{2+} and 0.89 to 3.1 m*M* for Ca^{2+} in the analysed saliva samples were claimed to be in good agreement with values obtained by ICP-atomic emission spectroscopy. No significant decrease in separation efficiency was shown over 20 subsequent injections, which suggested that the material was indeed resistant to protein fouling.

Zakaria *et al.* [75] developed a micro-IC system for the separation of anionic analytes based on a latex-coated methacrylate monolithic stationary phase immobilised in a fused silica capillary. The use of an in-house fabricated, hollow fibre micromembrane suppressor enabled suppressed conductivity detection to be performed. To allow for faster flow-rates, a polymerisation mixture yielding a monolithic template of 60% porosity and median pore diameter of 5 *μ*m was chosen. Dionex AS10 and AS18 quaternary ammonium functionalised latex particles were used for the coating procedure, yielding capacities of 0.6 and 1.6 *μ*equiv/g respectively. The intent was to create a general monolithic template that could then be post-modified using a variety of latex particles, thus simplifying the overall fabrication procedure in comparison to using and optimising new

polymerisation mixtures every time a different functionality was required. Separation of seven anions on the AS10 functionalised monolith was demonstrated in 2-3 min using a relatively weak eluent (40m*M* NaF) at flow-rates of 17 to 31 *µ*L/min with UV detection.

For hydroxide suppressed contactless conductivity detection, a monolithic column coated with hydroxide-selective Dionex AS18 latex particles was chosen. A hollow fibre micro-suppressor was fabricated based on previously published versions [76]. Separation of 5 anions was demonstrated in less than 3 min at hydroxide concentrations in the range of 0.5-5.0 m*M*. Detection limits of 0.4 to 1.2 *µM* were around 70 times more sensitive in comparison to UV detection, but suffered from band broadening and therefore relatively low efficiency (5,400 plates/m) which was attributed to the length (28 cm) of the micro-suppressor. While several limitations were encountered in this study, the results demonstrated the possibility of a micro-IC systems, which would also have the capability of direct coupling to mass spectrometric detection.

Further investigation by Hutchinson *et al.* [77] into the preparation of high capacity latex-coated monolithic stationary phases, focused on the synthesis of monolithic polymer templates with extensive surface functionalisation. Two alternative approaches were considered. First, the reactive modification of poly(styrene-*co*-DVB) monoliths by direct sulfonation was attempted, but was found to be ineffective even in only slightly crosslinked (8%) polymer networks. In the second approach, the polymerisation mixture included EDMA (16%), GMA (24%), cyclohexanol (30%), 1-decanol (30%) and AIBN (0.4%), a thermal initiator. The resulting

polymer network had an average pore size of 1.2 *μ*m, which afforded good permeability. The GMA-containing methacrylate monolith served as a template for three different post-modifications of the epoxide group.

Maximum conversion of epoxide groups was achieved with the first post-modification reaction, which was conducted in acetonitrile for better wettability of the hydrophobic polymer and to limit competing side reactions, such as hydrolysis. The second reaction consisted of a 3 step conversion which afforded lower epoxide group conversion due to reaction yields of only 60%. The third method was performed using the method of Ueki *et al.* [74] and resulted in the greatest increase in capacity and the resultant stationary phase was used for the separation of 7 anions using a linear hydroxide gradient. Reasonable separation efficiency of 6 anions was more recently achieved by Connolly and Paull [78] based on an earlier tested grafting approach using 2(methacryloyloxl)ethyl trimethylammonium chloride (META) as the functional monomer [79]. The authors claimed similar capacity and plate heights to latex coated analogues by Hutchinson [77] and Zakaria *et al.* [75]. Comparing columns with different types of terminating amine functionalities was recently performed by Kurganov *et al.* [80]. Based on a GMA copolymerised methacrylate monolith, the type of amination resulted in very differently performing IC columns. Inverse proportionality was claimed with capacity (and retention) over separation efficiency, such that post-modification with dimethylamine (DMA) resulted in strongly retaining columns with poor efficiency, while alteration with polyethyleneimine (PEI) yielded columns of low selectivity but with the best separation performance.

Unfortunately no experimental data was shown to support these findings. The authors chose a recipe with equal mix of DMA and PEI for optimal column performance. C-term variations in the Van Deemter equation as a result of different percentage of GMA monomer in the polymerisation mixture as well as changes in the polymerisation temperature were also demonstrated; however a clear correlation of results within the paper was not evident.

1.2.2 CEC – Capillary Electrochromatography

Coating of functionalised methacrylate monoliths in fused silica capillaries (50-533 *μ*m-*i.d*.) has been carried out by Hutchinson *et al.* [81] for the CEC preconcentration and separation of common anions. The monolithic template consisted of copolymerised BuMA, EDMA and AMPS at a ratio of 18wt%, 21wt% and 1.8wt% respectively. The coating procedure was performed by pumping a suspension of Dionex AS18 quaternary amine anion-exchange latex nanoparticles through the capillary-immobilised monolithic template until saturation point was reached, which occurred after approximately 10 column volumes. The presence of individual latex particles on the surface was confirmed both by SEM imaging and by the reversal of the electro-osmotic flow (EOF) as a result of the positively charged latex particles being adhered to the negatively charged substrate. Capacity measurements were conducted by bromide adsorption and subsequent elution. Despite a relatively low measured capacity of 1 *μ*equiv/g for a 75 *μ*m *i.d.* capillary-immobilised monolith (compared to 16 *μ*equiv/g for latex coated DVB beads), the separation of seven common anions was possible in less than 80 seconds using a CE instrument with UV detection. Capacity values for larger diameter

capillaries indicated that surface coverage of latex particles was distributed evenly throughout the monolith, even if a monolayer was not achieved. Reproducibility of the separations on different columns was highly dependent on variations in the coating procedure.

To achieve lower detection limits, a preconcentration method was included in the CE analysis. The determination of iodide in seawater by this technique was possible for concentrations as low as 75 p*M* (9.5 ng/L) after loading for 10 min at 1.2 MPa. Furthermore, iodide was reproducibly eluted in a very sharp band after 17 min, affording a separation efficiency of 51,300,000 plates. This was attributed to the high ion-exchange selectivity of iodide, which resulted in it being focused and eluted at the immediate front of the strong electrolyte gradient used in the separation. This process is referred to as frontal electro-elution with an isotachophoretic boundary, after terminology introduced by El Rassi [82] and is a popular and efficient technique for signal enhancement employed in capillary electrophoresis [83]. The detection limit for iodide using a 60 min preconcentration loading time was reported to be 11.5 p*M*.

1.2.3 Summary and Discussion

Monolithic polymers have found themselves in less popular demand for commercial IC applications in small ion analysis when compared to their silica counterparts. Initially this was simply a matter of reduced performance by the monolithic polymer stationary phases and the more reliable manufacture of silica monoliths in commercial production. The high degree in variation for polymer analogues has however given them much attention over

the years and many applications have been reported to date. These variations in the synthesis process have to some extend tailored the polymer analogues to be on par with the silica monolithic columns for specific applications [84-88].

A selection of organic modification techniques used to improve the separation efficiency of polymer monoliths for smaller analytes are discussed in the following results chapter. Some of these post-modification reactions go back several decades and have shown mixed success upon trial with monolithic analogues [89-90]. A recent combination of silica and polymer properties using silica beads as pore forming templates in a monolithic polymer materials has successfully been trialled by Thabano *et al.* [91] and highlights some of the potential in hybrid materials that could lead to new applications.

1.3 Improving polymer monoliths for better separations:

1.3.1 Reduction in polymerisation time

Separations of small molecules such as alkyl-benzenes are conducted with reverse-phase HPLC, based on hydrophobic interactions (van der Waals). Polymer monoliths have so far shown poor performance in comparison to their silica counterparts due to the low surface area of the methacrylate and styrene type scaffolds. However, recent advances in the synthesis process have resulted in larger surface area, polymer monolith stationary phases for the reverse phase HPLC separation of alkyl-benzenes and other small organic molecules. The high surface area analogues were obtained by either

reducing the polymerisation time [92-93] or alternatively through a second cross-linking step of the outer globule chains [94-95].

In the first instance, based on work pioneered by Trojer and Greiderer *et al.* [96-97], reduction in polymerisation time can provide significant improvements to the scaffold characteristics, in particular the mesoporous space, with claimed efficiencies of around 70,000 plates/m for some smaller organic molecules [96-97]. A study by Nischang and Brüggemann has likewise examined the effect of shorter polymerisation time and the resulting porous and hydrodynamic properties on the separation efficiency of small molecules. Using a classic poly(BuMA-*co*-EDMA) recipe with AIBN for thermal initiation, columns ranging from 30 min to 48 h reaction time were synthesised and compared [92]. Most notable were the hydrodynamic and porous properties of monoliths with less than 1 h reaction time, incorporating less than 50% of the BuMA monomer, however significantly higher proportions of EDMA cross-linker. The difference in the inclusion of the monovinyl and divinyl monomers was explained by their reactivity. In the initial reaction phase, the polymer nuclei are highly cross-linked and after phase separation become solvated with the BuMA monomer, which are subsequently incorporated into the swollen globules.

Most of the experimental assessment data was obtained with a column terminated after 30 min reaction time, with less than 30% EDMA and 14% BuMA monomer incorporated, which represents around a quarter of the total monomer volume. This would infer an overall porosity of around 90%, since 100% of both monomers only make up 60% of the solution. Hydrodynamic studies using uracil as the non-retained tracer appear to have

confirmed these values and BET adsorption studies related the findings to the porous properties in the nanometre range. As such the pore volume and surface area of pores up to 100 nm were significantly higher for the 30 min polymerised analogue, prompting the authors to deduce the complete absence of mesopores in the fully polymerised polymer globules in their dry state and confirm findings in an earlier study by Huo *et al.* [98].

Further velocity-based hydrodynamic permeability and total porosity calculations confirmed the higher porosity of the early reaction terminated monoliths and confirm the cross-sectional presence of both micro- and macro-globules as observed by SEM. In summary the flow and retention related studies of the methacrylate monoliths with various degree of polymerisation show that the column efficiency is governed by the analyte retention, which in turn is strongly influenced by the degree of gel porosity, a term used in reference to the amount of non-crosslinked chains in the outer globule layers.

In a previous study [98], the authors included a small percentage of monovinyl monomer with longer alkyl chain (lauryl) to emulate the reverse phase character of C_{18}-bonded silica monoliths. Increased retention of polycyclic aromatic hydrocarbons (PAHs) was observed at up to 15% under identical separation conditions. Further diffusion related studies attempted to isolate C-term dependent factors in the Van Deemter equation, predominantly relating to the diffusive surface action between mobile and stationary phase.

Despite the apparent lack of mesopores in all of the polymer materials, the swollen methacrylate monoliths provided better separation efficiencies

when THF was used in the mobile phase. The authors attributed the improvement to the enhanced surface diffusion of the analytes as a result of the swollen outer globule layers. Temperature variations during the separation provided a similar effect, reducing retention of the analytes with increasing temperature. The authors also hinted at a possible 'activated' restricted surface diffusion effect in the stationary phase [99].

Overall a combination of diffusive and retention driven factors within the polymeric monolithic substrates were deemed to govern the separation efficiency, with the parameters found to have a predominantly independent effect. However, it appears that the relationship depends on the type of stationary phase used and less influenced by the diffusion and retention factors in monolithic polymers. For example it would be plausible to assume reduced retention with THF-swollen globules due to a reduction in hydrophobicity caused by the swelling of the outer polymer globule layer. Similarly an increase in temperature would reduce retention and override the increase in diffusion that would normally occur with an increase in temperature.

In a following study, Nischang *et al.* [93] used poly(styrene-*co*-DVB) monolith analogues. The early terminated, thermally initiated polymerisation reaction yielded highly porous scaffolds with a bimodal pore distribution in the meso- and macro sized range as encountered previously by Bonn *et al.* [96-97]. In accordance with the methacrylate analogues, the styrene based polymer scaffolds exhibited significant surface area increases and good separation efficiency, however supposedly independent of their retention.

The authors used this finding to contrast popular assumptions held in regards to high surface area requirements for the efficient separations of small analytes such as alkyl-benzenes, thought to be only possible in the presence of mesoporous space. Nevertheless these findings demonstrate the improved synthesis of porous, large surface area polymer monoliths suitable for the reverse phase separation of small analytes. Comprehensive flow and hydrodynamic related studies such as backpressure and permeability analysis, analyte retention and separations confirmed the improved porous structure and made interesting correlations with the fully polymerised and swelling prone analogues, which have successfully been used for the separation of larger molecules (*i.e.* proteins). One interesting observation on the effect of the gel porosity of the fully polymerised polymer scaffolds is caused by the addition of organic modifier, affecting both retention and separation performance. This will be discussed further in conjunction with publications in the field of polymer chain hypercrosslinking.

1.3.2 Hypercrosslinking

Urban *et al*. [94-95] adopted a different approach to create a highly porous monolithic polymer stationary phase suitable for the separation of smaller analytes in reverse-phase (RP) mode. Based on a Friedel-Craft alkylation method pioneered by Davanakov *et al*. [100-104] initially with linear polystyrene and later extended onto poly(styrene-*co*-DVB) particles, Svec's group adopted the approach for successful modification of the polymer monolith analogues based on styrene and vinylbenzyl-chloride (CMS) monomers. The fully polymerised monolith globules in the precursor stage

exhibited gel porosity due to the presence of longer branches and chains in the outer globule layer, a result of the different reactivity of the mono and divinyl monomers in the reaction proceedings.

The hypercrosslinking approach incorporated a second reactive step using 1,2-dichloroethane (DCE) as the cross-linker and was catalysed by $FeCl_3$ at 80 °C for 2 h. Various optimisation procedures altered the mixture composition by varying the individual percentages of each monomer as well as porogen. The resulting columns exhibited no clear trend in relation to the mixture make-up, so a mathematical approach (second-order polynomial) was used to eliminate the less influencing factors of the mixture composition.

The optimised and hypercrosslinked stationary phase exhibited surface areas of over 600 m^2/g and column efficiencies of over 60,000 plates/m using a tailored ternary mobile phase composition and increased separation temperatures. At lower analyte concentrations (reduced loading) the chromatograms exhibited efficiencies of over 80,000 plates/m. Peptide separations and size exclusion chromatography were also successfully conducted using such columns, with the latter connecting two columns with a zero-volume union to achieve the required column length of 67 cm. The authors based the improved separation efficiency of the hypercrosslinked columns on the increased surface area of the material, as a result of the mesoporous morphology created by rigid cross-linking of the outer globule layer.

Although Nischang *et al*. [92-93] claim that their findings contrast those made by Svec's group, the two outcomes are not necessarily contradicting. Providing the gel porosity occurs only in the wet, solvated

state, MIP or BET measurements are only conducted in the dry state and are unable to measure the actual pore size and surface area distribution under operating conditions. As such the claim that gel porosity can be detrimental to the separation efficiency appears to be substantiated.

Different organic modifiers such as THF confirm the retention dependent behaviour in such circumstances. It may indeed be a result of the increased availability of surface area (an argument supported by the more efficient separations with reduced loading) that makes such porous polymer monoliths suitable for small analyte separations. Diffusive mass transfer is more evident in less porous analogues exhibiting gel porosity and only reduced when a retention limiting (stronger) mobile phase or higher temperatures are used in the separation process.

1.3.3 Nanoparticle coatings

Latex nanoparticles covered stationary phases have been available on the commercial market for some years now, with Dionex considered as the market leader. The latex coating of monolithic polymer columns has been predominantly pioneered by Hilder and Hutchinson *et al.* [61, 73, 75, 77, 81] and is presented in more detail in the following sections of this thesis. Since publication of the work presented here [105], Dionex has also introduced a commercial monolithic capillary column analogue (Ionswift™) based on the same post-modification proceedings.

A novel approach in the field of nanoparticle coated monolithic stationary phases employs the inclusion of gold nanoparticle (GNP) on the surface of polymer monoliths. First presented by Xu and Cao *et al.* [106-107],

the approach was also employed by Connolly *et al*. [108] on methacrylate monolith scaffolds grafted with vinyl azlactone and modified with ethylenediamine or cystamine to afford the required functionality for the gold particle attachment.

The resulting columns were flushed with a solution of 20 nm citrate stabilised GNPs. Due to cross-linking reactions of the functional amines, the terminating thiol group was of reduced availability for the attachment of the particles and thus provided a relatively sparse coverage. The coverage was measured at just over 20% (w/w) Au using energy dispersive X-ray spectroscopy. No applications were demonstrated; however it was addressed as possible future work in the conclusion chapter along with further modification of the self-assembled gold monolayer for chromatographic separations.

Frantisek Svec's group had employed a different approach to immobilise GNPs on a monolithic substrate [106]. A GMA-containing methacrylate monolith was modified by conversion of the epoxide group using cystamine and sodium hydrogen sulfide. The resulting thiol functionality could capture the gold nanoparticles either directly from preformed GNPs in solution or via reduction of chloroauric acid *in-situ.* The latter approach proved to be more convenient, taking only 1 h for saturation in comparison to 20 h with the coating of preformed GNPs.

The best columns were measured at 15% Au with average particle diameter of 40-50 nm. SEM images showed a similar amount of coverage to Connolly's work. Cystine (thiol) containing peptides could successfully be captured and subsequently eluded using a competing thiolated eluent

(mercaptoethanol). The bound mercaptoethanol could be eluded by water wash at elevated temperature (80 °C) thus regenerating the column within 2 h to above 80% of the original capacity. Due to the multivalent linkages, the GNPs were not eluded during the washing procedure. Given the relatively sparse coverage, the column was also useful in the separation of smaller analytes such as formamides and toluene, retaining some hydrophobic properties.

Following on from this work, Cao *et al.* [107] were able to use the GNPs as intermediates for exchangeable functionalities. In a similar manner to before, the thiol-containing ligands readily attached themselves to the GNPs, affording carboxylic acid, hydroxyl or amine functionalities for CEC separations. For RP mode, the GNPs were 'coated' with octadecylthiol and for ion exchange chromatography with sodium-2-mercapto-ethan-sulfonate. The authors suggested that in this way the one column could be used for multiple types of separation, *i.e.* CEC followed by HPLC.

In an attempt to selectively target phosphopeptides, Svec's group incorporated commercial hydroxyapatite nanoparticles in the polymerisation mixture [109]. These rod shaped crystals provide a zwitterionic type of interaction, allowing for simultaneous interaction of anions and cations.

Admixing the particles in the polymerisation mixture at approximately equal ratio followed by *in-situ* polymerisation provided the best results in regards to nanoparticle presence while retaining good flow-through properties. Due to aggregation of these particles in a variety of solutions, the alternative post-modification pathway proved to be not feasible due to column plugging. However the method of particle admixing provided up to 15% (w/w)

of hydroxyapatite inclusion and was found to successfully separate proteins and perform selective isolation of phosphopeptides from complex mixtures.

A recent publication [110] demonstrated the use of carbon nanotubes in the generation of functionalised polymer monoliths for small molecule IC. Both admixing of the nanotubes in the polymerisation mixture and post-polymerised attachment via surface functionalities of opposing charge were trialled. The first approach limited the incorporation of multi walled nanotubes (MWNT) to 0.25% of monomer content in the mixture, however resulted in a significant increase in efficiency (by more than one order of magnitude in comparison to the more polar, GMA methacrylate scaffold) to 15,400 plates/m. The second approach functionalised the GMA containing methacrylate substrate with ammonia to afford primary amine functionalities for the attachment of oxidised (carboxylic acid) nantotubes, resisting elution with organic modifiers (ACN). A separation of six alkyl benzenes was carried out in less than 30 min at efficiencies of 30,000 plates/m, which the authors attributed to the enhanced surface area and possibly specific affinity for aromatic compounds (π-π interaction). Addition of THF improved this figure to 44,000 plates/m, with the stability of the nanotube functionalisation confirmed after 6,000 column volumes, also including ACN in the eluent.

A similar study had previously been carried out by Li *et al.* [111] using single walled carbon nanotubes (SWNT). One of the difficulties in the synthesis process was the prior stable dispersion of SWNT in a suitable solvent which could act as the porogen in the following polymerisation mixture. A soft oxidative method using H_2SO_4/H_2O_2 resulted in hydroxyl

moieties on the nanotube surface and allowed for a solution of 0.1 mg/mL in 2-propanol.

The presence of SWNT in the polymer monolith was confirmed by Raman spectroscopy, with elemental analysis confirming the hydroxyl groups. SEM of the capillary columns was also conducted, showing reasonable morphology of the SWNT incorporated stationary phase. When tested chromatographically against a control column, higher backpressure and significantly increased retention for hydrophobic analytes (Toluene) was encountered. Despite these findings, no notable change in porosity was measured for the nanotube incorporated analogues. However an increase in surface area by about 30% was noted as a result of inclusion of SWNT.

Separation of 5 peptides by CEC could be performed more efficiently in comparison to the 'tubeless' control column. The authors concluded that more detailed studies are required to better understand the specific interaction between analytes and immobilised carbon nanotubes.

An altogether different nanoparticle coating was recently applied by Krenkova and Foret [112] in the form of co-precipitated iron-oxide colloids. Phosphopeptide enrichment based on metal oxide affinity chromatography (MOAC) has recently gained more attention due to the improvements in chromatographic supports.

Batch mode enrichment has recently been demonstrated with Fe_2O_3 [113] and Fe_3O_4 [114] nanoparticles. The iron oxide nanoparticles were synthesized by co-precipitation [115] with tri-sodium citrate and flushed through an quaternary amine functionalised GMA methacrylate column. Variations in the citrate concentration (0.5–3%) resulted in iron oxide

nanoparticles ranging from 33 to 15 nm. Only colloid suspensions with >1% citrate appeared to be sufficiently stable. Elemental analysis (EDAX) confirmed presence of iron on the monolith surface at 1%. The resulting binding capacity of 47.4 mg/mL (86 *µ*mol/mL column volume) was significantly higher than silica based monolithic columns containing immobilized titanium (1.4 *µ*mol/mL column volume) [116].

1.4 Current methods of quality control and characterisation

One of the recent trends in polymer monolith characterisation has focused on finding a suitable way to non-invasively assess polymeric monolithic capillary columns and monitor the reliability of manufacture. Although many monolith polymer recipes show good column-to-column reproducibility, some mixtures can include functional monomers in the polymerisation mixture to yield tailored stationary phases either by direct inclusion or through subsequent post-modification steps of the monolithic substrate. The required solubility balance of monomers and suitable porogens combined with the nature of the radical thermal or UV-initiation process create some challenges in regards to the reproducible synthesis of such porous polymeric capillary columns.

Post-functionalisation reactions conducted over several steps can be difficult to monitor, particularly when considering the different reactive yields of the individual modification steps where the following or final coating depends on the success of the previous functional group conversion.

Latex nanoparticle coverage based on the ionic interaction of functional groups of opposing charges can be monitored using ion

displacement measurements [77] and compared to visual imaging results carried out by scanning electron microscopy (SEM). This technique however requires the destructive preparation of capillary cross-sectional samples and is thus only viable as a secondary quantification method.

Self-assembled monolayers of such latex nanoparticles on a post-functionalised porous polymer monolith stationary phase were recently visualised for the first time [105]. While this technique provided an excellent way of showing the extent of the latex coverage in detail for the examined area, the high level of magnification resulted in only small sections of the monolith cross-section being visible at any given time.

Chromatographic column performance however is strongly related to the overall functional and morphological column uniformity, such that the information obtained by SEM on the overall homogeneity of the examined column cross-section was limited in providing a direct correlation. Non-destructive characterisation techniques can potentially provide a better understanding of the overall column uniformity and distribution of the functional surface coverage. Due to the non-invasive character of such an inspection, the functional column can still be used as a chromatographic medium and the uniformity profile directly related with the resulting separation performance.

1.4.1 C^4D

A recently published review by Connolly *et al*. [117] highlighted some of the areas where scanning contactless conductivity detection (sC^4D) was successfully used amongst other non-invasive ‘quality control’ tools. The

sC^{4}D technique and working principles are described in more detail in Chapter 4 of this thesis. The non-invasive scanning was generally carried out by manually shifting the C^{4}D detector head in mm increments with the help of a ruler along the length of 350 *µ*m *o.d.* fused silica capillaries. The readings were recorded after several seconds to allow the signal to stabilize.

By plotting the resulting conductivity readings along the axial length of the capillary, packing voids and crude irregularities were detected in packed particle bed capillary columns retained by monolithic porous polymer frits and also visually confirmed with digital photographs through the transparent capillary walls [118]. Measurements over areas with varying morphology showed an increased response over stationary phase gaps, a direct result of the higher conductivity of the mobile phase present in larger volumes when compared to the filled sections of the lower conducting polymer stationary phase.

Similarly using C^{4}D, the axial structural homogeneity of in-house functionalised C_{18} silica monoliths was compared with commercial analogues [119]. The difference in smoothness of the axial signal profile between the commercial and 'home-made' versions highlighted the difficulty in achieving such homogenously structured rods in a laboratory environment.

The conductivity profile of each scanned column was also related to the individual separation performance. Interestingly the commercial C_{18} functionalised silica column had exhibited a lower conductive response in the C^{4}D scanning, however when tested chromatographically exhibited a longer analyte retention time, which indicates a greater presence of immobilised C_{18} chains. Acetic acid (20 m*M*) was used as the conducting electrolyte and as a

result accounted for the largest portion in the conductive response, such that the profile was generated in relation to the porosity of the silica rod.

This was further confirmed by the highest signal conductivity profile of analogous open tubular columns. With a porosity of around 85% for the home-made silica monolith, the resulting surface area and thus amount of possibly immobilised C_{18} was deemed to be lower. Given the non-conducting nature of C_{18} chains the direct assessment of the carbon density is not possible with sC^4D and has thus been deduced indirectly through such relative factors like the overall surface area as a result of porosity.

Further illustration of the technique examined the morphological uniformity of UV-LED irradiated capillary polymer monoliths. The structural axial homogeneity was investigated in relation to the application of the light source (stationary vs. rotation) [120], such that the scanned profiles showed significantly different signal homogeneity for each approach. From these profiles it was concluded that the rotational approach yielded much more uniform columns, which was also loosely confirmed with SEM imaging of the respective column cross-sections. Another example of C^4D as a quality control tool was given with the analysis of empty and monolith filled microchips channels, using a commercial chip-C^4D detector [121]. The technique was able to differentiate between empty, void bearing (partially filled) and completely packed micro-fluidic channels and was thus considered useful in the analysis of channel packing density and uniformity in laboratory (home) fabricated chips.

Previously unpublished data was also presented in the review, some of which compared the conductivity signal response of individual surfactant

coating and washing steps of the C_{18} functionalised silica monolith capillary column. The results were discussed in relation to previous work by Gillespie *et al*. [122-123]. Over consecutive measurements it was noted that within the first 10 min of water washing, the signal reduction was most prevalent. No specific reason was given for the lower conductivity response; however the likely loss of surfactants from the polyelectrolyte layer was potentially responsible for this decrease in conductivity signal over time.

After the initial coating step, the signal response was nearly three times the original uncoated reading. Within one hour of water washing this had however decreased by 50%. This suggests a relatively poor stability of the multilayer polyelectrolyte coating. Due to the loss of polyelectrolyte, sC^4D was able to visualise changes in layer make-up in the nm range and deemed as a suitable technique for monitoring such thin ionic liquid coatings.

Similar measurements were also mentioned for coated GC columns [124] including the presence of salt to enhance the layer thickness [125-126]. Photo-initiated grafting zones of a functional monomer (AMPS) using a suitable photo-mask were also indirectly visualised using sC^4D [127]. The successful grafting extent of AMPS within these zones could be evaluated. In a similar manner, several columns grafted with increasing concentration (2, 4 and 6%) of SPM (3-sulfopropylmethacrylate) monomer were assessed by sC^4D and subsequently tested for chromatographic performance (unpublished data), showing a clear correlation between the increase in SPM concentration and conductivity and the resulting increase in retention time.

Utilizing this possibility, Currivan *et al*. [128] used sC^4D to evaluate functional stationary phase gradients of different polymerisation mixtures in

the same capillary, with one example using different co-monomer (AMPS) solution plugs of increasing concentrations and the other instance employing steps of higher intensity UV-grafting of the functional monomer sulfopropyl methacrylate.

In the solution plug approach, the scanning C^4D technique was able to clearly illustrate the diffusive mixing of the adjacent monomer solution plug boundaries, visualised by a predominantly steady conductivity increase in the scanned profile. The grafting approach on the other hand displayed a steplike conductivity profile, which was explained by the sharper grafting boundaries in the UV-irradiated approach, in which less monomer diffusion occurs during the shorter UV-polymerised timeframe. Some signal variations were insufficiently explained, such as a sharp signal drop near the end of the column. The authors attributed this to the higher stationary phase density, which would potentially provide more conducting groups and thus result in a signal increase.

A more likely explanation would be the apparent lack of sulfonated functionalities, caused either by a reduced surface area or less successful grafting near the capillary end. The grafted approach revealed sharper boundaries, however the displayed error bars were significantly greater than the claimed 1.7% RSD. Previous evaluation methods were performed chromatographically only and allowed no visualisation of the shape or profile of such a functional gradient. The exact visualisation of such profiles is considered very useful for complex gradient shape adjustments [129]. Unfortunately the authors failed to highlight the difficulty in attributing the

conductivity signal to either morphological inhomogeneities or the surface presence of ionisable groups.

Invasive quantification was achieved by Pucci *et al*. [130] at certain cross-sectional locations by destructive cutting of the columns and subsequent analysis of the bonded sulfur concentration using electron-probe microscopy (EPMA). Using sC^4D however allowed the longitudinal profile to be easily visualised and quantified while the column remained intact.

It is also of interest to observe that at locations of steeper conductivity profile gradient, the error bars from repeated manual scanning were much greater in comparison to both preceding and following points of measurement. Most likely this is a result of the error prone re-locations in manually conducted multiple scanning attempts, requiring the detector head to be shifted in millimetre increments by hand. Thus areas of higher conductivity with steeper change (slope) per mm section will display larger deviations when scanned again at that 'same' location.

Further examples of quality assessment by sC^4D listed in this review [117] include previous work of Connolly *et al*. in which this detection technique was published as a non-invasive characterisation tool for the first time [131]. Predominantly crude differences, such as larger voids in monolithic capillary columns, were visualized as zones of higher conductivity in the profile graph. The larger signal output for those voids is a result of the higher conductive response of the water, which is directly proportional to the displaced volume of the monolith filled sections, (which can take up to 50% of the capillary channel volume depending on the overall porosity of the polymeric stationary phase).

The technique was also adapted to successfully measure zones of immobilized protein [132] and the pH-dependent behaviour of weak acid functionalized monoliths [133-134] which could potentially be extended to on-column titrations in the authors opinion. Palladium loaded, flow-through capillary micro-reactors [135] were also be monitored for long term stability using sC^4D to observe the axial distribution, homogeneity and subsequent leaching and regeneration of the immobilised catalytic palladium metal [117].

In summary the authors deemed the technique of scanning C^4D suitable for conductivity profiling and non-invasive characterisation of many capillary and micro-chip applications and encouraged fellow researchers working in this field to consider the greater use of this technique, particularly as an additional analytical tool that can easily generate supplementary characterisation data without detrimentally affecting the designated use of such capillary columns or microchip reactors.

1.4.2 Fourier Transform near-infrared (FT-NIR) diffuse reflective spectroscopy

Heigl *et al.* [136] have employed the vibration response in the mid-infrared (MIR, 478 to 4000 cm^{-1}) and near-infrared (NIR, 4000 to 7800 cm^{-1}) range to non-invasively assess the morphological structure and surface area of polymethylstyrene-*co*-vinylphenylethane monolithic polymers. The spectral data were analysed by chemometric techniques (multivariate analysis) and evaluated in relation to changing polymer mixture compositions. The aim of simultaneously assessing both physical and chemical parameters of the porous substrates was realised by using a combination of spectroscopy and

principal component analysis with partial least-squares regression (standard error of prediction) due to the overlapping nature of the vibrational modes.

Specular reflectance within the porous substrate affects band shape and intensity and relates back to morphological and physicochemical properties of the sample. The absorption fraction, being the amount of light absorbed, directly relates to the volume of the material (globules), while the reflectance relates to the material surface area and porosity, providing information in turn by acting like an array of mirrors scattering the band components.

Data evaluation was conducted using a combination of raw spectral data evaluation as well as multivariate data analysis (MVA) and chemometric modelling. According to the authors, every material and surface structure has its unique physicochemical fingerprint in the near-infrared region, such that combined with chemometric and reference techniques, NIRS becomes a powerful tool for rapid and non-invasive assessment of morphological information with one set of measurements. The information generated by diffuse NIR spectroscopy correlated well with traditional techniques, such as nitrogen adsorption using the BET [137] and BJH [138] models.

The unique and probably most valuable information provided by this technique is the direct percentage of monomer and functional components integrated in the porous structure. Depending on the detail in spatial resolution and bandwidth of the integrated components, this technique may be very suitable in screening the extent of surface modifications. However, sufficient expertise in chemometric modelling and multivariate data analysis is required to extract useful information from the experimental data set.

1.4.3 Confocal Laser Scanning Microscopy (CLSM)

A relatively novel way of non-destructively visualizing and evaluating morphologies of monolith stationary phases was demonstrated recently by Bruns *et al*. [139]. The fluorescent dye V450 was immobilised on the silica monolith skeleton of a commercial Chromolith™ column in a multistep reaction pathway. The resulting modified stationary phase was excited with a UV diode laser at 405 nm and the emission spectrum was recorded around the maximum emission wavelength of 448 nm. Optical resolution was 30 nm per pixel and the resulting images were recorded in 61.5 μm planes with a total depth of 21.4 μm, resulting in 170 slices stacked at a distance of 126 nm between each slice.

The image stack was processed by iterative deconvolution software to remove high frequency noise and background interference and the slices segmented using a Gaussian kernel to blur the stack. The resulting segmented images were further analysed for pore size and distribution using an in-house written image processing software to calculate chord length distributions of 4×10^5 chords from random points within the void areas of the image in 32 angular directions (= 12,500 points). The average chord length of each point was used as a measure for the pore size around that point.

The same method was used for calculating the skeleton thickness and compared by statistical analysis of the pore median, mean, mode, variance and length values, corresponding well with TEM image analysis of Chromolith™ columns. The calculated mode of 2.2 μm for the pore size was quoted to be only slightly larger than the value measured by mercury

intrusion porosimetry and as the authors correctly noted a result of the 'bottle-neck-effect' of the latter method (underestimation).

The authors also highlighted the difference between the different averages (in particular variance) of Φ_{pore} since the values depend on the asymmetry of the analysed stationary phase and the resulting flow-through and mass transport properties. Further statistical analysis of the image stack included macroporosity determination by ratio of void pixels to all pixels in each slice. Interestingly there were significant variations of up to 5% in one stack of 160 slices (5 cropped on each side), with bulk macroporosity varying from 0.677 to 0.716 (mean 0.695).

In summary, the authors have conducted a very comprehensive and sophisticated characterisation method. Not only experimentally with fluorescent labelling chemistry, but also physically challenging by using an array of well-matched optical lenses. In mathematical terms the statistical analysis covered all aspects of morphological image processing, firstly by improving the image quality followed by the mathematical calculation of the porous properties. However besides the 'destructive' element of having a fluorescent-labelled column of no further use, the requirement for sophisticated chemical and physical preparation and mathematical analysis is a considerable drawback of this technique.

The chemical surface modification may be successfully reproduced by most other researchers in the field; however both optical scanning and deconvolution of the resulting images requires either a comprehensive knowledge or experience in those areas or the availability of technical

laboratories with such equipment and software processing. Nevertheless, it will be exciting to see what other findings will emerge following this work.

Notable characterisation work of silica monoliths using the confocal laser scanning micsroscopy technique was conducted by Tallerak *et al.* [183-185] providing further inside into the quality control aspect of this method.

The authors have hinted at several possibilities in their concluding statement, not only in regards to improving their developed technique, but also in combination with NMR and C^4D characterisation methods to determine individual contributions in the macroporous morphology responsible for eddy dispersion as a result of wall effects and integrate from the microscopic morphology to the macroscopic transport behaviour (monitoring mobile phase flow).

One further advantage of this technique is the ability to assess the morphology in the 'wet' state; the monolithic structure is not affected by shrinking and reflects more accurately the morphology of the column when in use, unlike SEM or MIP, which require the samples to be dry.

1.4.4 Transmission Electron Microscopy (TEM)

Somewhat more common is the measurement of porous properties by transmission electron microscopy. Courtois *et al*. [140] have applied this technique to a number of different monolithic stationary phases with different morphological properties. The samples are 'stained' with heavy metal-containing resin to increase the electron density and thereby the contrast of the resin-filled voids in the transmitting image. The capillary wall was removed with hydrofluoric acid and the embedded monolith encapsulated in

resin mix without the heavy metal component. 100 nm thick slices of the microtomed monolith-embedded resin were examined with the electron microscope (at 80kV) and the images recorded with a multiscan camera.

Using Corel Photo-Paint X3, the authors converted the TEM image into a binary black and white format to distinguish between the monolith globules and void sections filled with the lead-containing resin. These black and white images were subsequently analysed with chord length distributions (CLDs) as in the example above and the results compared to the values obtained by mercury intrusion porosimetry (MIP). Surprisingly there seems to be a consistent relationship between the two techniques, with all pore size measurements recorded by MIP being smaller by a factor of 2, regardless of the material analysed. While MIP underestimates the actual pore size due to the 'bottle-neck effect', it appears the CLD approach overestimates the median pore size due to longer chords distributed along the pore 'channel'. As such the mode value (peak value or highest number of chords with the same length) appears to be closer to the actual pore size value.

Besides the statistical analysis, the technique requires empirical preparation and time-consuming modification of the material to be analysed. Bubble formation is a potential problem during resin flush and the viscosity of the resin mixture limits the porosity of the material analysed. Once the material is stained and embedded in the resin component, the microtombing into thin slices can score the surface and cause some monolith fragments to dislodge from the resin bed and leave holes that show up in the resulting image. The image treatment is therefore more challenging and has to be matched with the original to assess any discrepancies.

However in comparison to techniques such as MIP, no bulk samples are required and the measurement made directly in the synthesised capillary. The advantages of this technique over MIP in assessing monolith morphology are relatively minimal since neither could be classified as non-destructive. The resin embedding appears to pose its own challenges, with bubble formation a likely occurrence and toxic materials used in the process. Furthermore TEM is carried out under vacuum and therefore similar to SEM imaging is not truly representative of the material morphology in the used (eluent wet) state.

1.4.5 Remote flow detection by NMR

A recent application of remotely detected (RD) magnetic resonance imaging (MRI) on monolithic columns has been able to visualize flow profiles within monolithic stationary phases [141]. The profiles of empty and hypercrosslinked monolith-filled capillaries show the parabolic distortion of the former *vs.* a more plug-like flow of the latter, porous scaffold containing capillaries. The authors suggest that the presence of the monolithic substrate disrupts the laminar flow profile and provides an even distribution of the mobile phase across the column.

Two dimensional nuclear magnetic resonance (NMR) spectra (transit time over chemical shift of the aromatic region) were able to illustrate the separation of three aromatic compounds at high flow-rates. This is a quite remarkable separation given that compounds so closely related would probably co-elute using more conventional chromatographic methods, while also offering the advantage of simultaneous identification and quantification.

Despite the unfavourably high flow-rates, the separations were also highly reproducible and the monolithic columns proved to be more physically stable than C_{18}-coated silica particle analogues. The authors conclude their findings with the current work on portable NMR spectrometers with tailored permanent magnet arrays, an exciting prospect for future studies into monolith morphology and separation performance in the field.

1.5 Summary and Discussion

Although the fast separations of small (inorganic) ions by IC using polymer monoliths do not yet match the speed of their silica counterparts, the potential of porous monolithic polymer stationary phases for fast IC and micro-IC is nevertheless very promising. Current publications demonstrating the use of polymer monoliths in IC are predominantly occupied with utilising the materials in the characterisation stage. The main concern involves matching of the functional material with suitable separation conditions. Further improvements, such as the development of shorter monolithic polymer-filled capillaries containing a higher degree of ion-exchange functionalities, have the potential to considerably reduce the separation time.

The unique advantage of using post-modification as the tailoring procedure on pre-synthesised polymer monoliths is the provision of a set of monolithic ‘templates’. In this way the morphology of the stationary phase is predetermined, allowing the user to simply introduce the surface properties required for the application without the need for prior optimisation of polymerisation conditions. Furthermore, post-modification of such templates

allows the incorporation of functional groups that are otherwise incompatible with the polymerisation mixture.

Nano-particle and multiple surfactant (polyelectrolyte) coatings appear particularly promising, providing high capacity, rapid mass transfer stationary phases for fast and efficient analysis. While monolithic polymer columns may so far appear to lack in efficiency, with the majority of values reported in the range of 10,000-100,000 plates/m, most Van Deemter plots for monolithic columns exhibit favourable mass transfers at higher flow-rates, without the detrimental loss in efficiency typically experienced with packed-particle columns under high flow conditions.

Polymeric monolith synthesis has a large range of factors influencing the structural and chromatographic properties [34]. Whilst this is advantageous for the specific tailoring of the material, such variability also entails a certain degree of confusion, as there seem to be a variety of factors responsible for the individual properties of the material structure. The dominant factor, porogen composition, influences the pore size and distribution. Similar effects are also observed when different monomers are being used, such that higher percentages of functional monomers (*i.e.* AMPS) can lead to different pore sizes without alteration of the porogen composition [142-144]. Furthermore, the incorporation of hydrophilic monomers such as AMPS, can considerably change the degree of swelling, particularly so in monoliths with small pore size, which can lead to a dramatic reduction of flow-rate and potentially the plugging of flow channels [73, 77].

Additionally, the influence of each constituent (*i.e.* porogens) varies with the type of polymerisation, such that the variety in polymeric monoliths

possible is quite large and the synthesis process requires re-optimisation after every change in composition and reaction parameters. However, recent studies in tailoring of porous properties by reducing the polymerisation time or by affording a second cross-linking step have further enhanced the possible applications of polymer monoliths and extended their useability to be on par with silica counterparts.

Morphology characterisations using SEM imaging provide a good indication of macroporous structure, but more rigorous characterisation methods are required for surface and mesopore analysis, on both wet and dry state materials using different techniques (*i.e.* solid state NMR), particularly for monolith compositions which are prone to swelling. A comprehensive optimisation characterisation study on thiol-converted GMA-*co*-EDMA polymer monoliths for use in CEC was conducted by Preinerstorfer *et al.* [145]. Using elemental analysis (%N), the authors measured up to 75% of the total amount of epoxide functionalities being accessible for further modification. A non-destructive, direct determination of thiol-groups on the monolith surface was performed by a disulfide-exchange reaction, yielding a UV-absorbing product, to allow quantification by photometric determination. Later research by the same research group [146] provided further characterisation of various methacrylate monoliths synthesised from a range of polymerisation mixtures. Such studies are critical to the further development and characterisation of polymer monoliths.

Recent quantitative advances using confocal laser scanning microscopy (CLSM), electron microscopy (SEM and TEM), near-infrared and NMR spectroscopy as well as sC^4D have significantly enhanced these

possibilities, however much more work is required to reliably provide detailed information on the composition of these monolithic materials to further improve their synthesis aspects. Less complicated, straightforward characterisation methods have also been developed to non-destructively monitor functional group presence, such as the pH-dependent ion-exchange capacity of carboxmethyl CIM disks (BIA Sep.) [147], supplementing as well as validating some of the more comprehensive analysis techniques.

Besides the success of these materials in protein separations by IC, no radical improvement for the analysis of small ions has yet been reported. The high degree of variability in the synthesis process, influencing the composition and behaviour of the polymeric structure, may limit the demand for these materials. This is further reflected in the low number of commercial porous polymer capillary columns of new generation (monolithic) with applications of interest to a wider sector of the market. Therefore, choice of the optimum material properties and mobile phase conditions for a desired analysis currently requires a good understanding of the material properties and developments in this field.

1.6 General Conclusions

Both silica and polymer monoliths have been demonstrated as useful stationary phases for CEC and conventional IC analysis. In current formats, CEC offers the advantages of miniaturised systems, such as low eluent and sample consumption and a relatively high degree of automation.

Furthermore, techniques such as gradient elution, isotachophoretic (ITP) focusing and electrokinetic injection enable improved detection limits.

The most promising aspect in this field is the use of preconcentration techniques, which can considerably improve detection limits. Limitations are predominantly confined to the instrumentation set-up, such that detection is usually restricted to UV absorbance and the pressure available for sample loading in commercial instrumentation is insufficient for fast flow.

On the other hand, current commercial IC instruments equipped for anion analysis simply require a suitable polymeric monolith column with sufficient capacity equivalent to the already available silica analogue, in order to achieve fast IC separations in a hydroxide eluent combination with suppressed conductivity detection. Based on research conducted within our group, monolithic polymer columns equivalent to the Chromolith range are now commercially available. Similar improvements have been made on the front of various nano-coatings, closing the gap to efficiencies so far only achieved with the silica counterparts.

Besides their advantages of improved flow characteristics and mass transfer, one of the most appealing aspects of the use of monoliths as stationary phase templates is the simplicity in post-modification of the column for the required application.

Reliable and straightforward coating and modification procedures as well as more exotic recent varieties have already been demonstrated for relatively simple sample solutions.

As the continued progress in this field generates further method improvement, it will be simply a matter of time until suitable column modifications for the analysis of complex sample matrices are developed and supported by the required design in instrumentation to permit real time

sample monitoring. However, unless these monolithic materials are developed to their full potential, micro-IC systems are likely to be available only as individual instrumental set-ups developed by different research groups. Neither CEC nor micro-IC systems are yet suitable for portability, which is ultimately the goal of most current research into microfluidic systems, *i.e.* Lab-on-a-chip. Nevertheless, the results obtained to date demonstrate that monolithic materials are not only highly useful for biological applications, but are now also on the verge of moving into the field of inorganic ion-exchange analysis, particularly for small molecules.

The demonstrated improvements in analysis speed and sensitivity form part of the initial steps towards a new era in inorganic IC, with the exciting prospects of miniaturised, fast, on-site monitoring becoming a more defined vision for ion chromatography.

1.7 Aims of this project

The aim of the study can be grouped into three main parts.

First, to establish a monolith synthesis and post-modification protocol for the development of a monolithic substrate with the right morphology and functionality to yield a complete monolayer latex nanoparticle coverage.

Second, to develop external characterisation methods that provide a better feedback throughout the column synthesis and thus improve the success rate of the latex coated monolith fabrication.

And third, to use existing and new instrumentation for Micro-IC with the desired performance in µL/min flow-rates, allowing for sensitive, low noise baseline detection.

Based on the promising results achieved prior to this work, the initial aim of this project focused on the strategies and pathways for achieving a monolayer latex coverage on monolithic polymer capillary columns and improve the separation performance for common anions with the columns synthesised. Subsequent variations in the outcome of the synthesis procedures prompted the quest for better characterisation methods besides the existing bulk assessments of MIP and BET (porosimetry and surface analysis).

The use of SEM allowed to visualise coating extents quite reliably, however the columns could then not be used for subsequent separation. Non-destructive characterisation methods were developed, in particular the use of sC^4D as a tool for stationary phase uniformity evaluation. Further study with latex nanoparticles of different size were undertaken to assess how the coatings affected capacity, separation characteristics and performance of the polymer monolithic columns.

2 General Experimental

This section describes the instrumentation, chemicals and general procedures used throughout this work, unless specified further in a particular chapter.

2.1 Instrumentation

Separations performed with hydroxide eluent generation using a Dionex Corporation (Sunnyvale, CA, USA) IC 2000 instrument were initially conducted with a modified flow-path. The unit was converted with a T-type flow-splitter connected to the capillary column on one end and backpressure coils (2000 psi total, Upchurch Scientific, Oak Harbor, WA, USA) on the other. The backpressure coils affected the split-ratio and converted the instrument's mL/min flow-rates to μL/min flow-rates. Injection was performed after the T-piece flow-splitting with an M-435 micro-injection valve (Upchurch Scientific) containing a 100 nL injection loop. A microsuppressor prototype manufactured by Dionex (Sunnyvale, CA, USA) was connected to the Chromeleon software panel, which allowed suppression current adjustment to suit the chosen hydroxide eluent gradients.

Subsequent separations described in Chapters 3, 4 and 5 were conducted with a Dionex Ultimate 3000 Capillary HPLC, which featured an integrated flow-splitter (ratio 1:100) connected to a continuously monitored flow-meter and control valve to maintain a constant flow-rate ranging from 0.1 to 10.0 μL/min. All separations on this instrument were performed at a temperature of 35 ^{o}C.

Detection was performed with the 5 nL UV flow cell at a wavelength of 214 nm. Sample injection was performed manually on the IC 2000 using a 10 μL micro syringe (SGE, Australia) and in automatic mode on the Ultimate 3000 Capillary LC system using the integrated autosampler, automatic injection valve and injection loops ranging from 1-5 μL.

2.1.1 Porosimetry and Surface Area Analysis

Bulk polymerisation was carried out in a glass vial (2-10 mL) to obtain bulk amounts of monolithic polymer for the determination of porous properties via surface area measurements using a Micromeritics ASAP 2400 BET Surface Area Analyzer (Norcross, GA, USA), and porosimetry measurements using a mercury intrusion Micromeritics Pore Sizer 9310.

2.1.2 Scanning Electron Microscopy

Scanning Electron Microscopy (SEM) images of the polymer monoliths and latex particles were obtained with a FEI Quanta 600 MLA environmental scanning electron microscope (Eindhoven, The Netherlands) in high vacuum mode, using an accelerating voltage of 20 kV. Secondary electrons were detected using an Everhard-Thornley scintillator-type electron detector. Conductive gold or platinum coatings were generated with a BalTec SCD 050 Sputter Coater (Balzers, Principality of Liechtenstein) of various thickness (10-50 nm depending on the surface area of the material analysed) to prevent charging of the material under the electron beam.

Best SEM results were achieved when the capillary cuttings were well washed with methanol and MilliQ water and vacuum dried overnight. The capillary was cut into sections of 2-3 mm in length and carefully adhered to the 12 mm pin-type aluminium SEM stub using either small amounts of superglue or epoxy resin. For lower magnification images, rows of capillary cuttings were immobilised onto 5 mm wide strips of conducting carbon tape and wound around the outside perimeter of the aluminium stud. This method was found to be more effective in assisting material conductivity and reducing electron charging effects, observed as white-out sections within the magnified image and found to occur more frequently with high porosity polymer monolith materials.

2.2 Reagents

Unless specified otherwise, all chemicals were of analytical reagent grade and are listed in Tables 2.1 - 2.3.

Table 2.1: Chemicals used to modify capillaries and monoliths

Name	Formula	Supplier
Acetic acid	CH_3COOH	BDH Chemicals, Kilsyth, Victoria, Australia
Acetone	$(CH_3)_2CO$	BDH Chemicals
Acetonitrile (ACN)	CH_3CN	BDH Chemicals
AS11 latex particles	N^+R_4	Dionex, Sunnyvale, CA, USA
AS18 latex particles	N^+R_4	Dionex
Dichloromethane	Cl_2CH_2	BDH Chemicals
N,N-Diisopropylethylamine	$C_8H_{19}N$	Sigma-Aldrich
Ethanol	C_2H_5OH	BDH Chemicals
Hydrochloric acid	HCl	BDH Chemicals

γ-methacryloxypropyl-trimethoxysilane	$C_{10}H_{20}O_5Si$	Sigma-Aldrich
Methanol	CH_3OH	BDH Chemicals
Phosphoric acid	H_3PO_4	BDH Chemicals
Sodium hydroxide	NaOH	Ajax Chemicals, Sydney, NSW, Australia
Sulfuric Acid	H_2SO_4	BDH Chemicals
Thiobenzoic acid	C_6H_5COSH	Tokyo Kasei Kogyo Co. Ltd. 6-15-9 Toshima, Kita-Ku, Tokyo, Japan
*tert-B*utyl hydroperoxide	$(CH_3)_3COOH$	Aldrich
Trimethylamine hydrochloride (TMAHCl)	$(CH_3)_3N$ HCl	Aldrich

Table 2.2: Chemicals used as analytes and eluents

Analyte	Formula	Supplier	Purity
Potassium Bromate	$KBrO_3$	Ajax	99%
Potassium Chloride	KCl	Sigma	99%
Potassium Iodate	KIO_3	Ajax	99%
Sodium Bromide	NaBr	Sigma	99%
Sodium Chlorate	$NaClO_3$	BDH Chemicals	99%
Sodium Chloride	NaCl	May and Baker	99%
Sodium Iodide	NaI	Aldrich	99%
Sodium Nitrate	$NaNO_3$	Ajax	99%
Sodium Nitrite	$NaNO_2$	Ajax	99%
Sodium Perchlorate	$NaClO_4$	Aldrich	99%
Sodium Sulfate	Na_2SO_4	BDH Chemicals	99%

Table 2.3: Chemicals used for monolith polymerisation

Chemical	Formula	Supplier
1,4-butanediol	$HO(CH_2)_4OH$	Aldrich
1-propanol	$CH_3(CH_2)_2OH$	Sigma
2,2'-azobisisobutyronitrile	$(CH_3)_2C(CN)N=NC(CH_3)_2CN$	Du Pont, Sydney

Chemical	Formula	Supplier
2-acrylamido-2-methyl-1-propanesulfonic acid	$H_2C=CHCONHC(CH_3)_2CH_2-SO_3H$	Aldrich
Basic alumina activity grade I, Type WB-2	Al_2O_3	Aldrich
Butylmethacrylate	$H_2C=C(CH_3)CO_2-(CH_2)_3CH_3$	Aldrich
Chloromethylstyrene	$ClCH_2-C_6H_5CH=CH_2$	Aldrich
Decane	$C_{10}H_{22}$	Sigma-Aldrich
Didecyldimethylammonium bromide (DDAB)	$[CH_3(CH_2)_9]_2N(CH_3)_2Br$	Sigma-Aldrich
Divinylbenzene (80%, diluted in 20% Ethylbenzene)	$H_2C=CH-C_6H_4-HC=CH_2$	Aldrich
Ethyleneglycol-dimethacrylate	$[H_2C=C(CH_3)CO_2CH_2]_2$	Aldrich
Lauryl Alcohol	$C_{12}H_{25}OH$	Aldrich
Toluene	$C_6H_5CH_3$	Aldrich
Styrene	$C_6H_5CH=CH_2$	Sigma-Aldrich

2.3 Procedures

2.3.1 Electrolyte and standard preparation

All electrolytes and analyte standards were prepared using MilliQ water (Millipore, Bedford, MA, USA). Electrolytes were filtered through a 0.45 μm membrane filter of Type HA (Millipore) and degassed in an ultra-sonic bath. Latex solutions supplied by Dionex were previously refined by dialysis through a cellulose membrane, as reported in work by Hutchinson *et al*. [60, 77]. The purpose of refinement was to remove surfactants designed to stabilise the emulsion. However in this work the presence of surfactants was shown to not have a negative influence on the coating procedure and

therefore these were not removed, which assisted in maintaining emulsion stability.

2.3.2 Measurement of ion-exchange capacity

Ion-exchange capacities for the columns were determined using an absorption/elution method [148], carried out using a sodium bromide or chloride solution which was flushed through the column to saturate the ion-exchange sites and then removed using a different eluent.

2.3.3 Capillary surface modification procedure

The standard procedure for covalent vinyl-group attachment to the capillary wall as outlined in [72] is described below. This procedure yields capillary sections of up to several metres in length with methacrylate groups attached to the fused-silica capillary inside surface. Fused-silica capillaries (100, 200 and 250 *μ*m *i.d.* with 365 and 650 *μ*m *o.d.* Polymicro Technologies, Phoenix, AZ, USA) of lengths up to one metre were surface-treated with a solution of γ-MAPS (3-(trimethoxysilyl)propyl-methacrylate) in ethanol to provide vinyl group functionalities for the covalent attachment of monolithic polymer globules to the capillary wall during radical polymerisation.

In summary, the capillaries were rinsed with acetone and water using a Hamilton syringe (250 *μ*L) by hand, activated with 0.2 *M* sodium hydroxide for 30 min using a syringe pump, washed with water by hand, then with 0.2 *M* HCl for 30 min, rinsed with water again and finally with ethanol. A 20% solution of 3-(trimethoxysilyl)propyl-methacrylate (γ-MAPS) in 95% ethanol adjusted to pH 5 using acetic acid was pumped through the capillaries at a

flow-rate of 0.25 μL/min for 60 min. The capillary was then washed with acetone, dried in a stream of nitrogen, and left at room temperature for 24 h to complete the condensation reaction of the silanol groups.

Note: Temperature effects were not taken into account. This procedure was conducted usually at around 20 °C (room temperature). Times and flow-rates can be varied in regards to the values given here (mostly the contact time of the derivatization agent is prolonged over several hours).

2.4 Preparation of monomer solutions

2.4.1 Monomer purification

Chloromethylstyrene (CMS, 90%) and divinylbenzene (DVB, 80%) were purified by distillation under reduced pressure before use. DVB (80:20 with ethylbenzene from Sigma-Aldrich) distillation required a high vacuum and the distillation temperature had to remain under 30 °C in the vapour space (using aluminium foil around flask and neck to aid insulation).

Firstly the ethylbenzene fraction was collected (25 °C) and as the condensation of ethylbenzene reduced, a temperature increase of 2-3 °C occurred prior to the condensation of the DVB. The first condensate fraction was collected in the same flask prior to rotating the set-up to collect the pure DVB distillate in the collection flask. CMS distillation was conducted in a similar manner, the temperature reached 32 °C in the first and about 40 °C in second collection (CMS) step. Again a high vacuum and careful temperature control was required.

2.4.2 Monolithic column synthesis

Specific monomer compositions are listed in the result sections of each chapter. The general synthesis procedure was conducted with surface-modified fused-silica capillary sections as outlined earlier (Section 2.3.3) and manually filled with the sonicated polymerisation mixture using a 250 μL Hamilton syringe and checked for air bubbles within the capillary cavity. Both ends of the capillary were then sealed with rubber septa and the capillary submerged in a water bath at 60 or 70 °C for 20 h for thermal polymerisation or placed in Teflon coated capillaries and irradiated under 254 nm UV light for 15 min. Upon completion of the radical polymerisation step, the unreacted porogens (such as toluene or dodecanol) were removed from the monolith by flushing the capillary with at least 250 μL of methanol at 1 μL/min for at least 6 h and then MilliQ or the chosen post-modification solution as required. The type and composition of which is described in each subsequent experimental chapter.

3 AS18 latex-coated polymer monolith capillary columns

3.1 Introduction

Separations of small anions on monolithic polymer stationary phases have not been explored to the extent of their silica counterparts [23]. Given the diffusive nature of small anions, such separations can provide an indication of the mass transfer characteristics of the monolithic scaffold. In theory these materials exhibit lower C-term dependence, which stems from the convective mass transfer of the open flow channels. In practice however it appears to be more complex in nature. Silica-based monolithic materials have gained popularity early on, with excellent separation performance as a result of highly reproducible and evenly distributed micro-globular monolithic structure, exhibiting bimodal pore distribution and high surface area. Polymeric monolithic scaffolds are more variable in synthesis, making it harder to achieve a similar degree of uniformity, and are prone to suffer from structural variations. These structural issues can be mostly overcome by carefully tailoring the fabrication conditions to suit the application.

It appears that a form of gel-porosity in the outer swollen globule layers has a detrimental impact on the mass transfer characteristics, particularly at higher flow-rates. A recent review by Nischang *et al.* identified the nanoscale gel porosity as a significant factor in reducing the performance of polymer monolith stationary phases in small ion separations [21]. Nevertheless, the possibility of direct *in-situ* fabrication of polymer monoliths in the column mould is particularly favourable for micro-analytical systems. Furthermore, the broader range of functional constituents and post-

modification reactions as well as mobile phase eluent conditions in polymeric rather than silica-based scaffolds allow for a higher degree of flexibility [12, 20]. One distinct advantage of polymeric stationary phases in anion-exchange chromatography is their superior stability at higher pH, which allows for better compatibility with hydroxide eluents.

Previous work on latex-coated porous polymer monoliths demonstrated the potential use of these materials as ion-exchange stationary phases in capillary IC [73, 75]. These stationary phases were synthesized by coating the surface of the negatively charged poly(butylmethacrylate-*co*-ethyleneglycoldimethacrylate-*co*-2-acrylamido-2-methyl-1-propanesulfonic acid) (BuMA-*co*-EDMA-*co*-AMPS) monoliths with positively charged quaternary ammonium functionalised latex nanoparticles, which were bound to the scaffold via their electrostatic attractions to the oppositely charged functional group. The capacity of such monolithic ion-exchange materials was measured in the range of 0.59 - 1.58 *µ*equiv./g [75]. This was attributed to the fact that only a relatively small amount of sulfonic acid functionalised monomer could be dissolved in the polymerisation mixture due to solubility limitations and only a percentage of these functionalities would be present at the pore surface, which in turn provided fewer sites for electrostatic interaction with the latex particles and thus resulted in poor surface coverage [81].

Following on from this work, different polymeric scaffolds and post-modification techniques were trialled, which led to improvements in latex coverage and an anion-exchange capacity of up to 29 *µ*eqiuv./g [77].

Hutchinson *et al.* found a direct correlation between the extent of terminating functional group presence on the scaffold and the resulting latex coverage.

Given the size and diffusive nature of small anions, sufficient ion-exchange capacity is essential for the material to exhibit superior separation performance under both isocratic and gradient elution conditions. Furthermore, it was demonstrated that post-modification of a poly(styrene-*co*-DVB) polymer scaffold by sulfonation gave a superior coverage of functional groups in comparison to the monoliths prepared using functional methacrylate monomers. In addition, the authors outlined several advantages of the post-modification, such as the versatility of tailoring the morphological and functional group properties independently from each other [77].

However, recent results have indicated that the distinction between the two techniques is generally not as clear as suggested by these two previous publications. Hutchinson *et al.* identified a pressing need for research on monolithic IC columns in relation to the coverage of functional groups on the surface of the monolith to improve the chromatographic performance. Early trials suggested that this might be achieved by investigating direct sulfonation of functional poly(styrene-*co*-DVB) monoliths via post-reactive modification pathways.

The aim of this study was to identify a robust method for the synthesis of fully latex agglomerated polymer monoliths as stationary phases for capillary columns in fast-IC and demonstrate their performance for the separation of small inorganic anions.

3.2 Experimental Section

3.2.1 Apparatus

Dionex IC 2000 and Ultimate 3000 instruments were used for chromatographic separations as described in Chapter 2.

3.2.2 Chemicals

2,2'-azobis(2-methylpropionitrile) (99%, AIBN), toluene (99%), 1-decanol (99%), 1-dodecanol (98%), acetonitrile (HPLC grade), methanol (HPLC grade), 3-(trimethoxysilyl)propyl methacrylate (98%), dichloromethane (99.5%), tert-butyl hydroperoxide (5.0-6.0 M in decane) were purchased from Aldrich (Milwaukee, WI, USA). Thiobenzoic acid (unknown purity) was purchased from TCI (Tokyo, Japan).

1 g of thiobenzoic acid (TGI T0195, left to warm up in the fumehood prior to opening) and 1 g of *N,N*-diisopropyl-ethylamine (Sigma-Aldrich > 99%) were added concurrently to 10 g of DCM to make 12 g (10% each in DCM). AS18 (65 nm diameter) latex particles with quaternary ammonium functionalities were obtained from Dionex as an 11% (w/v) suspension. DDAB was dissolved in 5% ACN to yield a 1 m*M* solution and filtered through 0.45 μm nylon filters. All other reagents were of the highest available grade and used as received.

3.2.3 Post-modification of CMS/DVB type monoliths

1st Step: The polymer monolith-filled capillaries were hand-flushed with 250 μL of dichloromethane (Hamilton Syringe) followed by freshly prepared thiobenzoic acid solution (10% (w/w) mixture with *N,N*-diisopropyl-ethylamine, adding 1 g of each to 10 g of DCM). The post-modification solution was dispensed using a Hamilton syringe on a Harvard syringe pump at 15 μL/h for 20 h with the capillary fully encased in a column heater (Phenomenex Thermasphere TS-130) at 60 °C (the typical monolithic capillary volume for a 30 cm section is approximately 10 μL).

2nd Step: Following the capillary monolith rinse with thiobenzoic acid solution, the second post-modification step required the column to be flushed with methanol (AR grade or better) using a 250 μL Hamilton syringe on the same syringe pump at a rate of 15 μL/h with the monolithic capillary encased in the column heater at 50 °C for 20 h.

3rd Step: The surface functionalisation was completed by flushing the capillary at room temperature overnight at a flow-rate of 15 μL/h with a solution of *t*-BuOOH (*tert*-butyl hydroperoxide, 5.0-6.0 M solution in decane). Washing of the capillary column with methanol and finally MilliQ water completed this final step.

3.2.4 Coating of CMS/DVB type monoliths

Latex solutions (AS18) were prepared by mixing the supplied 11% (w/v) latex suspension from Dionex with MilliQ Water at 1:50 or 1:100 dilution, followed by filtration through a 0.45 μm nylon syringe filter (Activon, Thornleigh,

Australia) and stored in sealed 10 mL vials. 1m*M* filtered DDAB solutions were used as prepared in 5% ACN.

Coating of the sulfonated monolith was achieved by placing the prepared solution (AS18 latex or DDAB) in a syringe, which was connected to the capillary casing with a microtight fitting, followed by flushing of the porous polymer filled capillary with the diluted solution at 60 μL/h for 4 h on a syringe pump. The coating procedure was completed upon rinsing of the monolith-filled capillary with MilliQ, either hand-flushing two syringe volumes or placing the syringe on a Harvard syringe pump for 1-2 h at 200 μL/h).

3.2.5 Preparation of Porous Polymer Monoliths

Poly(styrene-*co*-DVB) monoliths were prepared as described in Section 2.4. Bulk monoliths were prepared from the remaining polymerisation reaction mixtures by placing these in the sealed preparation vials in a 70 ^{o}C water bath for 20 h. The residual porogen in the bulk samples was removed by Soxhlet extraction over 8 h using methanol. Washed bulk samples were dried in a vacuum oven overnight and stored in airtight containers. These bulk samples were used for mercury intrusion porosimetry and BET surface area measurements and were considered to be representative of the morphological properties in the monolithic stationary phase.

3.2.6 Monolith comparison table

A summary of capillary columns prepared and used in this chapter is given in Table 3.1 below. All mixture constituents are given in % (w/w) relative to the total. AIBN was used as thermal initiator at 1% w/w relative to monomer.

Name	Monomer % w/w	Cross-linker %	Porogen %	Polymeris. Conditions	Dimensions	Post-mod.	Coating
DVB1	None	DVB 36	Tol,Dod 8, 56	Thermal (70°C, 24h)	0.25 x 180 mm	None	DDAB, AS18
20% x-link	Styrene 32	DVB 8	Tol, Dod 12, 48	Thermal (70°C, 24h)	0.25 x 409 mm	Chloro-sulfonic	AS18 latex
Cap 1	CMS 16	DVB 24	Tol,Dod 18, 42	Thermal (70°C, 24h)	0.25 x 300 mm	Thio-benzoic	AS18 latex
Cap 10	CMS 16	DVB 24	Tol,Dod 18, 42	Thermal (70°C, 24h)	0.25 x 200 mm	Thio-benzoic	AS18 latex

Table 3.1: Monolith composition for columns used in this chapter.

3.2.7 Measurement of Ion-exchange Capacity

The ion-exchange capacity of the monolithic stationary phases was determined by nitrate adsorption/desorption using the Dionex LC instrument. The capillary columns were first loaded with chloride using 20 m*M* potassium chloride solution. Excess chloride was flushed from the column using MilliQ water at a rate of 2.0 *µ*L/min for a period of 30 min. The capillary was disconnected from the pump and the system flushed with 1.0 m*M* nitrate solution for a period of 10 min using the same flow-rate. The capillary column was reconnected to the system and 1.0 m*M* nitrate solution pumped through the capillary at a rate of 2.0 *µ*L/min. The absorbance of the eluent was monitored at 215 nm until breakthrough was observed and the absorbance reached a stable value. The process was repeated twice more.

3.3 Results and Discussion

Highly magnified scanning electron microscopy images of latex particles on stationary phase substrates are rarely present in the literature, despite the availability of excellent latex coated ion-exchange columns since the 1990s. A comprehensive coverage on polymer particles was visualized by SEM in an early publication by Slingsby and Pohl [150]. In contrast, the best previously published SEM image of visualised latex particles on a monolithic substrate surface, prior to the results presented here, shows a relatively sparse coverage of these nanoparticles on the polymer globules [81]. The associated chromatogram illustrated reasonable separation performance, despite the poor latex coating. Considerable improvements have been achieved since this pioneering work.

Hutchinson *et al.* have recently published improved separation performances on capillary columns which were post-modified prior to coating with latex particles [77]. Although the capacity measurements of these columns suggested a more comprehensive latex coverage, no SEM images were available at the time of publication to demonstrate the correlation between the improved performance and the extent of the latex nanoparticle coating.

3.3.1 Surfactant coated polymer monolithic substrates

Previous work in this area demonstrated that functionalisation (in particular sulfonation) of highly cross-linked polymer monoliths is a very challenging task. Therefore alternative procedures to covalent modification were explored in this work. One example of non-covalent modification is surfactant coating,

which is well demonstrated for silica monoliths [28-29, 31-32, 51, 55, 60, 151] including electrostatic multilayer coatings [58] and is widely used in various modes of chromatography (dynamic coating). A plain DVB polymer scaffold can be coated with an ionic surfactant, such as didodecyl-dimethylammonium bromide (DDAB) to provide charged functional groups at the surface. An optimal coating concentration of filtered (0.45 μm) 1 m*M* DDAB in 5% ACN was chosen based on findings by Hatsis and Lucy [28].

Hydrophobic interactions between the polymer scaffold and the aliphatic chain of the DDAB formed the first coating, with the surfactant's negatively charged functional group allowing the positively charged latex particles to bond via electrostatic interaction. As seen in the cross-sectional SEM image in Figure 3.1, the coverage of particles over the surfactant coating was visulaized as irregular conglomerations. The chromatographic performance of the column however was found to be disappointing. The interspersed agglomerations on the globule surface are a result of the interaction between the charged surfactants and latex nanoparticles (AS18), similar to charged multilayer arrangements.

Other long-chain surfactants including *N*-dodecyl-*N,N*-(dimethylammonio) undecanoate (DDMAU) were also trialled in the coating procedure; however the resulting columns exhibited no improvement in visible coating extent or analyte retention.

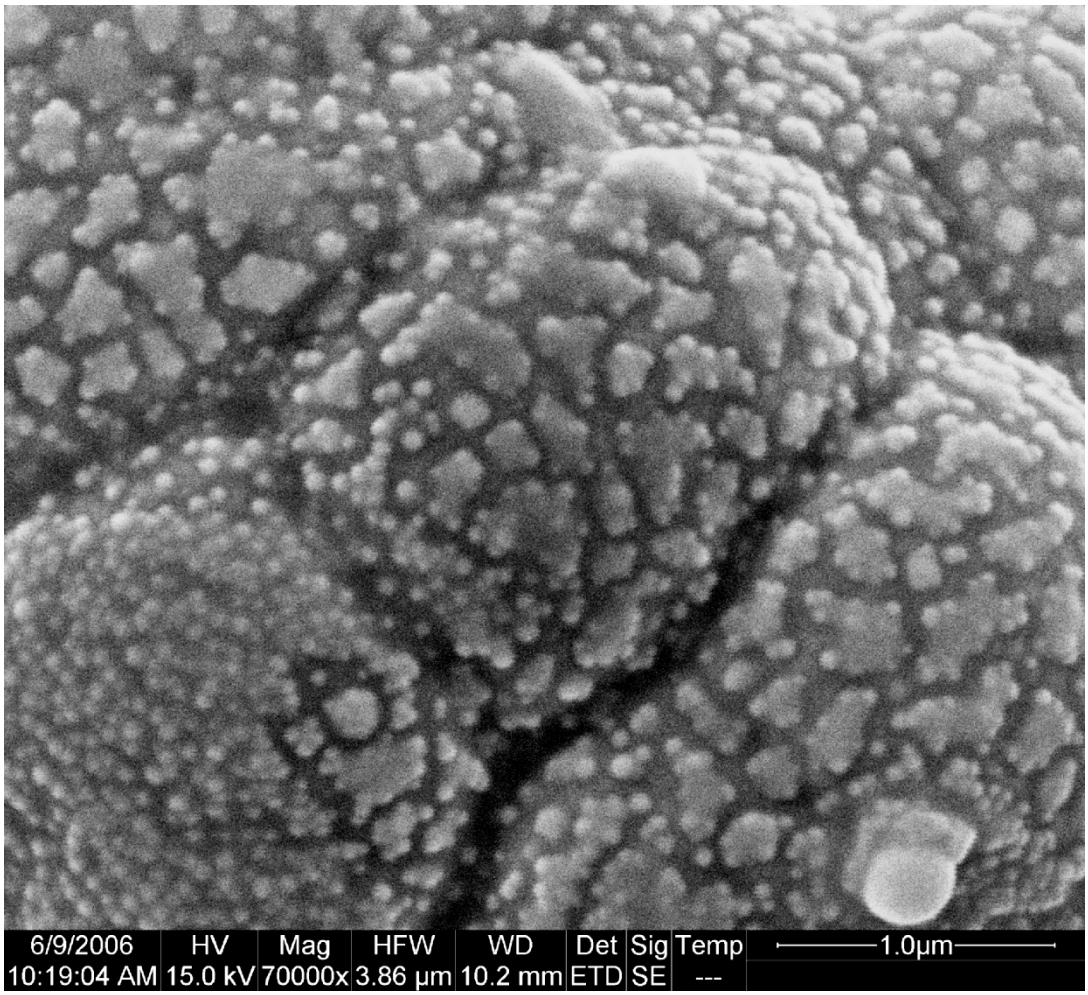

Figure 3.1: SEM of surfactant and latex coated hydrophobic DVB polymer monolith scaffold.

3.3.2 Sulfonated PS/DVB type monoliths

Commercially manufactured poly(styrene-*co*-DVB) polymer beads are typically functionalised using sulfuric acid at elevated temperatures. Based on this successful treatment of cross-linked polystyrene beads, a similar method was tested for monolithic polymers of similar monomer composition.

The degree of cross-linking was varied by changing the ratio of monomer to cross-linker (DVB) to allow for maximum sulfonation extent, while maintaining a rigid macroporous structure. A moderate coverage of latex nanoparticles was achieved by subjecting the 20% cross-linked poly(styrene-*co*-DVB) monolithic columns to hot concentrated sulfuric and chlorosulfonic acid treatment (column labelled 20% x-link), with the resulting chromatogram being shown in Figure 3.2. The separation shown represents a considerable improvement on the previous published results [77]. Seven anions were separated to near baseline resolution in 10 min, with efficiencies ranging from 1560 to 4560 theoretical plates/m.

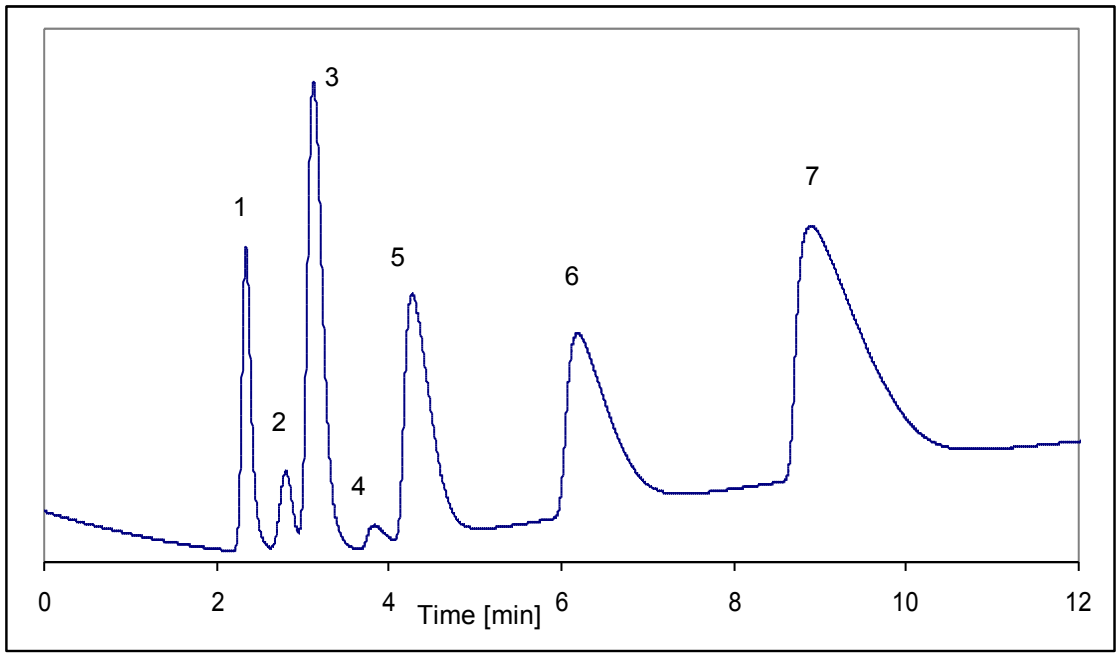

Figure 3.2: Separation of 7 anions, Column: 20% x-link PS-*co*-DVB, sulfonated with chlorosulfonic acid and coated with AS18, Length: 40.9 cm, Conditions: 10-50 m*M* NaOH gradient from 4 min at 4.8 *µ*L/min, Detection: UV (220 nm, Knauer),

Analytes: 1 - IO_3^-, 2 -BrO_3^-, 3 - NO_2^-, 4 - Br^-, 5 - NO_3^-, 6 - Benzene sulfonate, 7 - I^-.

The modified capillary column that yielded this separation was assessed for the extent of latex coating using scanning electron microscopy (SEM), which is shown in the highly magnified capillary cross-section in Figure 3.3. An even distribution of the latex nanoparticles (Dionex AS18) is clearly visible, although complete monolayer coverage was not achieved. The exposed section at the lower end of the image is a result of severed polymer globules, which occurred at the time the capillary was cut to obtain a cross-sectional image.

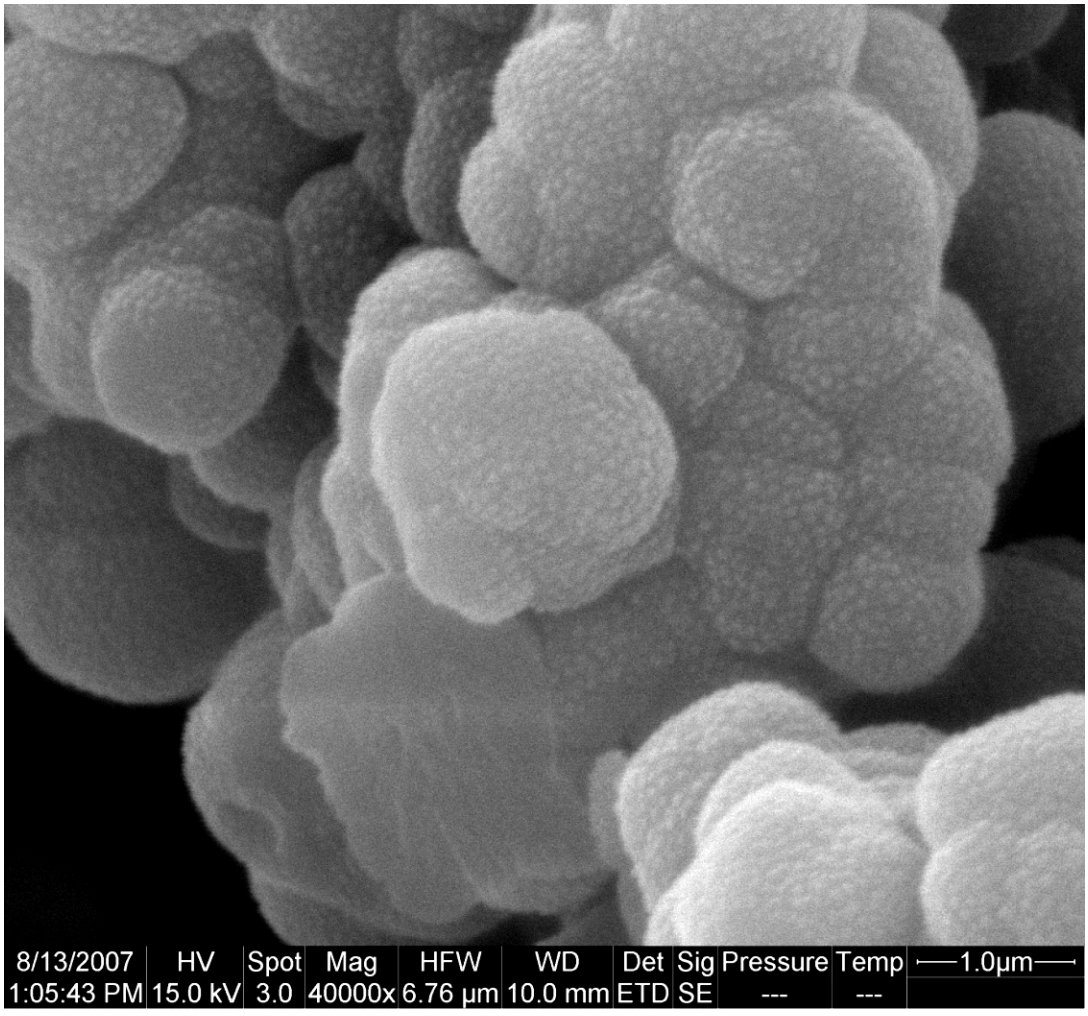

Figure 3.3: SEM of AS18 latex particle coated, sulfonated, 20% x-link PS-*co*-DVB monolith.

Despite not having obtained monolayer coverage, the resulting columns performed better than any previous approach using methacrylate monomers, which suggests that poly(styrene-*co*-DVB) based materials may provide more suitable morphological and post-reactive properties. Whilst achieving improvements over previous work, this approach did not represent a practical alternative for this column manufacture. The harsh reaction conditions damaged fittings and syringes used for the modification. Due to the different reaction kinetics and cross-linking in the polymer monolith compared to typical polymer beads, complete sulfonation appeared to have not been achieved using this method, supported by measured material composition using elemental x-ray analysis.

These limitations led to the evaluation of reactive styrene-based polymerisation mixtures as an alternative pathway to sulfonated styrene-based materials.

3.3.3 Reactive surface post-modification

Monoliths were prepared using CMS (chloromethylstyrene) as a reactive monomer based on previous recipes from Tripp *et al.* The choice to use a less polar monomer was firstly to avoid monomer solubility problems as reported earlier [75, 81] and secondly to obtain a good functional group distribution on the globule surface while maintaining the actual monolithic morphology of the scaffold.

Several post-reaction pathways were investigated to yield sufficient distribution of negatively charged sulfonate groups for electrostatic binding with the quaternary amine latex particles, including modification of the methyl

chloride group using Na_2SO_3 at 65 °C based on results published by Chonde *et al.* [90]. The most successful outcome was achieved with thiobenzoic acid as the precursor substituent, followed by cleavage with methanol and oxidation with tertiary butyl-peroxide to yield the final sulfonic acid functionality as depicted below.

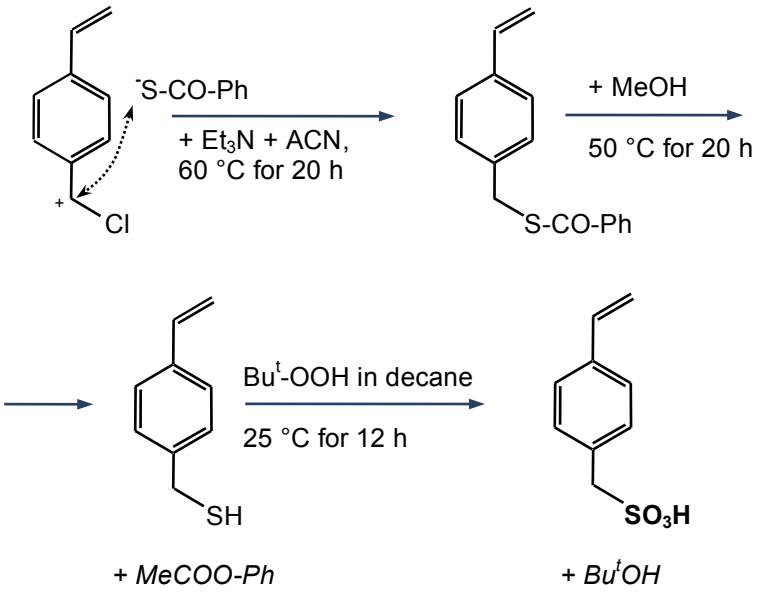

Initially, reproducibility proved to be quite poor. The preparation of the thiobenzoic acid solution was dependent on the order of addition of the constituents. Best results were achieved when the reactive ingredients were added to the dichloromethane (DCM). Furthermore the instability of the thiobenzoic acid solution once activated with *N,N*-diisopropyl-ethylamine, as outlined in Section 2.4.2, required it to be stored under nitrogen below 4 °C and used within 2-3 weeks. Given the limited options for assessing the yield of each individual reactive step, the success of each column was not known until the final latex coating, which could be screened visually using SEM.

A comparison of the coated and uncoated poly(CMS-*co*-DVB) monoliths is shown in the cross-sectional SEM images in Figure 3.4. The uncoated polymer substrate acts as the precursor for the latex-coated version (Cap 1), which was post-modified as shown above.

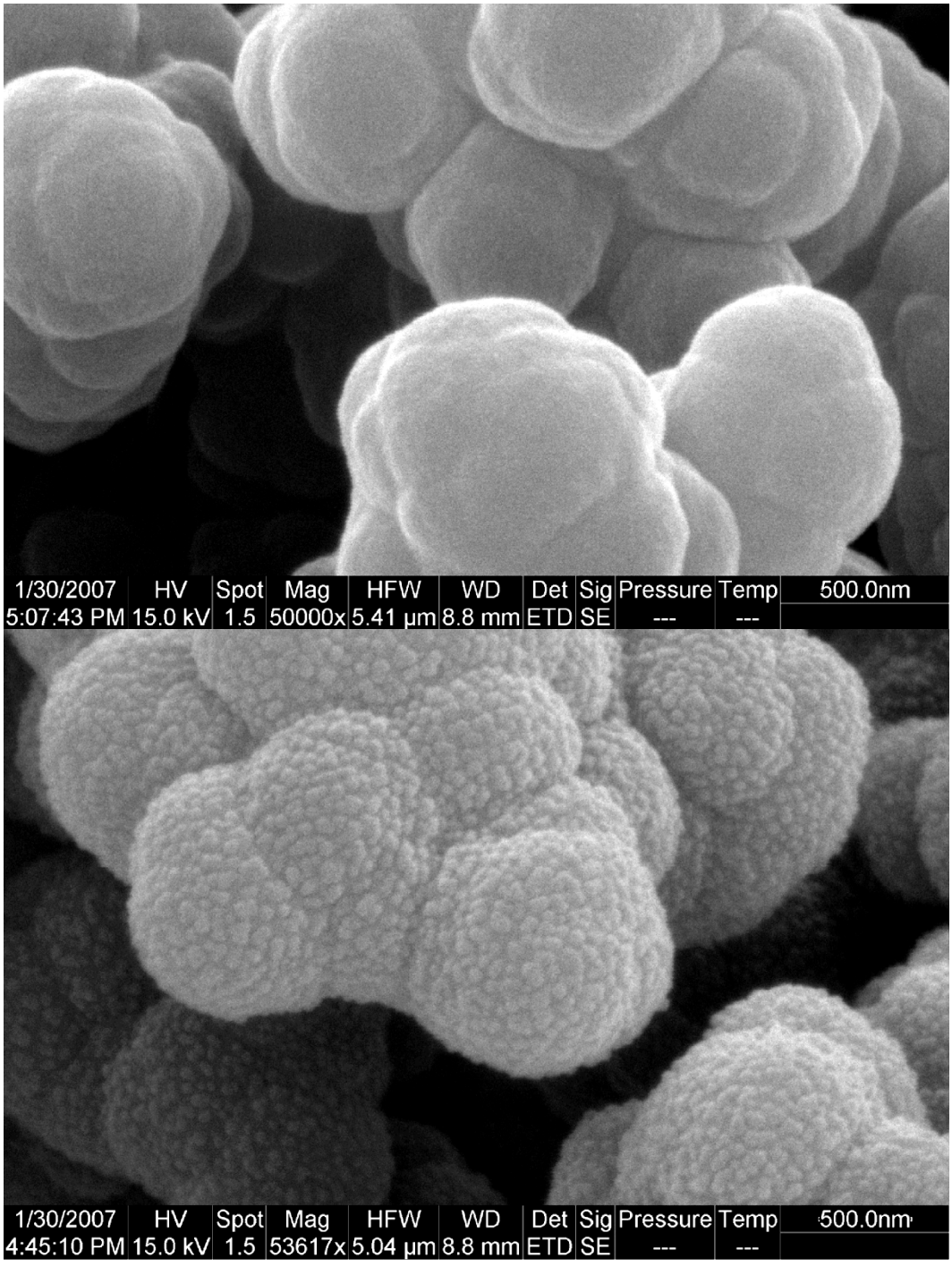

Figure 3.4: SEM of unmodified poly(CMS-*co*-DVB) monolith above and AS18 latex coated, sulfonated analogue below (Cap 1).

The separation performance of this capillary column is shown in the chromatogram of Figure 3.5. The instrumental configuration was based on the use of a backpressure coil to regulate flow-splitting of ml/min flow-rates to varying μL/min flow-rates, which resulted in fluctuating flow-rates in the capillary column and therefore chromatograms for which the retention factors varied considerably. However, the incorporation of an Atlas microsupressor allowed for highly sensitive contactless conductivity detection to be used and virtually provided the same instrumental set-up as the original configuration, which allowed the use of software-controlled gradient elution and suppression.

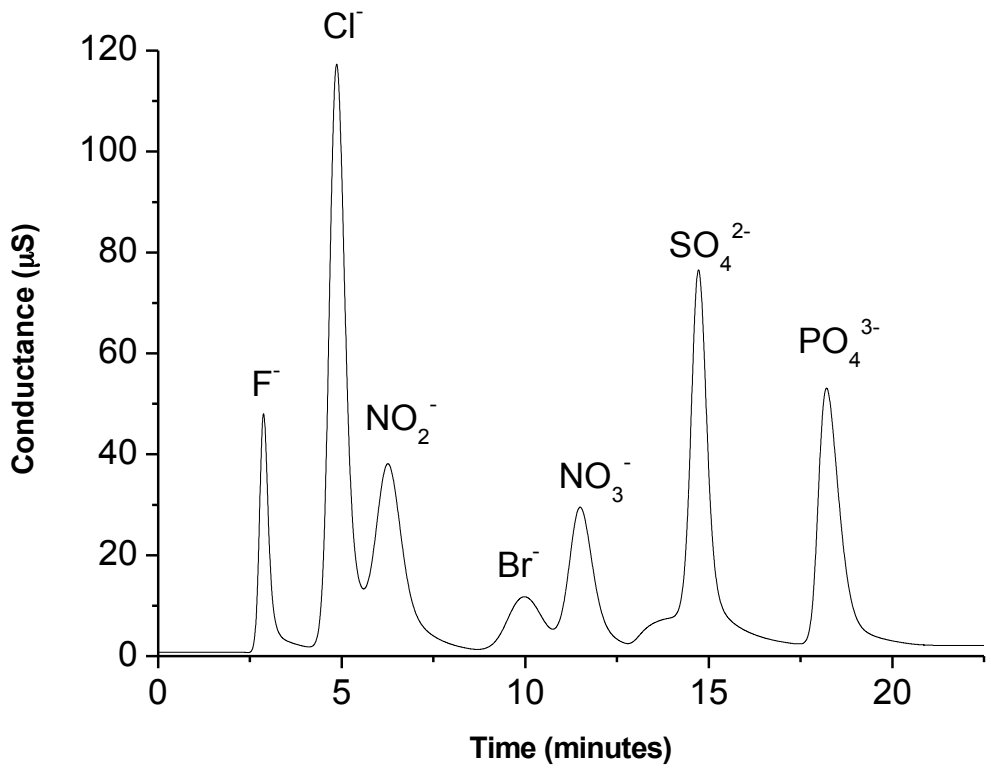

Figure 3.5: Separation of 7 anions using suppressed conductivity detection. Conditions: Eluent 2.0-20 m*M* KOH; Column: Cap 6 (250 μm *i.d.* × 30 cm, 2 μm pore size sulfonated CMS-DVB coated with AS18 latex nanoparticles (Dionex); Flow-rate: ~3 μL/min; Sample loop: 50 μm×5.0 cm (100 nL); Atlas microsupressor at 10 mA, flowing at 0.1 mL/min; Detector: TraceDec C^4D; Analytes as depicted.

Unfortunately, the use of hydroxide eluents degraded the fused silica capillaries to an extent where the silica walls developed micro-fractures and became quite brittle, which soon rendered them unsuitable as capillary columns. Cross-sectional SEM images of broken capillary sections showed excellent latex monolayer coverage on the monolithic substrate. Degradation of the coating was not observed over the lifespan of the capillary.

3.3.4 Anion separation using a Dionex *μ*HPLC system

A 20 cm section of 250 *μ*m *i.d.* fused-silica capillary containing the latex coated monolith was connected to a Dionex Ultimate 3000 instrument utilizing a 1:100 flow-splitter which allowed for stabilized flow-rates in the low *μ*L/min range. The uniformity of the flow was continuously regulated by an automated flow-control valve changing the backpressure of the splitter waste line to compensate for minor changes in column backpressure.

The instrument was fitted with internal UV-detection, which required the analyte composition to be changed to UV-absorbing species. The micro LC system did not permit hydroxide eluent generation, therefore a 60 m*M* KCl solution was chosen as the eluent, which further improved the lifespan of the fused silica capillaries and allowed for direct UV-detection to be employed. The chromatogram of five standard anions is shown in Figure 3.6. Chromatographic results for nitrate were reasonable, with measured plate counts of up to 26,000 plates/m, which was a considerable improvement on previous work [75] and on par with commercial polymer monolithic columns of larger format [152].

To date, the post-modification of CMS monomer with thiobenzoic acid reported here is the only reactive pathway that yields a functional polymer monolith with complete monolayer coverage of latex nanoparticles.

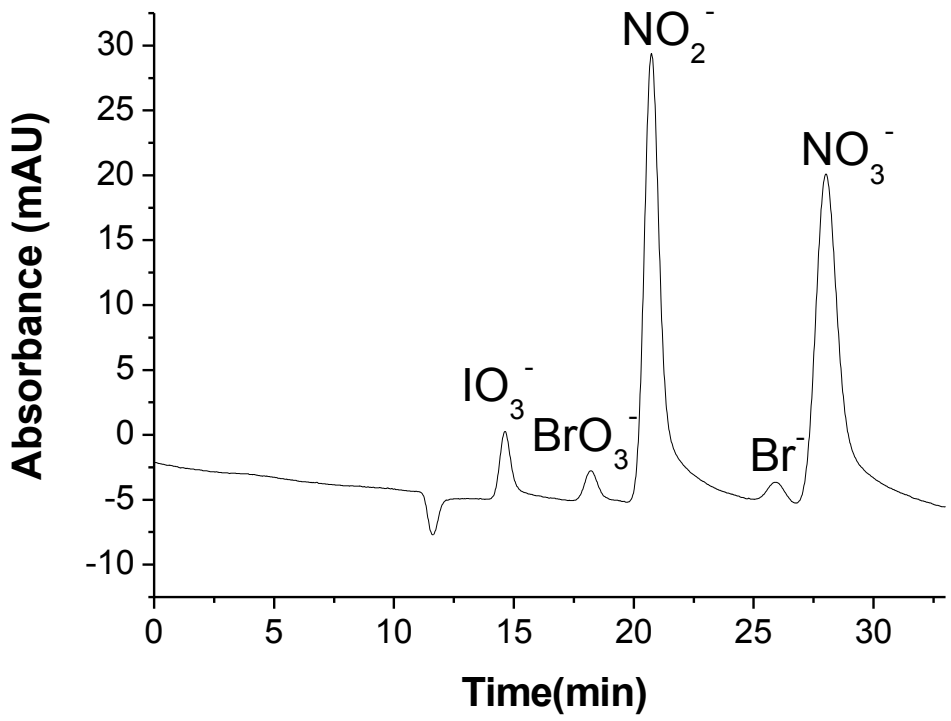

Figure 3.6: Separation of 5 anions using UV detection. Conditions: Eluent 60 m*M* KOH; Column: Cap 10 (250 *μ*m *i.d.* × 20 cm sulfonated CMS-DVB, coated with AS18 latex nanoparticles); Flow-rate: 2 *μ*L/min; Injection volume 1 *μ*L.

3.3.5 Column Characterisation

Column characterisation via SEM imaging of the capillary cross-section is shown in Figure 3.7. The extent of the latex monolayer coverage and the presence of a uniform morphology is slightly surprising based on the average performance of the column as shown earlier (Figure 3.6). One possible reason for the lower than expected separation efficiency is a result of the open flow morphology of the substrate, which exhibits good flow-through properties on the one hand, but in turn does not allow enough time for ions to diffuse to the monolith surface and interact with the latex particles.

Figure 3.7: SEM of Cap 10, AS18 coated, sulfonated poly(CMS-*co*-DVB) monolith.

Better results were achieved when the flow-rate was reduced. Further characterisation studies were undertaken to evaluate the column performance in relation to the material flow-through properties and functional group distribution. Van Deemter plots for iodate and bromate are shown in Figures 3.8a and b, respectively. Unlike separations of these analytes in silica type monoliths [28, 50] or separation of larger ionic analytes in functionalised polymer monolithic columns, the optimal performance at relatively low flow-rates deteriorated very quickly with linear velocity above 0.2 mm/s in both cases. Kinetic performance at higher flow-rates was also found to decrease in commercial polymer monolith columns of larger format, however it was not as pronounced [152-153].

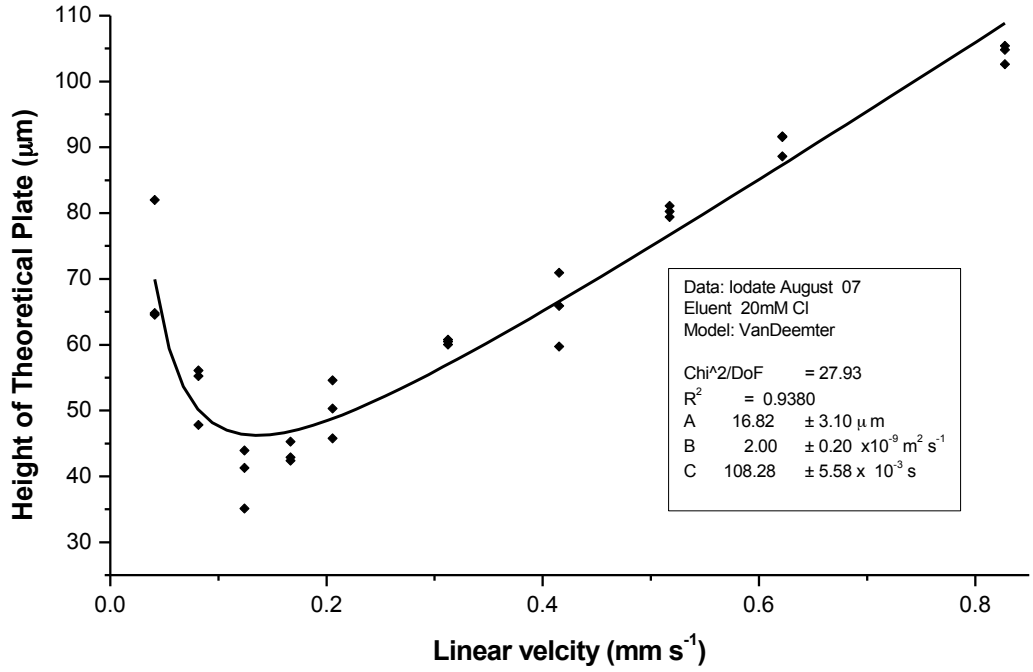

Figure 3.8a: Van Deemter plot for Iodate. Conditions: Length of monolith 287 mm. Flow-rate (0.1-2.0 *μ*L/min) T= 35 °C, n=3. Eluent: 20 m*M* KCl. Curve fitting with Origin.

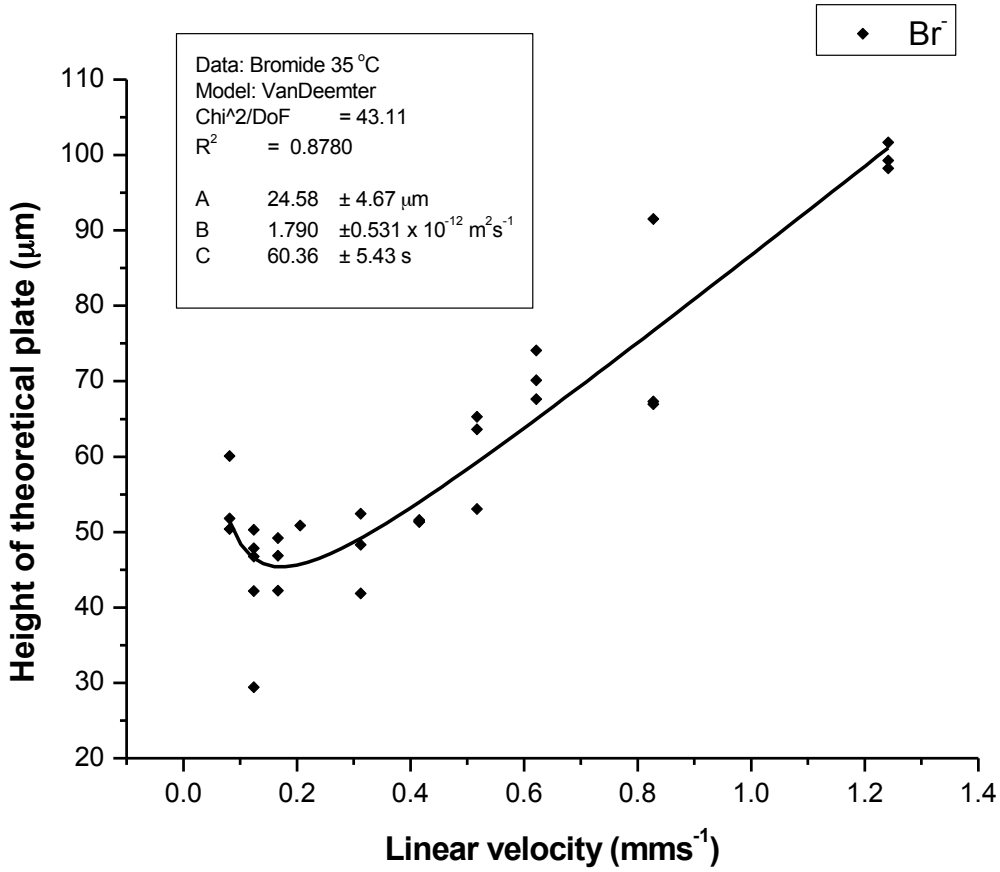

Figure 3.8b: Van Deemter plot for bromate. Conditions: Length of monolith 287 mm. Flow-rate (0.1-2.0 μL/min) T= 35 °C, n=3. Eluent: 20 m*M* KCl. Curve fitting with Origin.

Capacity measurements of the column were performed by displacement of chloride ions with nitrate, as shown in Figure 3.9. The average time taken for breakthrough to occur was 83.87 min (n = 3), with RSD = 14.0%. The ion-exchange capacity of the column expressed per gram of monolith was estimated at 34 *μ*equiv/g using an average porosity value of 70% and a mean density for the solid material of 1.2 g/mL.

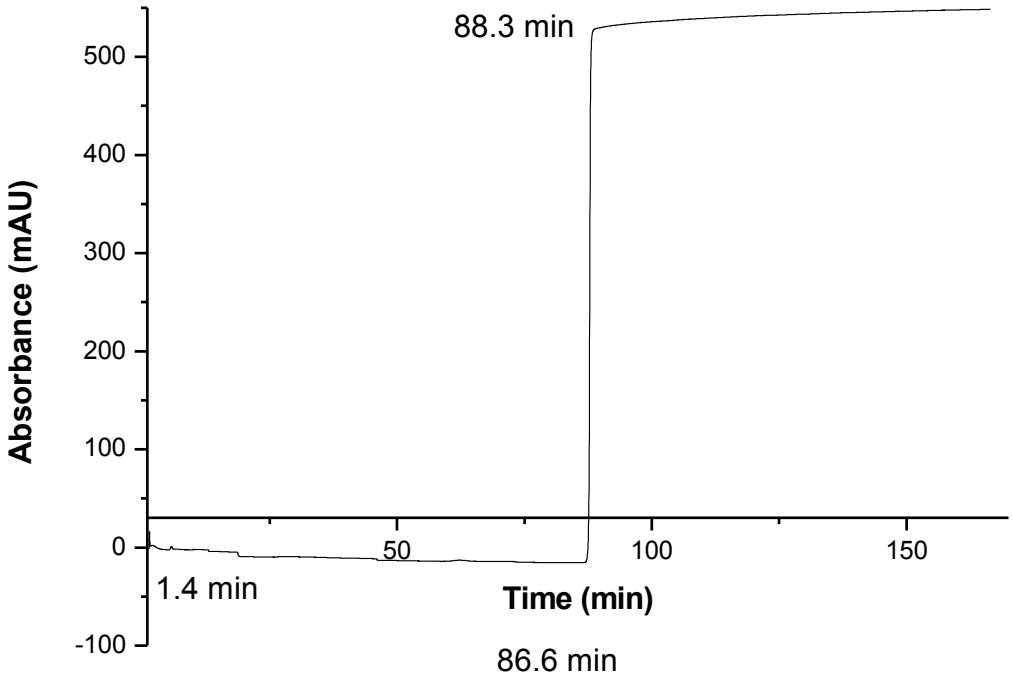

Figure 3.9: Breakthrough of nitrate ions. Conditions: Eluent: 1.0 m*M* KNO_3 (aq), flow-rate 2.0 *μ*L/min. Detection by UV diode array detection at 215 nm.

In an early publication by Slingsby and Pohl [150], capacity figures for latex-coated particle-packed columns were listed at up to 24 *μ*equiv/column. The Dionex website [154] lists figures of 2.85 *μ*equiv for an IonPac® AS18 Anion-Exchange 0.4 × 250 mm capillary column. Porosity measurements of the unmodified styrene scaffolds indicate macropores of around 1-2 *μ*m, with surface area values of around 30-100 m^2/g.

The results presented here are predominantly based on traditional chromatographic assessments of ion-exchange stationary phases coupled with more technical characterisation techniques such as SEM, BET and porosimetry. In Chapter 4 the use of a non-destructive assessment technique is discussed with the aim of providing a direct measurement of the polymer monolith synthesis and modification completion in the individual capillary column manufacturing steps, prior to testing the chromatographic performance of the column.

3.4 Conclusions

The aim to establish a monolith synthesis and post-modification protocol for the development of a monolithic substrate with the correct morphology and functionality to yield complete monolayer coverage of latex nanoparticles has been successfully realized. The synthesised capillary columns were examined by SEM to visualise the extent of the coverage and were tested for their chromatographic performance using a mixture of small inorganic anions. The reliance on the success of the latex coverage on the porous substrate suggests a requirement for some external form of characterisation, to provide

a degree of feedback during the column synthesis and thereby help to improve the success rate of the latex-coated monolith fabrication.

The original aim of this study was to consistently achieve the best monolayer coverage of latex nanoparticles on the polymer monolith substrate surface, which was expected to rival traditional latex-coated packed particle columns in terms of selectivity, while simultaneously offering the advantages of monolithic formats, such as reduced backpressure and better mass transfer at higher flow-rates.

Complete and reproducible monolayer coverage of latex nanoparticles was achieved, with efficiencies of 16,000 to 26,000 plates/m for a range of UV-absorbing anions. This represents a significant improvement over previously published results for monolithic columns, but falls short of the performance achieved by traditional packed particle columns. These results do not challenge silica or particle type counterparts with regard to speed or efficiency. Nevertheless, the results show significant advances in the latex coating of polymer monolith scaffolds.

The separation performance of these latex-coated styrene-based polymer monoliths is to date the best reported for small anions analysed on functional polymer monoliths. The fact that silica-based monoliths and the commercially available particle-based columns still outperform monoliths in this area suggests that further inspection of the morphologically inherent properties of styrene-based polymer monoliths is required. Typical flow-related advantages of monolithic columns have not been apparent in this system, which suggests a strong interaction between the type of analytes and the morphology of the porous polymer structure. The chromatographic

separation of small molecules is generally more diffusion driven, such that the benefits of convective mass-transfer properties in porous polymer monolithic materials with irregular morphology are negated by non-uniform flow-profiles through the porous scaffold. Polymer monoliths still require extensive research and development to tailor the wide variety of properties available to suit the system at hand. It has become apparent in this study that taking something that works in one system (latex-coated, sulfonated poly(styrene-*co*-DVB) particles) and applying it to another (latex-coated, sulfonated poly(styrene-*co*-DVB) monoliths) does not necessarily achieve the results anticipated. While the initial goals included the development of a better monolithic porous polymer material in direct comparison to the currently available latex-coated particle columns for the separation of small inorganic analytes, the course of research has revealed some of the advantages and disadvantages of polymer monoliths in relation to small molecule chromatography and that the inherent flow and mass transfer properties of the materials tested herein may be more suited for larger ionic analytes.

Ongoing research is investigating not only different types of latex particles to better address the nature of small inorganic analytes, but also addressing different scaffold preparations with specifically tuned porous structures [91]. Further development of non-destructive assessment techniques that provide step-by-step feedback on the manufacture of the capillary column prior to chromatographic performance testing will also be undertaken. These techniques are potentially useful for monitoring capillary column manufacture in industry.

4 Non-invasive inspection of columns using C^4D

4.1 Introduction

In recent years capacitively coupled, contactless conductivity detection (C^4D) has gained popularity for universal on-column detection in capillary electrophoresis (CE) and related chromatographic techniques, partially attributable to the limited range of detection techniques available for such capillary systems for non-UV absorbing ions [123]. When compared to conventional contact conductivity detection, further advantages of C^4D include the possibility of on-column, low interference detection and non-invasive inspection.

The basic principles of C^4D as a viable detection alternative in CE and related techniques are well described in reviews by Guijt [155] and Zeeman [156]. Prior to the commercial availability of a C^4D instrument, a comprehensive study into the effects of cell design, frequency variations, amplification voltage, stray capacitance and a number of other parameters affecting the conductivity readings was published as a two part series by Hauser and Kuban [157-158]. The operational principles of C^4D are discussed in more detail in Section 4.3.2 of this chapter.

Since the original independent development by both da Silva [159] and Zeeman [160] of a simple C^4D setup and the subsequent availability of a commercial capillary C^4D instrument, a rapid increase in publications utilising this detection method has been noted [161]. The two most commonly used, stand-alone commercial instruments (TraceDec from Istech, Austria and C^4D

by eDAQ, Australia) both consist of a main instrument unit that connects to an external sensor head and offers both analogue and digital signal outputs. Besides the intended use of the C^4D instrument as a fixed detection unit for capillary chromatography, recent publications have reported the facilitation of C^4D in the non-invasive inspection of surfactant-coated monolithic scaffolds in fused-silica capillaries [122] and for measuring the pH-dependence of boronic acid functionalised zones in polymeric capillary columns [133].

Inspection of the longitudinal homogeneity of the monolithic structure and grafted zones in a capillary column format was undertaken by Connolly *et al*. [131], where conductivity measurements were taken at manually adjusted 1 mm increments along the capillary to demonstrate the difference between UV-initiated polymerised and unpolymerised (shielded during radiation) capillary sections. After flushing of all porogens and rinsing of the partially monolith filled capillary with deionised water at 1 μL/min, the sections containing the porous polymer monolith yielded signal zones of lower conductivity, whereas the empty capillary sections responded with higher conductivity readings. Since the signal output is relative to the volume of conducting eluent (the main conducting medium in non-functional columns), which is inversely related to the presence of the porous polymer substrate, the location of the shielded, material void capillary section could be directly measured.

Deionised water can be considered as an adequate conducting medium for use with non-functionalised polymer scaffolds due to the polarity and auto-dissociation properties of H-O-H, responding adequately in the alternating electric field. The authors performed subsequent C^4D inspection

of photografted zones on an otherwise plain monolithic scaffold, with an increase in the recorded signal correlating with the presence of these templated functional groups at specific masked locations [131]. The increase in conductivity over these zones was a direct result of the functional group ionisation in water, easily detectable by C^4D. In conclusion, the authors suggested that this technique has the potential to serve as a simple means to determine ‘zone capacity'.

A TraceDec C^4D instrument was used for this work and the parameter settings were chosen according to instrument specifications (Frequency 3xHigh, Amplification Voltage -12 dB, Gain 50% and Offset 0). The TraceDec manual suggests the use of higher frequency settings with larger *i.d.* capillaries and the reduction of amplification voltage and gain (particularly in the case of signal overflow), consequently the measurements were of lower resolution. Nevertheless, these measurements demonstrated the feasibility of the technique to detect gross differences in substrate homogeneity.

Manual detector handling to obtain point-based readings as well as the lack of parameter optimisation are currently the main limitations of the technique. These establish the need for further investigations to confirm the viability of C^4D as a quality control technique for porous polymer capillary columns. In a recent review [117], a number of publications and previously unpublished results were presented, in which monolithic polymer capillary columns were assessed by sC^4D, with the resulting conductivity profile demonstrating the potential and wider applicability of this technique to characterise functional and plain porous polymer scaffolds.

As noted by Kuban and Hauser [161]: "*Conductivity detection has its distinctive characteristics, which need to be understood by the user in order to make best use of the technique. The fact that a bulk signal is measured has bearing on the optimization of the operating parameters and of the separation buffer and affects the performance of the detector.*"

Aim of this work

Having identified the necessary conditions for producing latex-coated monoliths in the previous chapter, the aim of this work was to develop strategies for non-invasive evaluation of column performance as a measure of quality control. This specifically builds on previous work in this area where factors such as the effect of changing porosity or pore size as well as correlation with separation performance were not reported.

4.2 Experimental

4.2.1 Instrumentation

The system for on-column ion-exchange analysis consisted of a Dionex Ultimate 3000 capillary HPLC, which features automatic flow adjustment in the low μLmin^{-1} range as described in Chapter 2.

For conductivity measurements, a TraceDec C^{4}D was connected to a Dionex Universal Interface and the analogue output signal recorded with the Dionex Chromeleon Software on a Windows XP operated PC.

A custom-built moveable stage controlled by two stepper motors with continuous rod screws (see Figure 4.1) allowed the detector head to be continuously moved along the capillary at speeds ranging from 1 cm/min up to 1 cm/s. The capillary column remained stationary by attaching it to a syringe (Hamilton) in a syringe pump (Harvard Instruments). Due to the capillary immobilisation, the detector head was unable to assess the first 2 cm of the attached capillary.

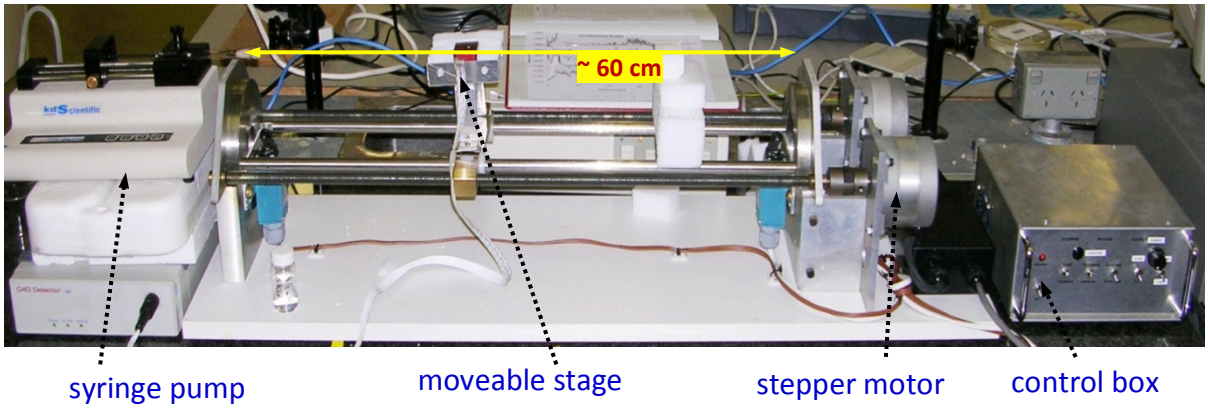

Figure 4.1: A motorized stage allows the C^4D unit to be pulled along the capillary at a rate of 1 cm/min to produce a continuously recorded conductivity profile.

Instrumentation for SEM visualisation of latex coatings and monolithic cross-sections is described in Chapter 2. Capillary sections were cut into 5 mm lengths and dried under vacuum before gold plating the cross-sections for 200-400 s, to avoid charging of the sample with stray electrons during the SEM procedure, the thickness of which depended on the vacuum mode (low/high). The cut capillary cross-sections were immobilised onto the perimeter of the aluminium stubs using carbon tape. Scanning Electron Microscopy (SEM) Images were taken at magnifications between 2,000 to 20,000 fold.

4.2.2 Chemicals

1-propanol (99%), 1,4-butanediol (99%), 2,2'-azobis(2-methylpropionitrile) (99%, AIBN), cyclohexanol (99%), 1-decanol (99%), 1-dodecanol (98%), acetonitrile (HPLC grade), methanol (HPLC grade), toluene (99%), 2-acrylamido-2-methyl-1-propanesulfonic acid (99%, AMPS), trimethylamine hydrochloride (TMAHCl, 98% Fluka), 3-(trimethoxysilyl)propyl methacrylate (γ-MAPS, 98%), dichloromethane (99.5%) and basic alumina (Brockman activity I, 60-325 mesh) were purchased from Aldrich (Milwaukee, WI, USA). Butyl methacrylate (BuMA), glycidyl methacrylate (GMA), ethylene glycol dimethacrylate (EDMA) (all Aldrich) were purified by passage through a bed of inhibitor removal beads (Aldrich) and distilled under reduced pressure.

4.2.3 Reactive post-modification solution

The ring opening (for GMA-containing monoliths), reactive post-modification solution was made by dissolving 24.8 g of TMAHCl (trimethylamine hydrochloride >98% from FLUKA) in 50 mL of MilliQ to give a 5 M solution of clear orange colour.

4.2.4 Monolith comparison table

A summary of capillary columns prepared and used in this chapter is given in Table 4.1 below. All mixture constituents are given in % w/w relative to the total. DMPAP was used as UV-initiator and AIBN as thermal initiator, each at 1% w/w relative to monomer %.

Name	Monomer % w/w	Cross-linker %	Porogen %	Polymeris. Conditions	Dimensions	Post-mod.	Coating
Buma2 B16	BuMA 24	EDMA 16	1-Decanol 60	UV (254 nm, 15 min)	0.1 mm x 50 mm	None	None
Buma2 B27	BuMA 24	EDMA 16	1-Dec: 44 Cyclo: 16	UV (254 nm, 15 min)	0.1 mm x 50 mm	None	None
Buma2 B18	BuMA 24	EDMA 16	1-Dec: 40 Cyclo: 20	UV (254 nm, 15 min)	0.1 mm x 50 mm	None	None
Buma3 B16	BuMA 24	EDMA 16	1-Decanol 60	UV (254 nm, 15 min)	0.1 mm x 10 cm	None	None
Buma3 B15	BuMA 30	EDMA 20	1-Decanol 50	UV (254 nm, 15 min)	0.1 mm x 9 cm	None	None
Buma3 B14	BuMA 36	EDMA 24	1-Decanol 40	UV (254 nm, 15 min)	0.1 mm x 8 cm	None	None
SAX5	GMA 16	EDMA 24	1-Dec: 42 Cyclo: 18	Thermal (60°C, 22h)	0.25 x 200 mm	TMAH Cl	None
SAX13	GMA 16	EDMA 24	1-Dec: 42 Cyclo: 18	Thermal (60°C, 22h)	0.25 x 200 mm	TMAH Cl	None
SAX14	GMA 16	EDMA 24	1-Dec: 44 Cyclo: 16	Thermal (60°C, 22h)	0.25 x 300 mm	TMAH Cl	None

Table 4.1: Monolith composition for columns used in this chapter.

4.2.5 Preparation of polymer monolith capillary column

The monolith mixture was prepared by dissolving the radical initiator (AIBN) in respective proportions of monomers and porogens (see Table 4.1) and the solution was sonicated for 10 min followed by purging with N_2 for 1 min.

The surface-modified fused-silica capillary segment (modification procedure outlined in Section 2.3.3) was filled with the chosen pre-sonicated polymerisation mixture using a 250 μL Hamilton syringe. Both ends of the capillary were then sealed with rubber septa and the capillary submerged in a water bath at 60 °C for 20 h. Upon completion of the radical polymerisation step, the unreacted porogens (1-decanol and cyclohexanol) were removed

from the monolith by flushing the capillary with at least 250 μL of methanol at 1 μL/min for 6 h.

BuMA-*co*-EDMA monoliths of various pore size and porosity were prepared in 100 μm *i.d.* UV-transparent and Teflon-coated fused silica capillaries (Polymicro Technologies, Phoenix, AZ), using DMPAP (2,2-dimethoxy-2-phenylacetophenone) as the UV-initiator and irradiated at 254 nm for 15 min, then flushed with MeOH to remove porogens.

4.2.6 Surface Modification of Porous Polymer Monoliths

GMA-*co*-EDMA type monoliths were modified by firstly removing the porogens, hand-flushing the capillaries with acetone and acetonitrile (one syringe volume of each was sufficient). This was followed by flushing the monolithic capillary column with greater than one column volume of TMA HCl (trimethylamine hydrochloride) solution prepared as described in Section 4.2.3 using a 250 μL Hamilton syringe. The remainder of the syringe volume was further pumped through the porous polymer containing capillary using a Harvard syringe pump, during which the capillary was fully encased in a column heater (Phenomenex Thermasphere TS-130) at 25 °C for 6 h at 20 μL/h (alternatively the capillary was capped with rubber septa and place in a water-bath at 25 °C for 6 h). The modification procedure was concluded by rinsing the capillary column with sufficient volumes of MilliQ water (1 syringe volume minimum) over 4-5 h (at 60 μL/h).

4.3 Results and discussion

4.3.1 C^4D scanning setup

Monolithic ion-exchange capillary columns fabricated for small anion separations were initially characterised manually at discrete points using a TraceDec C^4D. Similar to the work published by Connolly [162] and Gillespie [122], a syringe pump was used to flush the porous stationary phase with MilliQ water and KCl solutions, while a 60 cm metal ruler served as a guide to adjust the position of the detector head at 1 cm increments. The resulting conductivity measurements were recorded once the signal had stabilised and the procedure was repeated over the entire length of the capillary. Figure 4.2 illustrates the incremental conductivity measurements along the unmodified CMS-*co*-DVB monolith (a), conducted along the same capillary after sulfonation (b) and the subsequent measurements following the coating with latex particles (c). (Remove Fig 4.2a-c altogether?)

Early on, a number of inconveniences became apparent in the manual handling of both capillary and detector. Shifting of the detector head at 1 cm increments by hand required a signal stabilization period of around one minute. Furthermore, the reproducibility of the readings was found to be relatively poor, with significant variations in signal output being recorded over subsequent measurements, evident in the size of the displayed error bars. Besides the difficulty of manually locating the same discrete points of measurements, some of these variations were also attributed to temperature influences incurred by the manual handling, secondary static electrical effects and surface contaminations.

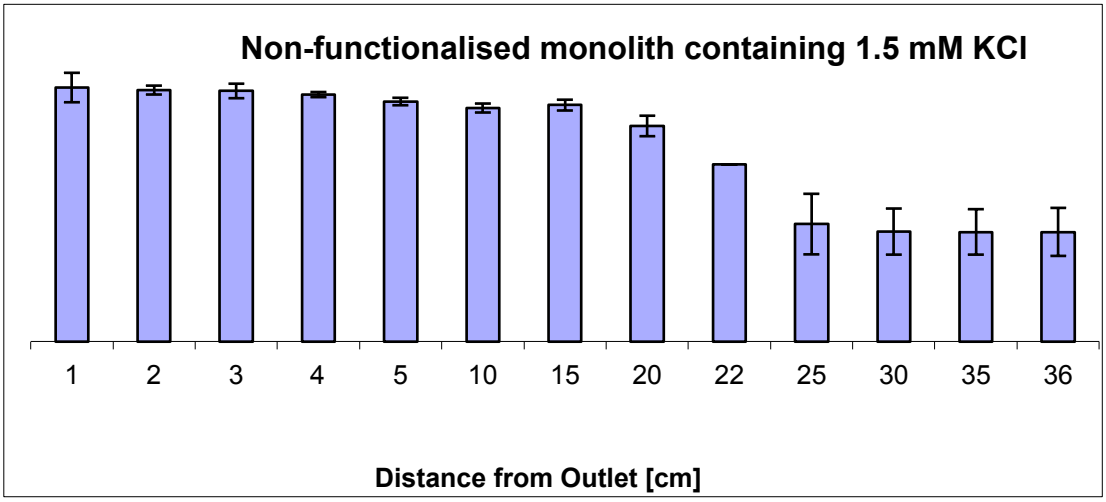

Figure 4.2a: Measurements were initially made by manually moving the C^4D detector along the capillary column (average values from 3 successive measurements).

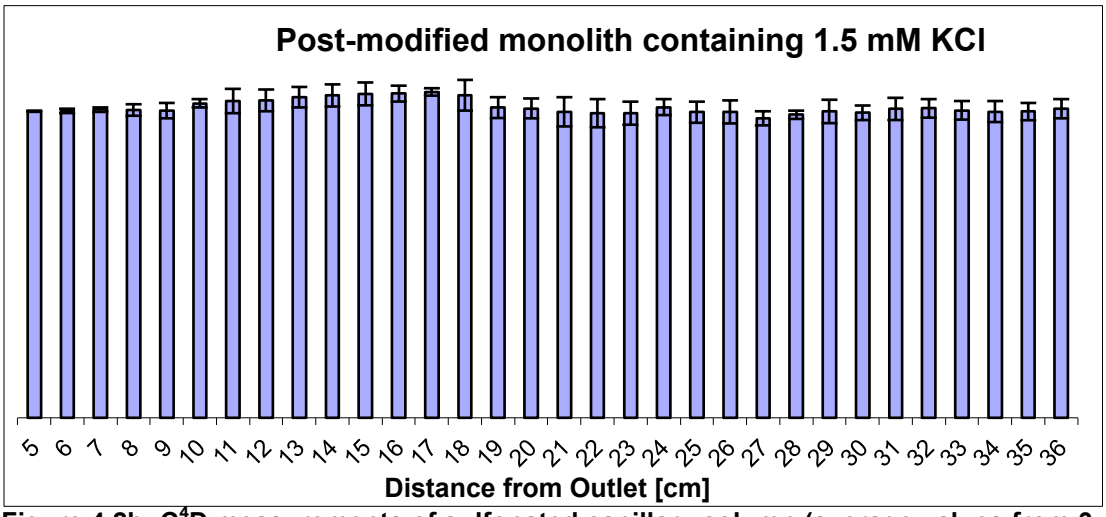

Figure 4.2b: C^4D measurements of sulfonated capillary column (average values from 3 successive measurements).

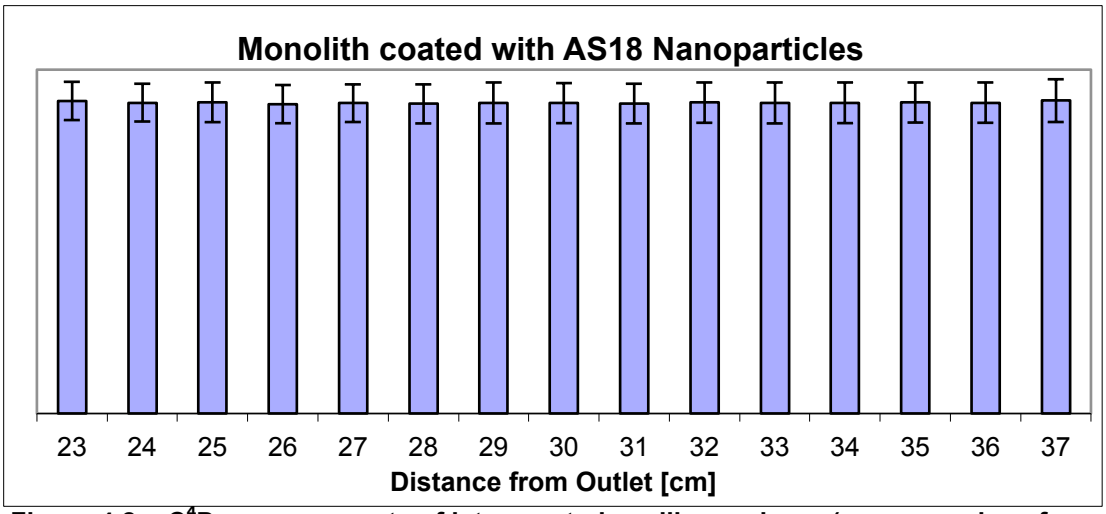

Figure 4.2c: C^4D measurements of latex coated capillary column (average values from 3 successive measurements).

As a result, an automatic approach was considered as the critical next step for a systematic evaluation of the signal composition to better understand the origin of the signal variations occurring over a number of repeated scans.

Figure 4.2d illustrates the comparative conductivity profiles of automated, continuous vs. manual conductivity-scanning of a 100 *µ*m *i.d.* fused silica capillary filled with MilliQ water. The profiles are both generated in continuous recording mode at highest detector sensitivity, with the conductivity signal of the continuous set-up displayed in red above the blue profile recorded by manual shifting of the detector head in 1 cm increments during continuous recording of the conductivity response.

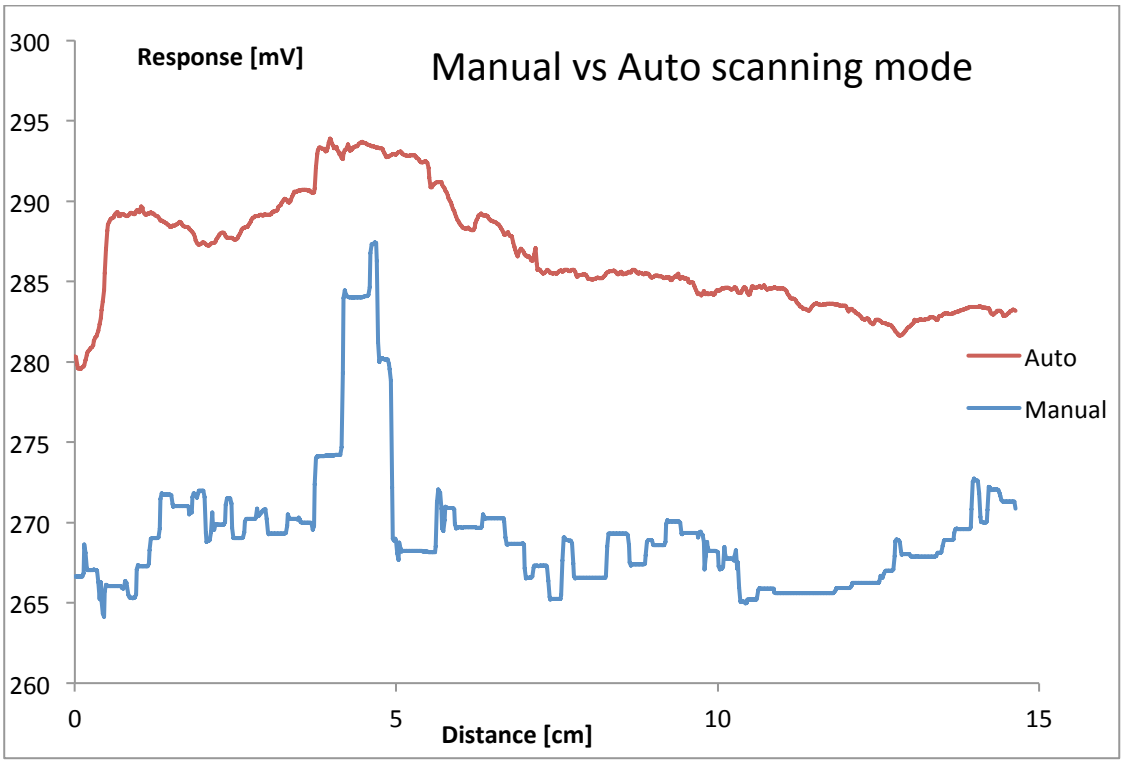

Figure 4.2d: MilliQ filled 100 *µ*m *i.d.* fused-silica capillary scanned continuously in automatic (red) and manual (blue) mode. TraceDec settings at maximum sensitivity: Frequency 3xHigh, Full Amplification (0 dB), Gain 200%, 0 Offset.

Further detector interferences were also addressed, such as static noise from the syringe pump during capillary flushing procedures and the drifting of the conductivity signal at a stationary point on the capillary over time. It was concluded that pre-flushing of the capillary before rather than during the scanning procedure resulted in the most stable and reproducible signal profiles.

4.3.2 Theoretical Model

Connolly *et al.* have successfully demonstrated the differences in conductivity response of empty and filled capillary sections using C^4D [162]. The utility of this technique to determine more subtle discontinuities in the stationary phase beds however has not yet been fully explored. Whilst C^4D is reasonably mature as a detection technique for ions, with the optimum analyte detection parameters well described in the literature [160], the same optimisation has not been undertaken for the stationary phase scanning applications of this detector as a characterisation technique.

In order to optimise the system conditions and instrument parameters for optimal signal-output capable of detailed morphological assessment of chromatographic columns, a theoretical model was developed to gain a more comprehensive insight into the workings of the C^4D instrument. This required separate assessment of the capacitive and resistive components in the electric circuit in relation to the physical configuration of the scanned capillary column. For example, changes in capillary internal diameter were found to affect capacitive coupling of the electrodes as well as axial resistance, which is reflected in the overall conductivity signal.

The theoretical impedance model is based on the TraceDec instrument configurations, as measured with an oscilloscope, to model the electrical configuration of the detector unit. The instrument is configured with a 10 V output voltage over the range of frequencies as selected in the main unit panel in parameter settings. 38 kHz (Low), 76 kHz (Medium), 153 kHz (High), 306 kHz (2xHigh) and 612 kHz (3xHigh) can be chosen.

The sensor head is made up of an approximately 3x2x1 cm aluminium box encompassing two small ring electrodes around an inner tube, which allows for capillaries of 350 *μ*m outer diameter (*o.d.*) to slide through. The physical make-up of the ring electrodes inside the detector head are illustrated in the schematic of Figure 4.3. The width of the ring electrodes for the TraceDec instrument is listed as l = 1 cm and the distance between the inside edge of the electrodes is d = 0.8 mm, with a shielding electrode placed in between (set-up b.).

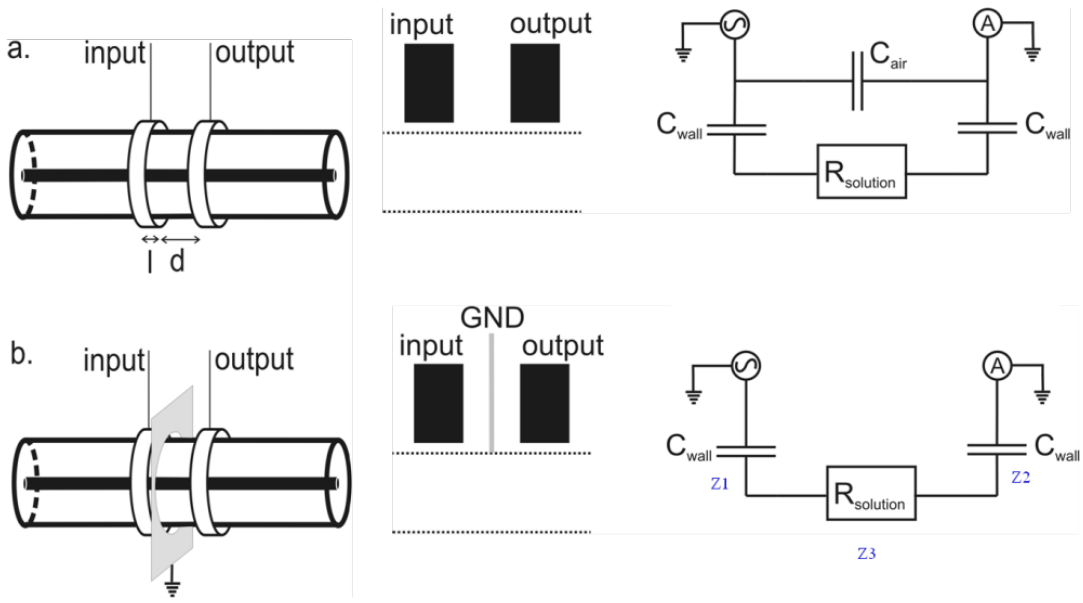

Figure 4.3: Schematic drawing of the different electrode set-ups: unshielded (a.) and shielded (b.) using a grounded plate (GND) between the two ring electrodes around the outside of the capillary to cancel out C_{air} (Reprinted with permission from [155]). Notations Z1 (= Z2) and Z3 were added to denote the individual resistive and capacitive impedances.

An oscillating (AC) voltage is applied to the input electrode and transferred through the conducting medium to the output electrode and transmitted to the main detector unit for signal processing.

The magnitude of the transmitted signal depends on the Ohmic resistance of the solution ($R_{solution}$ = Z3) as well as the capacitive (coupling) impedance of the ring electrodes with the capillary wall (Z1 and Z2), illustrated in the circuit drawing of Figure 4.3(b.). The overall impedance Z, which is inversely related to the conductivity signal response, is given as a combination of the solution resistive component and the capacitive coupling of the electrodes with the solution filled capillary and displayed in Equation 4.1 [155, 157-158].

$$\boldsymbol{Z = R_{solution} + \frac{1}{j*\pi*f*C_{wall}}} \qquad \textbf{Eqn 4.1}$$

J represents the parameters involved in AC circuits with associated phase shift, *f* the applied AC frequency and C_{wall} the capillary wall capacitance. This approximation is deemed adequate for the ground-shielded electrode set-up, which eliminates the capacitive impedance of the air outside the capillary [155]. The overall impedance (reciprocal of conductivity) is frequency dependent in relation to the capacitive reactance of the capillary material.

Although the equation can be considered a sufficiently accurate approximation for larger *i.d.* capillaries filled with conducting electrolyte (the conditions used to detect analytes), it fails to acknowledge the axial impedance of the capillary wall, generated by the direct coupling of the two ring electrodes through the capillary (and stationary phase) material. The

amended theoretical model therefore includes a fourth impedance (Z4) across the fused-silica material through direct capacitive coupling of the two ring electrodes, depicted in Figure 4.4, with the associated capacitance of Z4 expressed as $C_{wall\text{-}ax}$. Unlike the C_{air} term in the unshielded electrode set-up, the $C_{wall\text{-}ax}$ capacitance is not significantly affected by the shielding GND electrode. The impedances Z1, Z2 and Z3 are in series and can be combined into the single impedance Z5, which is parallel to Z4. The overall impedance, Z, is the reciprocal of the sum of the reciprocals of Z4 and Z5, such that Z = 1/(1/Z4 + 1/Z5) according to the equation $1/R = 1/R_1 + 1/R_2$ for the addition of parallel impedances.

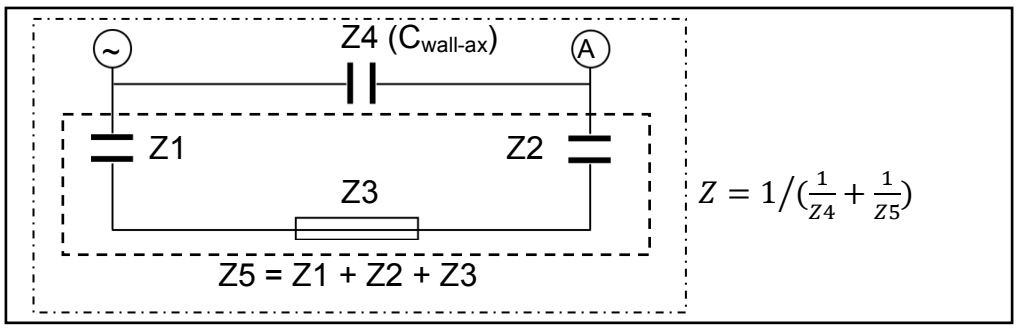

Figure 4.4: Theoretical modelling of the capacitive and resistive impedances in the detector set-up.

The resistive and capacitive components of the individual impedances were calculated by using the relative permittivity of quartz in the applied electric field. The relative permittivity of the material depends on the inherent dielectric properties and can be measured by recording the material dielectric relative to vacuum when placed in the electric field of a flat plate capacitor.

The axial capacitance $C_{wall\text{-}ax}$ was calculated by approximating the relative plate area with the cross-sectional annulus of the capillary as

illustrated in the schematic of Figure 4.5. This approximation is considered adequate since the cross-sectional annulus area forms the restricting region for the field lines to pass through, since it is considerably smaller than the plate area of the electrodes.

The calculation of the axial capacitance is based on two flat plate capacitors of annular area A (annulus of the capillary wall cross-section surface area). The corresponding equation for flat plate capacitors of area A separated over a distance d is:

$$\boldsymbol{C_{wall-ax} = 2 * \pi * \varepsilon_0 * \varepsilon_r * A/\mathrm{d}} \qquad \textbf{Eqn 4.2}$$

Where $\varepsilon_0 = 8.842 * 10^{-12}\ F/m$ is given as the absolute permittivity in vacuum and $\varepsilon_r = 4.06\ F/m$ the relative permittivity of silica (quartz) [163]. The distance between electrodes is d = 0.8 mm and for 100 μm *i.d.* fused-silica capillaries A = A_o - A_i = 9.39*10^{-8} m^2, such that $C_{wall-ax}$ = 4.22*10^{-3} pF.

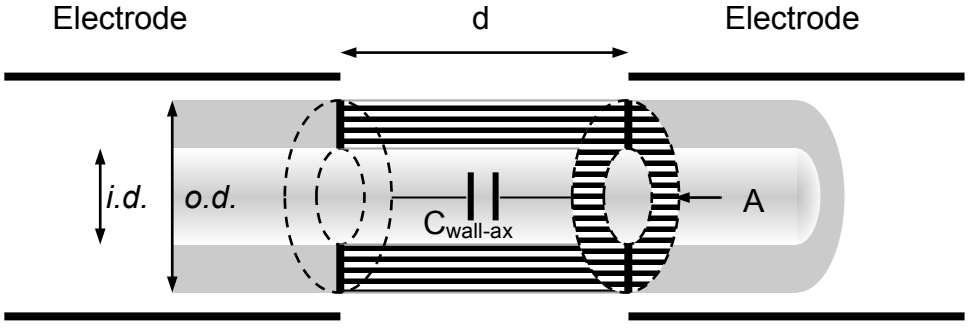

Figure 4.5: Schematic drawing of axial capillary wall coupling between electrodes over the distance d.

The variation of axial capillary wall capacitance with increasing capillary internal diameter is shown in Figure 4.6. The variation of the axial capacitive impedance Z4 with frequency is shown in Figure 4.7.

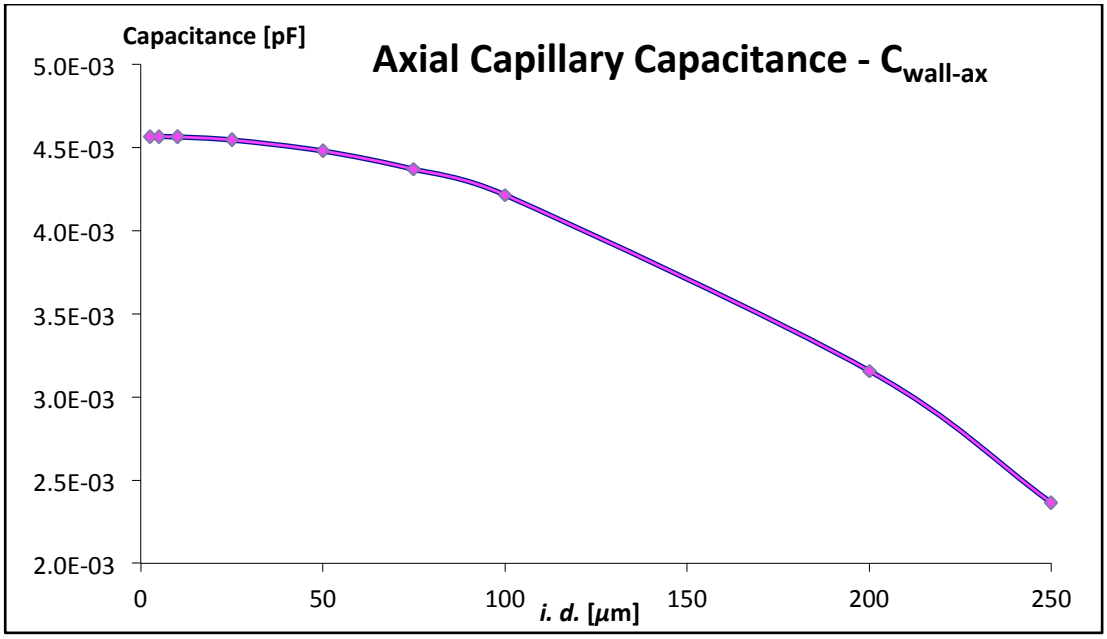

Figure 4.6: Calculated axial capillary wall capacitance ($C_{wall-ax}$) for different capillary internal diameters.

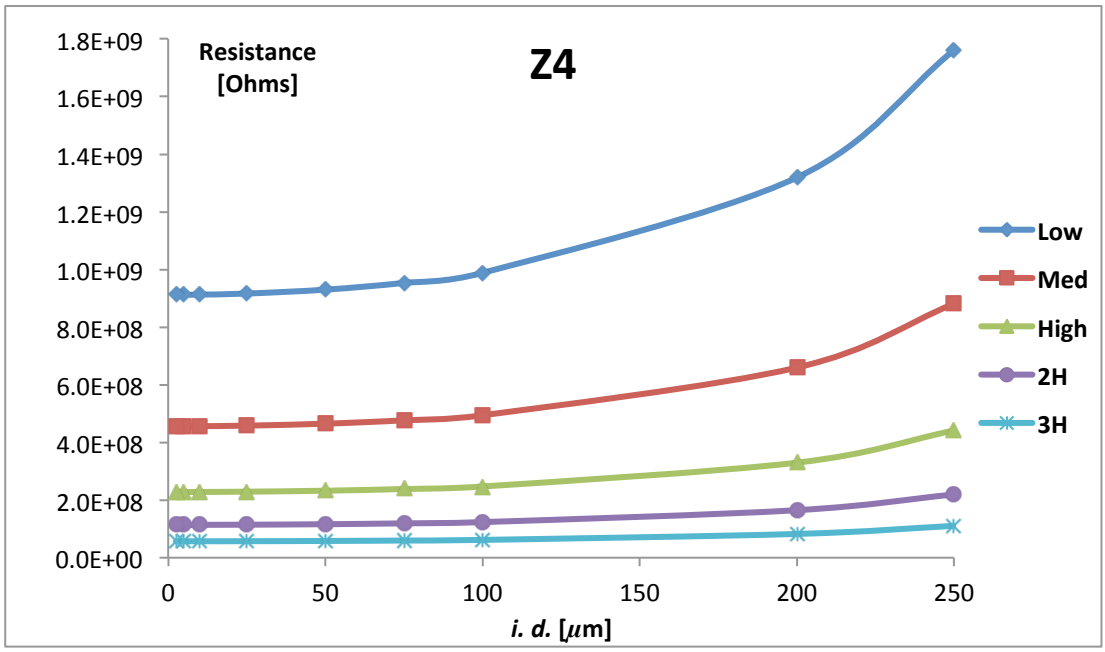

Figure 4.7: Axial capacitive impedance Z4 at Low to 3xHigh frequencies.

Axial solution impedance (Z3) was calculated as the sum of solution impedances, including the radial solution capacitance in combination with the solution resistance $R_{solution}$, which is a relationship of the solution resistivity for a given distance over the solution cross-sectional area A as illustrated in equation 4.3 below.

$$\boldsymbol{R_{solution} = \frac{\rho * d}{A} = \frac{d}{A * \sigma}} \qquad \textbf{Eqn 4.3}$$

For 100 *µ*m *i.d.* fused-silica capillary, using A = πr^2 = π*(50 *µ*m)^2 and σ = 2x10^{-4} S/m the conductance of water [163], the solution resistance is calculated as

$$R_{solution} = \frac{8 * 10^{-4} m}{\pi (5 * 10^{-5})^2 * 2 * 10^{-4}} = 1.6 * 10^9\ \Omega.$$

Figure 4.8 illustrates the combination of Z1/Z2 and Z3 for the relative surface areas of the capillary inner wall and cross-section.

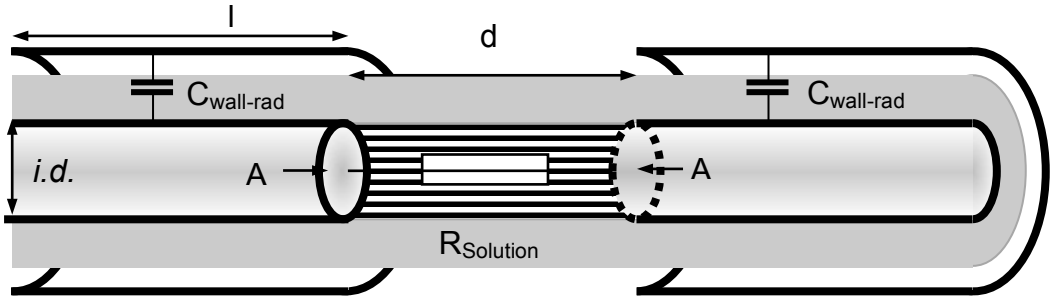

Figure 4.8: Schematic drawing of axial solution impedance and capacitive coupling of electrodes with capillary inner wall surface area over the same width l.

Z1 and Z2, the radial wall capacitance of the fused-silica capillary extends over the length of the ring electrodes and can be calculated as follows [164]:

$$C_{wall-rad} = 2 * \pi * \varepsilon_0 * \varepsilon_r * l/ln\left(\frac{o.d.}{i.d.}\right) \qquad \text{Eqn 4.4}$$

Where *l* = 0.01 m is the width of the ring electrodes, $\varepsilon_0 = 8.842 * 10^{-12}\ F/m$ the absolute permittivity in vacuum and $\varepsilon_r = 4.06\ F/m$ the relative permittivity of quartz [163].

For a 100 *µ*m *i.d.* fused-silica capillary, the radial wall capacitance is 1.761 pF, calculated with the equation for radial capacitors (Equation 4.4), using the surface area of the electrodes of length l (1 cm) and the capillary inner wall surface area over the same length l. The resulting plot of radial capacitance over various capillary diameters for a given frequency is given in Figure 4.9.

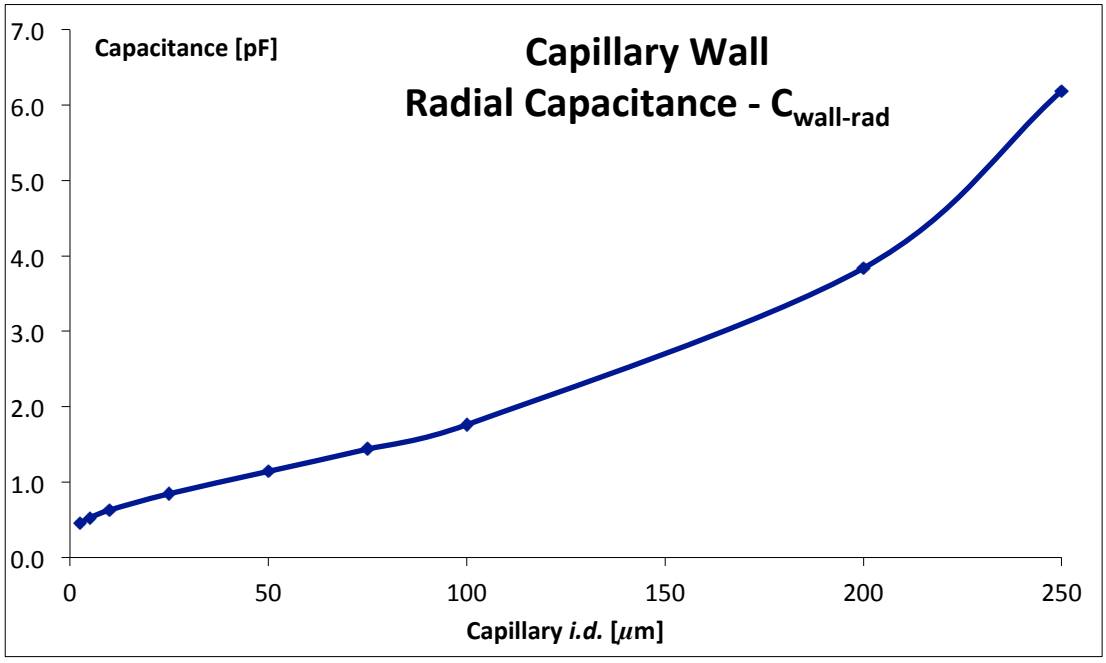

Figure 4.9: Radial Capacitance with varying capillary internal diameter.

Since the permittivity of materials depends on the frequency of the alternating electric field, the resulting impedance (Z1 = Z2) is also frequency dependent. Figure 4.10 displays the frequency dependent behaviour of Z1/Z2 over the range of capillary internal diameters. As expected the resistance across the capillary wall is reduced with higher frequencies and larger internal diameters.

Similary the individual impedances respond differently to the chosen frequencies over the range of capillary wall thickness, which relates back to the dipole moments of the material components. Figure 4.11a shows the change in individual and overall impedances for capillaries with internal diameters ranging from 2 to 250 μm at 38 kHz (Low) and Figure 4.11b the same impedances and range of capillaries at 612 kHz (3xHigh).

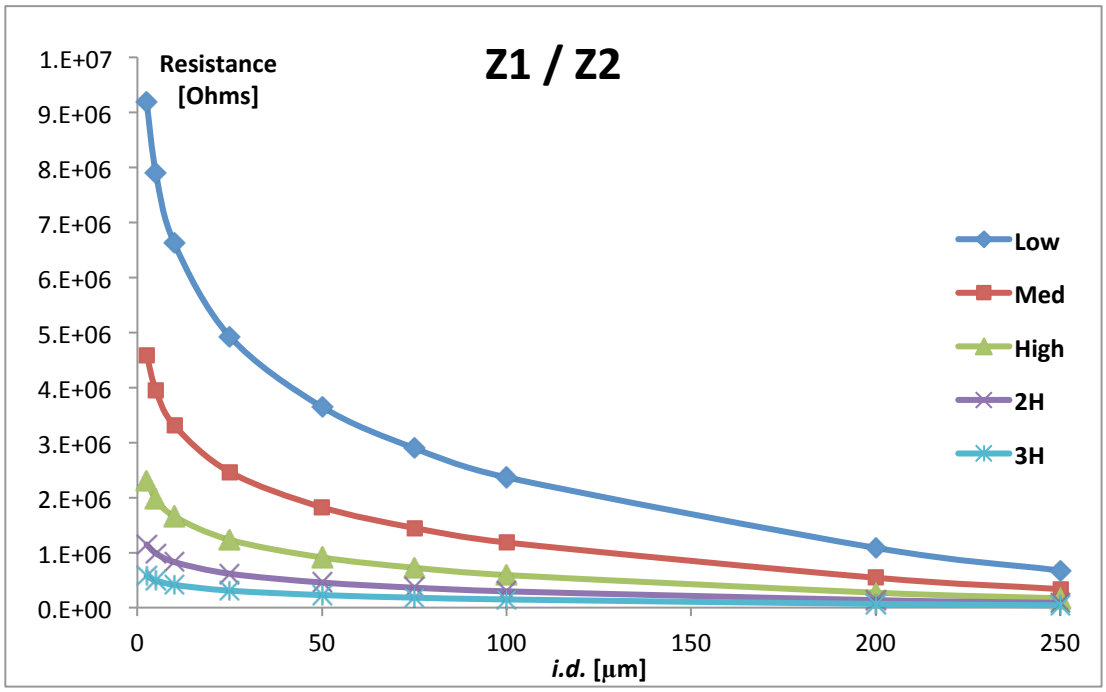

Figure 4.10: Capacitive radial wall impedance Z1/Z2 of fused-silica capillaries with varying internal diameters over a range of frequencies.

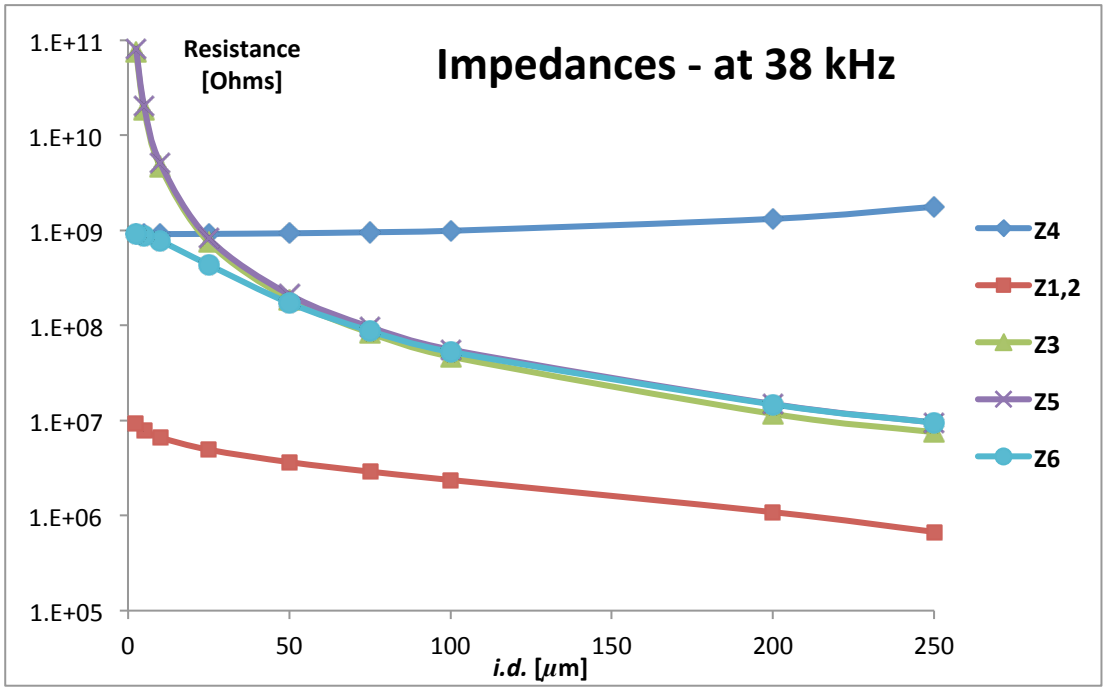

Figure 4.11a: Individual impedances Z1 - 4 and their relative influence on the combined impedance Z5 and overall impedance Z6 at Low frequency (38 kHz) for the different capillary internal diameters.

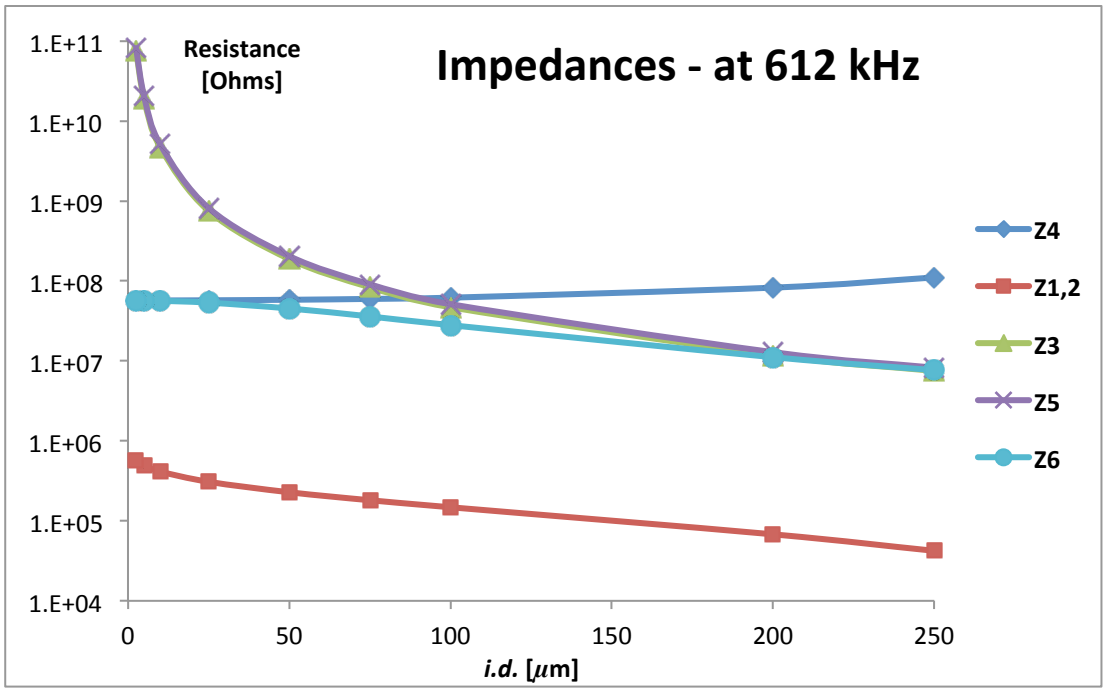

Figure 4.11b: Individual impedances Z1 - 4 and their relative influence on the combined impedance Z5 and the overall impedance Z6 at 3xHigh frequency (612 kHz) for the different capillary internal diameters.

In theory, the separate capacitive and resistive components have complementary or opposing effects on the signal output depending on physical and chemical arrangements. In low conductivity conditions, material (physical) properties are predominant, such as stationary phase (porosity) and capillary dimensions. If functional groups on the material surface provide 'films' of higher conductivity, then the physical properties of the substrate material may be dominated by the response of the lower resistive component of the surface film. In summary, the model separately assessed capacitive coupling of the electrodes and the solution, coupling between electrodes and capillary wall as well as the axial resistance of the stationary phase and of the solution itself. The theoretical signal response is given as a function of solution resistance at a given frequency and is shown in Figure 4.12.

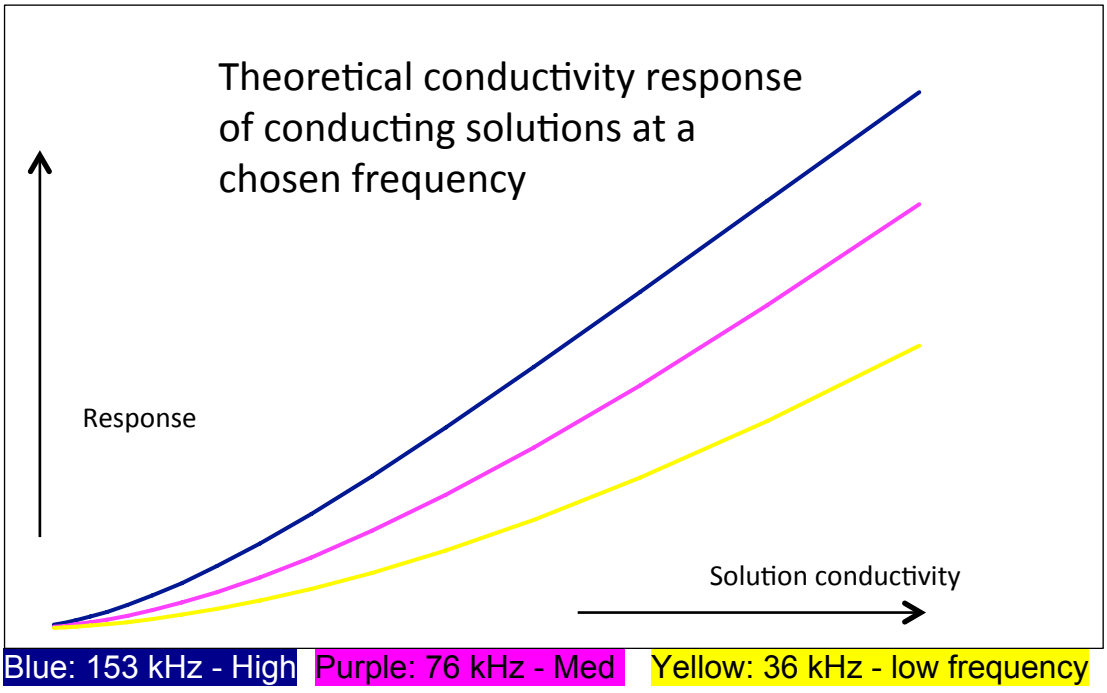

Fig 4.12: Theoretical model predicts a stronger increase in conductivity response with higher frequencies (as observed in the practical measurements, minus the C_{wall} - term generated by the silica material).

4.3.3 Experimental Validation

The model was experimentally validated using small *i.d.* capillaries filled with MilliQ and KCl solutions of increasing concentrations (0.2 – 100 m*M*), which were measured with a conductivity meter for comparative purposes on conductivity readings. The instrument parameter settings allow for arbitrary choice of Input Frequency, Amplification Voltage, Gain and Offset to adjust the detector response, yielding measurements over a broad range of conductivities.

The relationship between capillary wall capacitance C_{wall} and the solution resistive component ($R_{solution}$) resulted in an increase in detector response with increasing solution conductivity (= 1/R) over the range of frequencies (3xHigh = 612 kHz, 2xHigh = 306 kHz, High = 153 kHz, Medium = 76 kHz and Low = 38 kHz) as demonstrated in Figure 4.13. MilliQ water and low concentration KCl solutions exhibit a gradual rise in conductivity response early on for the lower frequencies. For measurements conducted at higher frequencies, no change in the conductivity signal is observed for MilliQ water and dilute KCl solutions, until moderately conducting solutions (1 m*M* KCl or greater) are introduced into the capillary. As illustrated in the enlarged lower conductivity graph, not only the capillary wall capacitance (y-intercept) varies with the chosen frequency, but also the response to solution conductivity, which is delayed further for higher frequencies, increasing more rapidly once the solution response overrides the capillary wall capacitance.

Consideration of very small *i.d.* capillaries with significant silica wall material relative to the capillary lumen, means that the capillary wall

capacitance, C_{wall}, forms a dominant component in the overall impedance when using higher frequency, AC input voltage.

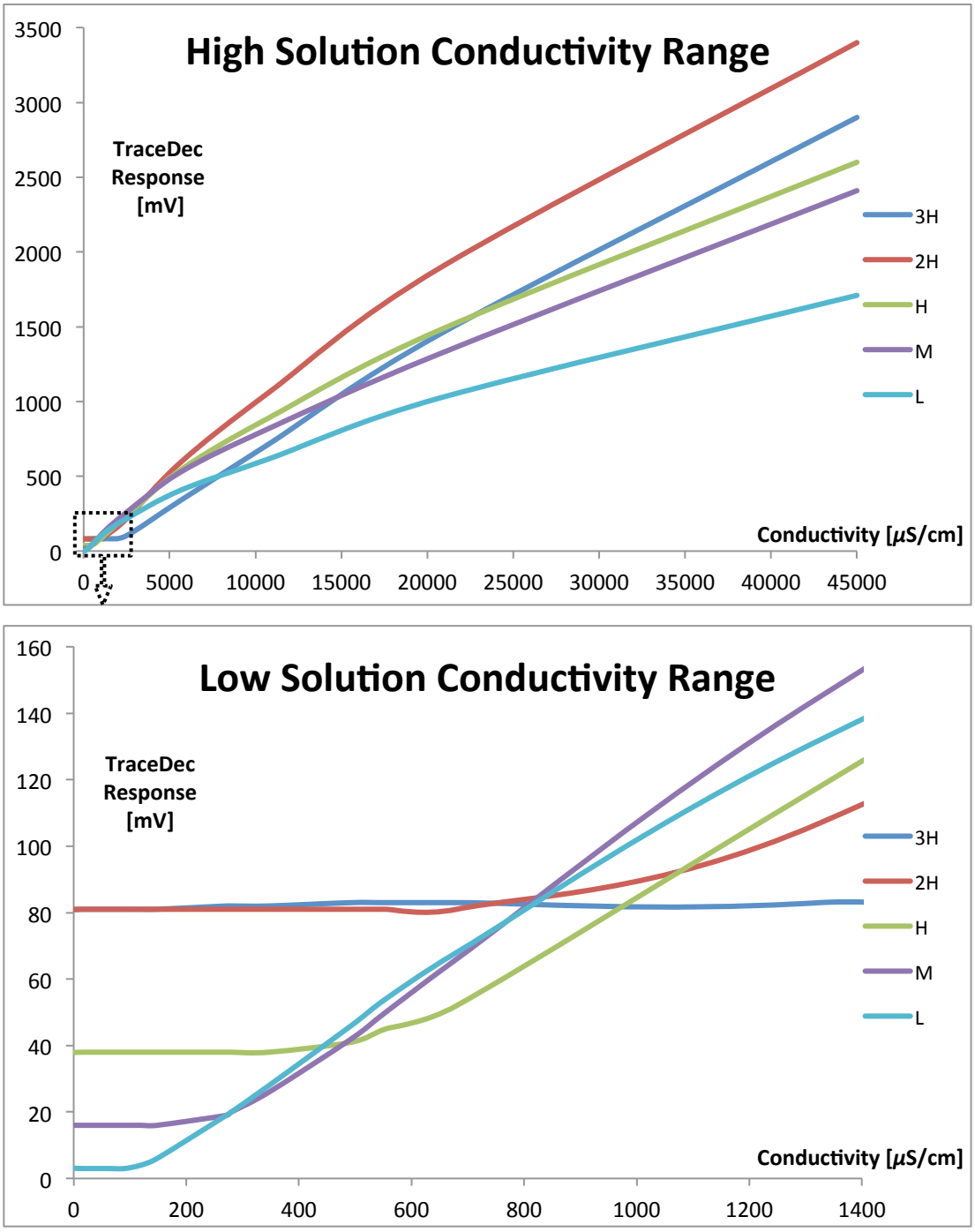

Figure 4.13: TraceDec response of 5 µm *i.d.* capillary flushed with KCl solutions ranging from 0.2 m*M* to 10 m*M* (expressed in relative conductivity readings). Profiles illustrate the different C^4D signal response at the respective frequencies (L=Low, M=Medium, H=High).

This is further illustrated in Figure 4.14, where the capacitive component of empty capillaries of various internal diameters (*i.d.*) is measured over a range of frequencies, with both the 2xHigh and 3xHigh frequencies initially exhibiting the same wall capacitance for the smaller *i.d.* capillaries, before crossing over for capillaries with internal diameters above 75 μm.

While the fused-silica material is technically non-conductive, it has a considerable dielectric constant, such that the polar nature of the material allows for temporary distortion of the dipole in the alternating electric field. The relaxation of the distorted dipole moment of the silica material reduces the capacitance of the fused-silica capillary wall, which is more evident at the lower AC frequencies. The capacitive effects of the silica capillary wall is evident in the radial coupling from the electrodes to the lumen (capillary internal) and the axial coupling between the electrodes through the capillary walls (in parallel with the solution).

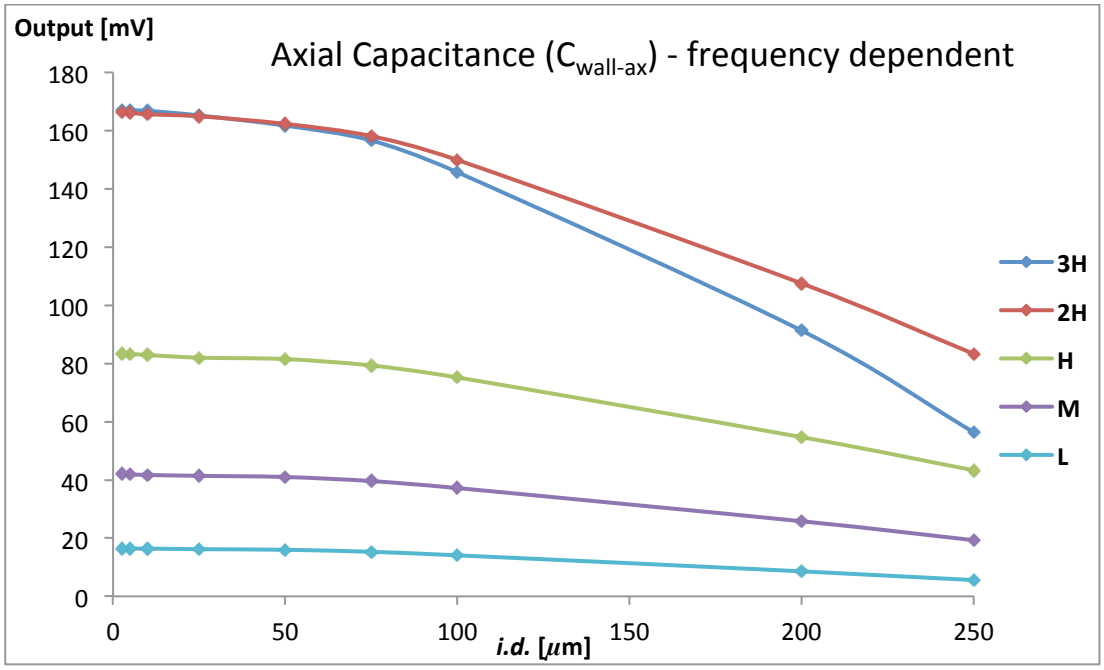

Figure 4.14: Capillary wall capacitance C_{wall} of empty fused silica capillaries with various internal diameters, using the TraceDec C^4D – Signal response is relative to the volume of silica material (= cross-sectional area / annulus).

Note: *If a capacitor is driven with a time-varying voltage that changes rapidly enough, then the polarization of the dielectric cannot follow the signal. As an example of the origin of this mechanism, the internal microscopic dipoles contributing to the dielectric constant cannot move instantly, and so as frequency of an applied alternating voltage increases, the dipole response is limited and the dielectric constant diminishes. A changing dielectric constant with frequency is referred to as dielectric dispersion, and is governed by dielectric relaxation processes, such as Debye relaxation.*

Several strategic experiments were designed to separately evaluate the parameters of the conductivity sensor and to assist in the validation of the conductivity technique as a quality control tool with the aim to reliably predict the separation performance of an axially profiled capillary column by scanning C^4D. The mathematical model of the sensor illustrates the frequency dependence of the output voltage, as a combination of capacitive reactance (radially and axially) and the axial resistive coupling of the solute (and substrate). The model addressed the various impedances in the electronic circuit to predict the signal response. The theory was tested with practical conductivity measurements in smaller *i.d.* capillaries filled with KCl solutions of different concentration, one of which is shown earlier in Figure 4.13. Capillaries with internal diameters of 2-10 *μ*m exhibited the same trend. The different y-intercept of each frequency is indicative of the axial capacitive coupling of the electrodes through the capillary wall, which was more pronounced at higher frequencies.

For the lower frequencies, the axial C_{wall} 'interference' is less pronounced, thus the measurements on lower conducting solutions produce

an earlier rise. Furthermore, the smaller the internal diameter of the capillary, the lower the radial capacitive coupling, since the plate distance between electrode and the capillary inner wall is increased and the surface area of the inner wall 'plate' is dramatically reduced. This leads to an overall low sensor conductance at low frequencies and a consequent faster rise in signal response for the higher frequencies in higher conducting solutions.

The idea behind testing such small *i.d.* capillaries was to investigate if there is a specific concentration range at which different pore size materials can be discerned – referring to a range in solution conductivity, where the magnitude in signal change can differentiate between the pore sizes (discontinuity over the same average porosity) of such materials based on the distance of solution filled pores relative to the electrodes. However, measurements on a non-uniform monolithic capillary column showed that higher conducting eluents only decrease the resolution of the scanned porous polymer profile, compared to lower conducting eluents such as MilliQ, which allow for more sensitive detection parameters.

Having identified the necessary conditions for optimum scanning C^4D performance, this work extends on the previous results in this area to determine the limitations of this approach for the assessment of column properties. The scanned capillary axial conductivity profiles provide information on the

- Average stationary phase material porosity;
- Capacity (presence of ionisable functional groups);
- Surface area variations of functional substrates.

Whilst each of these factors cannot be considered in isolation and every conductivity profile of a functional capillary stationary phase is always a combination of the above-mentioned properties, the relative influence of each factor was systematically investigated. Only a plain, non-functional material substrate can yield conductivity profiles that reflect the morphological continuity alone, where the signal response is predominantly related to the average porosity filled with the conducting mobile phase.

Evaluation of the combined porosity, capacity and surface area profiles could potentially be related to separation performance. Physical characterisation by scanning electron microscopy (SEM) can either confirm or extend the evaluation of the conductivity profiling. A combination of uniform porosity, high capacity and surface area of the monolithic substrate is an indication for a high efficiency anion exchange capillary column.

4.3.4 Scanning Porous Polymer Substrates

To further examine this argument, three different, well-studied BuMA-*co*-EDMA recipe mixtures of different (interglobular) pore size but identical porosity (60%) were prepared. Using a 15 cm piece of 100 *μ*m *i.d.* capillary (labelled Buma2), the three different solutions were introduced as 5 cm sections in progressive order (B16, B27 and B18) and polymerised using UV irradiation. After flushing of the porogens with MeOH and subsequently MilliQ water, the scanned capillary sections showed no noticeable zone differences in the conductivity profiles, as illustrated in Figure 4.15. This result confirms the theoretical prediction in that both capacitive and resistive impedances are

related to the volume of the conducting solution, as long as there is no overriding substrate surface charge effect.

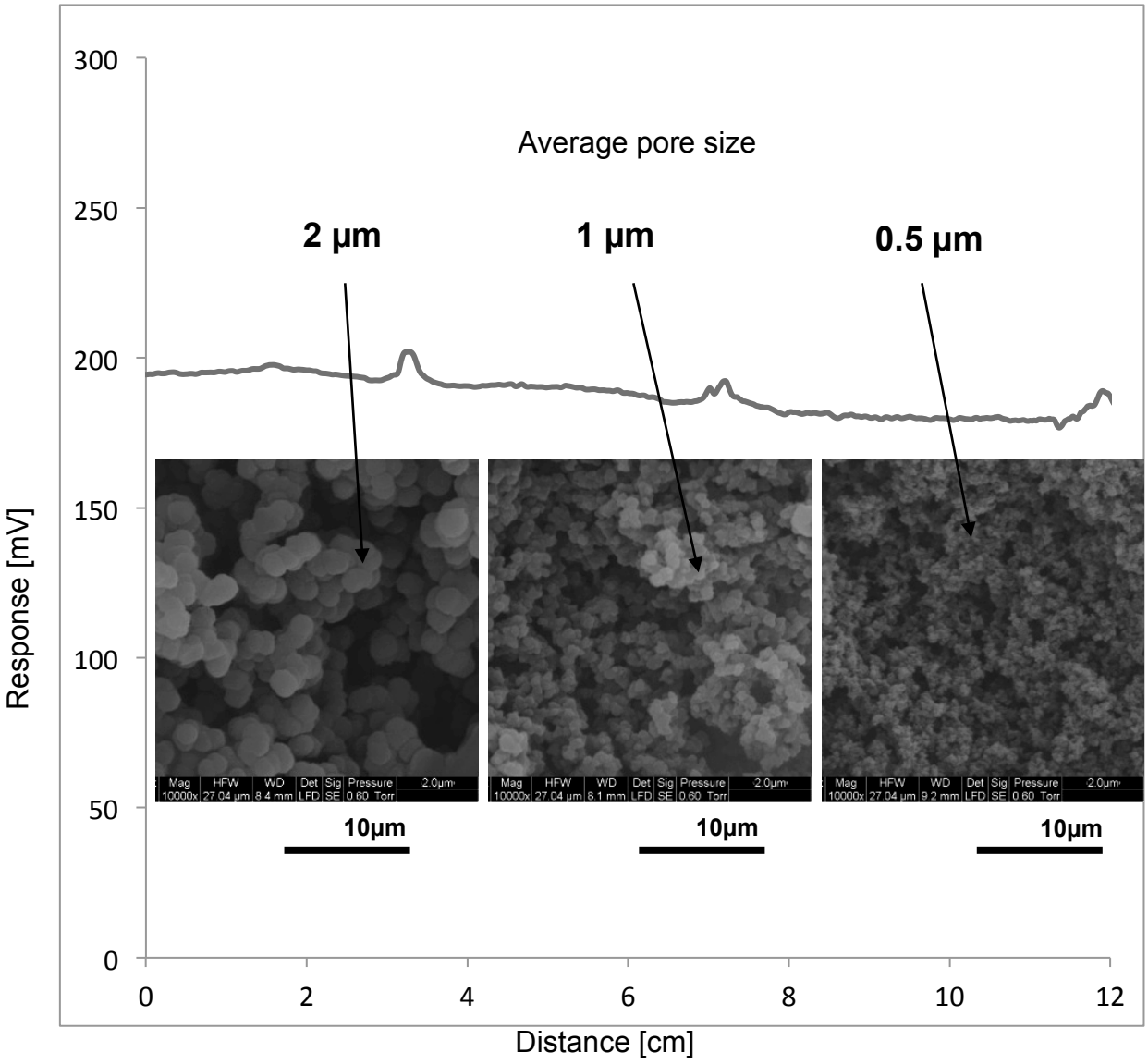

Figure 4.15: TraceDec conductivity profile of Buma2 (100 *µm i.d.* Teflon coated capillary with 5 cm sections of B16, 27 and 18) flushed with MilliQ, showing corresponding SEM images of each cross-section. Detector settings: Frequency 3xHigh, Amplification Voltage 0 dB, Gain 100%, Offset 0.

Similarly, three BuMA-*co*-EDMA monolith recipies of different porosity (which were 40, 50 and 60% respectively using porogen ratios of monomers to dodecanol 60:40, 50:50 and 40:60 respectively) were polymerised in 8-10 cm sections in the one capillary. The different monomer solutions were introduced as solution plugs with micro-syringes and polymerised under UV-light, limiting the time of diffusion between the solution zones boundaries.

Scanning C^4D was again used to detect zones of different porosity, which were a result of the different porogen ratios. The scanned C^4D profile of the MilliQ flushed capillary containing monolith sections is illustrated in Figure 4.16.

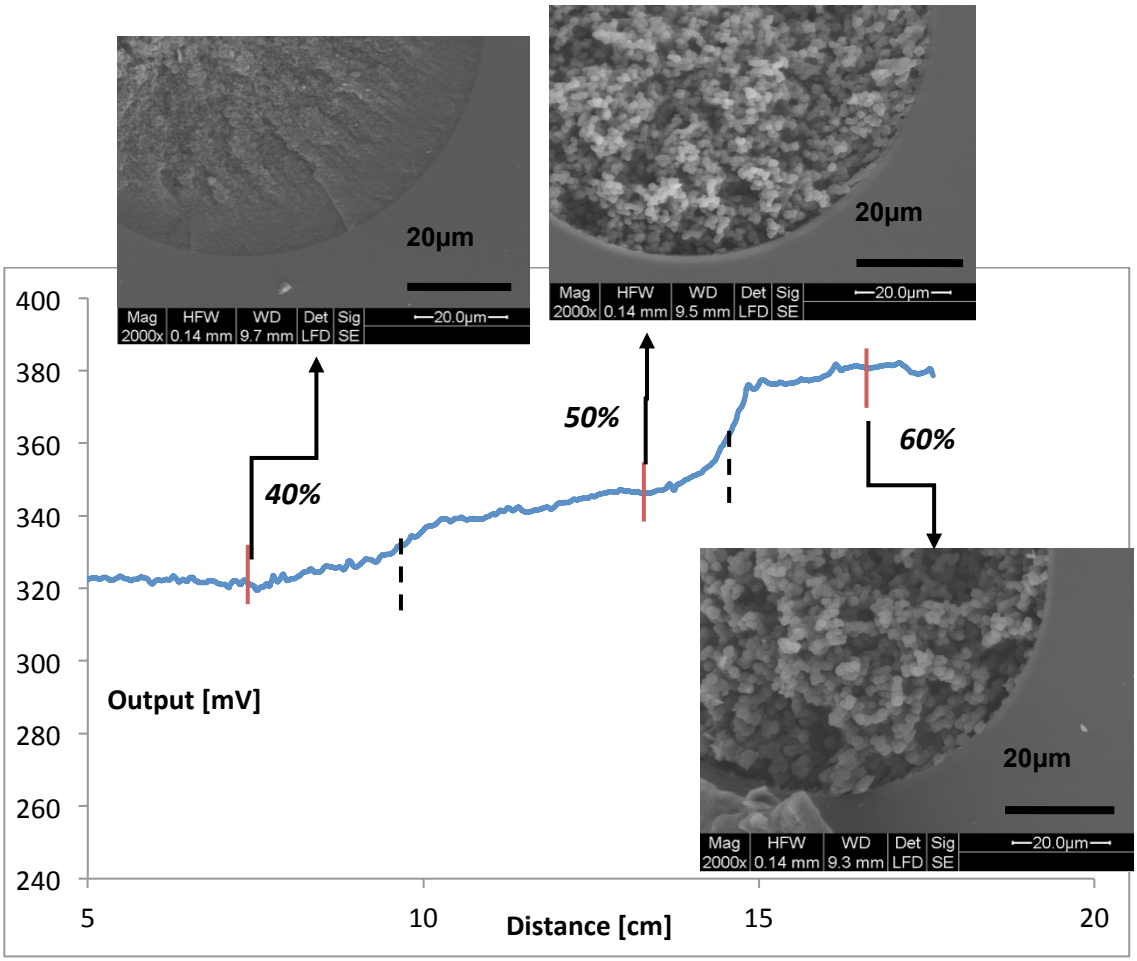

Figure 4.16: TraceDec profile of Buma3 (100 *µm i.d.* Teflon coated capillary with varying porosity monolith sections of 40, 50 and 60% from solution plugs of B14,15 and 16 respectively) flushed with MilliQ and displaying corresp. SEM cross-sections.

Due to variations in material uniformity as a result of solution mixing at the zone boundaries (and possibly during the injection step), the zone differences were not strictly defined. The variation in zone conductivity observed in the scanned conductivity profile correlates well with the change in porosity, as visualized in the SEM images of the cross-sectional cuts of each respective section. Changes to the porogen ratio typically results in less uniform and reproducible polymer morphologies, which explains the irregular C^4D profile of Figure 4.16.

Post-functionalisation of a poly(GMA-*co*-EDMA) porous polymer monolith column was conducted as outlined in the experimental section. Two quaternary amine functionalised monolithic, strong anion-exchanger (SAX) stationary phases were synthesised. Subsequent conductivity profiling with MilliQ water resulted in uneven and drifting signal profiles of the larger pore and globule sizes, but lower surface area SAX5 material as evident in Figure 4.17a. Longer 'residence' times of MilliQ within the porous substrate resulted in more strongley 'amplified' signal variations. In contrast, the scanned conductivity profile of the SAX13 capillary (Figure 4.17b) exhibits an even and smooth signal outline when presented at the same scale (small variations upon scale enlargement visible), which relates to the general uniformity in morphology and capacity.

Imaging by SEM visualized porous polymer substrates of different pore-size, albeit both of uniform material morphology. The signal variations of the scanned SAX5 column were therefore a result of surface area variations and the presence of functional groups, and were surprisingly reproducible in the respective scans along the longitudinal profile outline.

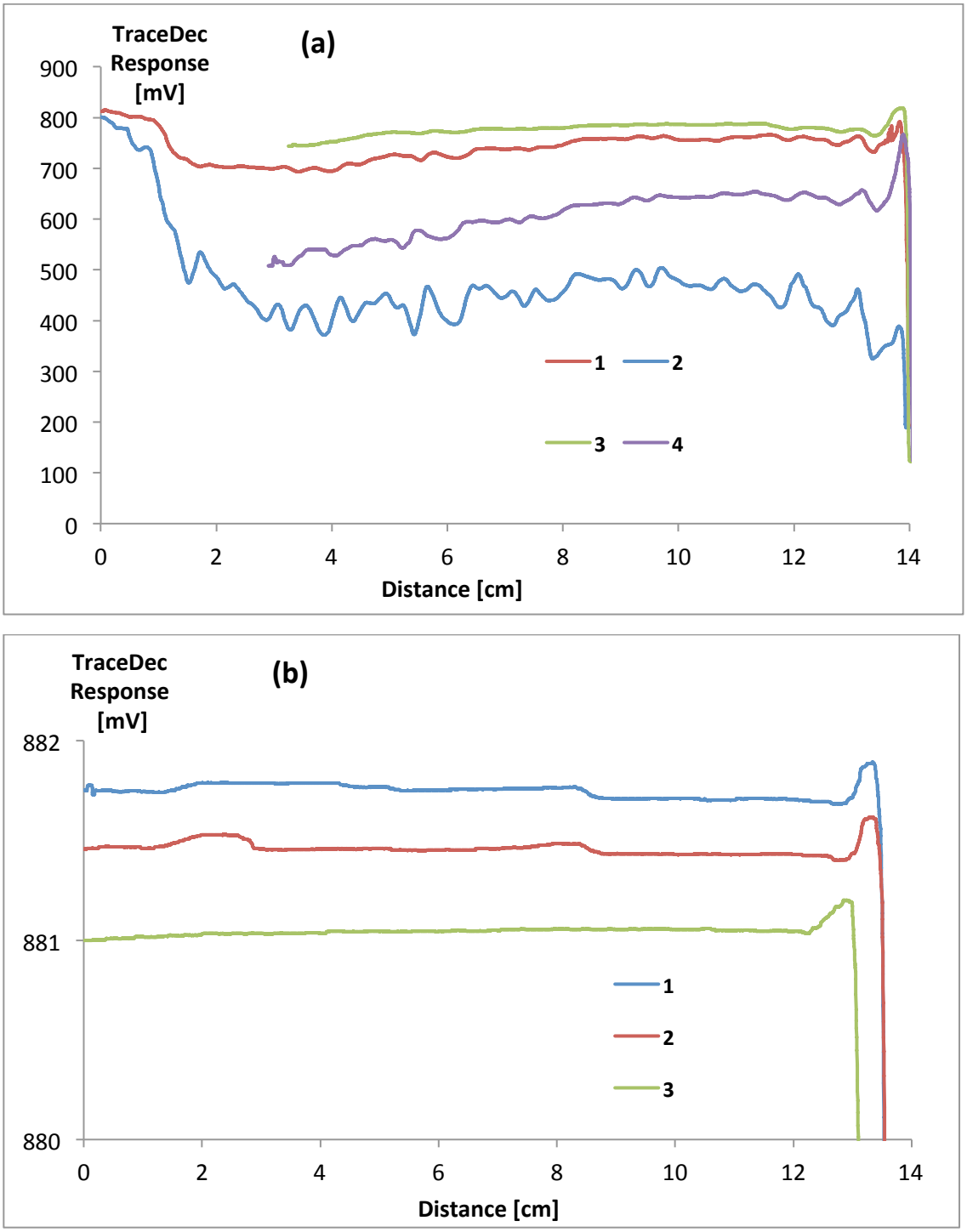

Figure 4.17a and b: Conductivity profiles of 15 cm capillary column sections (250 *µm i.d.*) of SAX5 (a) and SAX13 (b) flushed with MilliQ water: Frequency 3xHigh, Amplification Voltage -6 dB, Gain 100%, Offset 0. Profile numbers 1 to 4 correspond to the respective consecutive scanning runs.

Given that the conductivity signal of the stationary phase is directly linked to the amount of functional groups present on the surface of a stationary phase section (capacity), the surface area and subsequent degree of functional group conversion (post-modification) of the material plays an important role in conductivity profiling and separation performance. A possible link between signal drifting and the conversion of functional groups may be established with further signal deconvolution, such that leaching of ions into the mobile phase or similar functional group effects can be directly attributed to the change in conductivity signal.

The columns were both tested chromatographically under similar conditions and returned quite different chromatograms as shown in Figure 4.18a and b. SAX5 exhibited lower peak resolution and efficiency as reflected in the lower plate count. SAX13 on the other hand achieved baseline separation of five common anions in less than 5 min, with efficiencies of 25,000 plates/m.

The differences in capacity are also reflected in the eluent strengths required, 400 m*M* for SAX5 and 1 *M* KCl for SAX13. Performance variations can be attributed to the morphology and related ion-exchange capacity of the two columns, which was evident in the different conductivity profiles as shown earlier. Both chromatograms exhibited symmetrical peak shapes, so the morphology of the monolithic polymer can be considered uniform and the variations are a result of variations in general flow-through profiles as well as functional surface area properties.

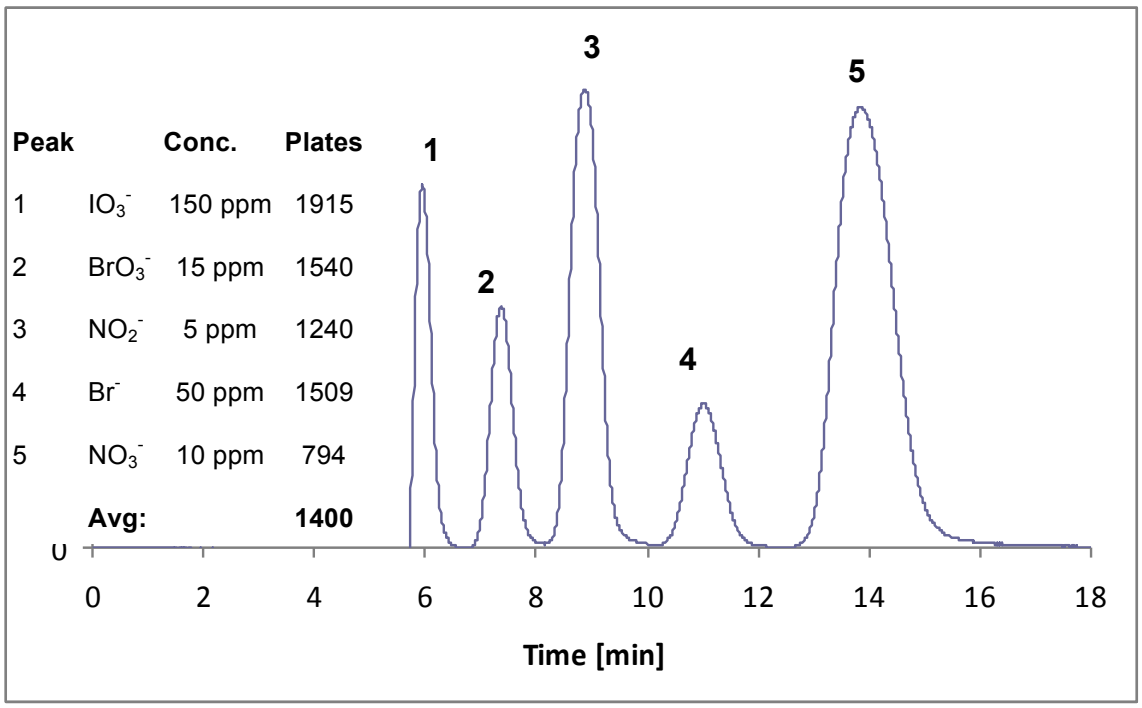

Figure 4.18a: Separation of 5 common anions on the SAX5 capillary column, Flow-rate: 1.5 µL/min, 0.4 *M* KCl, 1 µL inj. Backpressure around 2200 psi, Efficiency up to 8,000 plates/m for IO_3^-. Detection: UV absorbance at 254 nm.

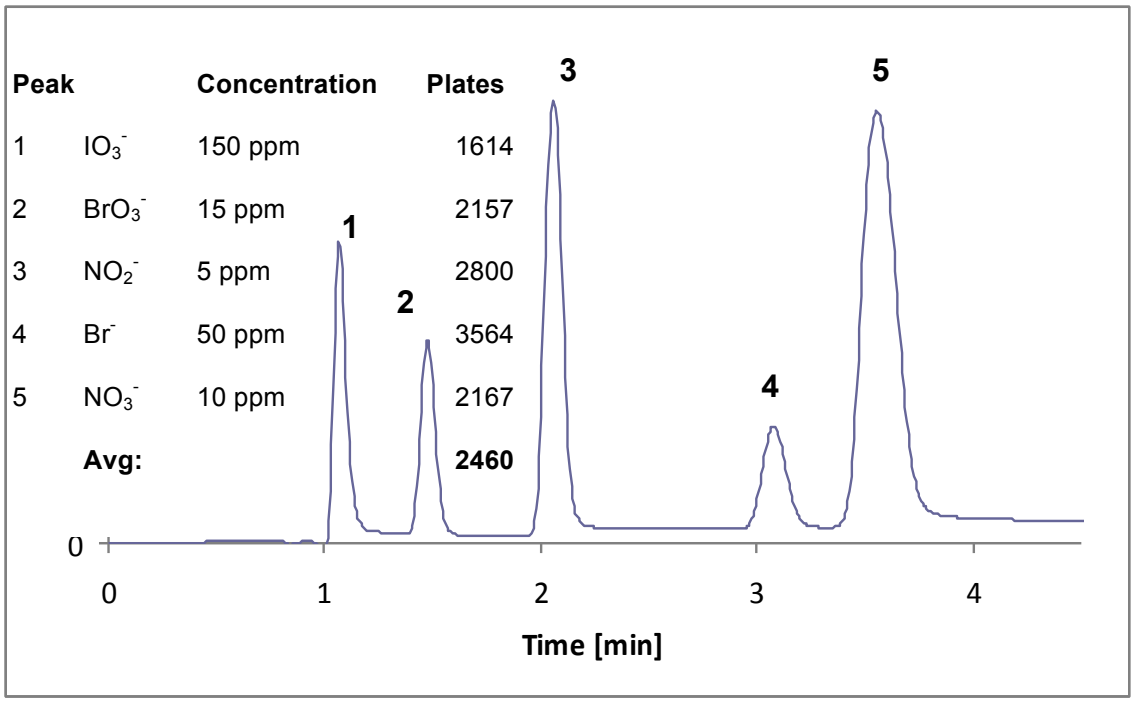

Figure 4.18b: Separation of 5 common anions on the SAX13 capillary column, Flow-rate: 7 µL/min, Eluent: 1 *M* KCl, Injection: 1 µL, Backpressure around 2500 psi, Efficiency up to 25,000 plates/m for Br^-. Detection: UV absorbance at 254 nm.

Further examination was however required to specifically locate the parameters responsible for both the variation in conductivity signal and the resulting difference in separation performance. SEM was chosen as a method to further visualise the differences in the morphological make-up of the columns. Each capillary column was cut and examined using the visual magnification technique. Comparative assessment of the cross-sectional images highlights morphological differences in the form of differently sized polymer globules as illustrated in the SEM images of Figure 4.19a and b. The difference in chromatographic performance cannot be predicted from the SEM images alone. The larger polymer globule material (SAX5) exhibited higher backpressures at lower flow-rates, suggesting that differences in the pore size distribution of the flow-through pores are partly responsible.

No morphological discontinuities were evident from the SEM images, partly as the examined cross-sections only provide a low depth view of the porous material at the axial location where the capillary was cut.

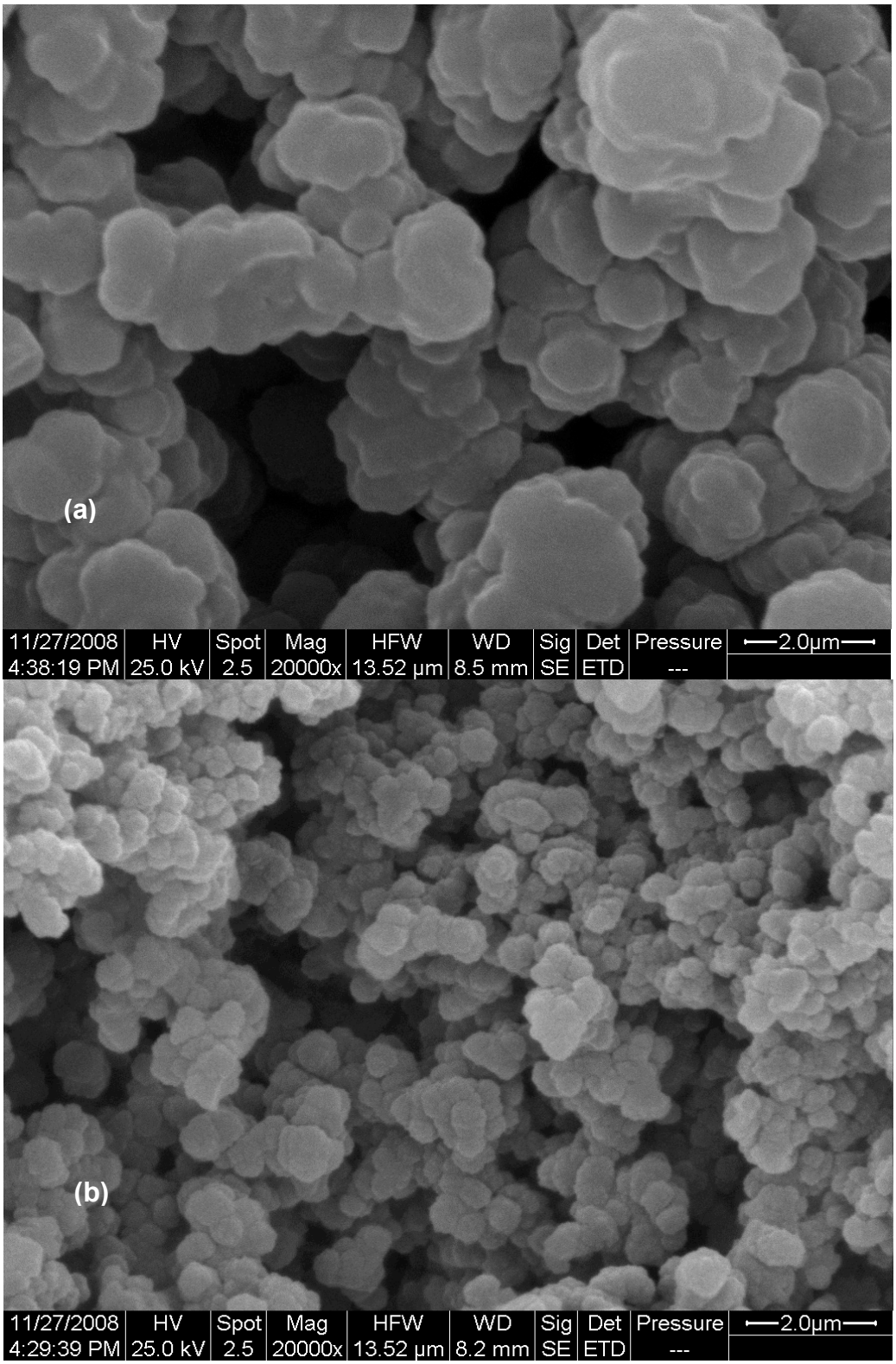

Figure 4.19: SEM of SAX5 (a) and SAX13 (b) at 20,000x magnification.

In theory, such axial inhomogeneity can be observed in the C^4D profile of the plain monolithic scaffold prior to post-modification, since the conductivity of the ion-exchange groups is 'deducted' from the overall signal of the conducting liquid (MilliQ water) and a reflection of the porous uniformity as described earlier.

A more marked example of this interaction was observed in the synthesis of another strong anion-exchange column (SAX14). The presence of physical material voids within the column, visible through the capillary wall with completely empty capillary sections of several mm, allowed for improved conductivity profile visualisation and optimisation of signal sensitivity. The plain (initially unfunctionalised) GMA-*co*-EDMA material exhibited a scanning conductivity profile as shown in Figure 4.20. The decrease in signal response occurred wherever there was polymeric material present, which resulted in a volume reduction of the conducting electrolyte (MilliQ water), as predicted in the theoretical model.

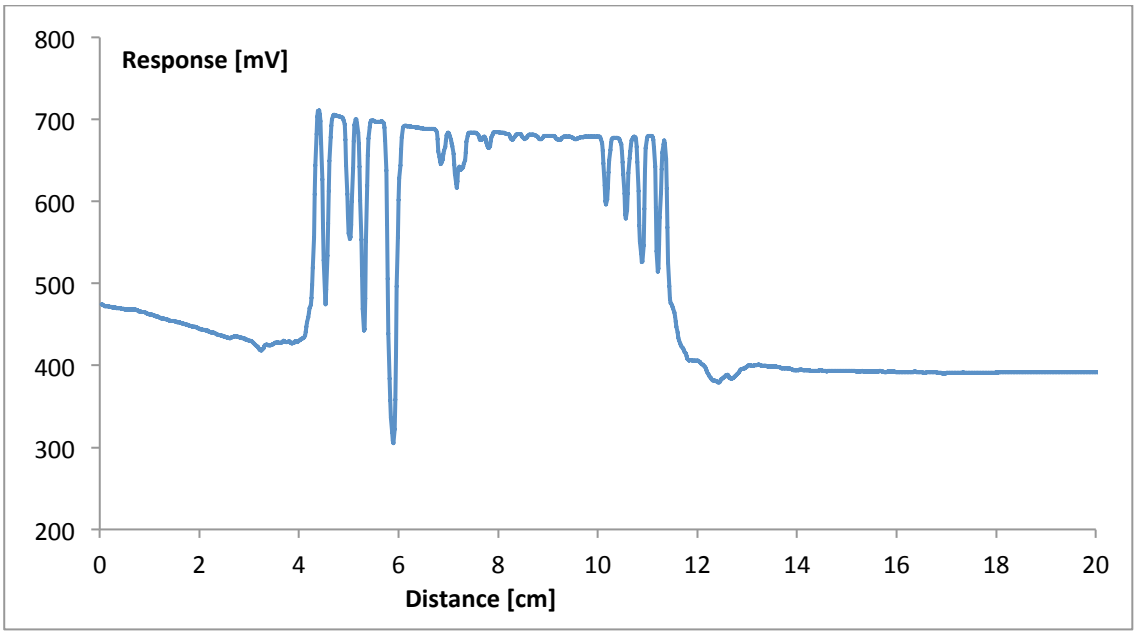

Figure 4.20: C^4D of the unfunctionalised SAX14 scaffold after MilliQ flush, Conditions: Frequency 3xHigh, Amplification Voltage -6 dB, Gain 100%, Offset 0.

Upon surface functionalisation of the porous polymer substrate with TMAHCl, the signal profile inverts and the peaks in the C^4D profile reflect the actual presence of conducting stationary phase, which has a higher conductivity response in comparison to the lower conducting MilliQ water response (Figures 4.21 and 4.22a and b). The nature of the physical material gaps in SAX14 also allowed for a direct demonstration of parameter optimisation on the resolution of the profile. Low frequency scanning produced a less sensitive conductivity profile of low resolution, while high frequency scanning resulted in the detection of minor differences (Figure 4.21). The parameters were tuned to full gain and amplification, revealing minor material variations. Sections of continuous functionalised material responded with signal overflow and were not recorded at the same settings, as shown in Figure 4.22a.

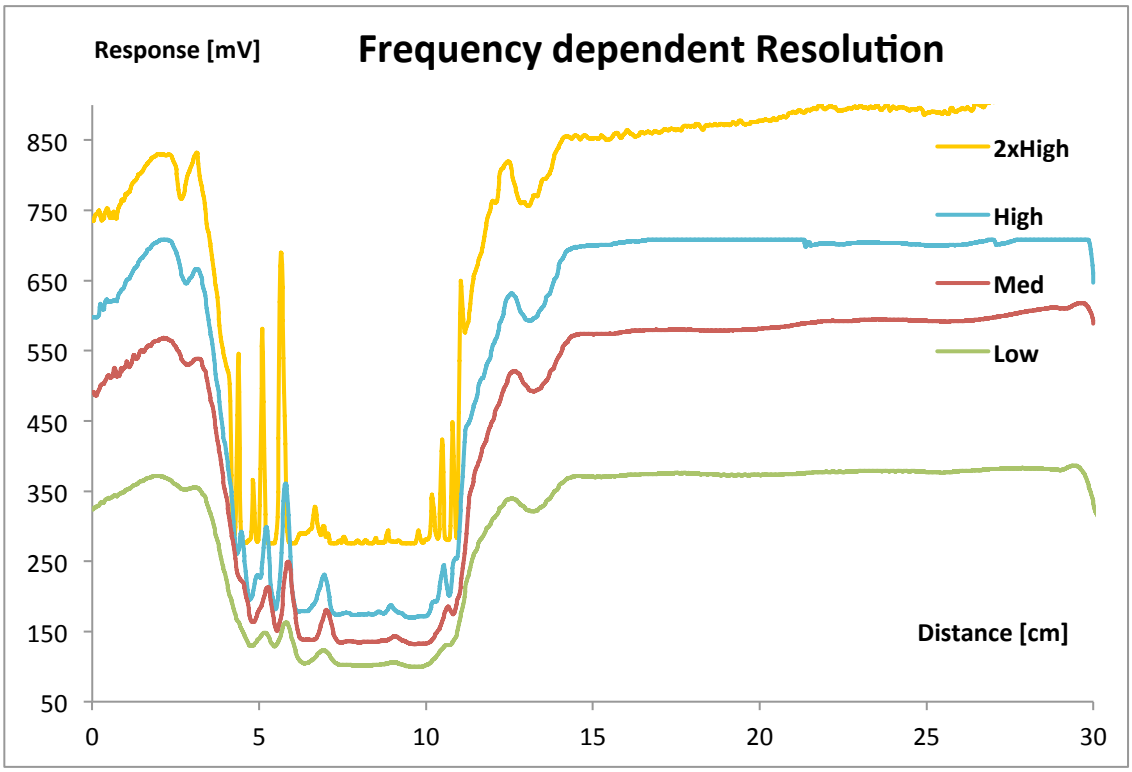

Figure 4.21: Overlayed C^4D profiles of low to high frequencies for capillary SAX14; Conditions: MilliQ flushed, Frequency as depicted, Amplification Voltage -6 dB, Gain 100%, Offset 0.

Trials with highly conducting eluents also confirmed the theory of decreasing resolution by resulting in a loss of fine structure in the conductivity profile, as shown in Figure 4.22b.

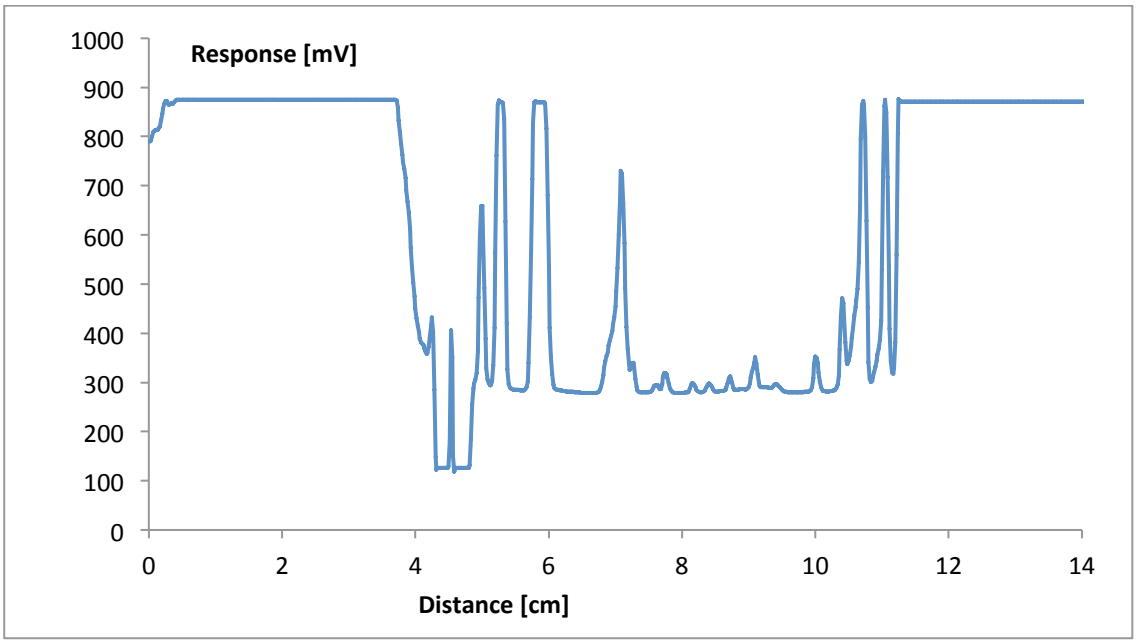

Figure 4.22a: C^4D scan with highest signal sensitivity and resolution of capillary column SAX14; Conditions: MilliQ flushed, Frequency 3xHigh, Gain 200%, Amplification Voltage 0 dB.

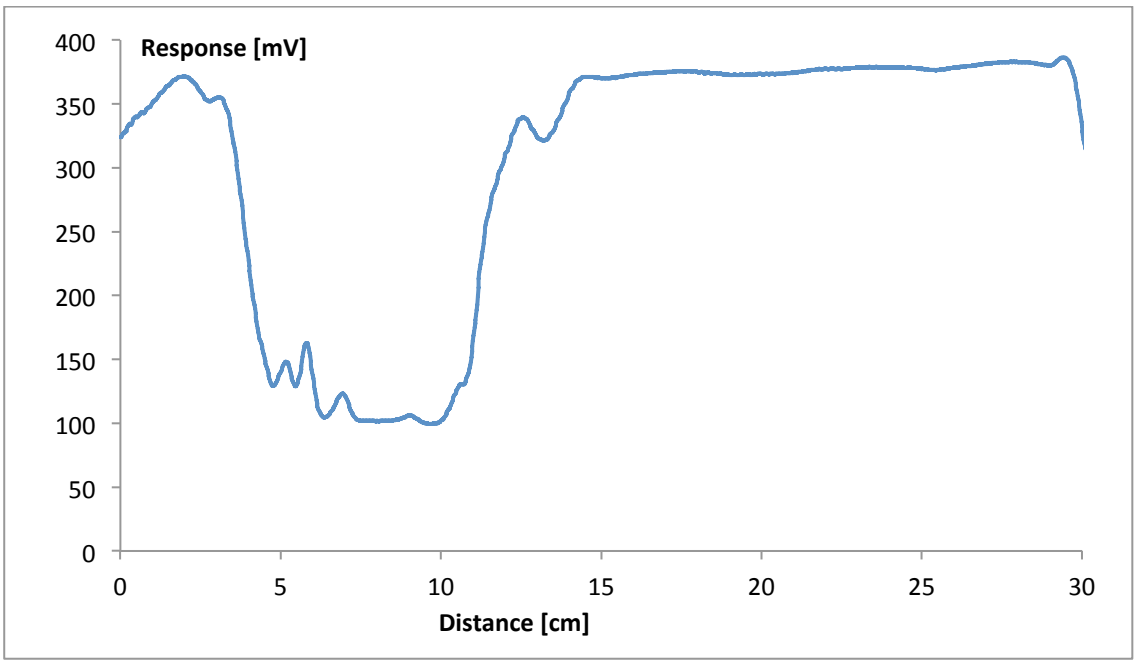

Figure 4.22b: C^4D profile of SAX14 capillary column filled with 100 m*M* KCl; Conditions: Frequency 3xHigh, Amplification Voltage -6 dB, Gain 100%, Offset 0.

The axial placement of two ring electrodes in series, each 1 cm in length and 0.8 mm apart, allows for a theoretical capacitor plate distance anywhere between 0.8 mm and 2.08 cm. The axial arrangement results in a different capacitor plate area in comparison to flat plate capacitors. This effect is evident when assessing the scanning resolution at various frequencies.

Figure 4.21 illustrates the signal output over scanned material variations with different parameter conditions. The frequency effect appeared more prominent than anticipated, with lower frequencies providing very little longitudinal scanning detail. As the modelled response indicates, higher frequencies maximised the axial resolution and sensitivity towards the morphological and functional variations of the substrate, however the wall effect of the fused-silica material also becomes more prominent.

To illustrate the findings in context with actual column performance, the scanned capillary (SAX14) was cut in half as illustrated in Figure 4.23. The capillary section which had exhibited material discontinuities in the early C^4D scanning (Section 1), performed poorly when tested for chromatographic performance.

In contrast, the evenly conducting Section 2 of the cut capillary was chromatographically a much better performing column. Eddy diffusion and capacity variations as a result of the physical material discontinuities within the capillary, are considered to be the main factors responsible for the poor separation performance of Section 1, as indicated by the strongly tailing peak shapes.

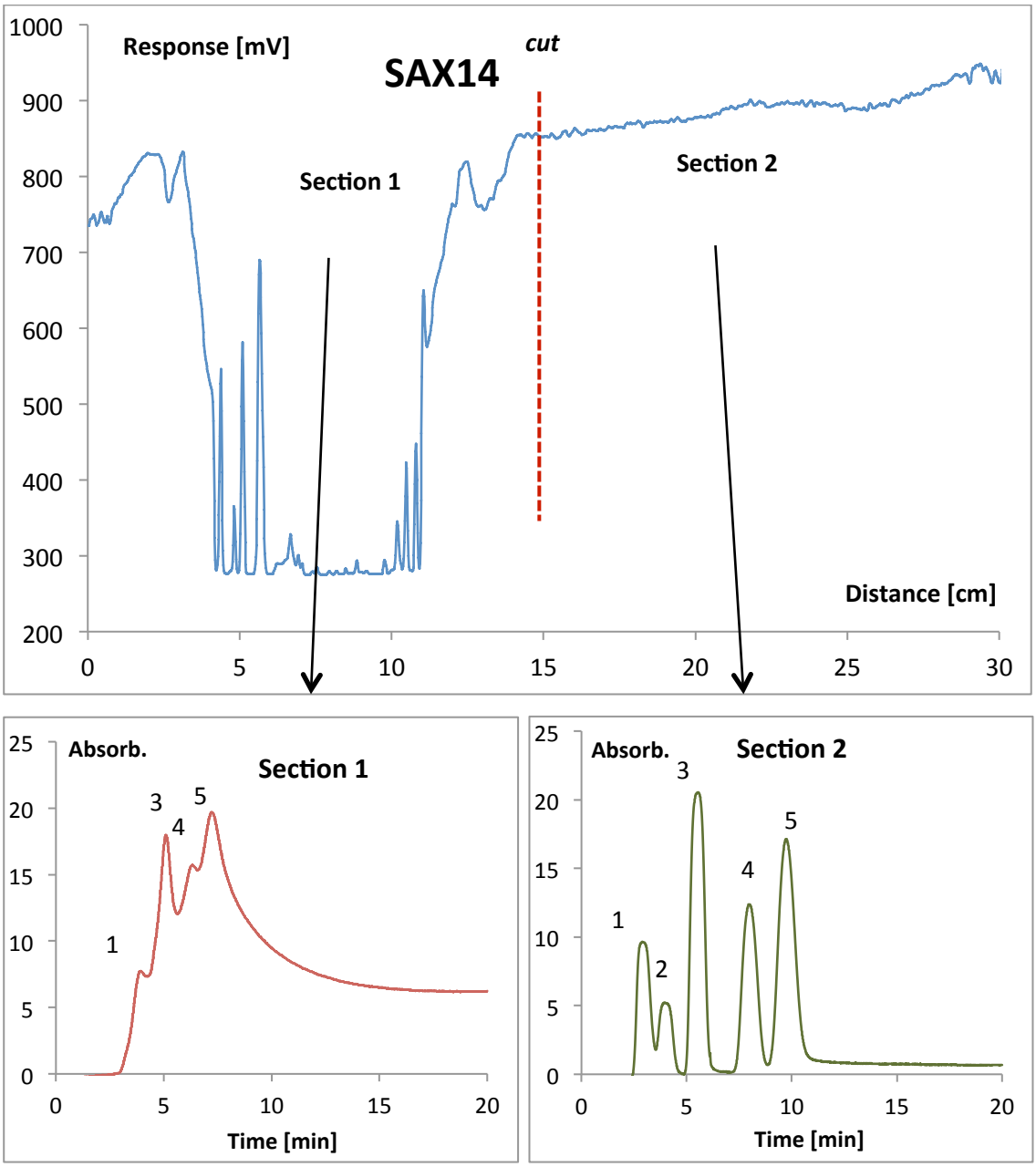

Figure 4.23: Respective chromatograms of each capillary section, illustrating effectively that material discontinuities (detectable by C^4D) lead to peak broadening and thus reduced resolution and efficiency. Separation: 1 NO_2^- (5 ppm), 2 NO_3^- (10 ppm), 3 IO_3^- (15 ppm), 4 BrO_3^- (50 ppm), 5 Br^- (50 ppm), Injection: 0.5 µL, Eluent: 20 m*M* KCl at 0.5 µL/min.

4.4 Conclusion

Chromatographic column performance can generally be attributed to the morphological and functional group uniformity of the incorporated stationary phases, which in this case were quaternary amine functionalised methacrylate polymer monoliths in capillary format.

The results presented in this chapter demonstrate that uniformity of axial porosity and the presence of functional groups on the material surface can be assessed in sequence and correlated with the separation performance of the scanned column. Capillary C^4D can be used to visualise porosity uniformity in non-functionalised (non-ionic) porous polymer filled capillaries. Using a low conducting mobile phase such as MilliQ water, the method permits measurements of small volumetric changes in porosity of the cross-sectional monolithic profile down to axial resolutions of less than 1 mm.

While the surface area and distribution of a typical porous polymer correlates to the pore size and can be visually assessed by SEM imaging of cross-sectional capillary slices, C^4D cannot reliably detect differences in the pore size of plain, non-functionalised materials, since the overall porosity is the governing factor in the signal response. Surface area and pore size uniformity cannot be separately assessed from the conductivity response alone, since the overall solution resistance predominantly influences the conductivity signal variations. Once functional groups are present on the porous polymer surface, the conductivity variations correlate more strongly with the distribution of the conducting functionalities over the surface of the porous substrate.

The potential exists for the reliable determination of pore size variations in functionalised materials, however any disparity in the surface charge uniformity, the main contribution to the signal composition, will make such an attempt very difficult to confirm. In respect to the influences of the individual impedances on the overall signal profile as illustrated in the theoretical model, this will most likely require extensive conductivity profiling in combination with frequency differentiations, such that the respective difference in signal response between the frequencies is indicative of the pore distribution. In other words, the simultaneous scanning of the frequency range at discrete axial locations with such morphological material variations should provide a relative differentiation of the physical material variations.

However, the combination of capacitive effects of electrode, capillary, material and resistive components of solution and material make it very difficult to standardise and assess the influencing factors separately. The high sensitivity of this technique implies a high susceptibility to signal fouling through capillary wall contamination (manual handling), temperature changes and (static) electrical charge build-up.

The exact physical influences are difficult to model, as the design of the ring electrode complicates the effect of their physical properties on the signal in comparison to flat plate capacitors, where the plate area and uniform distance between plates provide a simpler framework to model. The application of finite element (multivariate) analysis of the electric fields in the capillary confines could provide both numerical and graphical insights into this complex, three dimensional situation. However the scope of the present study does not include this level of detail.

In summary the technique, once optimised to the conditions of the examined material, allows prediction of the separation performance of functional polymer monolith capillary columns, by longitudinal uniformity assessment of the porous polymer material morphology and the distribution of surface functionality. C^4D can visualise in a non-invasive and operational wet-state manner, which conventional methods such as SEM fail to do.

5 Monolith coating using differently sized AS11 latexes

5.1 Introduction

Initial attempts to increase the surface area and functional density of a monolithic stationary phase by coating the negatively charged substrate formed with a functional monomer with positively charged quaternary amine latex nanoparticles yielded only a moderate surface coverage of the functional particles [77]. As the presence of particles is directly correlated with the opposing charge on the substrate surface, it was assumed that the AMPS-incorporated polymer lacked sufficiently accessible sulfonic acid functionalities [73, 75, 81].

As demonstrated in Chapter 3, a monolayer coverage could be achieved by employing a multi-step conversion of the chloromethyl group in the poly(CMS-*co*-DVB) substrate into the sulfonic acid group, to which the latex particles adhered by electrostatic forces [105]. This method was deemed successful in that sufficient amounts of the convertible functional monomer could be dissolved in the polymerisation mixture, previously not possible with the more polar AMPS monomer, as it required a change in porogen composition and a limit of 1.8% (w/w of total mixture) of the functional monomer [165]. The poly(styrene-*co*-divinylbenzene) type monoliths also showed better permeability in comparison to the methacrylate analogues and were less affected by the reduction in pore diameter through the coating procedure, as previously reported [73].

The method of this post-modification reaction is described in Chapter 3, with the same polymer recipe and stepwise conversion being used in this

successive work. Positively charged, the nanoparticles attached themselves to the negatively charged polymer substrate. The extent of the coverage varied between the different particle types, morphology of the substrate and extent of negative surface charge, demonstrating that both core chemistry and surface functionality influenced the interaction with the monolith.

An earlier study by Slingsby and Pohl [150] examined the effect of the quaternary amine terminal group alkylation on the latex nanoparticles surface in relation to the selectivity of the coated stationary phase towards common anions. It appeared that the hydrophilicity of the terminating amine functionality had a greater influence on selectivity and retention of the corresponding analytes (calculated by the free energy of hydration) than the particle size or ion-exchange capacity of the coated stationary phase. Information about the IonPac AS18 and AS11 columns provided by Dionex (www.dionex.com) lists both latex types as alkanol quaternary amine ions with different hydrophobicity values (medium low to very low).

The hydration of the latex functionality, the analytes and the eluent ion plays a significant role in the separation characteristics, as well as the extent of coating and stability of the latex layer. The type of amine alkylation strongly affects the hydration, which in turn governs the retention and selectivity of the anions. The publication further suggests possible analyte interactions beyond the amine functionality into the styrene chains of the swollen latex particle for π-π interactions with the benzene rings. This theory was confirmed with the addition of *p*-cyanophenate in the eluent, competing in the π-orbital overlap and reducing the retention of halides, nitrate and chlorate.

For the columns manufactured in this chapter, contactless conductivity detection (C^4D) was used to monitor the synthesis and post-modification of the polymer substrate as well as the extent of the latex-coating on the functionalised monolithic scaffold. Being a non-invasive characterisation technique, the capillaries could be examined through their scanned conductivity profile to locate sections of uniform conductance, which were cut from the capillary to yield a suitable column for the IC separations of 5 common anions.

Signal variations of the scanned conductivity profile can be attributed to two main factors, namely the distribution and extent of surface functionalities on the one hand and morphological uniformity, specifically in terms of the overall porosity and distribution on the other. Cross-sectional images as well as surface magnified images by SEM at specific locations along the capillary allowed correlation of the changes in conductivity with the origin of the signal variation since the functional latex particles were clearly visible. Directly incorporated functionalities with no separate visible structure, such as the SAX columns in Chapter 4, cannot be directly visualized by SEM and require other methods of quantification. Electron probe microanalysis (EPMA) and scanning electron microscopy (SEM) are closely related techniques for high-magnification imaging and spatially resolved chemical analysis of solid samples. EPMA is mainly used for quantitative chemical analysis of micrometer-sized structures, line profiles or two dimensional element maps and allows elemental analysis of incorporated functionalities. Non-conductive samples are coated with a layer of carbon for chemical analysis or gold for imaging. The samples also have to withstand the high

vacuum in the instruments. Secondary electrons (SE) show surface morphology, backscattered electrons (BSE) local differences in average atomic number, x-rays are detected by wavelength and energy dispersive spectrometers (WDS, EDS) for chemical analysis.

The aim of testing three different sized quaternary amine latex particles of 54 nm, 75 nm and 180 nm average particle diameters was to examine the effect of particle type and size on surface coverage and resulting chromatographic performance. Since monolayer coverage was not easily achieved in a reproducible manner using AS18 latex, the influence of particle size and type on the successful coverage of identical functional scaffolds should provide further insight into the coating mechanism and the effect on capacity and resulting performance of the anion-exchange capillary column.

5.2 Experimental

5.2.1 Instrumentation

The Ultimate 3000 Micro LC was operated with KCl solutions of 20-100 m*M* at flow-rates of 0.1 to 5 μLmin^{-1}. Chloride rather than hydroxide eluent was used to reduce the degenerating effect of alkaline hydroxide solutions on the various metal components and fused-silica capillaries in the system. Nevertheless, the ionic strength of the salt solutions was sufficiently strong for corrosion to occur on the stainless steel components of the instrument when left without being operated over a longer period of time. As a consequence, the entire system was flushed with MilliQ water after each set of experiments to reduce ionic enhancement of the material degradation. The

C^4D scanning set-up was operated in automated mode as described in Chapter 4. SEM imaging was performed as described in Chapter 2.

5.2.2 Chemicals

AS11 (45, 75 and 170 nm in diameter) latex particles with quaternary ammonium functionalities were obtained from Dionex as an 11% (w/v) suspension. The latex suspension was filtered through a 0.45 μm nylon syringe filter (Activon, Thornleigh, Australia) and diluted in MilliQ at a ratio of 1:50 and 1:100 (latex solution volume to MilliQ volume).

5.2.3 Monolith Column Composition

Capillary columns were prepared as described in Chapter 3 and coated with the chosen AS11 latex nanoparticles by flushing the sulfonated, post-modified CMS-DVB monolith with diluted AS11 solutions as prepared above. The resulting columns were labelled as outlined in Table 5.1 below.

Table 5.1: Monolith composition for columns used in this chapter.

Name	Monomer % w/w	Cross-linker %	Porogen %	Polymeris. Conditions	Dimensions	Post-mod.	Coating
Cap 5	CMS 16	DVB 24	Tol,Dod 18, 42	Thermal (70°C, 24h)	0.25 x 700 mm	Thio-benzoic	AS11 54nm
Cap 12 S1 1,2H	CMS 16	DVB 24	Tol,Dod 18, 42	Thermal (70°C, 24h)	0.20 x 160 mm	Thio-benzoic	AS11 54nm
CMS S1	CMS 16	DVB 24	Tol,Dod 18, 42	Thermal (70°C, 24h)	0.20 x 220 mm	Thio-benzoic	AS11 54nm
Cap 11 S2	CMS 16	DVB 24	Tol,Dod 18, 42	Thermal (70°C, 24h)	0.20 x 200 mm	Thio-benzoic	AS11 75nm
CMS S2	CMS 16	DVB 24	Tol,Dod 18, 42	Thermal (70°C, 24h)	0.20 x 160 mm	Thio-benzoic	AS11 170nm
Cap 11 S1	CMS 16	DVB 24	Tol,Dod 18, 42	Thermal (70°C, 24h)	0.20 x 150 mm	Thio-benzoic	AS11 170nm
Cap 12 S2	CMS 16	DVB 24	Tol,Dod 18, 42	Thermal (70°C, 24h)	0.20 x 400 mm	Thio-benzoic	AS11 Mixture

5.3 Results and Discussion

The morphology of monolithic scaffolds, such as pore size, pore size distribution and surface area, can vary significantly in magnitude depending on the polymerisation mixture and reaction conditions used. The pore size distribution and surface area are interconnected, such that the presence of micropores (pores smaller than 2 nm) [12] significantly increases the measured surface area. However these pores are not deemed useful in the coating of the material with latex particles and are therefore not desirable in the synthesis of functional scaffolds. The post-modification procedure requires all of the functionalities to be accessible for coating on the surface of the larger flow-through pores. These macropores form the basis of a favourable flow to mass transfer ratio, the defining property of monolithic stationary phases. It is on the surface of these pores where the ionic functionalities are the most relevant. The polymerisation mixture yielding macropores of 1-2 μm was therefore considered to be suitable.

As mentioned earlier, the mechanism of latex coatings is predominantly governed by the electrostatic interaction between the negatively charged sulfonic acid groups on the monolith surface and the positively charged quaternary amine groups of the latex nanoparticles. As such it was deemed necessary to provide a sufficient amount of negatively charged sulfonic acid functionalities on the pores surface for the electrostatic interaction between the nanoparticles and material surface, to yield a complete monolayer latex coverage.

The presence of elemental sulfur was examined by electron beam induced x-ray emission lines of the outer sulfur electrons present in the

sulfonic acid groups on the material surface. Values of around 0.5% (w/w) were typically encountered for the sulfonated, post-modified CMS scaffold. Columns with full monolayer coverage exhibited values higher in magnitude, as seen by the sulfur line spectral electron count equivalent to 1.63% (w/w) as shown in Figure 5.1a for Cap 5.

In contrast the unmodified (plain) CMS-*co*-DVB material exhibited no presence of sulfur and 1.44% (w/w) for chloride as seen in Figure 5.1b. Similar to the approach of industrially prepared sulfonated polystyrene beads where hot sulfuric acid is used to impart the necessary functionality, unmodified poly(styrene-*co*-DVB) materials treated with fuming sulfuric acid returned values up to 7% (w/w) for sulfur in the elemental analysis, although not very consistently.

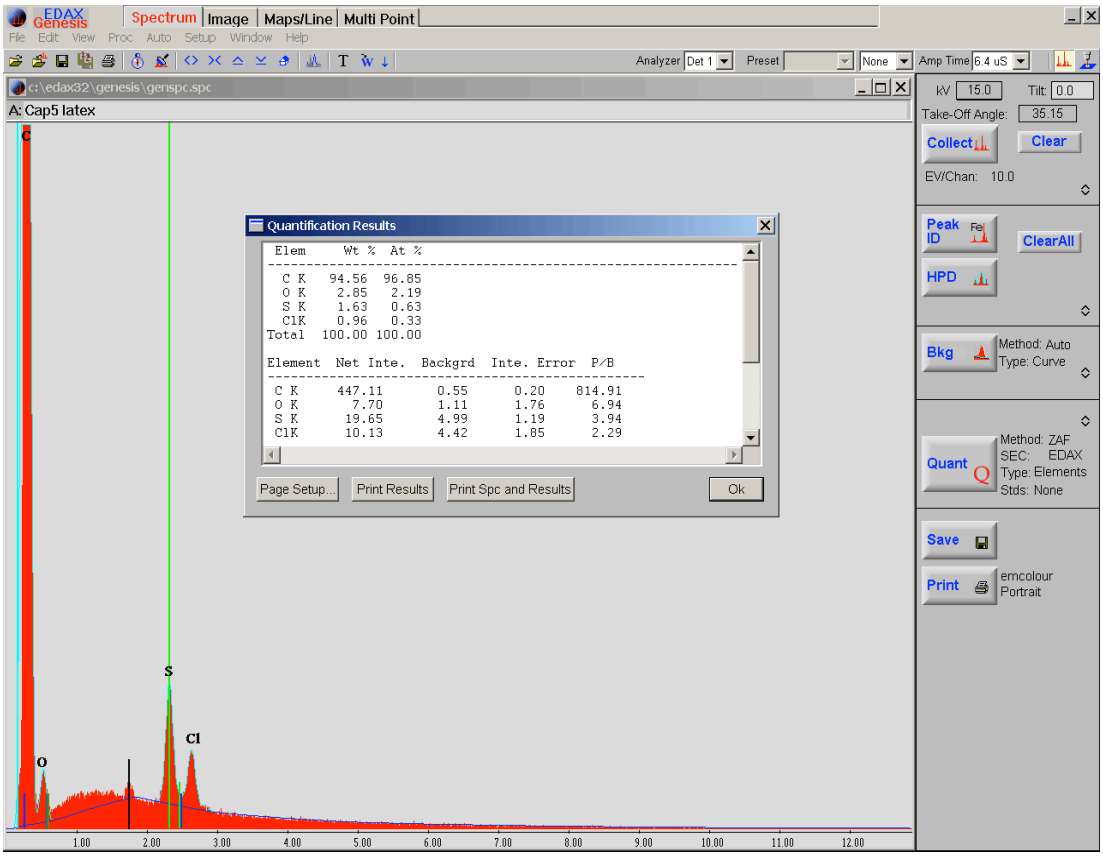

Figure 5.1a: Elemental X-ray spectral lines show presence of sulfur and chloride in modified and latex coated poly(CMS-*co*-DVB) monolith Cap 5.

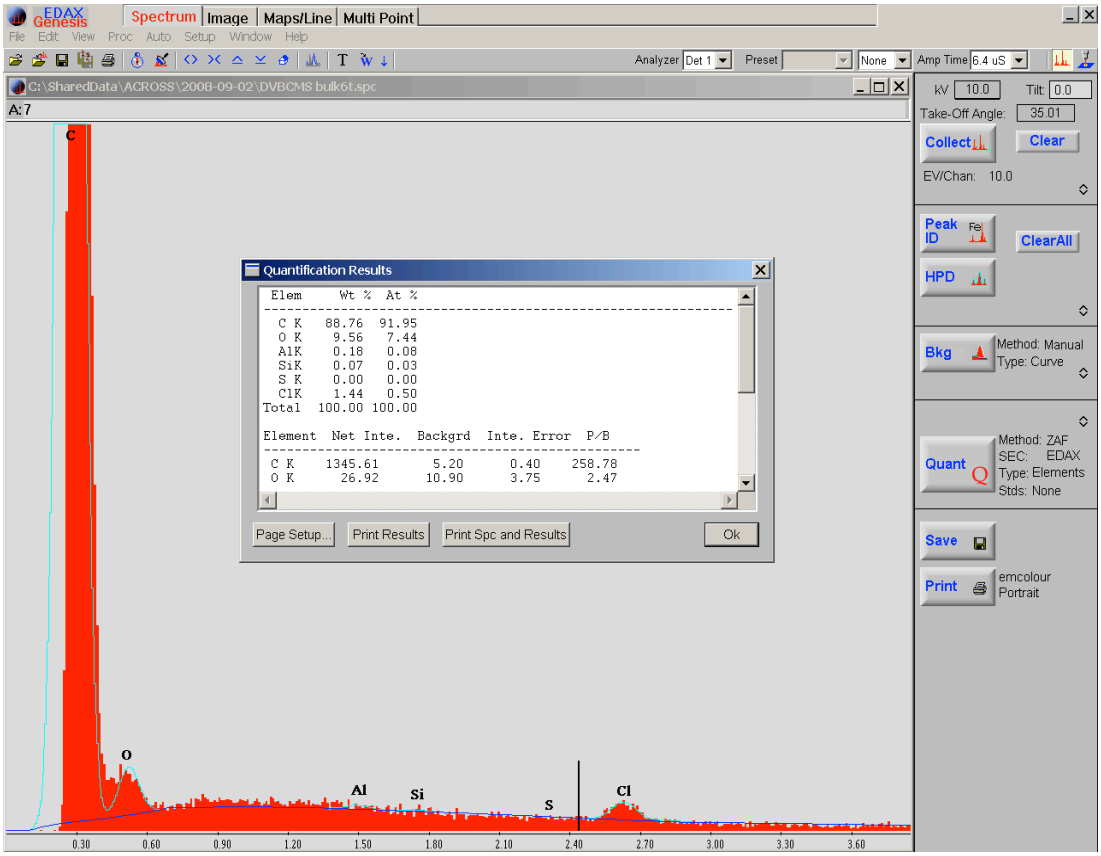

Figure 5.1b: Elemental X-ray spectral lines show presence of chloride groups in unmodified bulk polymerised poly(styrene-*co*-DVB) monolith.

Subsequent SEM images of the acid pre-treated and latex-coated scaffolds showed limited coverage of the latex nanoparticles on the material surface (see Figures 3.1 and 3.3 in Section 3.3). In contrast, low presence of sulfur was observed amongst the remaining materials sulfonated by post-modification of the included functional monomers. Significant disparities in the extent of the latex coating were observed with SEM imaging amongst the coated scaffolds of different modification methods. In theory, one would expect a higher surface coverage with smaller particles, when sufficient sulfonic acid groups are present on the scaffold to retain the positively charged latex particles via electrostatic attraction.

To test this theory, a number of these sulfonated CMS-*co*-DVB monoliths were prepared and subsequently coated with different latex particles dispersed in an aqueous solution. The three latex samples examined were prepared by Dionex, using the same synthetic approach and having the same quaternary amine surface chemistry. The main difference between them was their respective size, averaging 54, 75 and 170 nm each with highly uniform monodispersity.

Figure 5.2 shows three proposed scenarios of possible latex particle distribution over the functionalised stationary phase surface. The theoretical coverage of a well functionalised material with smaller latex particles is illustrated in Figure 5.2a, larger latex particles in Figure 5.2b and the deduced actual coverage as observed under SEM in Figure 5.2c. The fact that stabilizing surfactants were used in the latex suspension as supplied by Dionex, has so far been mostly ignored in terms of its effect on the coating procedure.

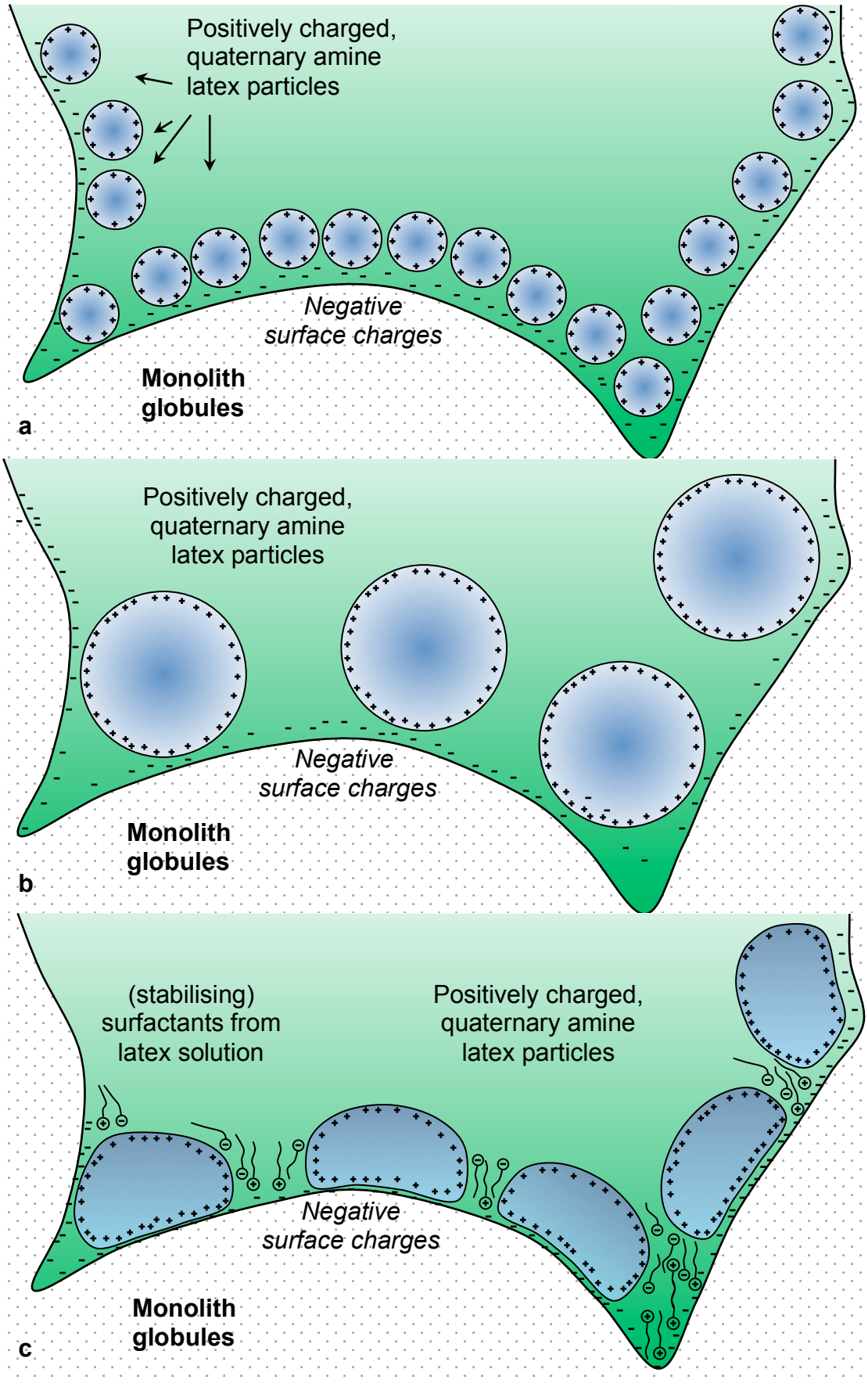

Figure 5.2: Expected theoretical coverage of smaller latex particles (a), larger latex particles (b) and actual coverage as observed under SEM (c).

It can be expected that these surfactants also remain present in the coating layer and assist in stabilizing the latex coating on the polymeric monolith substrate. Since the quaternary amine latex particles have positive charges distributed over the surface, it is safe to assume that electrostatic repellent forces results in some distance being established between adjacent particles in the coating layer. As mentioned earlier however [150], secondary π-π interactions and possible charge dissociation of the amine functionality due to interaction with surfactants of opposing charge is likely to reduce the electrostatic repulsion between particles.

Images of latex layers obtained by SEM show the various extents of coatings and resulting spaces between the particles. Highly magnified segments of the differently sized AS11 latex particle coatings are shown in Figure 5.3a (54 nm), b (75 nm) c (170 nm) and d (mixture of all three), all taken at the same level of magnification, illustrating a cross-section of just over 4 μm. The notable difference in substrate morphology, particularly the globule size, is discussed at a later stage.

The observed combination of surfactants and latex particles as shown earlier (Figure 3.1 in Chapter 3) illustrates an interaction of these charged molecules and particles that is not easily dispersed by simple flushing with aqueous solutions. This interaction is deemed relatively stable and appears to have a configuration similar to polyelectrolyte layers, which are known for their surprising stability and longevity [58].

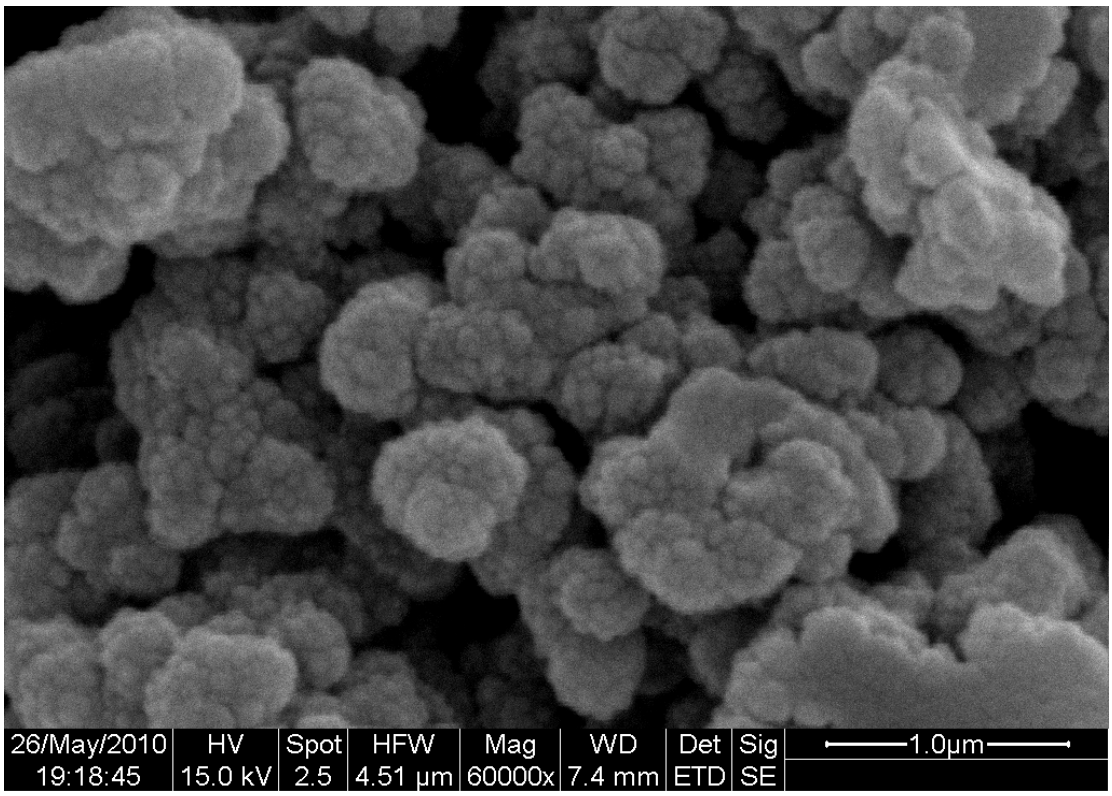

Figure 5.3a: SEM of 54 nm AS11 latex coating on sulfonated CMS-*co*-DVB scaffold.

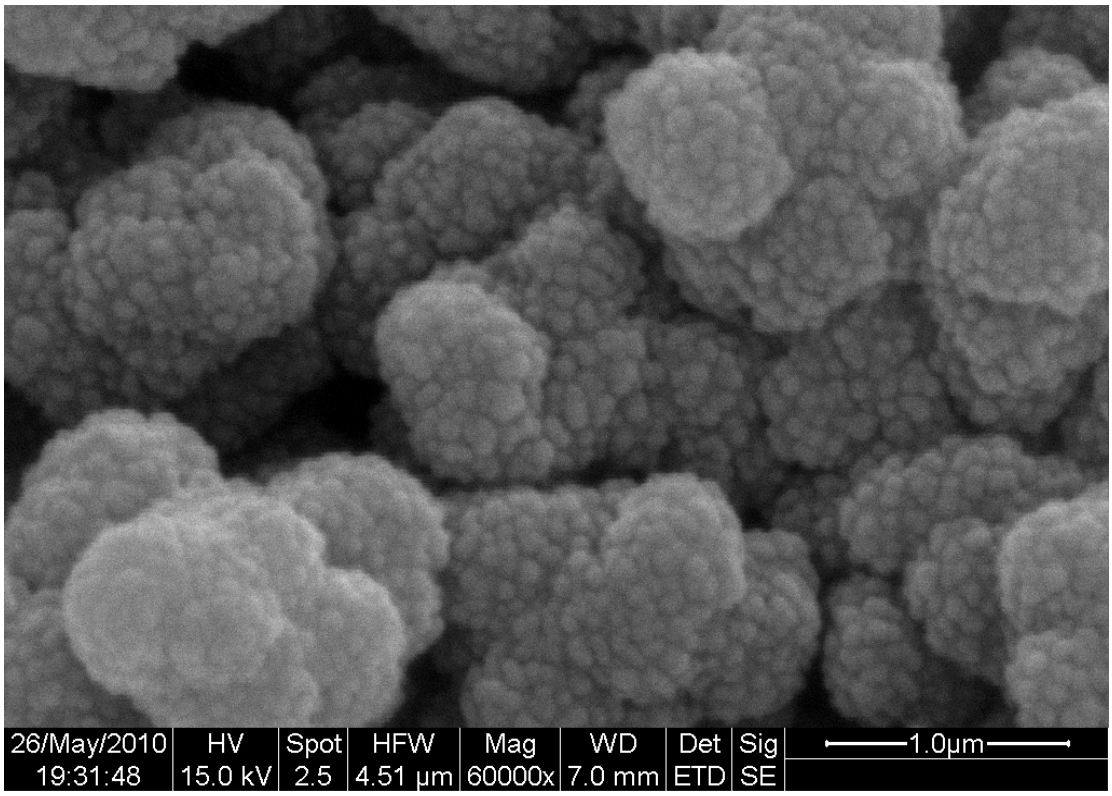

Figure 5.3b: SEM of 75 nm AS11 latex particle coating.

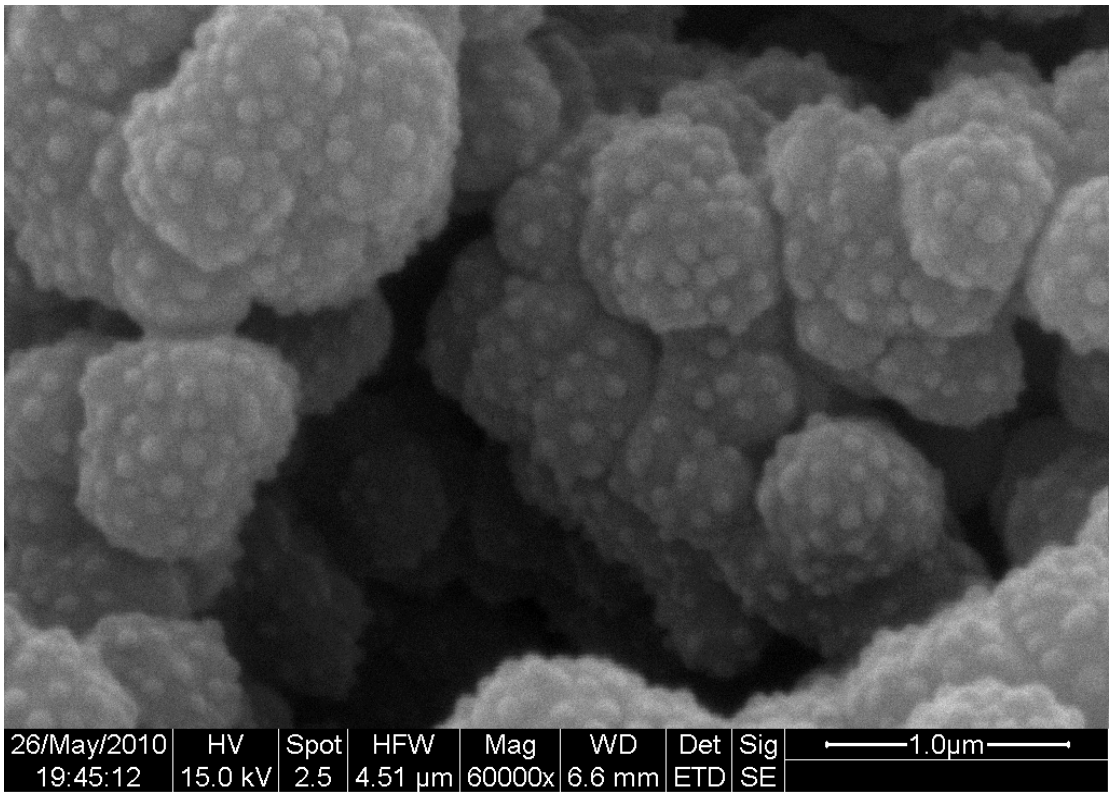

Figure 5.3c: SEM of 170 nm AS11 latex particle coating.

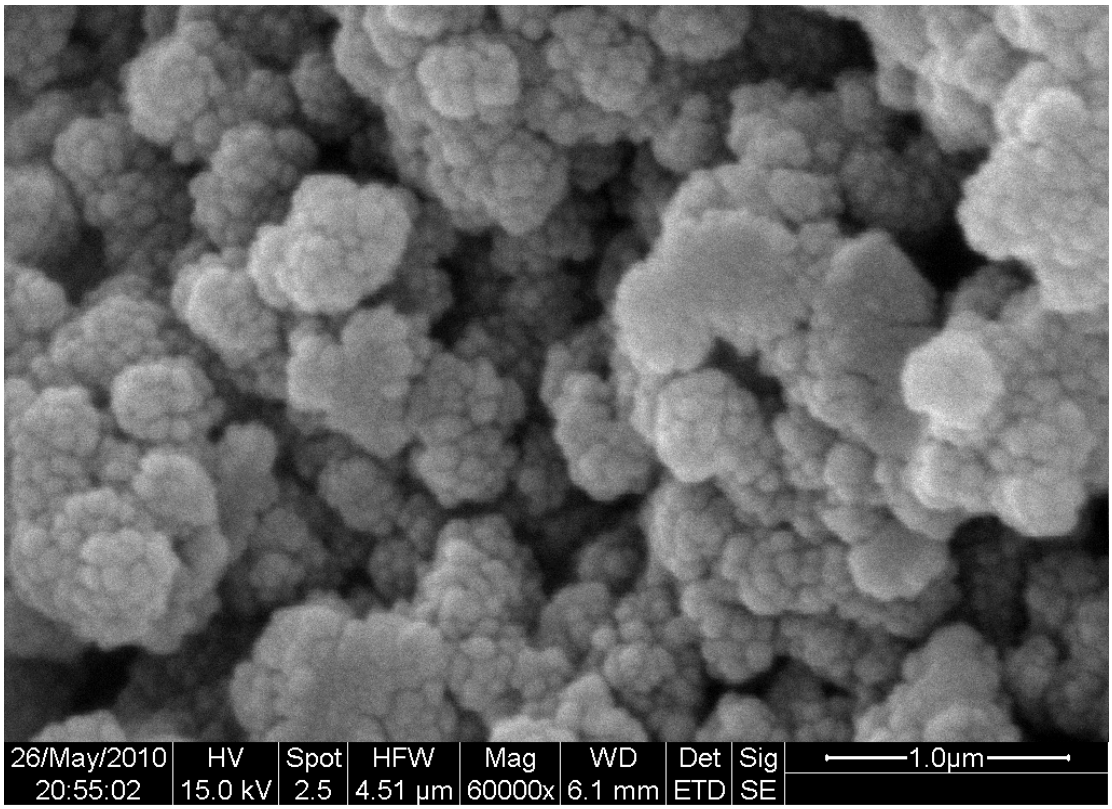

Figure 5.3d: SEM of AS11 latex particle mixture coating.

5.3.1 AS11 - 54 nm latex-coated capillary columns

CMS-*co*-DVB monolith filled capillaries were post-functionalised as described in Chapter 2 and cut into smaller workable sections prior to coating with the different latex solutions. Cap12, Section 1 was coated with the 54 nm AS11 solution and subsequently cut into two halves, 1st and 2nd (1H and 2H). Each half was then tested chromatographically using a standard 5 anion mixture. The resulting chromatogram of the first half (Figure 5.4) shows some analyte retention but suffers from band-broadening effects as evident by the tailing and distorted analyte peaks.

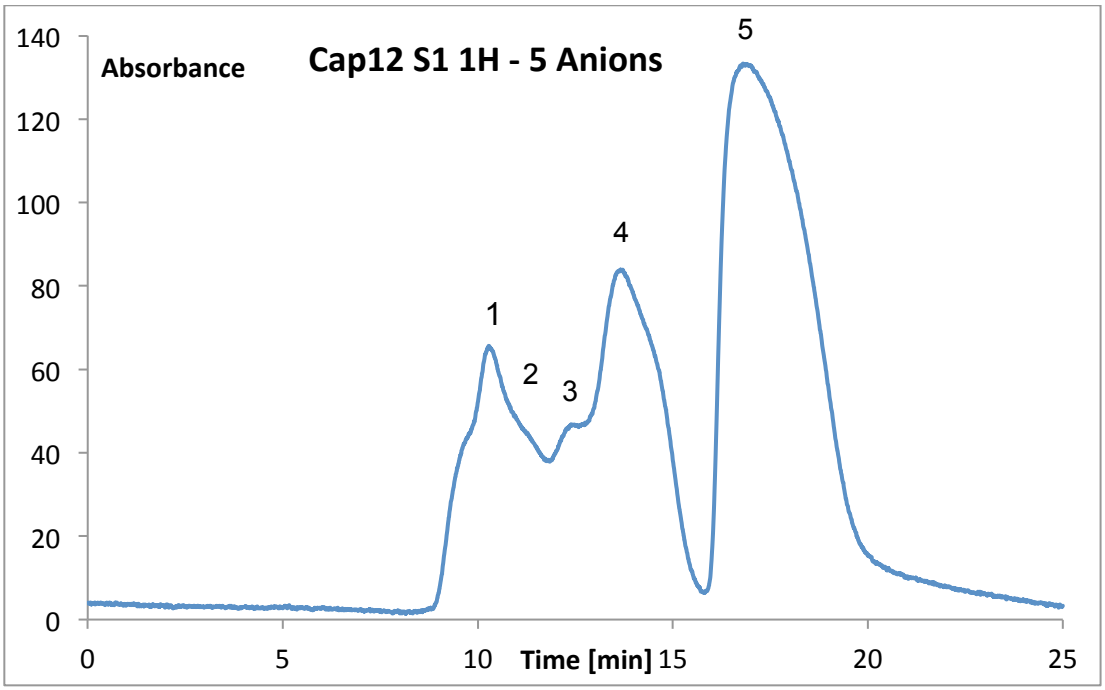

Figure 5.4: Chromatogram of Cap12 S1 1H (0.2 x 150 mm AS11 latex coated capillary column): 5 Anions: 1 NO_2^- (5 ppm), 2 NO_3^- (10 ppm), 3 IO_3^- (15 ppm), 4 BrO_3^- (50 ppm), 5 Br^- (50 ppm), Injection: 0.5 µL, Eluent: 20 m*M* KCl at 0.5 µL/min.

The capillary section was flushed several times with MilliQ water and then scanned with the contactless conductivity detector (C^4D) as described in Chapter 4, starting with a high conductivity reading followed by a gradual decrease along the first third of its length. A multi-step drop-off occurred in the centre part of the capillary column, as shown in Figure 5.5. These steep signal reductions were surprising and possible reasons could be a reduction in latex coating in the latter part of the capillary, morphological discontinuities or a combination of both.

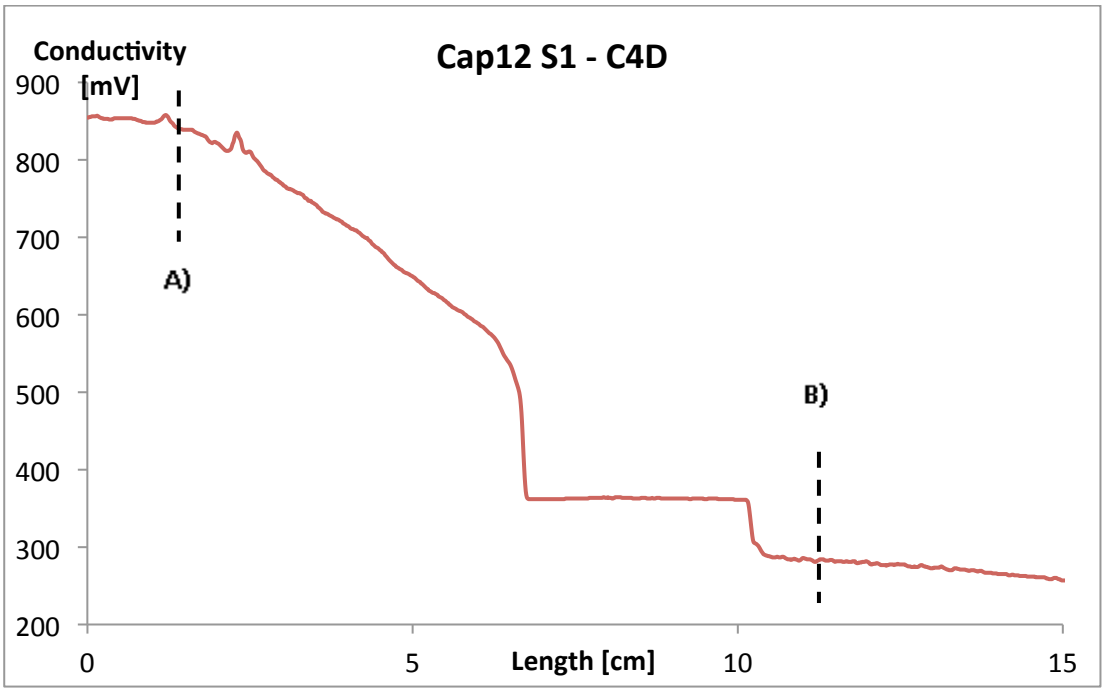

Figure 5.5: C^4D scan of Cap12 S1 1st half (Post MilliQ flush): Frequency 3xHigh, Gain 200%, full Amplification (Voltage 0), Offset 0. The capillary was cut at location A) and B) for SEM analysis.

The corresponding SEM images correlate well with the C^4D findings, with the sampling location A) in the higher conducting section in Figure 5.6a showing a relatively uniform morphology distribution across the entire cross-section. The corresponding high magnification image exhibits a clear presence of latex particles on the substrate surface. The highly magnified segment of the cross-sectional image of the latter, low conducting part of the monolith filled capillary at location B is however not showing any visible latex coverage (Figure 5.6b). In the cross-sectional capillary image of Figure 5.6b, some morphological disparity in the capillary centre is also visible, which would explain some of the band broadening issues of the resulting chromatogram.

The second half of Cap12 S1 was analysed in the same way, with the resulting chromatogram shown in Figure 5.7. Again the anions are well separated but the peaks are broadened due to possible eddy diffusion and flow-mixing, usually caused by uneven flow-channels as a result of likely morphological inconsistencies. Following the same procedure as with the first half, the section was scanned by C^4D after being flushed multiple times with MilliQ. The resulting conductivity profile is shown in Figure 5.8.

The scanned profile exhibits a relatively smooth contour for the initial 8 cm followed by a slight signal dip, before regaining most of the initial conductivity value. The sharp drop off at the end of the capillary indicates some material inconsistency before the final spike at the capillary end cut-off (the conductivity spike is a likely result of higher ion concentration due to eluent evaporation at the open end).

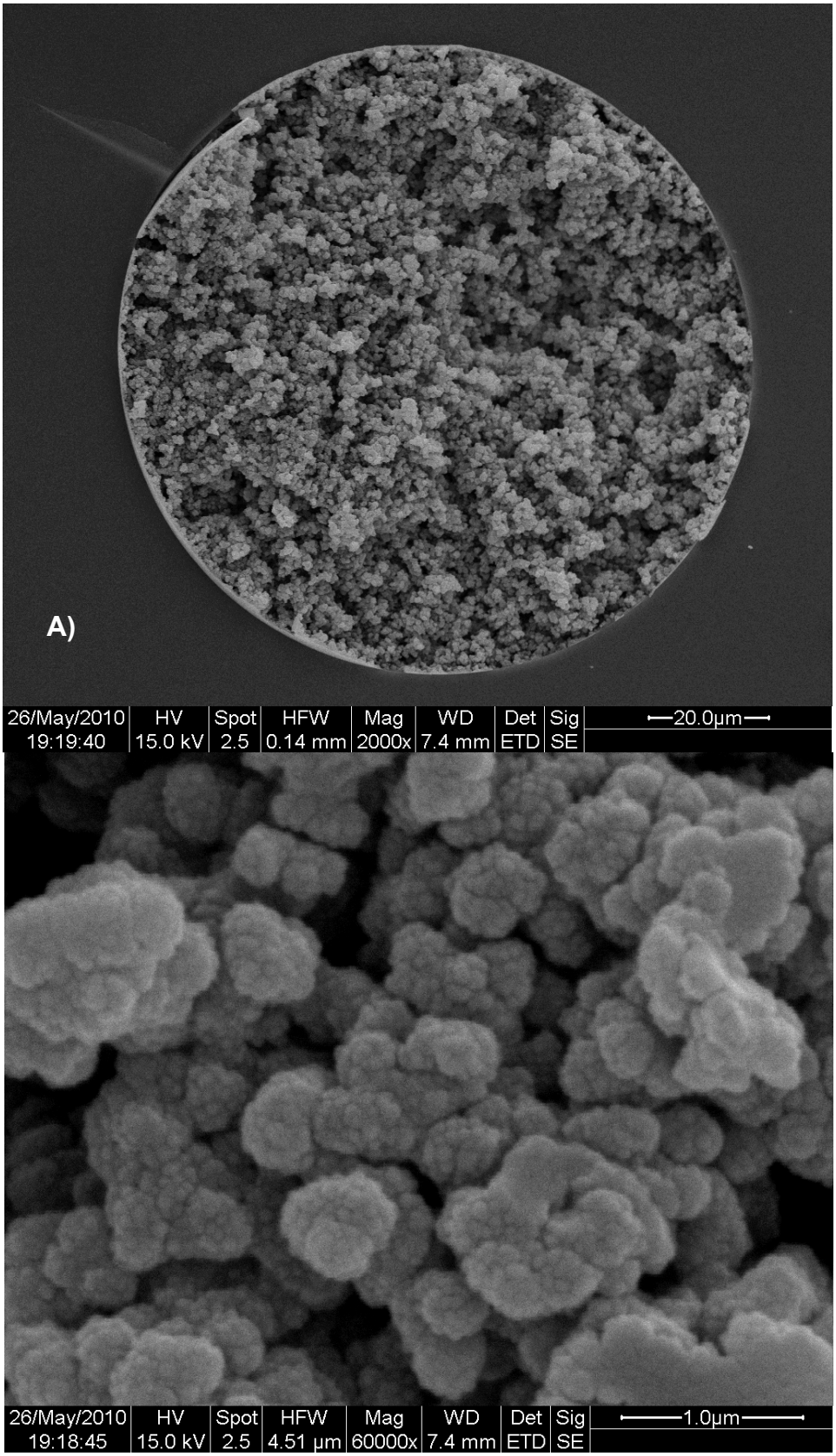

Figure 5.6a: SEM of capillary cross-section at location A) and highly magnified segment presenting latex coverage below.

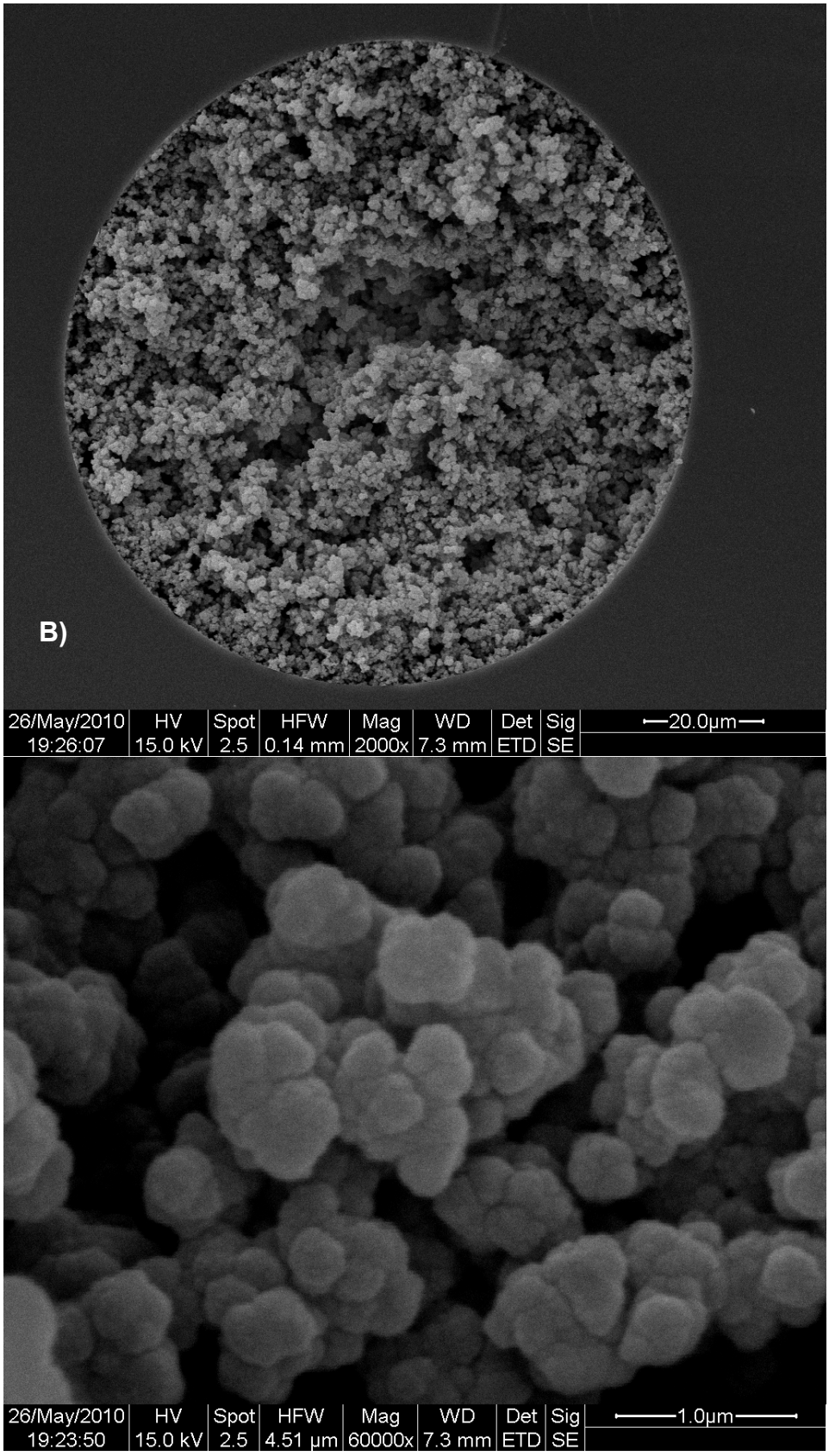

Figure 5.6b: SEM of capillary cross-section at location B) and highly magnified segment presenting no visible latex coverage below.

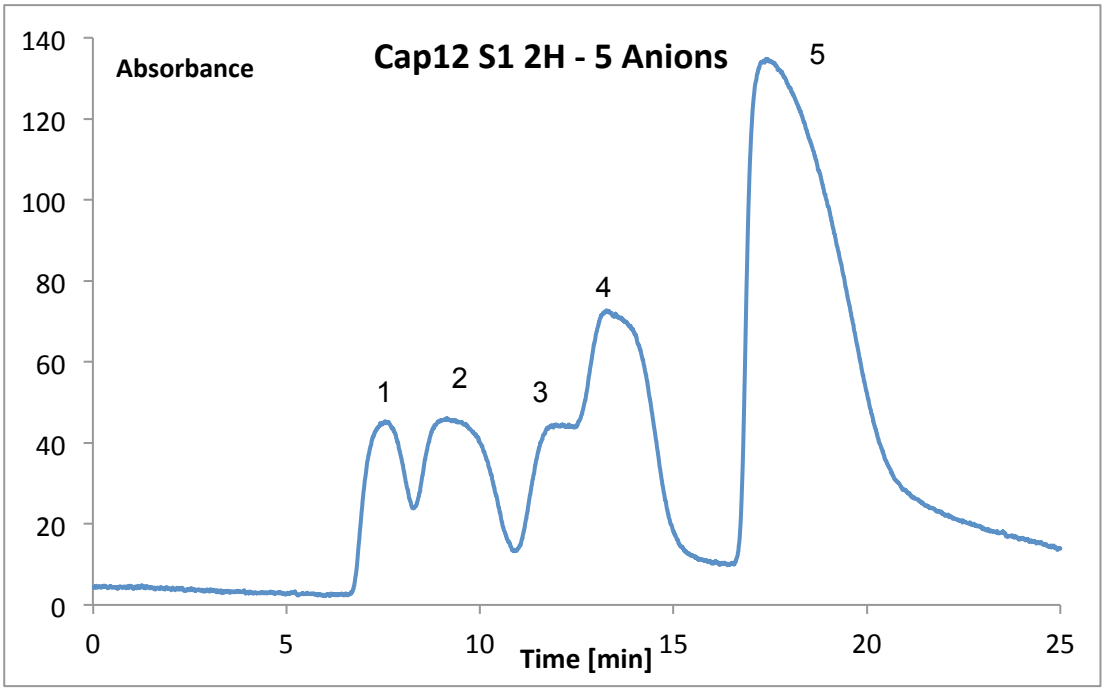

Figure 5.7: Chromatogram of Cap12 S1 2H, 5 Anions: 1 NO_2^- (5 ppm), 2 NO_3^- (10 ppm), 3 IO_3^- (15 ppm), 4 BrO_3^- (50 ppm), 5 Br^- (50 ppm), Injection: 0.5 μL, Eluent: 20 m*M* KCl at 0.5 μL/min.

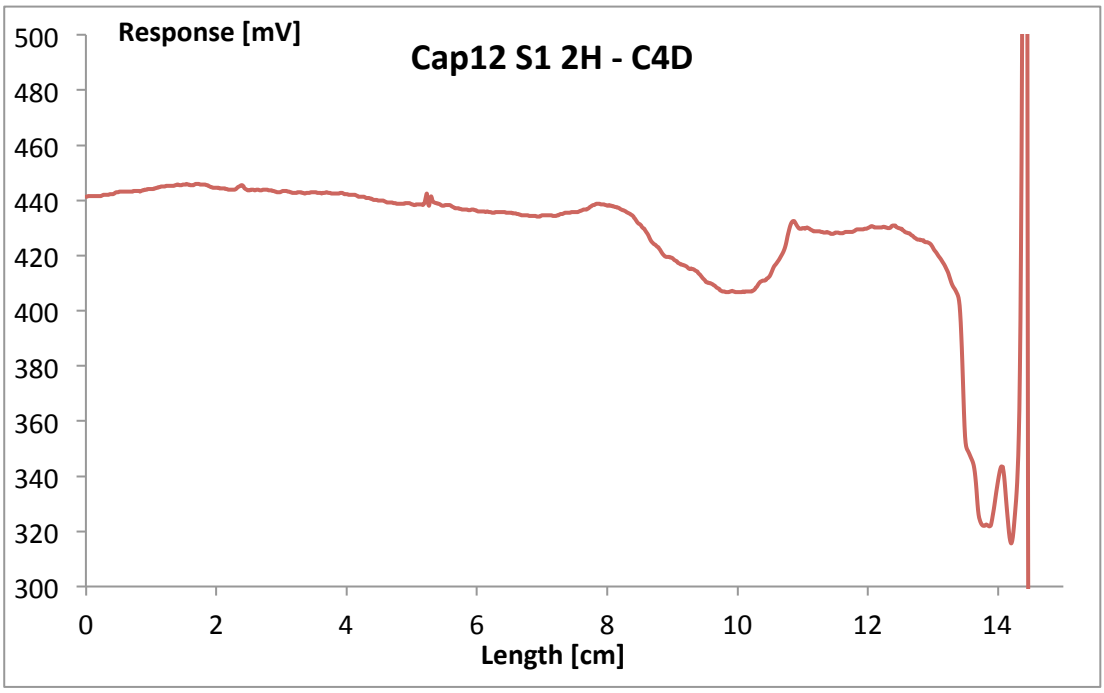

Figure 5.8: C^4D scan of Cap12 S1 2nd half (Post IC MilliQ flush): Frequency 3xHigh, Gain 200%, Amplification Voltage 0 (full), Offset 0.

Another trial was conducted with a freshly prepared polymerisation mixture of the same recipe and subsequently post-modified using the same procedure. The resulting scaffold was again coated with the diluted 54 nm AS11 latex solution and labelled CMS S1. A small section of the polymerised capillary was retained without subsequent modification (in the chloromethyl form) and tested chromatographically as an anion-exchange stationary phase for comparative purposes.

Figure 5.9 illustrates the elution of the five anions as one broad peak, as a result of insufficient surface functionality. In comparison, the post-modified and latex coated analogue shows clearly separated peaks, as illustrated in Figure 5.10. The corresponding SEM images (Figure 5.11) of the column cross-section are unfortunatly of poor quality, however at closer examination exhibit a good latex coverage, as well as a reasonably uniform substrate morphology, which would explain the better seperation performance evident by the lesser degree of peak broadening.

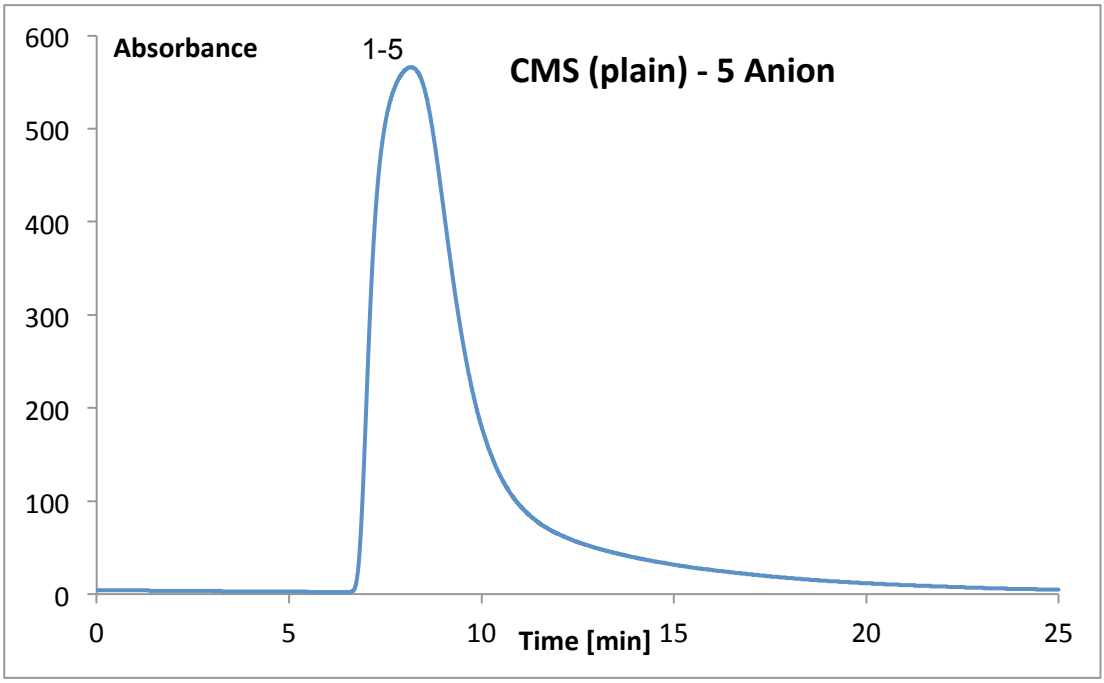

Figure 5.9: Chromatogram of the unmodified CMS-*co*-DVB capillary, Separation: 5 Anions co-eluted: 1 NO_2^- (5 ppm), 2 NO_3^- (10 ppm), 3 IO_3^- (15 ppm), 4 BrO_3^- (50 ppm), 5 Br^- (50 ppm), Injection: 0.5 µL, Eluent: 20 m*M* KCl at 0.5 µL/min.

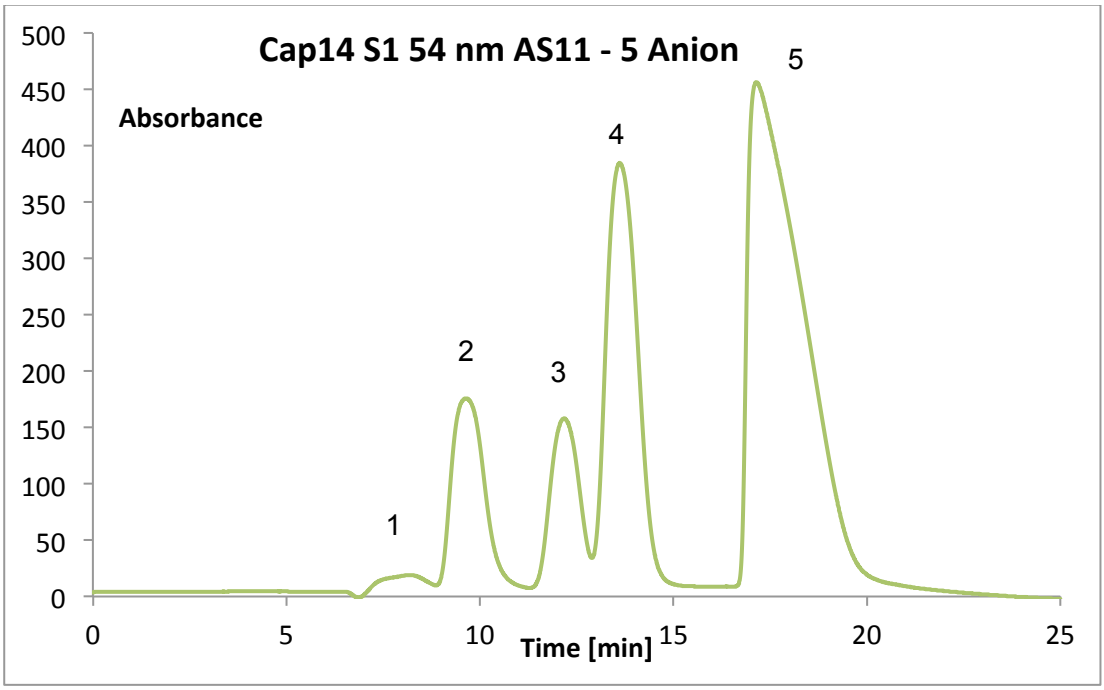

Figure 5.10: Chromatogram of CMS S1 (54 nm AS11), 5 Anions: 1 NO_2^- (5 ppm), 2 NO_3^- (10 ppm), 3 IO_3^- (15 ppm), 4 BrO_3^- (50 ppm), 5 Br^- (50 ppm), Injection: 0.5 µL, Eluent: 20 m*M* KCl at 0.5 µL/min.

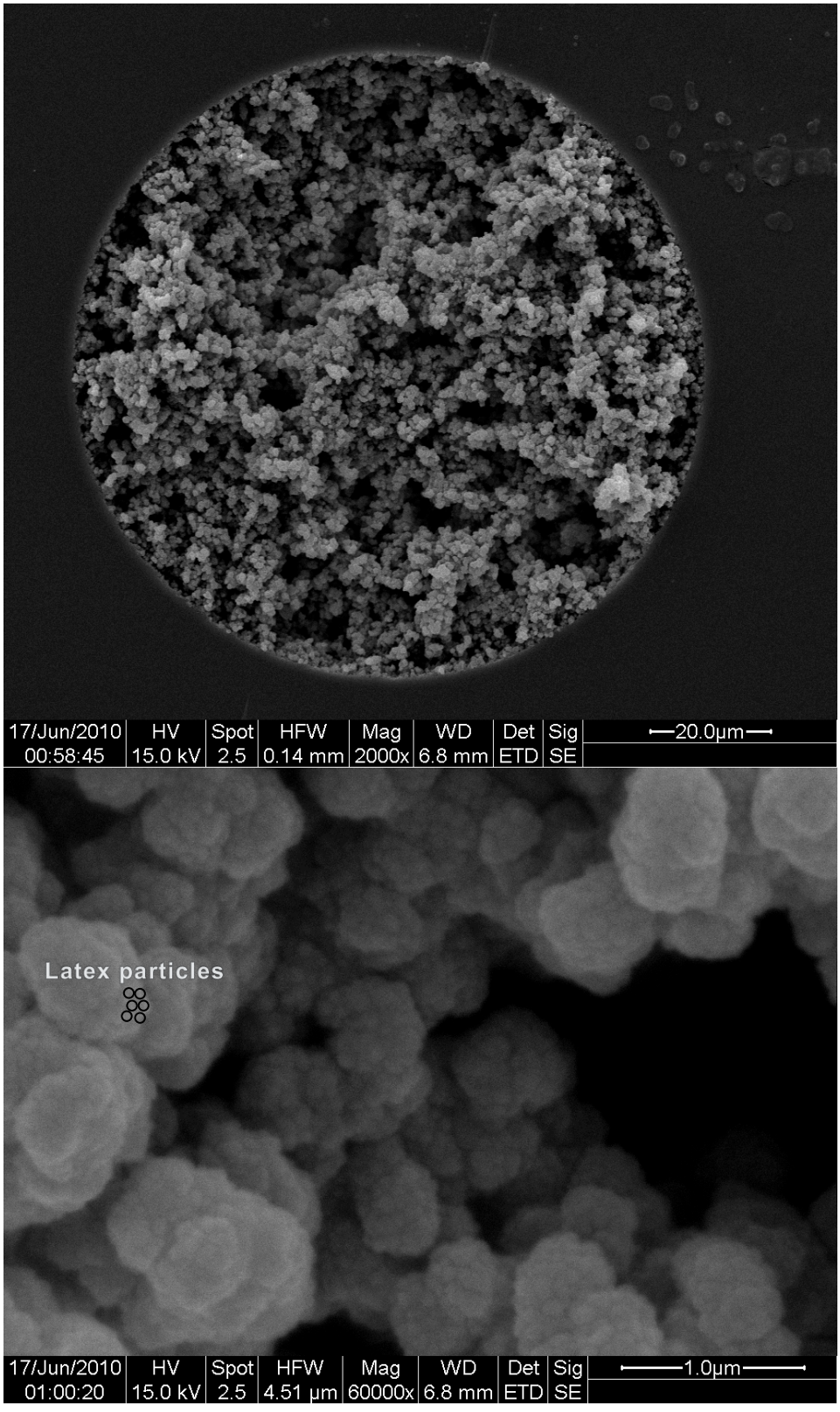

Figure 5.11: SEM images of latex coated (54 nm) sulfonated poly(CMS-*co*-DVB) monolith CMS S1.

The C^4D profile of the unmodified column exhibited a high degree of signal variations, resulting from numerous discontinuities within the stationary phase morphology, as seen in the corresponding conductivity profile in Figure 5.12. The irregular conductivity signal profile relates to the structural variations within the morphological makeup. The material was not functionalised, so the response correlates to the volume of MilliQ water present in the porous space, reflecting on the variations of the average cross-sectional porosity.

Since these variations are quite pronounced over distances of less than one cm, it appears that the axial resolution of the detector is close to the physical gap between the ring electrodes, which are 0.8 mm apart. C^4D used as a scanning characterisation technique allows physical examination of average capillary cross-section conductivity at axial resolutions of less than 1 mm. This level of detail is sufficiently precise to detect material inconsistencies, which may be affecting the chromatographic performance.

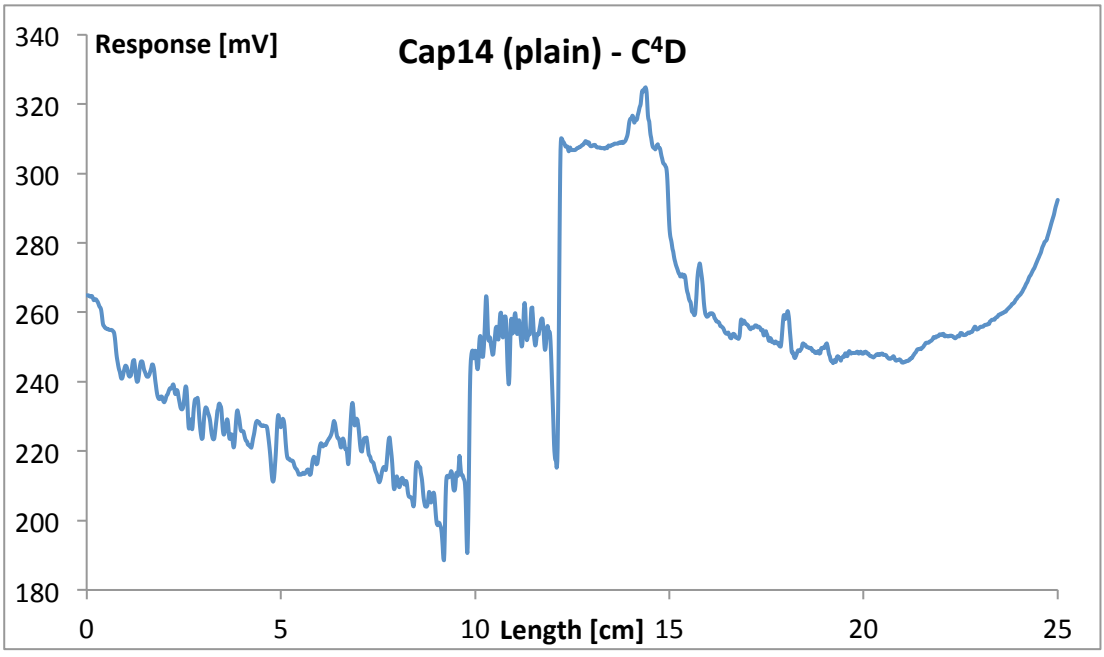

Figure 5.12: C^4D scan of CMS S1 prior to modification: Frequency 3xHigh, Gain 100%, full Amplification (Voltage 0), Offset 0.

5.3.2 AS11 - 75 nm latex-coated capillary columns

Another section of sulfonic acid functionalised monolith capillary section was coated in the same manner as described earlier by flushing the capillary column with a 1:100 AS11 75 nm latex solution in MilliQ from both ends and labelled Cap11 S2. The dilution ratio was doubled to 100, due to blocking issues at 1:50. The separation of 5 common anions was also conducted as described before with various injections ranging from 0.1 to 0.5 μL to test for overloading of the column. The resulting chromatograms with injections of 0.3, 0.4 and 0.5 μL are shown in Figure 5.13 as three overlaid colours. SEM imaging of the material after IC separation is illustrated in Figure 5.14. The cross-sectional images exhibit uniform, near monolayer coverage of the latex particles (75 nm) and a relatively even distribution of pores.

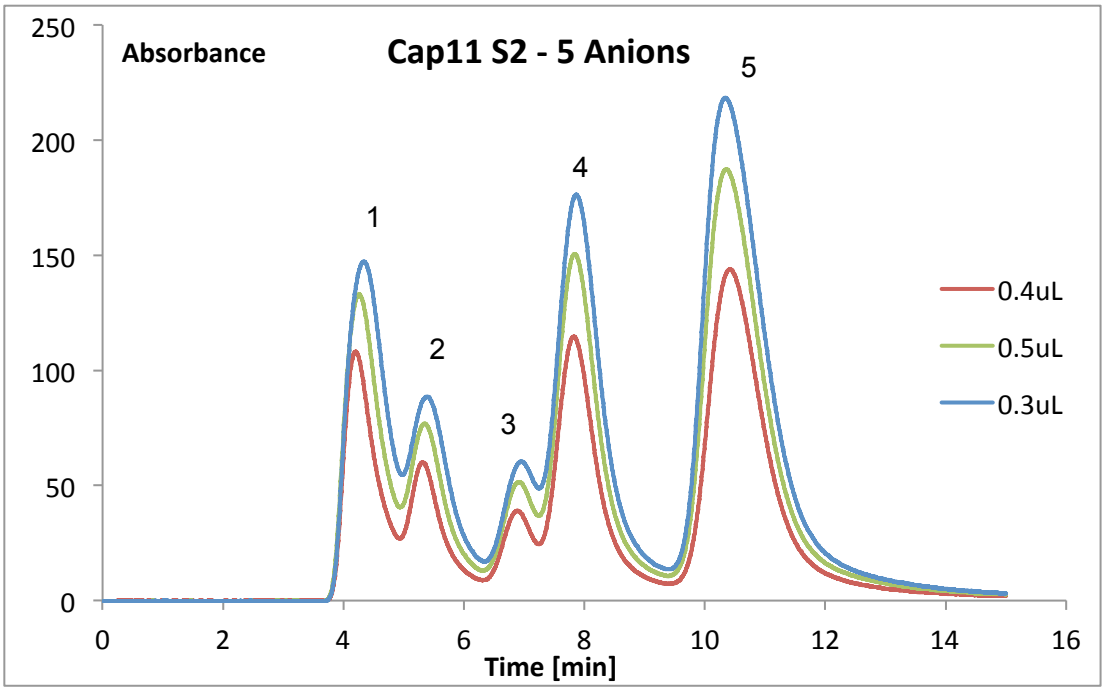

Figure 5.13: Chromatogram of Cap11 S2 (200 μm *i.d.* fused silica capillary filled with sulfonated CMS-*co*-DVB monolith and coated with 75 nm AS11 latex particles); 5 Anions: 1 NO_2^- (5 ppm), 2 NO_3^- (10 ppm), 3 IO_3^- (15 ppm), 4 BrO_3^- (50 ppm), 5 Br^- (50 ppm); Eluent: 50 m*M* KCl, at 0.5 μL/min, Injection volumes: 0.3 (red), 0.4 (beige) and 0.5 μL (blue).

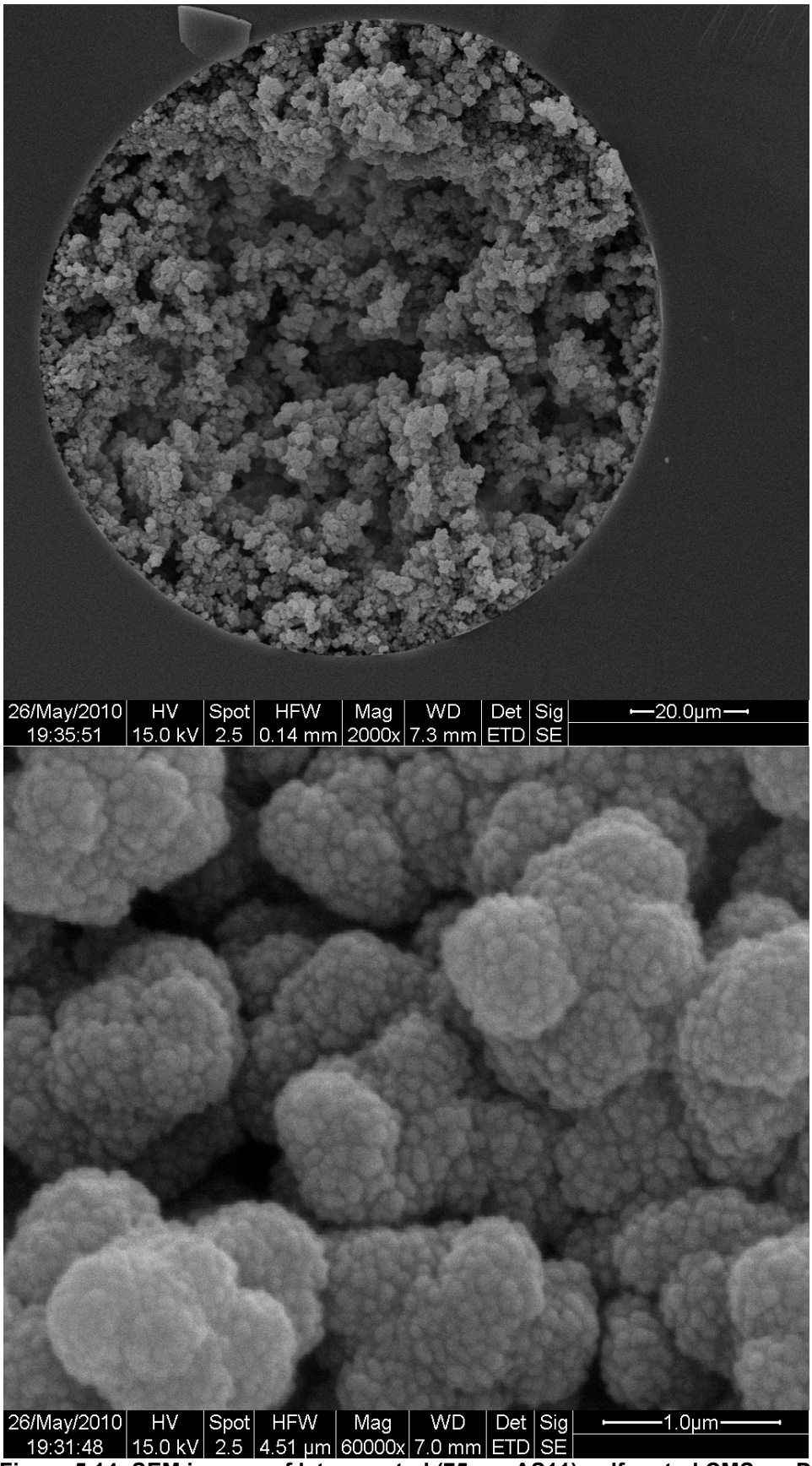

Figure 5.14: SEM images of latex-coated (75 nm AS11) sulfonated CMS-*co*-DVB monolith capillary column Cap11 S2.

Plotting of the conductivity response using scanning C^4D produced a uniform profile along the majority of the capillary length, as shown in Figure 5.15. Small variations along the middle section indicate a degree of morphological inconsistency. The steep drop at the 19 cm mark indicating a sharp decrease in conductivity could either be a result of an abruptly lesser extent of functional latex coating or a sudden morphological discontinuity.

SEM imaging of cross-sectional cuts at the low conducting section confirm that it is the latter cause (Figure 5.16). While a monolayer coverage of latex nanoparticles can be observed at close range (60,000 x magnification), the cross-sectional image (2,000 x magnification) shows gross morphological disparities, which would lead to an uneven flow-profile resulting in broader peaks.

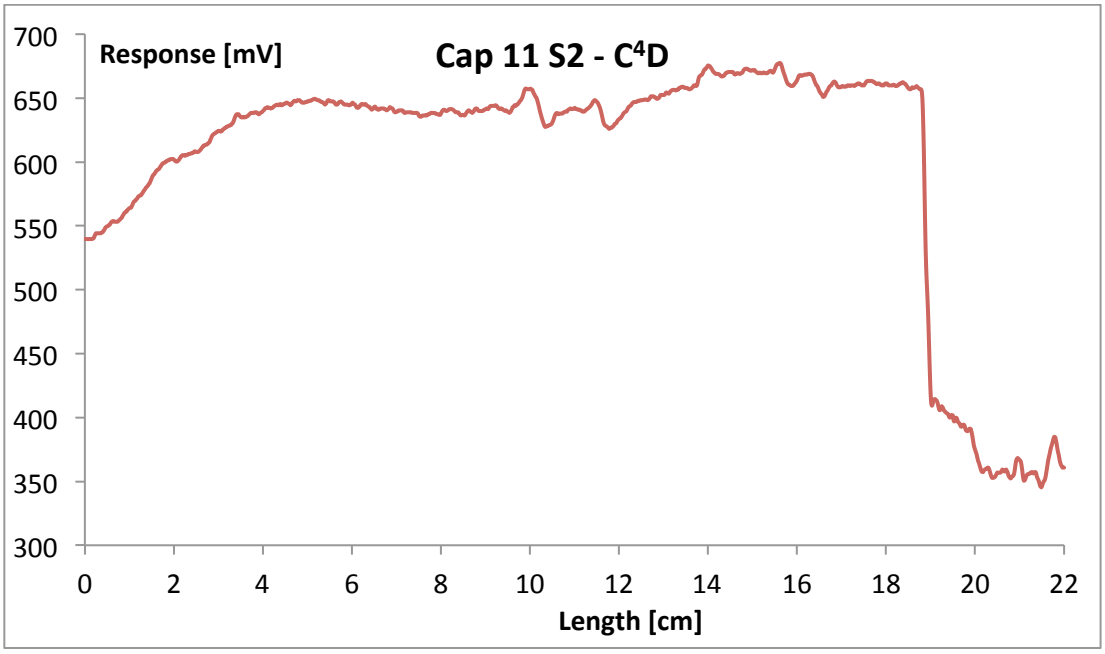

Figure 5.15: C^4D Profile of Cap11 S2, AS11 (75 nm) latex-coated, sulfonated poly(CMS-*co*-DVB) capillary column after MilliQ flushing, Frequency 3xHigh, Gain 200%, Amplification Voltage 0 (full), Offset 0.

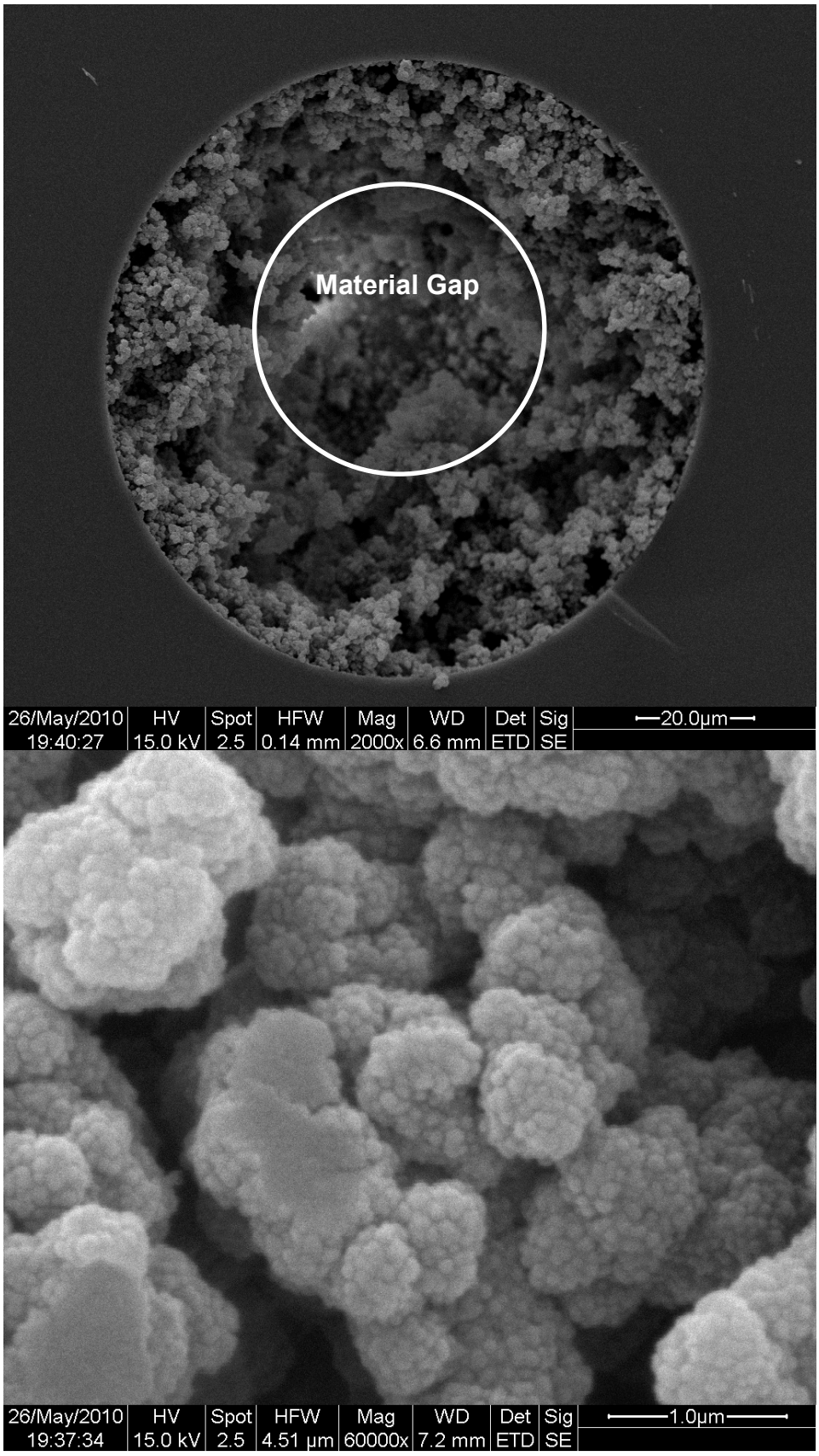

Figure 5.16: SEM images of latex-coated (75 nm AS11) functional styrene-*co*-DVB monolith cross-section, cut at the lower conducting capillary end of Cap11 S2, showing good latex coating of the polymer globules, however large morphological disparities in the capillary centre.

5.3.3 AS11 – 170 nm latex-coated capillary columns

The first section of Cap11 (S1) was coated with 170 nm sized AS11 latex particles by subsequent flushing of the 1:100 solution in MilliQ from either end of the monolith filled capillary. Chromatographic analysis of the column (Cap11 S1) showed little retention and no separation of the 5 anion mixture. The C^4D response (shown in Figure 5.17) of the MilliQ flushed column conducted post IC testing and using a detector setting of maximum amplification and 200% gain, resulted in a signal response half in magnitude to the 75 nm AS11 latex coated version earlier. The C^4D profile shows relative uniformity but is of relatively low conductivity along the majority of the capillary length with the exception of noticeable conductivity spikes towards the end of the column.

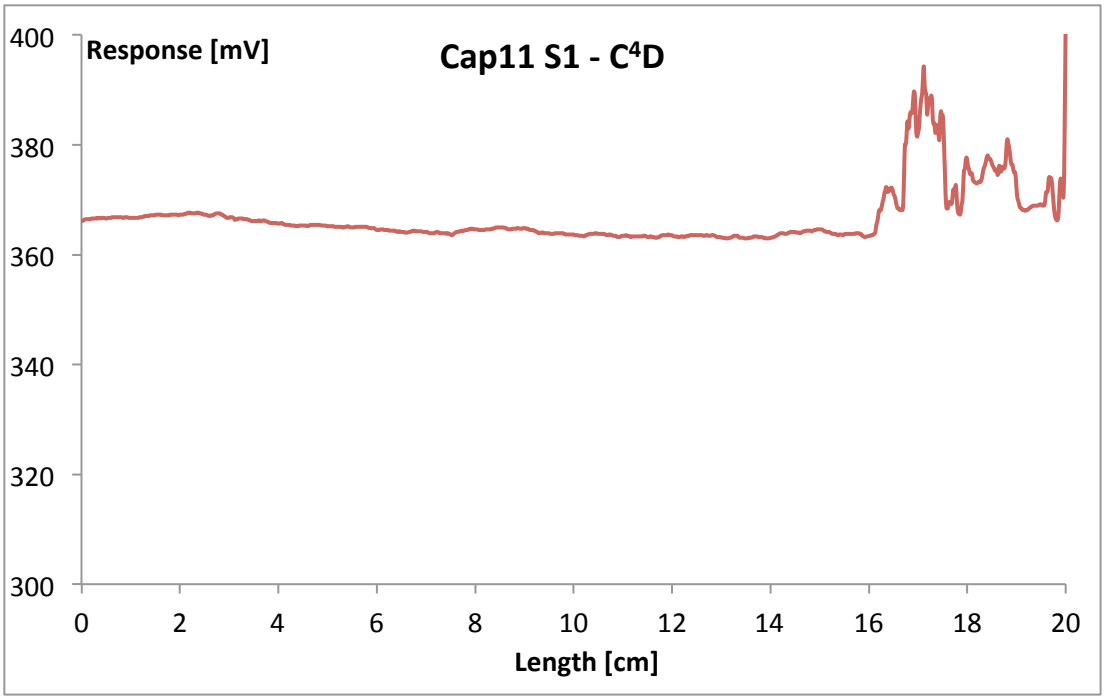

Figure 5.17: C^4D profile of AS11 (170 nm) latex-coated Cap11 S1 sulfonated CMS-*co*-DVB column, MilliQ flushed, Frequency 3xHigh, Gain 200%, Amplification Voltage 0 (full), Offset 0.

Analysis by SEM shows the evenly dispersed presence of some latex particles at the location of the conductivity spikes in the conductivity profile above. Cross-sectional cuts at the remainder of the column however reveal a total lack of functional latex particles (Figure 5.18c), which would explain the low conductivity reading along the majority of the column. Besides the lack in functionality, the column shows an otherwise good morphological uniformity.

The reason for this sporadic coating is not known and requires further analysis of the contributing factors, such as the extent of post-modification and the possible influence of gel porosity in the latex coating process.

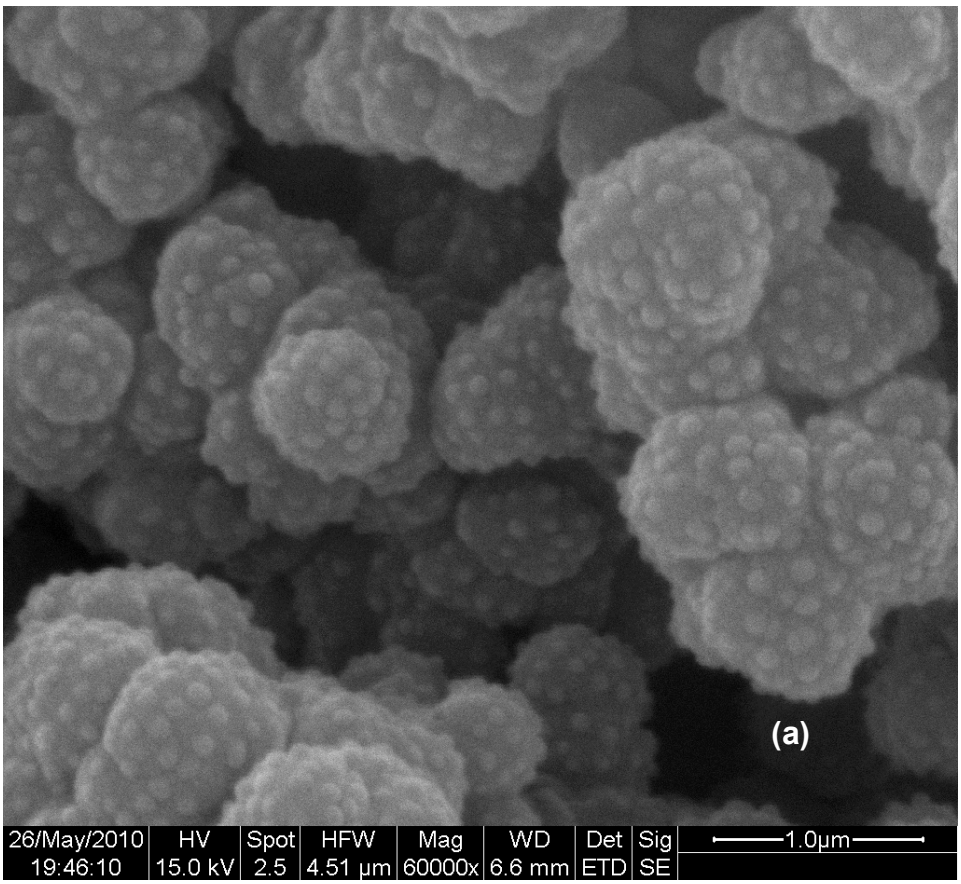

Figure 5.18: SEM images of AS 11 (170 nm) latex-coated Cap11 S1, spike response section (a) and uniform lower conducting section (b and c).

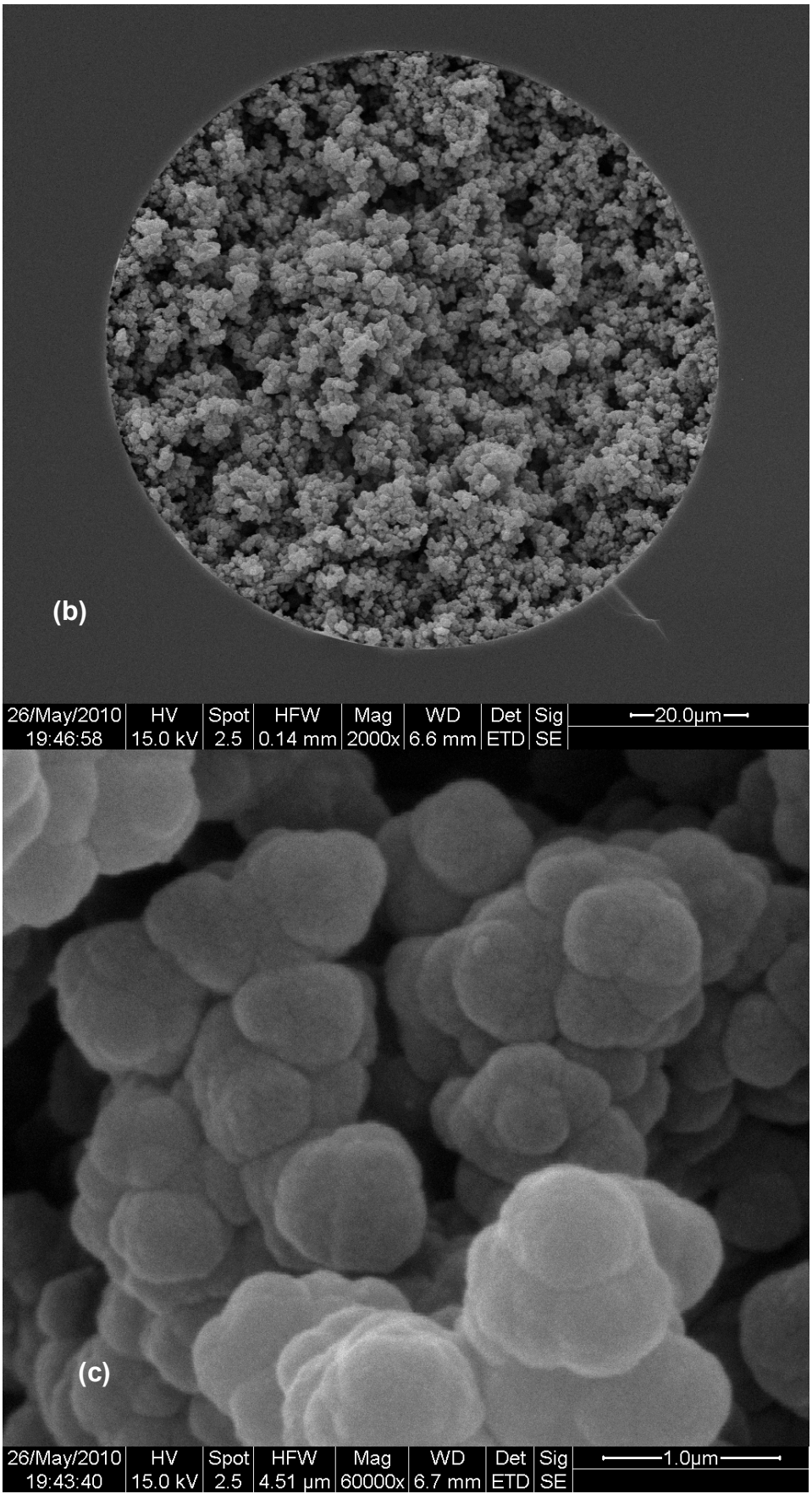

Figure 5.18: SEM images of AS 11 (170 nm) latex-coated Cap11 S1, spike response section (a) and uniform lower conducting section (b and c).

A capillary column prepared with fresh monomer mixture of the same composition and post-functionalised in the same manner was also coated with the AS11 (170 nm) 1:100 latex solution and labelled CMS2 S2. The separation of 5 anions using this column in the Nano 3000 Micro LC is shown in Figure 5.19.

Although the 5 anions are separated within 30 min, the individual peaks suffer from band broadening, which is most likely caused by factors other than the diffusion driven mixing that normally arises from lengthier separation times. This is evident in the similar tailing peak shape of the early and later eluted ions, suggesting that it is not a time based diffusion mechanism that is causing the broadening of analyte bands.

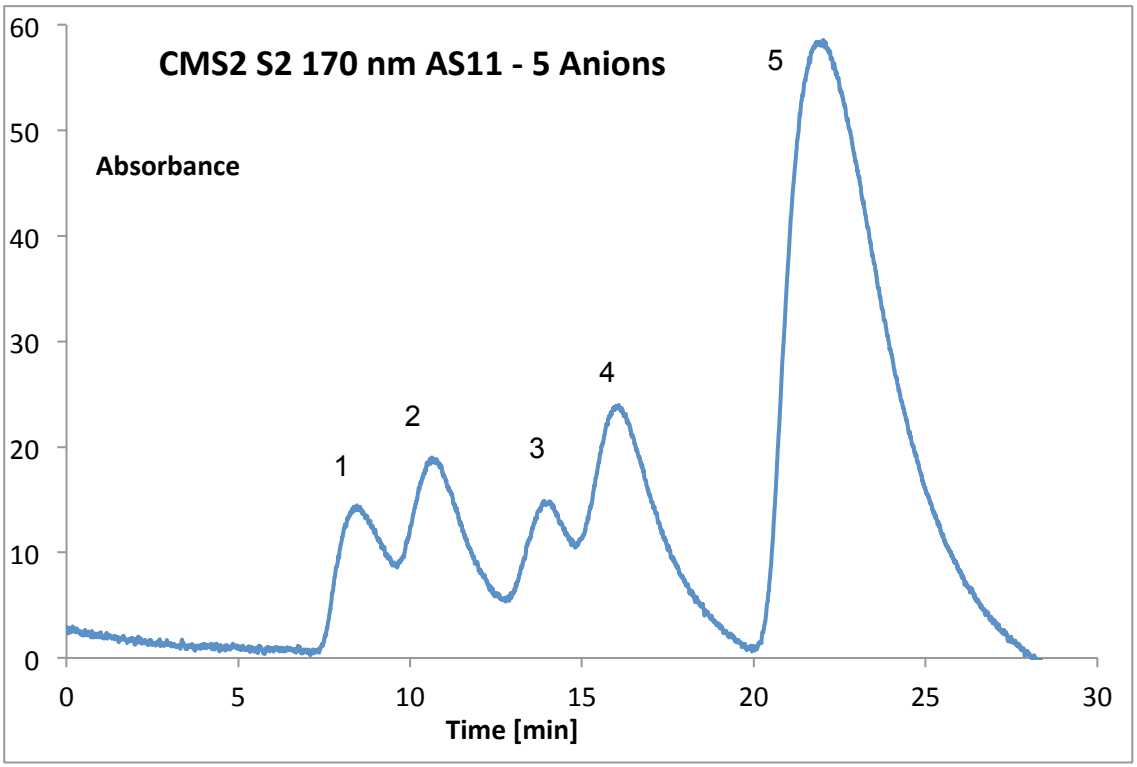

Figure 5.19: Chromatogram of CMS2 S2 (0.2x160 mm sulfonated CMS-*co*-DVB column coated with 170 nm AS11), 5 Anions: 1 NO_2^- (5 ppm), 2 NO_3^- (10 ppm), 3 IO_3^- (15 ppm), 4 BrO_3^- (50 ppm), 5 Br^- (50 ppm), Injection: 0.5 µL, Eluent: 20 m*M* KCl, at 0.5 µL/min.

SEM images show good latex coverage (Figure 5.20), which is confirmed by the analyte retention in the chromatogram. The cross-sectional image however illustrates uneven pore distribution resulting in likely flow-mixing and therefore band broadening of the analyte peaks.

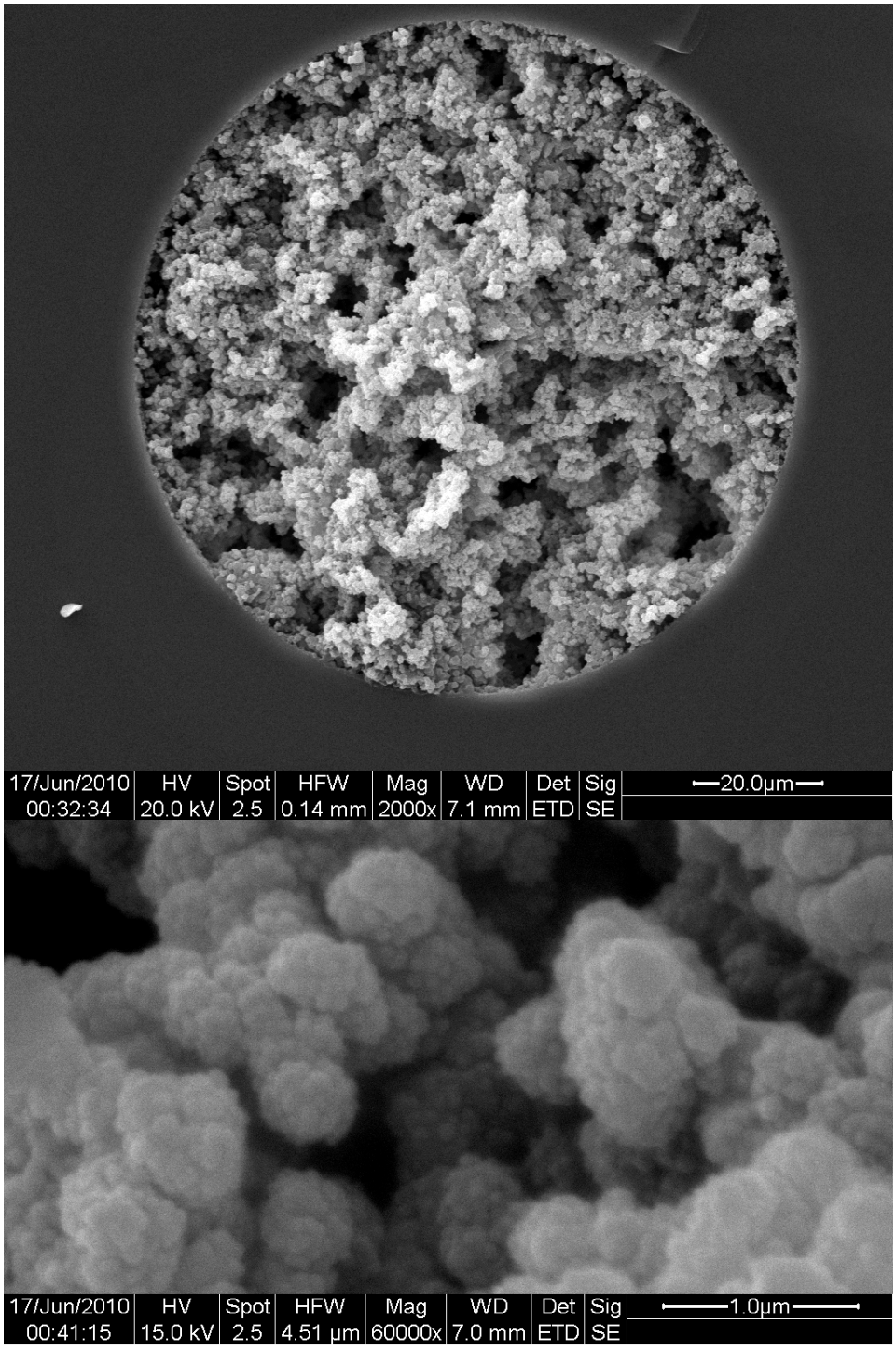

Figure 5.20: SEM images of latex-coated (170 nm AS11) CMS2 S2.

Conductivity scanning of the column after chromatographic testing was performed by C^4D and illustrates the irregular morphology and latex-coverage in the resulting irregular conductivity profile as shown in Figure 5.21. The difference in conductivity over the first 8 cm in comparison to the latter half is a direct result of the extent of latex coating. The higher conducting section has a higher surface charge and therefore higher response in the alternating field of the detector electrode due to the higher presence of latex particles.

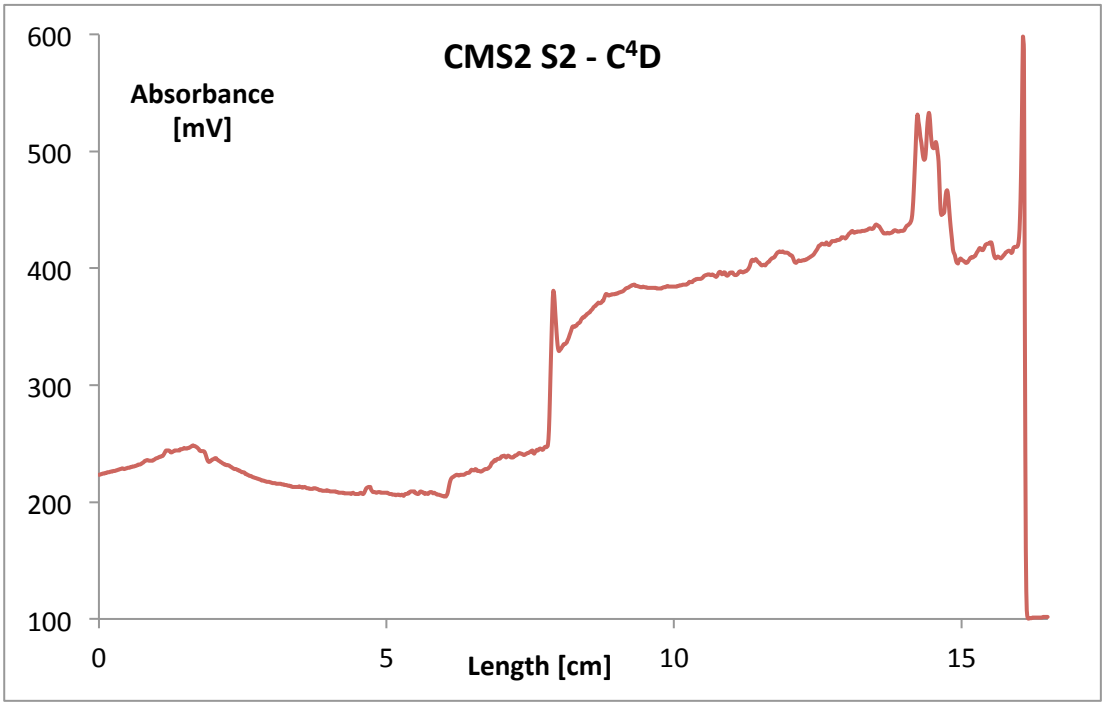

Figure 5.21: C^4D profile of AS11 (170 nm) latex-coated CMS2 S2 column, MilliQ flushed, Frequency 3xHigh, Gain 100%, 0V, Offset 0.

5.3.4 AS11 latex mixture coated capillary columns

In an attempt to achieve maximum surface density of the different sized particles, the sulfonated CMS-*co*-DVB monolith was coated with an equal mixture of the three different sized (54, 75 and 170 nm) latex particles as a 1:100 solution in MilliQ. The resulting column, Cap12 S2 was cut into two halves, 1st and 2nd (1H and 2H), the latter tested for chromatographic performance using the same anion mixture. Different eluent concentrations were tested to examine time-based diffusion as a possible indicator of column morphology variation, responsible for peak broadening in monolithic IC separations (Figure 5.22).

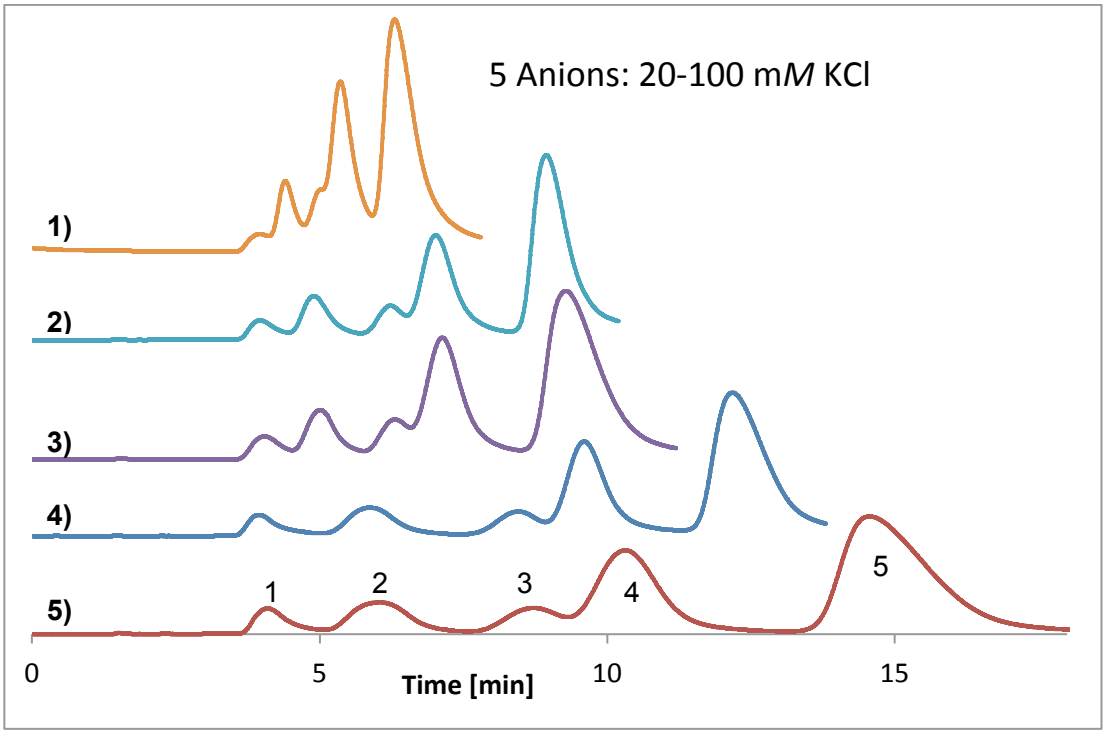

Figure 5.22: Cap12 S2 2H (0.2x200mm sulfonated poly(CMS-*co*-DVB monolith coated with AS11 mixture of 54, 75 and 170 nm latex particles), Separation: 5 Anions: 1 NO_2^- (5 ppm), 2 NO_3^- (10 ppm), 3 IO_3^- (15 ppm), 4 BrO_3^- (50 ppm), 5 Br^- (50 ppm), Injection: 0.25 l*µ*L, Eluent: 1) Isocratic 20 m*M*, 2) Gradient 20-50 m*M*, 3) Isocratic 50 m*M*, 4) Gradient 50-100 m*M*, 5) Isocratic 100 m*M*.

Assessing the progression in peak resolution, it appears that some broadening is caused by possible inconsistencies within the monolith structure. Experimental verification was conducted by SEM with the resulting images shown in Figure 5.23.

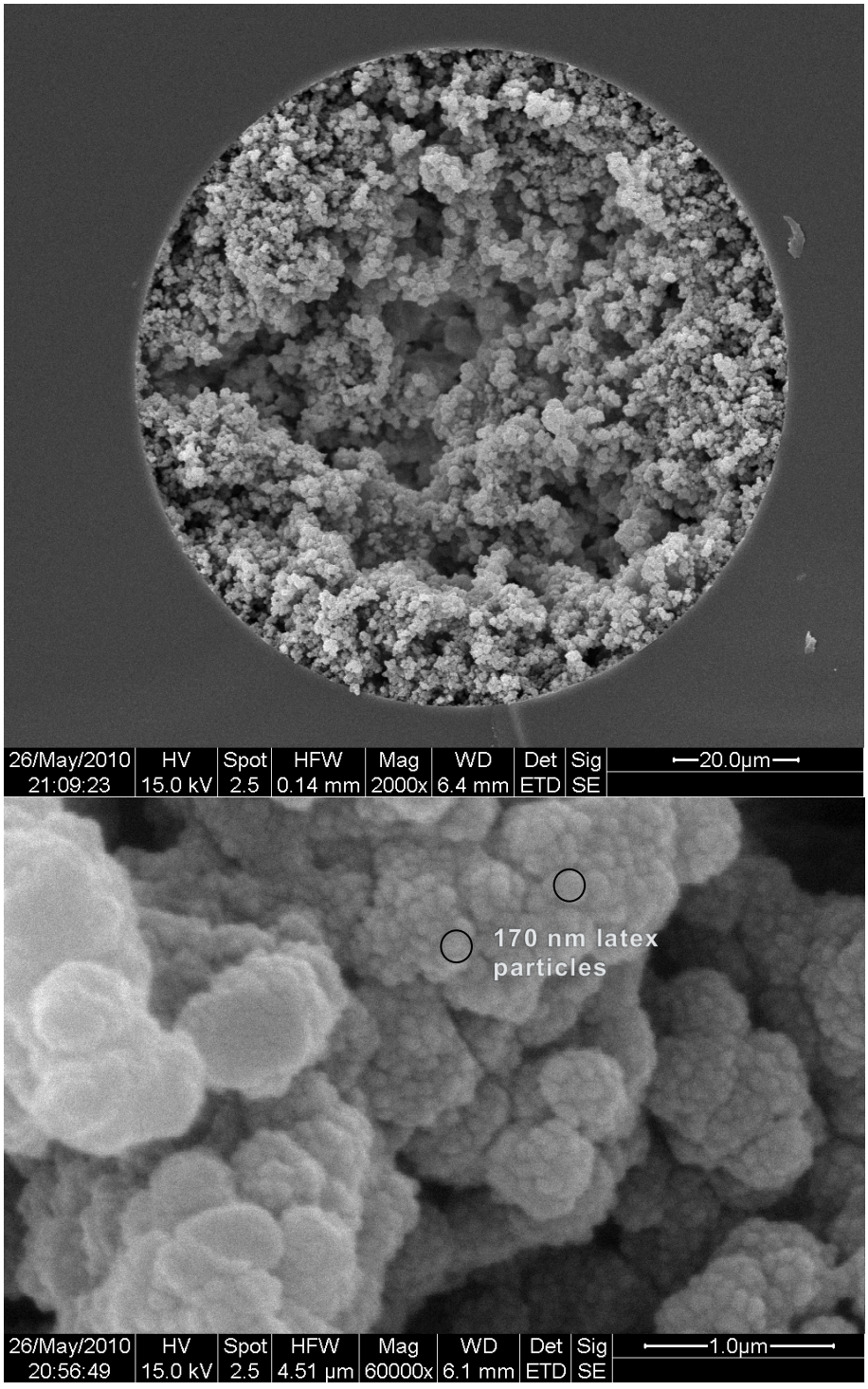

Figure 5.23: SEM images of latex-coated (AS11 mixture) Cap12 S2 2nd half.

The highly magnified segment illustrates uniform latex monolayer coverage of the different sized particle mixture over the postmodified CMS-*co*-DVB scaffold, with some larger 170 nm latex particles visible amongst the coating. The majority of the particle layer appears to be made up of the smaller latex nanoparticles. The lower magnification image shows the non-uniform morphology over the entire capillary cross-section, with bigger pores in the centre region and inconsistent globule sizes. Again these variations would account for significant peak broadening effects due to uneven flow-paths in the porous material, where larger flow-paths experience lower resistance and analytes progress faster through the capillary column.

The C^4D scan of the entire capillary Cap12 S2 following latex coating is shown in Figure 5.24. The different conductivity readings can be linked directly to the extent of the coating as shown by the SEM images. As before, the section with good latex coverage outperformed any other sections of reduced or no latex coating and remained stable over several IC separations. The small signal variations of the higher conducting 2^{nd} half account for more subtle variations arising from small morphology differences. Columns exhibiting smooth, high conductivity readings have so far shown to produce the best chromatographic results. Complete latex monolayer coverage has been achieved with the 54 and 75 nm AS11 latex solution and the mixture of all three, which appeared to exhibit the highest degree of coating. The large 170 nm sized particles were only loosely attached by themselves, suggesting that it is less the monodisperse size selection of particles that results in a well coated column than a matching of particle properties to the surface functionality of the scaffold. As such a polydisperse mixture of particles may

well result in the highest degree of coating and separation of smaller molecules.

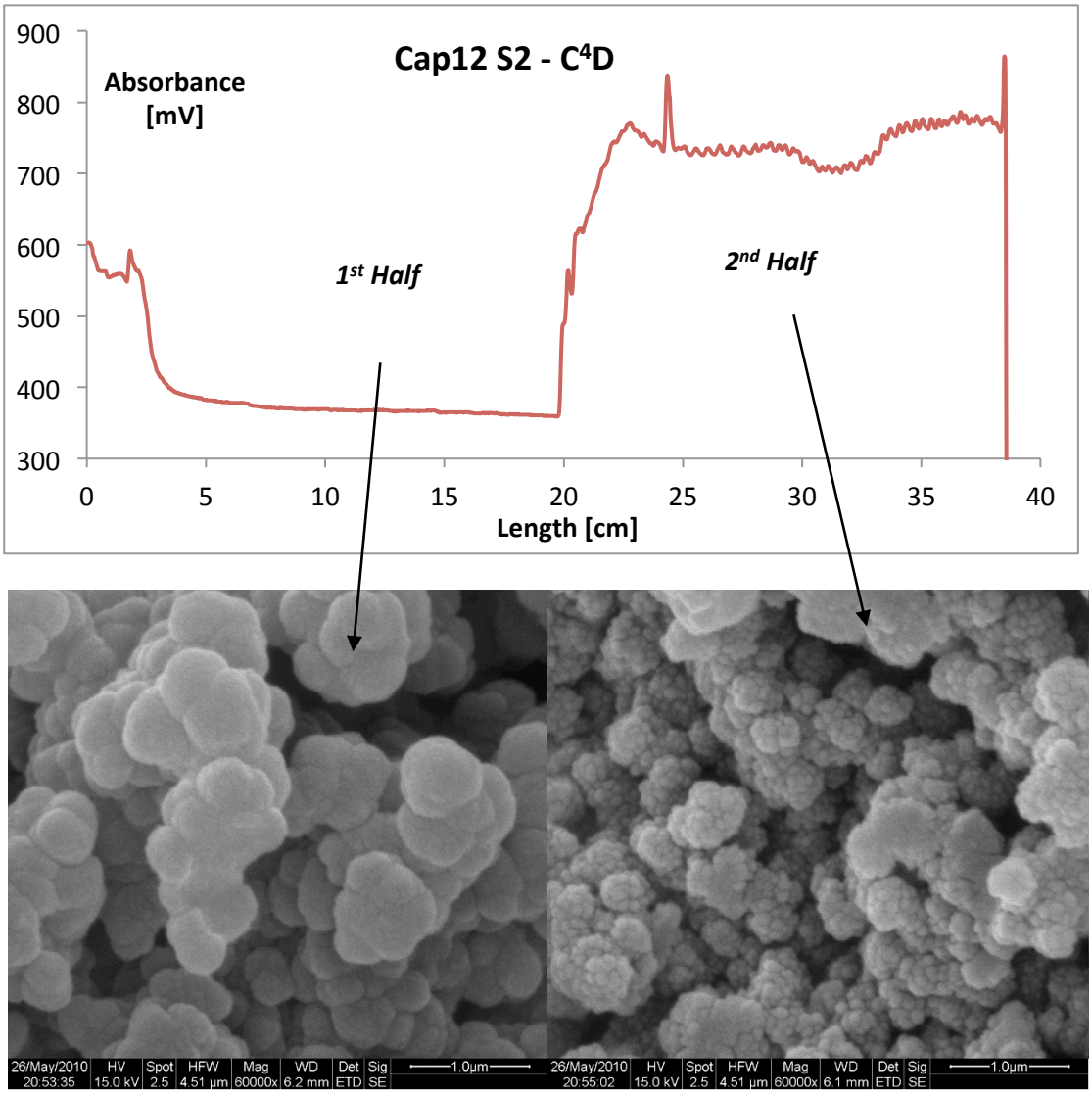

Figure 5.24: C^4D scan of Cap12 S2, both 1st and 2nd half after latex-coating (MilliQ flushed), exhibiting significantly lower conductivity over the first half, Frequency 3xHigh, Gain 200%, full Amplification, Offset 0.

SEM images of the corresponding halves directly below: 1st half (left) showing no latex particles and 2nd half (right) with the latex particles visible on the monolith surface.

5.3.5 Column performance summary

The individual columns described in this chapter are outlined below with each chromatograms analysed for the respective performance indicators.

Colum name (coating) Figure	Peak no. Analyte	Peak ret time [min]	Peak width [min]	Resolution	Asym-metry	Plates
Cap 5	Not tested					
Cap 12 S1 1H (54 nm AS11) Figure 5.4	1 NO_2^-	9.9	n.a.	n.a.	n.a.	n.a.
	2 NO_3^-	10.3	0.90	2.34	1.94	1584
	3 IO_3^-	12.5	n.a.	0.73	0.64	3549
	4 BrO_3^-	13.7	3.40	0.94	1.32	497
	5 Br^-	16.8	3.55	n.a.	2.24	252
Cap 12 S1 2H (54 nm AS11) Figure 5.7	1 NO_2^-	7.55	1.49	0.66	0.94	289
	2 NO_3^-	9.13	2.24	1.24	1.58	147
	3 IO_3^-	12.15	1.40	0.48	0.66	674
	4 BrO_3^-	13.27	2.16	1.20	1.74	353
	5 Br^-	17.42	5.53	n.a.	2.67	284
CMS plain (no latex) Figure 5.9	All 5 co-eluted	8.17	3.09	n.a.	1.24	81
CMS S1 (54 nm latex) Figure 5.10	1 NO_2^-	8.07	1.90	0.94	0.86	193
	2 NO_3^-	9.83	1.30	1.94	1.17	720
	3 IO_3^-	12.53	1.23	1.09	1.00	1433
	4 BrO_3^-	14.04	1.35	1.87	1.27	1504
	5 Br^-	17.86	2.99	n.a.	3.57	725
Cap 11 S2 (75 nm latex) Figure 5.13	1 NO_2^-	4.26	0.83	1.35	1.30	375
	2 NO_3^-	5.35	0.71	2.25	1.09	835
	3 IO_3^-	6.91	0.60	1.10	0.86	1766
	4 BrO_3^-	7.84	1.02	1.92	n.a.	912
	5 Br^-	10.35	1.56	n.a.	n.a.	684
CMS S2 (170 nm latex) Figure 5.19	1 NO_2^-	8.45	3.64	1.13	1.07	279
	2 NO_3^-	10.64	2.30	1.89	1.16	518
	3 IO_3^-	13.89	1.17	1.11	0.96	1231
	4 BrO_3^-	16.07	3.33	1.61	1.33	735
	5 Br^-	22.03	6.46	n.a.	1.81	305
Cap 11 S1 (170 nm latex)	Chromatogram not depicted					
Cap 12 S2 (AS11 mix) Figure 5.22	1 NO_2^-	3.96	0.64	1.37	1.15	565
	2 NO_3^-	4.90	0.69	2.07	1.21	756
	3 IO_3^-	6.23	0.52	1.11	0.86	1903
	4 BrO_3^-	7.02	0.84	2.03	1.23	1071
	5 Br^-	8.94	1.02	n.a.	1.47	1185

Table 5.2: Monolith column performance based on chromatograms shown in this chapter.

5.3.6 Conclusion

Latex-coated polymeric monolith capillaries are becoming more useful as micro-columns for the separation of common anions as demonstrated earlier in Chapter 3. The actual size of the latex nanoparticles used in the coating process appears to affect the level of coating more significantly. The impact on the actual separation performance of the column, once the monolayer coverage has been achieved is of lesser influence.

The main factors influencing the peak and resolution capacity of the monolithic stationary phase are determined by the extent of latex-coating and the uniformity of the axial and longitudinal morphology. For reasons not directly obvious, the distribution of surface functionalities can vary strongly within the one capillary column, containing the same monolithic polymer. These functional variations seem to occur independently of the morphology characteristics imposed during the earlier polymerisation process, such that the properties need to be addressed and optimised separately. However, the difficulty remains in detecting these variations. The combination of non-invasive detection such as C^4D and subsequent invasive analysis by SEM imaging allows visualization of the type of discontinuity, the extent of latex coating (from individual particles to dense layers, 'surfactant' covered or not) and the morphological changes in the polymer structure.

The actual impact of latex particle size on the separation performance of the column could not be reliably deduced, because of the existence of more significant factors which influence the conductivity of the material and impart overshadowing effects on the column performance. The most influential factors were predominantly in the form of irregular monolithic

substrate morphology and the overall extent and uniformity of the latex coating, which was dominated by the latex particle size in relation to the scaffold morphology, exhibiting a reduced coverage for the larger monodispersed latex solutions. Best results were achieved for the polydispersed mixture of all three sizes, which allows for each individual particle to be more adequately fitted to the corresponding micro-surface morphology and functional density.

The actual latex particle size appears to be a relevant factor in the coating process, since the required amount and distribution of the sulfonic acid counter-charge has to match the distribution of positively charged amine groups on the latex particle surface for a successful retention and coating via electrostatic interaction. It is nevertheless encouraging to use C^4D as a reliable characterisation and coating quantification technique to detect such material disparities at the precise longitudinal location without destroying the potential column. There is sufficiently of room to further develop the C^4D scanning tool, preferably in a 3 dimensional frequency variation inspection, such that a 3D scanning profile is produced for every scanned length unit with the respective conductivity response recorded for each frequency cycle.

6 General Discussion

Monolithic stationary phases have received much attention in recent literature. The problems encountered with their synthesis are however rarely mentioned in these publications. While one could say this suggests that there are not any problems, the more likely reason is that on the one hand the publication of results of experimental 'failure' is not deemed overly popular, while on the other hand some problems stem from the complexity and multitude of the polymerisation methods. This is a likely result of possible small errors in the preparation process, which are not accounted for in the synthesis protocol.

Simple systems with a low degree of variation tend to have more reliable outcomes. As such the distinct benefit of monolithic polymers, their flexibility in manufacture and specific tailoring ability, also poses the prime restriction in their manufacture, as evident in the deficiency of reliable and reproducible preparation and the anticipated improved separation performance for smaller molecules.

This has recently been brought into renewed focus by a series of publications that outline variations of the traditional synthesis procedure and are summarized in a recent review by Nischang *et al.* [21]. The common denominator in the publications summarized in this review was identified as mass transfer resistance of analytes resulting from gel porosity on the stationary phase material. The term, gel porosity, is defined by Nischang as the gel-like porous structure on the outer polymerisation layer of the monolith polymer globules, which exhibits a lower degree of cross-linking due to the kinetically favoured inclusion of the (cross-linking) divinyl monomers in the

early stages of the polymerisation [25]. The forming polymer nuclei swell with residual monomers, predominantly monovinyl, such that the outer globule layers mostly consist of longer chain 'branches' which are prone to swelling by suitable solvents/eluents. Early examination of this soft matter, gel porosity was noted by Jerabek [166] using size exclusion chromatography (SEC) on swollen styrene-*co*-DVB gels:

'*Cross-linked polymers are used as carriers in a number of various applications - ion exchangers, sorbents, catalysts, polymer reagents, carriers for the peptide synthesis in the solid state, and the like. These materials mostly swell in the medium in which they are wed, which considerably changes their structure compared with the dry state. For this reason, successful correlations between structural parameters determined for dry materials of this type by classical porosimetric methods, on the one hand, and their functional properties, on the other, are rather an exception than a rule. Steric exclusion chromatography is probably the only method capable of providing such information on the structure of swollen polymer gels.'*

An earlier study by Jerabek [167] tested the method of pore volume determination by SEC using materials of known properties (porous glass). For the polymer study, the author referred to the Ogston-Killander theory [168] as the means of modelling the pore distribution most accurately, based on the distribution of pores as random spaces amongst spherical rods of hard material.

Gel filtration was used as a means of size exclusion chromatography based on the assumption that the volume in the gel grains available for a particular substance will determine its position in the gel chromatogram. It

appears that this diffusive driven mechanism occurs independent of the flow-rate and relates predominantly to the gel porosity (gel grain size) and the rate of diffusion. More recently the hydrodynamic separation on polymer monoliths has gained in momentum as a similar separation technique that also has the secondary characterisation outcome for the porous scaffolds by size dependent separation of macromolecules [93, 169-171]. The porous properties of the polymeric separation medium were tailored to obtain macropores (of radius R) that are relative to the size of the analysed (macro)molecules (of radius r), such that the ratio $\lambda = r/R = 0.2$ or less (channel diameter is 5-50 times the size of molecules to be separated [171].

The hydrodynamic separation mechanism requires small flow-channels that exhibit laminar flow, such that molecules are separated according to size within this flow-profile. Size exclusion chromatography on the other hand occurs through diffusion of the separating molecules into the mesoporous space of the same size as the analytes and therefore offer a simultaneous characterisation of the porous scaffold, referred to as inverse size-exclusion chromatography (ISEC) [172]. Porosity data obtained by ISEC is based on the molecular standards used and measurements with more conventional materials to correlate the retention data.

Besides the limited availability, this method does not take swelling effects (such as gel porosity) into account. Nevertheless it appears to accurately describe wet-state porosity over certain range of pore sizes (the findings would benefit from comparative assessment by BET surface adsorption and mercury intrusion porosimetry).

A review by Vegvari [173] examined the use of homogenous (charged) gels in CEC in comparison to continuous beds (monoliths). Due to their non-particular structure, the beds were performing more efficiently, exhibiting lower diffusion terms and resistance to mass transfer as expressed in the Van Deemter equation:

$$H = A + B/v + Cv$$

Where A is the term expressing the eddy diffusion, B the longitudinal diffusion, C is the resistance to mass transfer and v the mobile phase velocity. The time required for an analyte molecule to diffuse from one interaction site to another is much shorter in a gel than in continuous or particular beds as the distance between the 'walls' of a gel pore is much smaller than the average distance of the pore walls in a continuous bed or between beads in a packed bed.

Both longitudinal diffusion (time dependent) and the resistance to mass transfer are therefore smaller in homogeneous gels. It is therefore somewhat confusing when considering the resistance to mass transfer generated by the gel porosity in polymer monoliths as described by Nischang *et al*. [21, 92-93]. It appears that this 'gel layer' in monolithic polymer scaffolds is solvent dependent and tends to retain analytes with hydrophobic character more strongly. Additions of organic modifiers affect the gel porosity and tend to decrease retention to benefit the separation performance.

The effect of gel porosity on post-modification processes and coatings appears to have been largely ignored in the literature. While research into this matter has been very limited in the work presented here, it is safe to assume that the solvents used in the post-modification and coating process

have a strong influence on the success of the procedure, since the accessibility of the functional groups will depend greatly on the level of swelling of the outer porous layer. The strongly hydrophobic properties of styrene and DVB based polymer monoliths impose restrictions on the analytes and separation conditions.

Modifications of the surface chemistry based on similar CMS scaffolds to those used in this work have been described by Wang *et al.* [174]. Infra-red spectroscopy was successfully used to monitor the conversion of the chloromethyl group. Retention factors of alkylbenzenes from chromatographic elution illustrated the differences in hydrophobicity for the original and modified hydrophilic material. The level of hydrophilicity was found to be comparable to a typical hydrolysed GMA-*co*-EDMA material. The results further suggest that any hydrophobic groups are well hidden in the polymer matrix and not accessible to even small analytes, resulting in a completely hydrophilic stationary phase in chromatographic terms.

Resistance of flow due to swelling of photografted chains has also been addressed by Potter [175] in reference to the “polyelectrolyte effect” [176]. Similar to the mechanism that results in the good stability of PEMs, it is described as ionic strength dependent swelling of solvated charged polymers.

Considering the findings in this context, it appears that the solvation of the outer polymer globule layer has varying influences on the stationary phase performance, much of it dependent on the hydrophobic or ionic interaction with the mobile phase, analytes and coating particles or surfactants. More rigorous analysis of this interaction in context of post-

modification and coating procedures as well as small anion analysis on the functionalised materials may shed more light on possible detrimental effects and how they could be negated.

Possible examination techniques for the assessment and characterisation of the morphology and functionalisation of the stationary phase have been reviewed in the Introduction chapter. However none of these are able to assess the specific interaction between scaffold surface chemistry, coating materials and analytes. Scanning capacitively coupled conductivity detection (sC4D) provides good average conductivity profiles that reflect on functional distributions as well as morphological uniformity within the capillary confined porous polymer material. It has been used to successfully demonstrate levels of characterisation similar to other techniques [117]. C^4D is however still very much at the early stage of being developed as a reliable characterisation tool, with instrumental configuration simply having been adapted from its original use as a detection technique for ionic species.

Exact measurements of material homogeneity (interstitial voids) can only be obtained for non-functionalised, hydrophobic stationary phases conducted in purified water, which provides a reasonably accurate reflection of the porous make-up based on the volume of water displaced by the monolithic polymer and therefore exhibiting direct proportionality to the signal response. However any functionality on the stationary phase surface will impede and dominate the signal response otherwise generated by the purified water. The increase in signal response stems from a rise in conductivity, either through the higher number of free ions in the ‘eluent’ or

buffer, in this case deionised water, or as bound charges along the surface of the functionalised porous polymer.

Given that C^4D is conducted using alternating current, various other factors besides the buffer or stationary phase material composition contribute to the signal make-up. Any dipole and electron charge displacement in the surrounding field has an effect on the signal output, whether it be in the air, glass (capillaries), electric field interferences from other equipment or static electricity. Unfortunately current publications so far shy away from examining the experimental circumstances that lead to fluctuations in measurements and to pinpoint these individual parameters using a combination of multivariate analysis or deconvolution software and standardisation of the readings through relative measurements.

As highlighted by the theoretical modelling and experimental validation using small *i.d.* capillaries, frequency related signal responses of the different material dipoles can discern physical properties to some extent. With adequate modifications to the instrumental set-up and implementation of auto-tuning, deconvolution and signal standardisation tools in the data processing software, further details in physical material make-up could be revealed.

7 Conclusion and Future Directions

The work described in this thesis offers significant improvements in the manufacture of monolayer latex-coated polymeric monolithic stationary phases. The successful post-modification procedure for poly(CMS-*co*-DVB) monolithic scaffolds has been adapted by Dionex to produce the IonSwift™ new generation commercial latex-coated monolithic capillary column for the rapid separation of organic acids and inorganic anions using a hydroxide eluent generation system. The monolithic porous polymer column is a novel development on the commercial IC market since the silica analogues have not been able to withstand degradation of the monolithic material in alkaline conditions.

Conventional C^4D instrumentation, which has previously been used for the sensitive analysis of inorganic anions, was successfully adapted to scan the manufactured and post-modified capillary columns. A theoretical model based on the impedances within the electronic circuit was able to successfully model the behaviour of conducting material between the electrodes and confirm the relationship experimentally using small bore capillaries. The non-invasive C^4D findings were successfully correlated with the separation performance of the scanned ion-exchange capillary columns in conjunction with visualisations of the material morphology and coating extent using SEM.

The specific outline and intensity of the column conductivity profile visualized not only major material discontinuities, but could also locate areas of minor inconsistencies and inspect the degree of surface functionalisation, which allowed for predictions of the separation performance. The various

parameters influencing the conductivity signal were partially acknowledged, such as capillary wall capacitance and solution conductivity, however further work is required to accurately identify the individual signal components and quantify their contribution on the overall signal magnitude.

7.1 Further work

Current in-house research on latex particle synthesis of various surface chemistry and hydrophobicity will provide further insight into the surface and particle chemistry that heavily influences the separation performance of coated polymeric monolith columns and has so far been predominantly an industry clandestine. Micro-formats besides fused silica capillaries are also being tested and developed, such as small *i.d.* peek tubing (IonSwift^{TM}) and various microchip channel fabrication techniques.

The advantages of fused-silica capillaries, such as offering covalent attachment of the polymer monolith scaffold to the inner wall, are still relevant for eluent systems where a high pH mobile phase is not required. Recent publications by Nischang *et al.* [177-178] examined the influence of varying channel geometry and downscaling in narrow bore capillaries on the separation performance of BuMA-*co*-EDMA monolithic columns. Besides a confinement effect of the capillary wall for very small internal channel diameters (10 μm or less) and the impact on reaction kinetics using lower polymerisation temperatures, the actual channel geometry did not impact on the separation performance, which suggests that other micro fluidic channel designs may become more available for IC applications.

Hybrid type materials [91, 170] and cryogel like combination of latex and silica nanoparticles as freeze dried colloidal mixtures [179] have also gained in recent interest. Similarly specific bicontinuous monolithic porous polymers have been obtained using 2,2,6,6-tetramethylpiperidin-1-yl oxide (TEMPO)-mediated living radical polymerisation of divinylbenzene [180]. These types of developments are poised to further generate porous polymer stationary phases with specific surface properties.

A combination of characterisation techniques as mentioned earlier in Chapter 1.4 would also improve the understanding of the various polymerisation and post-modification techniques. In particular the flow-related NMR studies [141], near-infrared porous property analysis [136] and material composition analysis by IR in conjunction with elemental analysis [174] have further potential in material characterisation. Modified C^4D equipment with better data processing and deconvolution software would significantly improve the level of detail in examined columns. The detector set-up could also include physical longitudinal vibrations of the capillary or conversely the actuator and pick-up electrodes during the scanning process to perform response sensitive analysis, which is material depth dependent rather than relating to the overall cross-sectional average. Other electrode designs could incorporate small plate electrodes on either side of the capillary, which could be rotated around the circumference during the scanning process.

Analysis of material composition and modification by infrared spectroscopy could potentially be conducted non-invasively and on-column with a laser type arrangement pinpointing the examined locations through the capillary wall.

7.2 Future predictions

Frantisek Svec has stated in a recent review [11]: *"The monolithic arena is still young and may largely be a terra incognita. But, like this unknown land got eventually mapped, explorations in the field of monoliths will certainly discover many novel materials with new unexpected properties and applications. Let us wait and see."*

In this review entitled "My favourite materials: Porous polymer monoliths" Svec examines the evolution of monolithic materials, in particular as polymer stationary phases in IC. The numerous applications of monoliths reported to date in this field are considered in relation to their potential applicability in future. In summary, Svec addresses the applications that may suit the monolithic stationary phase and suggests that the novel and different ways for preparation and modification may see monolithic materials becoming more strongly established as one of the major stationary phase materials in IC.

With respect to the literature review outlined in the introduction chapter and the developments since publication in 2006, the predicted trend in the specific field of fast IC of small inorganic anions has been somewhat slower for capillary polymer monoliths, but is also much broader in the sense of tailored applicability of the modified stationary phases and equipment design for a range of different techniques. These include such specialty fields as – chelating, chiral, protein, peptide, CEC, mirco-LC, simultaneous anion and cation analysis (TSKgel-Super IC) and microchips. Analysis of literature published in the last decade shows that an early rise in publications has plateaued in most fields using capillary monoliths since around the time of

the review publication (2006), however an increasing trend in monolithic materials, particular polymeric, is noticeable.

containing the concept:	*"capillary ion-exchange"*	In Publication Year "2000-2006"	In Publication Year "2006-2010"
# of references found	559	232	109
% of total using monoliths	4.6%, half polymer, half silica	6.0%, more silica	15.6%, half polymer, half silica
capillary	288	132	60
electrophoresis	114	64	20
chromatography	106		24
ion-exchange	86	45	17
CEC	68	52	
review	57	28	11
anion	43	28	
protein	42	25	12
preconcentration	28		
monolithic	26	14	17
cation	23	8	
silica	18	10	11
polymer	16		11
latex-coated	11	11	8

Developments of commercial micro-IC instrumentation have resulted in the official market launch of suitable micro-IC systems with reagent-free eluent generation, matching recent capillary stationary phase developments in ion-exchange chromatography. The Dionex ICS 5000 instrument can provide reagent-free eluent generation for in-house manufactured polymer based

capillary columns in Peek at flow-rates between 1-30 μL/min, with claimed capillary pump specifications allowing flow-increments as low as 0.1 μL/min (see www.dionex.com for more information). Depending on market developments, further micro-IC instruments are likely to be available, since most manufacturers have micro- and nano-LC instrumentation and related equipment already in circulation.

As quoted by Chambers [17]:

Polymer monoliths can produce excellent separations of macromolecules and biomolecules such as peptides, proteins, oligonucleotides, and nucleic acids. However, to date the efficiency of IC separations performed with polymeric monoliths have been poor compared to those achieved with silica monoliths. Nonetheless, due to their relative ease of preparation and commercial availability, the potential of polymer monoliths to provide fast separation is just starting to crossover from theory and thought to real world use and practicality. With regard to IC, the enhanced mass transfer demonstrated with latex-coated polymer monoliths makes this a promising means of developing polymeric IC monoliths. In 'As You Like It', Shakespeare broke the life cycle of any person into seven ages. In a classic editorial, Herb Laitinen, then editor of Analytical Chemistry, applied these seven ages to characterize the development and maturity of analytical methodologies [181]. Laitinen's seven ages are: conception and initiation; demonstration and validation; acceptance by nonspecialist; maturation through detailed studies of principle and mechanisms; widening breadth of application; standardization of the methodology such that it is described in

compilations of standard methods but not in research papers; senescence as techniques of greater speed, economy, etc. surpass the method. A decade ago IC was characterized as being in the sixth age [182]. The introduction of monoliths to IC has revitalized the field such that monolith IC or fast IC is now just entering the third age – bringing monoliths from a laboratory curiosity into the hands of the nonspecialist. Modern research is starting to characterize what monoliths can do for IC separations. Nevertheless, as new forms of IC monoliths are prepared, research easily can revert to new conceptions of how monoliths can be used and optimized for IC. With continuing advances, the future of monolithic columns for use in IC holds exciting prospects for fast ion analysis.

With this in mind it will be exciting to see what future applications and material modifications await the field of functionalised monolithic polymer substrate ion-exchange chromatography.

8 References

[1] H. Small, T. S. Stevens, W. C. Baumann, *Anal. Chem.* **1975**, *47*, 1801-1809.

[2] P. R. Haddad, P. E. Jackson, *Ion Chromatography - Principles and Application*, Elsevier, Amsterdam, **1997**.

[3] C. A. Lucy, *J. Chromatogr. A* **2003**, *1000*, 711-724.

[4] T. Greibrokk, *J. Sep. Sci.* **2004**, *27*, 1249-1254.

[5] P. Kuban, P. K. Dasgupta, *J. Sep. Sci.* **2004**, *27*, 1441-1457.

[6] Z. Liu, R. a. Wu, H. Zou, *Electrophoresis* **2002**, *23*, 3954-3972.

[7] C. J. Evenhuis, R. M. Guijt, M. Macka, P. R. Haddad, *Electrophoresis* **2004**, *25*, 3602-3624.

[8] B. Paull, P. Nesterenko, *Analyst* **2005**, *130*, 134-146.

[9] B. Paull, P. Nesterenko, *TRAC* **2005**, *24*, 295-303.

[10] F. Svec, *J. Sep. Sci.* **2004**, *27*, 1419-1430.

[11] F. Svec, *J. Sep. Sci.* **2009**, *32*, 3-9.

[12] F. Svec, *J. Chromatogr. A* **2010**, *1217*, 902-924.

[13] E. F. Hilder, F. Svec, J. M. J. Fréchet, *Electrophoresis* **2002**, *23*, 3934-3953.

[14] F. Svec, E. C. Peters, D. Sykora, C. Yu, J. M. J. Fréchet, *J. High Res. Chromatogr.* **2000**, *23*, 3-18.

[15] H. Zou, X. Huang, M. Ye, Q. Luo, *J. Chromatogr. A* **2002**, *954*, 5-32.

[16] C. Legido-Quigley, N. D. Marlin, V. Melin, A. Manz, N. W. Smith, *Electrophoresis* **2003**, *24*, 917-944.

[17] S. D. Chambers, K. M. Glenn, C. A. Lucy, *J. Sep. Sci.* **2007**, *30*, 1628-1645.

[18] D. Josic, A. Buchacher, A. Jungbauer, *J. Chromatogr. B* **2001**, *752*, 191-205.

[19] E. F. Hilder, A. Nordborg, *Anal. Bioanal. Chem.* **2009**, *394*, 71-84.

[20] F. Svec, *J. Chromatogr. A* **2011**, *1218*, doi:10.1016/j.chroma.2011.1007.1019.

[21] I. Nischang, I. Teasdale, O. Brüggemann, *Anal. Bioanal. Chem.* **2011**, *400*, 2289-2304.

[22] A. Nordborg, E. F. Hilder, P. R. Haddad, *Annu. Rev. Anal. Chem.* **2011**, *4*, 197-226.

[23] D. Schaller, P. R. Haddad, E. F. Hilder, *J. Sep. Sci.* **2006**, *29*, 1705-1719.

[24] F. Svec, J. M. J. Fréchet, *Anal. Chem.* **1992**, *64*, 820-822.

[25] F. Svec, J. M. J. Fréchet, *J. Chromatogr. A* **1995**, *702*, 89-95.

[26] H. Minakuchi, K. Nakanishi, N. Soga, N. Ishizuka, N. Tanaka, *Anal. Chem.* **1996**, *68*, 3498-3501.

[27] Q. Xu, M. Moria, K. Tanaka, M. Ikedo, W. Hu, *J. Chromatogr. A* **2004**, *1026*, 191-194.

[28] P. Hatsis, C. A. Lucy, *Anal. Chem.* **2003**, *75*, 995-1001.

[29] D. Connolly, D. Victory, B. Paull, *J. Sep. Sci.* **2004**, *27*, 912-920.

[30] Q. Xu, M. Mori, K. Tanaka, M. Ikedo, W. Hu, P. R. Haddad, *J. Chromatogr. A* **2004**, *1041*, 95-99.

[31] C. Ó Ríordáin, P. N. Nesterenko, B. Paull, *J. Chromatogr. A* **2005**, *1070*, 71-78.

[32] C. Ó Ríordáin, L. Barron, E. Nesterenko, P. N. Nesterenko, B. Paull, *J. Chromatogr. A* **2006**, *1109*, 111-119.

[33] F. Svec, T. Tennikova, Z. Deyl, *Monolithic Materials: Preparation, Properties and Application, Vol. Vol. 67*, J. Chromatogr. Library ed., Elsevier, Amsterdam, **2003**.

[34] F. Svec, J. M. J. Fréchet, *Ind. Eng. Chem. Res.* **1999**, *38*, 34-48.

[35] F. C. Leinweber, D. Lubda, K. Cabrera, U. Tallarek, *Anal. Chem.* **2002**, *74*, 2470-2477.

[36] P. Hemström, A. Nordborg, k. Irgum, F. Svec, J. M. J. Fréchet, *J. Sep. Sci.* **2006**, *29*, 25-32.

[37] R. Asiaie, X. Huang, D. Farna, C. Horváth, *J. Chromatogr. A* **1998**, *806*, 251-263.

[38] D. Allen, Z. E. Rassi, *Electrophoresis* **2003**, *24*, 3962-3976.

[39] N. Tanaka, H. Kobayashi, K. Nakanishi, H. Minakuchi, N. Ishizuka, *Anal. Chem.* **2001**, *73*, 420A-429A.

[40] A.-M. Siouffi, *J. Chromatogr. A* **2003**, *1000*, 801-818.

[41] K. Nakanishi, N. J. Soga, *Non-Cryst. Solids* **1992**, *139*, 1-24.

[42] N. Ishizuka, H. Minakuchi, K. Nakanishi, N. Soga, H. Nagayama, K. Hosoya, N. Tanaka, *Anal. Chem.* **2000**, *72*, 1275-1280.

[43] E. Vasbinder, G. Van der Weken, Y. Vander Heyden, W. R. Baeyens, A. Debunne, J. P. Remon, A. M. Garcia-Campãna, *Biomed. Chromatogr.* **2004**, *18*, 55-63.

[44] E. Sugrue, P. N. Nesterenko, B. Paull, *J. Chromatogr. A* **2005**, *1075*, 167-175.

[45] E. Sugrue, P. N. Nesterenko, B. Paull, *Analyst* **2003**, *128*, 417-420.

[46] E. Sugrue, P. N. Nesterenko, B. Paull, *J. Sep. Sci.* **2004**, *27*, 921-930.

[47] J. P. Hutchinson, E. F. Hilder, M. Macka, N. Avdalovic, P. R. Haddad, *J. Chromatogr. A* **2006**, *1109*, 10-18.

[48] D. Connolly, B. Paull, *J. Chromatogr. A* **2001**, *917*, 353-359.

[49] D. Connolly, B. Paull, *Anal. Chim. Acta* **2001**, *441*, 53-62.

[50] P. Hatsis, C. A. Lucy, *Analyst* **2002**, *127*, 451-454.

[51] D. Connolly, B. Paull, *J. Chromatogr. A* **2002**, *953*, 299-303.

[52] R. M. Cassidy, S. Elchuk, *J. Chromatogr. Sci.* **1983**, *21*, 454-459.

[53] D. Victory, P. N. Nesterenko, B. Paull, *Analyst* **2006**, *129*, 700-701.

[54] Q. Xu, K. Tanaka, M. Mori, M. I. H. Helaleh, W. Hu, K. Hasebe, H. Toada, *J. Chromatogr. A* **2003**, *997*, 183-190.

[55] J. S. Fritz, Z. Yan, P. R. Haddad, *J. Chromatogr. A* **2003**, *997*, 21-31.

[56] E. Sugrue, P. N. Nesterenko, B. Paull, *Anal. Chim. Acta* **2005**, *533*, 27-35.

[57] M. C. Breadmore, S. Shrinivasan, K. A. Wolfe, M. E. Power, J. P. Ferrance, B. Hosticka, P. M. Norris, J. P. Landers, *Electrophoresis* **2002**, *23*, 3487-3495.

[58] M. C. Breadmore, S. Shrinivasan, J. Karlinsey, J. P. Ferrance, P. M. Norris, J. P. Landers, *Electrophoresis* **2003**, *24*, 1261-1270.

[59] M. W. Kamande, K. A. Fletcher, M. Lowry, I. Warner, M., *J. Sep. Sci.* **2005**, *28*, 710-718.

[60] J. P. Hutchinson, E. F. Hilder, M. Macka, N. Avdalovic, P. R. Haddad, *J. Chromatogr. A* **2006**, *1109*, 10-18.

[61] J. P. Hutchinson, M. Macka, N. Avdalovic, P. R. Haddad, *J. Chromatogr. A* **2004**, *1039*, 187-192.

[62] M. T. Dulay, J. P. Quirino, B. D. Bennett, M. Kato, R. N. Zare, *Anal. Chem.* **2001**, *73*, 3921-3926.

[63] K. Morishima, M. T. Dulay, J. P. Quirino, B. D. Bennett, R. N. Zare, *J. Sep. Sci.* **2002**, *25*, 1226-1230.

[64] M. T. Dulay, J. P. Quirino, B. D. Bennett, R. N. Zare, *J. Sep. Sci.* **2002**, *25*, 3-9.

[65] M. Kato, K. Sakai-Kato, H. Jin, K. Kubota, H. Miyano, T. Toyo'oka, M. T. Dulay, R. N. Zare, *Anal. Chem.* **2004**, *76*, 1896-1902.

[66] C. Yu, F. Svec, J. M. J. Fréchet, *Electrophoresis* **2000**, *21*, 120-127.

[67] E. C. Peters, F. Svec, J. M. J. Fréchet, *Adv. Mater.* **1999**, *11*, 1169-1181.

[68] C. Viklund, E. Ponten, B. Glad, K. Irgum, P. Horstedt, F. Svec, *Chem. Mater.* **1997**, *9*, 463-471.

[69] C. Viklund, F. Svec, J. M. J. Fréchet, K. Irgum, *Chem. Mater.* **1996**, *8*, 744-750.

[70] E. C. Peters, M. Petro, F. Svec, J. M. J. Fréchet, *Anal. Chem.* **1997**, *69*, 3646-3649.

[71] R. Kala, V. M. Biju, T. P. Rao, *Anal. Chim. Acta* **2005**, *549*, 51-58.

[72] T. Rohr, E. F. Hilder, J. J. Donovan, F. Svec, J. M. J. Fréchet, *Macromolecules* **2003**, *36*, 1677-1684.

[73] E. F. Hilder, F. Svec, J. M. J. Fréchet, *J. Chromatogr. A* **2004**, *1053*, 101-106.

[74] Y. Ueki, T. Umemura, J. Li, T. Odake, K.-i. Tsunoda, *Anal. Chem.* **2004**, *76*, 7007-7012.

[75] P. Zakaria, J. P. Hutchinson, N. Avdalovic, P. R. Haddad, *Anal. Chem.* **2005**, *77*, 417-423.

[76] A. Sjorgen, C. B. Boring, P. K. Dasgupta, *Anal. Chem.* **1997**, *69*, 1385-1391.

[77] J. P. Hutchinson, E. F. Hilder, R. A. Shellie, J. A. Smith, P. R. Haddad, *Analyst* **2006**, *131*, 215-221.

[78] D. Connolly, B. Paull, *J. Sep. Sci.* **2009**, *32*, 2653-2658.

[79] S. Eeltink, E. F. Hilder, L. Geiser, F. Svec, J. M. J. Fréchet, G. P. Rozing, P. J. Schoenmakers, W. T. Kok, *J. Sep. Sci.* **2007**, *30*, 407-413.

[80] A. A. Kurganov, A. A. Korolev, E. N. Viktorova, A. Y. Kanat'eva, *Russ. J. Phys. Chem.* **2009**, *83*, 303-307.

[81] J. P. Hutchinson, P. Zakaria, M. Macka, N. Avdalovic, P. R. Haddad, *Anal. Chem.* **2005**, *77*, 407-416.

[82] T. Tegeler, Z. EL Rassi, *J. Chromatogr. A* **2002**, *945*, 267-279.

[83] M. C. Breadmore, M. Boyce, M. Macka, N. Avdalovic, P. R. Haddad, *Analyst* **2000**, *125*, 799-802.

[84] W. Yan, R. Gao, Z. Zhang, Q. Wang, C. V. Jiang, C. Yan, *J. Sep. Sci.* **2003**, *26*, 555-561.

[85] C. Zheng, Y.-P. Huang, Z.-S. Liu, *J. Sep. Sci.* **2011**, *34*, 1988-2002.

[86] M. Laemmerhofer, W. Lindner, *Journal of Chromatography Library* **2003**, *67*, 489-559.

[87] J. Haginaka, *J. Sep. Sci.* **2009**, *32* 1548-1565.

[88] J. Spross, A. Sinz, *J. Sep. Sci.* **2011**, *34*, 1958-1973.

[89] C. M. A. Ribeiro, J. Hradil, F. Švec, J. Kálal, *Angew. Macromol. Chem.* **1980**, *87*, 119-126.

[90] Y. Chonde, L.-J. Liu, I. M. Krieger, *J. App. Polym. Sci.* **1980**, *25*, 2407-2416.

[91] J. R. Thabano, M. C. Breadmore, J. P. Hutchinson, C. Johns, P. R. Haddad, *J. Chromatogr. A* **2009**, *1216*, 4933-4940.

[92] I. Nischang, O. Brüggemann, *J. of Chromatog. A* **2010**, *1217*, 5389-5397.

[93] I. Nischang, I. Teasdale, O. Brüggemann, *J. of Chromatog. A* **2010**, *1217*, 7514-7522.

[94] J. Urban, F. Svec, J. M. J. Fréchet, *J. of Chromatog. A* **2010**, *1217*, 8212-8221.

[95] J. Urban, F. Svec, J. M. J. Fréchet, *Anal. Chem.* **2010**, *82*, 1621-1623.

[96] L. Trojer, C. P. Bisjak, W. Wieder, G. K. Bonn, *J. Chromatogr. A* **2009**, *1216*, 6303-6309.

[97] A. Greiderer, L. Trojer, C. W. Huck, G. K. Bonn, *J. of Chromatog. A* **2009**, *1216*, 7747-7754.

[98] Y. Huo, P. J. Schoenmakers, W. T. Kok, *J. of Chromatog. A* **2007**, *1175*, 81-88.

[99] K. Miyabe, G. Guiochon, *Anal. Chem.* **2000**, *72*, 1475-1489.

[100] V. A. Davanakov, S. V. Rogozhin, M. P. Tsyurupa, in *Vol. 729*, U.S. Patent 3, **April 24, 1973**, p. 457.

[101] V. A. Davanakov, M. P. Tsyurupa, *React. Polym.* **1990**, *13*, 27-42.

[102] A. V. Pastukhov, M. P. Tsyurupa, V. A. Davanakov, *J. Polym. Sci., Polym. Phys.* **1999**, *37*, 2324-2333.

[103] V. A. Davanakov, M. P. Tsyurupa, M. Ilyin, L. Pavlova, *J. Chromatogr. A* **2002**, *965*, 65-73.

[104] M. P. Tsyurupa, V. A. Davanakov, *React. Funct. Polym.* **2006**, *66*, 768-779.

[105] P. R. Haddad, E. F. Hilder, C. Evenhuis, D. Schaller, C. Pohl, K. Flook, *Abstr. Pap. Am. Chem. Soc.* **2009**, *236*.

[106] Y. Xu, Q. Cao, F. Svec, J. M. J. Fréchet, *Anal. Chem.* **2010**, *82*, 3352-3358.

[107] Q. Cao, Y. Xu, F. Liu, F. Svec, J. M. J. Fréchet, *Anal. Chem.* **2010**, *82*, 7416-7421.

[108] D. Connolly, B. Twamley, B. Paull, *Chem. Commun.* **2010**, *46*, 2109-2111.

[109] J. Krenkova, N. A. Lacher, F. Svec, *Anal. Chem.* **2010**, *82*, 8335-8341.

[110] S. D. Chambers, F. Svec, J. M. J. Fréchet, *J. Chromatogr. A* **2011**, *1218*, 2546-2552.

[111] Y. Li, Y. Chen, R. Xiang, D. Ciuparu, L. D. Pfefferle, C. Horváth, J. Wilkins, *Anal. Chem.* **2005**, *77*, 1398-1406.

[112] J. Krenkova, F. Foret, *J. Sep. Sci.* **2011**, *34*, 1-7.

[113] L. Han, Z. Shan, D. Chen, X. Yu, P. Yang, B. Tu, D. Zhao, *J. Colloid Interface Sci.* **2008**, *318*, 315-321.

[114] A. Lee, Y. H.-J., E.-S. Lim, J. Kim, Y. Kim, *Rapid Commun. Mass Spectrom.* **2008**, *22*, 2561-2564.

[115] A. Bee, R. Massart, S. Neveu, *J. Magn. Mater.* **1995**, *149*, 6-9.

[116] C. Hou, J. Ma, D. Tao, Y. Shan, Z. Liang, L. Zhang, Y. Zhang, *J. Proteome Res.* **2010**, *9*, 4093-4101.

[117] D. Connolly, P. Floris, P. N. Nesterenko, B. Paull, *TrAC* **2010**, *29*, 870-884.

[118] D. Connolly, L. P. Barron, E. Gillespie, B. Paull, *Chromatographia* **2009**, *70*, 915-920.

[119] T. D. Mai, H. V. Pham, P. C. Hauser, *Anal. Chim. Acta* **2009**, *653*, 228-233.

[120] Z. Walsh, P. A. Levkin, V. Jain, B. Paull, F. Svec, M. Macka, *J. Sep. Sci.* **2010**, *33*, 61-66.

[121] Z. Walsh, M. Vasquez, F. Benito-Lopez, B. Paull, M. Macka, F. Svec, D. Diamond, *Lab. Chip* **2010**, *10*, 1777-1780.

[122] E. Gillespie, M. Macka, D. Connolly, B. Paull, *Analyst* **2006**, *131*, 886-888.

[123] E. Gillespie, D. Connolly, M. Macka, P. N. Nesterenko, B. Paull, *Analyst* **2007**, *132*, 1238-1245.

[124] M. Takeuchi, Q. Li, B. Yang, P. K. Dasgupta, V. E. Wilde, *Talanta* **2008**, *76*, 617-620.

[125] R. Nehme, C. Perrin, H. Cottet, M. D. Blanchin, H. Fabre, *Electrophoresis* **2009**, *30*, 1888-1898.

[126] J. B. Schlenoff, S. T. Dubas, *Macromolecules* **2001**, *34*, 592-598.

[127] E. Gillespie, D. Connolly, B. Paull, *Analyst* **2009**, *134*, 1314-1321.

[128] S. Currivan, D. Connolly, E. Gillespie, B. Paull, *J. Sep. Sci.* **2010**, *33*, 484-492.

[129] A. Maruska, A. Rocco, O. Kornysova, S. Fanali, *J. Biochem. Biophys. Methods* **2007**, *70*, 47-55.

[130] V. Pucci, M. A. Raggi, F. Svec, J. M. J. Frechet, *J. Sep. Sci.* **2004**, *27*, 779-788.

[131] D. Connolly, V. O'Shea, P. Clark, B. O'Connor, B. Paull, *J. Sep. Sci.* **2007**, *30*, 3060-3068.

[132] V. o'Shea, *The detection by conductivity of the effect of protein tagging on immobilization within monolith columns and development of a novel free sialic acid detector* Dublin City University (Dublin, Ireland), **2009**.

[133] E. Gillespie, D. Connolly, P. N. Nesterenko, B. Paull, *Analyst* **2008**, *133*, 874-876.

[134] E. Gillespie, D. Connolly, P. N. Nesterenko, B. Paull, *J. Sep. Sci.* **2009**, *32*, 2659-2667.

[135] A. Gömann, J. A. Deverell, K. F. Munting, R. C. Jones, T. Rodemann, A. J. Canty, J. A. Smith, *Tetrahedron* **2009**, *65*, 1450-1454.

[136] N. Heigl, A. Greiderer, C. H. Petter, O. Kolomiets, H. W. Siesler, M. Ulbricht, G. K. Bonn, C. W. Huck, *Anal. Chem.* **2008**, *80*, 8493–8500.

[137] S. Brunauer, P. H. Emmett, E. Teller, *J. Am. Chem. Soc.* **1938**, *60*, 309-319.

[138] E. P. Barrett, L. G. Joyner, P. P. Halenda, *J. Am. Chem. Soc.* **1951**, *73*, 373-380.

[139] S. Bruns, T. Müllner, M. Kollmann, J. Schachtner, A. Höltzel, U. Tallarek, *Anal. Chem.* **2010**, *82*, 6569-6575.

[140] J. Courtois, M. Szumski, F. Georgsson, I. Knut, *Anal. Chem.* **2007**, *79*, 335-344.

[141] T. Z. Teisseyre, J. Urban, N. W. Halpern-Manners, S. D. Chambers, V. S. Bajaj, F. Svec, A. Pines, *Anal. Chem.* **2011**, *83*, 6004-6010.

[142] N. Delaunay-Bertoncini, C. Demesmay, J.-L. Rocca, *Electrophoresis* **2004**, *25*, 3204-3215.

[143] E. C. Peters, M. Petro, F. Svec, J. M. J. Fréchet, *Anal. Chem.* **1998**, *70*, 2288-2295.

[144] M. Bedair, Z. EL Rassi, *Electrophoresis* **2002**, *23*, 2938-2948.

[145] B. Preinerstorfer, W. Bicker, W. Lindner, M. Lämmerhofer, *J. Chromatogr. A* **2004**, *1044*, 187-199.

[146] B. Preinerstorfer, W. Lindner, M. Lämmerhofer, *Electrophoresis* **2005**, *26*, 2005-2018.

[147] N. Lendero, J. Vidič, P. Brne, A. Podgornik, A. Štrancar, *J. Chromatogr. A* **2005**, *1065*, 29-38.

[148] P. E. Jackson, *Ion-exchange Chromatography* University of NSW, PhD thesis (Sydney), **1990**.

[149] D. K. Roper, E. N. Lightfoot, *J. Chromatogr. A* **1995**, 3-22.

[150] R. W. Slingsby, C. A. Pohl, *J. Chromatogr.* **1988**, *458*, 241-253.

[151] K. M. Glenn, C. A. Lucy, P. R. Haddad, *J. Chromatogr. A* **2007**, *1155*, 8-14.

[152] C. J. Evenhuis, W. Buchberger, E. F. Hilder, K. J. Flook, C. A. Pohl, P. N. Nesterenko, P. R. Haddad, *J. Sep. Sci.* **2008**, *31*, 2598-2604.

[153] T. J. Causon, R. A. Shellie, E. F. Hilder, *J. Chromatogr. A* **2010**, *1217*, 3765-3769.

[154] http://www.dionex.com/en-us/products/columns/ic-rfic/hydroxide-selective-packed/ionpac-as18/lp-73261.html.

[155] R. M. Guijt, C. J. Evenhuis, M. Macka, P. R. Haddad, *Electrophoresis* **2004**, *25*, 4032-4037.

[156] A. J. Zemann, *Electrophoresis* **2003**, 2125-2137.

[157] P. Kuban, P. C. Hauser, *Electrophoresis* **2004**, *25*, 3387-3397.

[158] P. Kuban, P. C. Hauser, *Electrophoresis* **2004**, *25*, 3398-3405.

[159] J. A. F. da Silva, C. L. do Lago, *Anal. Chem.* **1998**, *70*, 4339-4343.

[160] A. J. Zemann, E. Schnell, D. Volgger, G. K. Bonn, *Anal. Chem.* **1998**, *70*, 563-567.

[161] P. Kuban, P. Hauser, *Electrophoresis* **2009**, *30*, 176-188.

[162] D. Connolly, V. O'Shea, P. Clark, B. O'Connor, B. Paull, *Journal of Sep. Science* **2007**, 3060-3068.

[163] W. P. Mason, *Properties of Piezoelectric Crystals in Physical Acoustics and the Properties of Solids*, Princeton, New Jersey, US, **1958**.

[164] W. J. Duffin, *Electricity and Magnetism*, London, **1965**.

[165] J. P. Hutchinson, M. Macka, N. Avdalovic, P. R. Haddad, *J. Chromatogr. A* **2006**, *1106*, 43-51.

[166] K. Jerabek, *Anal. Chem.* **1985**, *57*, 1598-1602.

[167] K. Jerabek, *Anal. Chem.* **1985**, *57*, 1595-1597.

[168] T. C. Laurent, J. Killander, *J. Chromatogr.* **1964**, *14*, 317-330.

[169] E. N. Viktorova, A. A. Korolev, S. V. Rodionov, A. A. Kurganov, *Russ. J. Phys. Chem. A* **2011**, *85*, 125-129.

[170] P. Jandera, J. Urban, D. Moravcova, *J. Chromatog. A* **2006**, *1109*, 60-73.

[171] R. Edam, S. Eeltink, D. J. D. Vanhoutte, W. T. Kok, P. J. Schoenmakers, *J. Chromatog. A* **2011**, *1218*, 8638-8645.

[172] M. Al Bokari, D. Cherrak, G. Guiochon, *J. Chromatogr. A* **2002**, *975*, 275-284.

[173] A. Vegvari, *J. Chromatog. A* **2005**, *1079*, 50–58.

[174] Q. Wang, F. Svec, J. M. J. Fréchet, *Anal. Chem.* **1995**, *67*, 670-674.

[175] O. G. Potter, *New Materials and Techniques for Miniaturised Chromatography* University of Tasmania, PhD Thesis (Hobart), **2011**.

[176] S. Graham, P. A. G. Cormack, D. C. Sherrington, *Macromolecules* **2004**, *38*, 86-90.

[177] I. Nischang, F. Svec, J. M. J. Fréchet, *J. Chromatogr. A* **2009**, *1216*, 2355-2361.

[178] I. Nischang, F. Svec, J. M. J. Fréchet, *Anal. Chem.* **2009**, *81*, 7390-7396.

[179] C. A. L. Colard, R. A. Cave, N. Grossiord, J. A. Covington, S. A. F. Bon, *Adv. Mater.* **2009**, *21*, 2894-2898.

[180] K. Kanamori, K. Nakanishi, T. Hanada, *Adv. Mater.* **2006**, *18*, 2407-2411.

[181] H. A. Laitinen, *Anal. Chem.* **1973**, *45*, 2305-2305.

[182] C. A. Lucy, *J. Chromatogr. A* **1996**, *739*, 3-13.

[183] D. Hlushkou, S. Bruns, A. Höltzel and U. Tallarek, *Anal. Chem.* **2010**, *82*, 46-58.

[184] S. Bruns, T. Hara, B. M. Smarsly and U. Tallarek, *J. Chromatogr. A* **2011**, *1218*, 5187-5194.

[185] K. Hormann, T. Müllner, S. Bruns, A. Höltzel and U. Tallarek, *J. Chromatogr. A* **2012**, *1222*, 46-58.